ONE MINUTE AT A TIME:
ADVANCING OUR ABILITY TO ESTIMATE EFFECTS OF HUMAN SOUND ON MARINE LIFE.

by

S. Bruce Martin

Submitted in partial fulfillment of the requirements
for the degree of Doctor of Philosophy

at

Dalhousie University
Halifax, Nova Scotia
April 2019

DEDICATION

This thesis is dedicated to my wife Katherine for all her support and encouragement the past four years, as well as my children Cameron, Isaac, Andrew and Michael who have put up with my studying and being distracted.

To Dr. Greg Hirsch and NP Karen Withrow at the QE2 Cardiac Unit – thanks for keeping me going so that I could get this done!

Contents

LIST OF TABLES

LIST OF FIGURES

ABSTRACT

Mitigating the effects of sound from man-made sources is an important component of marine conservation of marine mammals, fish and crustaceans. Sound travels from its source, through the ocean, to the animals that perceive it. Natural sounds include wind, waves, rain, ice, mammals, fish, and crustaceans. Man-made sounds include non-impulsive sources such as vessels and oil rigs, and impulsive sources such as seismic airguns, pile driving, and sonars. To protect animals from these sounds, safe thresholds are defined based on animal's hearing and the daily sound exposure level (SEL). Safe thresholds for impulsive sounds are about $1/10^{th}$ those of non-impulsive. To mitigate the effects of sound on marine life we need to better quantify the properties of man-made sources and the differences between non-impulsive and impulsive. This thesis provides such information.

It is shown that seismic arrays have more energy above 1 kHz than previously reported and therefore have greater effects on marine life. Sound levels from impact pile driving depend on strike energy, pile penetration and the angle between pile and seabed. These factors change the distance that must be monitored to protect marine life by a factor of ten.

The daily SEL and the autocorrelation of the one-minute sound exposure are used to describe the acoustic environment. These metrics are used to identify environments with and without human sound sources and the difference between different types of soundscapes, especially coral reefs from all others.

Safe thresholds for sound exposure are based on the daily impulsive and non-impulsive SEL. Impulsive sounds change to non-impulsive-like over ranges of kilometers, and at some transition point they should accumulate with the non-impulsive SEL. Using kurtosis as a measure of impulsiveness and a proposed threshold for no possible injury, a new categorization of man-made sounds as impulsive or non-impulsive is presented that depends on the source and functional hearing group but not on range.

This work will inform the development of regulatory protocols to help mitigate the effects of man-made sound on marine life.

LIST OF ABBREVIATIONS USED

Abbreviation	Meaning
AIC	Akaike Information Criterion
ADEON	Atlantic Deepwater Ecosystem Observation Network
dB	decibel
EOV	Essential Ocean Variable
FFT	Fast Fourier Transform
FHWG	Fisheries Hydro-acoustic Working Group
FIR	Finite Impulse Response
GOOS	Global Ocean Observing System
IMO	International Maritime Organization
ISO	International Organization for Standards
MERIDIAN	Marine Environmental Research Infrastructure for Data Integration and Application Network
MMO	Marine Mammal Observer
NIOSH	National Institute of Occupational Safety and Health
NMFS	National Marine Fisheries Service
NOAA	National Oceanic and Atmosphere Administration
NPI	No Possible Injury
NRC	National Research Council
PCAD	Population Consequences of Acoustic Disturbance
PCoD	Population Consequences of Disturbance
PP	Pile Penetration
PSD	Power Spectral Density
PTS	Permanent Threshold Shift
SE	Strike Energy
SEL	Sound Exposure Level
SONAR	Sound Navigation and Ranging
SPL	Sound Pressure Level
TTS	Temporary Threshold Shift
UN	United Nations

ACKNOWLEDGEMENTS

I never planned to do a PhD, but here it is – there are a lot people along the way who gave me the support, guidance and wisdom I needed to complete this work. David Hannay, Alex MacGillivray, Roberto Racca, Julien Delarue and the rest of the fantastic team at JASCO taught me the value of a μPa, how to do a sound source characterization, what a marine mammal is and how they are all intertwined through acoustics. They encouraged and supported my early conference presentations that gave me an appreciation for sharing science with others. Over the years Karen Hiltz has helped me learn subtleties of Microsoft Word, Endnote and active writing, which made it much easier to assemble this document. I am also extremely grateful to JASCO for funding my tuition.

I also want to acknowledge the researchers I've met along the way who have shared their time both professionally and socially, which helped me know that I could accomplish this goal. In particular thanks to Drs. Art Popper and Jen Miksis-Olds. Dr. Popper was especially important for making me understand that there are a lot of fish in the sea. To Dr. Pete Cott who suggested we co-author my first paper – it turned out not to be *that* hard …

To my advisor Dr. David Barclay, and my committee – Drs. Christopher Taggart, Corey Morris, Alex Hay and Sean Pecknold – you have given me the freedom to explore my topic and the guidance when I needed it to stay focussed and make sure I did 'good science'.

CHAPTER 1 INTRODUCTION

Contributions of human sound sources to the marine soundscape are increasingly regarded as an environmental effect that we have an ability to measure and control, particularly with respect to recovery of endangered species or maintaining the health of commercial fish stocks. Measuring baseline sound levels and mitigating the effects of sound are important elements of the Canadian Government's Ocean Protection Plan (https://bit.ly/2Tcqnq9). Management of noise is third on the list of actions that we can take to help in the recovery of north Atlantic right whales (after reducing ship strikes and fishing gear entanglement (https://bit.ly/2BSeUlC)). In the United States ocean noise management is a priority for the National Oceanic and Atmospheric Administration (https://cetsound.noaa.gov/road-map), including the establishment of a network of Noise Reference Stations (https://bit.ly/2Ec8Pkv). The European Union has identified annual average sound levels and the number of days with impulsive sounds as indicators of Good Environmental Status within the Marine Strategy Framework Directive (https://bit.ly/2NpksZl). In May 2018 the Global Ocean Observing System (GOOS) added Ocean Sound as only the second cross-disciplinary essential ocean variable (EOV) that observatories should measure and report (https://bit.ly/2VisS7O).

These high-level management directives have led to increases in baseline monitoring programs and dedicated sound measurement campaigns, both facilitated by lower cost and higher performance autonomous acoustic data loggers. The programs in turn have led to rapid growth in the available acoustic data that needs to be processed to extract information from the raw data. There is a need for both standardized metrics and tools, and research to advance our understanding of how to collect, process, and interpret

marine acoustic data. Basic acoustic metrics are defined in the recent ISO Standard 18405 (2017a), and the Atlantic Deep-water Ecosystem Observation Network (ADEON) project in the United States has produced a Soundscape Specification and Data Analysis Specification that go into more detail on what metrics to produce and how to compute them (https://www.adeon.unh.edu/). These initiatives provide definitions for fundamental measurements of sound levels, however, they do not proscribe measurement details relevant to studying the effects of noise on marine life such as integration times for sound pressure level or metrics for describing how sounds evolve from impulsive to non-impulsive as they propagate.

Marine sound is a source – medium – receiver system. We require knowledge of all three components to understand the operation of the whole. Of the three, we know the most about how sound propagates through the medium. Modeling of sound propagation is well understood, especially for frequencies below 1 kHz where the physical scales of our environmental data are within a few orders of magnitude of the sound's wavelength (Jensen et al. 2011). At higher frequencies the resolution of environmental data is no longer sufficient, and the medium's effect become more probabilistic. Most energy from vessels, seismic surveys and pile driving is also below 1 kHz, so the analysis of the properties of these sound sources has also been predominantly below 1 kHz. However, we know that many sound receivers in the ocean, especially pinnipeds and odontocetes, only start hearing at 1 kHz and above (Finneran 2015b). We know very little about the hearing sensitivity of most other marine life in terms of absolute thresholds as a function of frequency (to pressure or particle motion), ability to distinguish sounds that are close

in time or frequency, ability to localize sound sources, or their sensitivity to impulsive versus non-impulsive sounds (Popper et al. 2014b).

There is a mismatch between our knowledge of the sources, medium and receivers in the marine sound system. This thesis provides new information on the characteristics of human sound sources and proposes new analysis tools and standardized methods for describing the sounds received by marine life.

This thesis is organized as follows:

- The remainder of this Chapter introduces the effects of sound on marine life and how we currently quantify them.
- Chapter 2 introduces basic acoustic metrics, long range acoustic propagation effects and the fundamental data analysis tools employed throughout the thesis.
- Chapter 3 is a detailed analysis of a 2-month long seismic survey which investigates the frequency content of seismic sounds as a function of distance, the auditory frequency weighted SEL, and how the data integration duration affects results.
- Chapter 4 uses a linear mixed model to analyze over 27,000 impact pile driving strikes measured at ranges between 540 – 9100 m to determine how sound levels change with distance, pile inclination, strike energy and pile penetration into the sediment.
- Chapter 5 examines the SEL from 12 long-term data sets. The results are used to recommend a minimum protocol for measuring auditory frequency weighted SEL: a sampling rate of 64 kHz and recording for at least 1 minute every 30 minutes. The error in the daily SEL estimates are determined by the autocorrelation of the one-minute sound exposures. The autocorrelation is also shown to provide information on whether a soundscape is affected by human sounds.

- Chapter 6 examines the transition of sounds from impulsive to non-impulsive and whether that matters. Four impulsiveness metrics are compared by computing their values using short-term and long-term real-world data as well as numerous synthetic and random data. Kurtosis is recommended as the best metric. It is proposed that the threshold for no possible injury is the auditory frequency weighted sound pressure level given by the NMFS (2018) TTS threshold for non-impulsive sound minus 50 dB. The Chapter concludes with a new categorization of sounds as impulsive or non-impulsive based on animal's functional hearing groups.
- Chapter 7 summarizes the results from all of the Chapters as a consistent set of recommendations on how to record and analyze acoustic data for assessing the effects of sound on marine life.

1.1. Sound in the Ocean and the Responses of Marine Life.

There is a complex relationship between the oceans and human society. The oceans are critical to the health of our planet and humankind. Estimates of the oxygen production by marine phytoplankton range from 50-80% of the world's consumption. The productivity of the ocean relies on a healthy ecosystem, including the role of large predators (birds, whales) as nutrient recyclers (Roman et al. 2014, Doughty et al. 2016). Humans interact with the oceans in diverse ways. Seventeen percent of the world's human population obtain their protein from the ocean (https://bit.ly/2Gwxe84). Ninety percent of world trade is carried on the ocean (UN 2017), carried by an ever increasing fleet of merchant ships that rose from 38,000 vessels in 2010 to 55,000 in 2016. Control of shipping lanes has been a military priority since the days of the Roman Empire. Thirty percent of the world's oil and gas is obtained from offshore sources (https://bit.ly/2SM6aIx) and offshore renewable energy installations are increasing world

wide. Our activities in the ocean generate wastes of many types that may affect marine life, including sound (IMO 2014).

Sound is everywhere in the ocean and is the most important sensory modality for most marine animals. The acoustic landscape, or soundscape, is the sum of sounds from all sources that arrives at an animal or acoustic recorder. When we analyze recorded sound, we characterize it with typical engineering measurements – such as sound pressure levels, weighted sound exposure levels, and the type and number of detectable sources like ships, seismic airgun pulses and sounds from marine mammals or fish. The meaning of sounds to marine life depend upon their hearing capabilities, time and spatial evolution of the sounds, the relative contribution of each source, the direction to each source and how the sound has changed as it propagates through the environment (Figure 1-1; Jennings and Cain (2013), (NOAA 2016, Southall et al. 2019a)). A sound's meaning also depends on the history of the listener with similar sounds and what the animal is presently doing, which makes studies of the effects of sound challenging (Ellison et al. 2012, Hall et al. 2013).

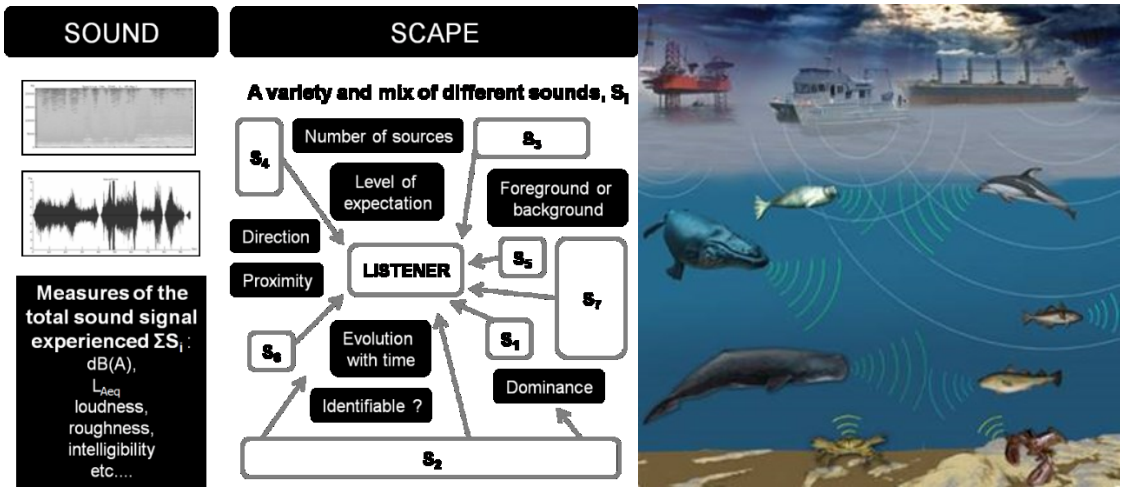

Figure 1-1. Conceptual views of a soundscape A soundscape is composed of 'sound' – the physical measurements of the sound field, and the 'scape' which conveys how all of the sound sources overlap and are perceived by the listener [Figure from (Jennings and Cain 2013)]. Right - Graphic representation of the multiple ocean sources contributing to an ocean soundscape [Figure from NOAA (2016); figure was contributed to Miksis et al. (2018)]

Underwater soundscapes are dynamic -- they vary in space and time. The contributors to the in-air soundscape that humans are accustomed to are generally within several hundred meters of the listener. Underwater soundscapes are influenced not only by local conditions (within 1 km) but also by distant sound sources (10's to 100's of km away) because sounds propagate long distances in water. The natural underwater soundscape is composed of contributions from natural abiotic or geophysical processes (e.g., wind, rain, ice), as well as contributions from biological sources (e.g., sound produced from animal movement and vocalizations from marine mammals, fishes, and invertebrates (Figure 1; Pijanowski et al. 2011). In the last 200 years humans have added new sounds into the ocean from machine driven shipping, seismic airgun surveys, pile driving, oil and gas extraction and sonars. From the 1950's-1990's ship sound increased by 3 dB / decade then became steady (Andrew et al. 2011). The development of seismic

airgun arrays to survey search for oil and gas below the seabed has created a new low frequency sound source throughout the world's oceans (Nieukirk et al. 2012, Nowacek et al. 2015).

Man-made sound sources in the soundscape can affect marine life that generates sounds or listens in the same frequency bands. Sounds that are ecologically relevant to marine animals include conspecific calls, predator and prey sounds, natural sounds like surf used for orientation, and echolocation calls from odontocetes (Clark et al. 2009). It is well known that marine mammals use sound for foraging and navigation (Payne and Webb 1971, Au et al. 1974, Madsen et al. 2004), social communications (e.g. Whitehead and Rendell 2014), mother-calf bonding (Dombroski et al. 2016), and mating displays (Payne and McVay 1971). All fish and sea turtles have hearing organs and all individuals measured to date respond to sound in some way (Popper et al. 2014b). There have been multiple evolutions of sound production for courtship and agonistic displays in fish (Parmentier et al. 2017) which implies a significant advantage is gained by being able to produce sound. Reef fish are know to select or avoid settlement areas based on sound (Parmentier et al. 2015), and it appears that both coral and fish larvae use the intensity and transient content of the soundscape to select settlement locations (Vermeij et al. 2010, Piercy et al. 2016). This shows that sound is important to these species at all life stages. Invertebrates also produce and perceive sound. Oysters have a valve closing response to sound (Charifi et al. 2017) as do scallops, which also make distinctive 'cough' sound associated with clearing sediment from their valves (Di Iorio et al. 2012). Snapping shrimp generate bubbles by rapid movement of their claws that are believed to be used for signalling and hunting. These sounds vary widely in space and time

(Lammers et al. 2006). Lobsters and many other crustaceans sense sound and generate sounds which are believed to be associated with mating (Pye and Watson 2004)

Short and long term studies of passive acoustic data in conjunction with observation of marine life behaviour have shown a wide range of impacts from human activities on marine life including: diversion of migrating of bowhead whales around seismic surveys (Richardson et al. 1999); a change in bowhead whale calling rates in response to seismic surveys (Blackwell et al. 2015); porpoise avoiding areas within 20 km of impact pile driving (Tougaard et al. 2009, Brandt et al. 2016); stress hormones dropping in right whales when shipping was reduced after 9/11 (Rolland et al. 2012); small boat sound affecting the settlement of larvae fish (Simpson et al. 2016), affecting fishes orientation responses (Holles et al. 2013) and increasing fish cortisol (stress) levels (Spiga et al. 2012); seismic survey sound affecting scallops and lobsters months after exposure (Day et al. 2016); alarm and startle reactions in fish and squid to seismic surveys (Fewtrell and McCauley 2012); possible mortality of zooplankton exposed to seismic surveys (McCauley et al. 2017); a wide variety of responses by benthic animals to substrate borne vibrations (Roberts and Elliott 2017); beaked whales responding and stranding to naval sonars (D'Amico et al. 2009, Tyack et al. 2011, Deruiter et al. 2013); blue whales changing behaviour and calling patterns when exposed to naval sonars (Melcon et al. 2012, Goldbogen et al. 2013) or seismic surveys (Di Iorio and Clark 2010); vessel sound restricting the communication space for baleen whales (Hatch et al. 2012); pile driving sounds injuring fish (Halvorsen et al. 2012a, Casper et al. 2013); blue mussels changing their metabolic state when exposed to pile driving (Spiga et al. 2016);

and a marked difference in beaked whale echolocation clicks in the presence of vessels with echosounders running (Cholewiak et al. 2017).

The Population Consequences of Acoustic Disturbance (PCAD) model was developed to provide a framework for understanding what happens when human sounds interfere with animals' lifecycle functions (NRC 2005). To complete PCAD models we require information on existing population sizes, fecundity, mortality and feeding rates, the sound sources, the behavioural effects that result from exposure, and the consequences of changes to these factors. Obtaining this breadth of information is a challenge, even for better understood mammal populations such as the North Atlantic right whales and Southern resident killer whales (https://bit.ly/2T0AdLJ). Adding to the complexity of modeling population consequences of acoustic effects are other stressors to mammal populations, which led to the more general Populations Consequences of Disturbance model (PCoD, Harwood et al. 2014, King et al. 2015). Extensive research is still required on the effects of disturbing migrations, foraging, mating, and predator-prey detection to serve as inputs to the models. There is sufficient evidence in place now to recommend measures to mitigate auditory injury to marine mammals but not most other marine life.

1.2. Quantifying the Effects of Sound

The effects of sound on humans and animals has traditionally been visualized as a series of four zones or concentric rings around the sound source (Figure 1-2). In Zone 1 the sound exposure leads to barotrauma injury (for examples see Halvorsen et al. 2012b) or permanent threshold shift (PTS) meaning that hearing is damaged and does not

recover. In Zone 2 the sound exposure causes a temporary threshold shift (TTS) where hearing recovers from after some period of time (e.g. the morning after a rock concert). In Zone 3 the sound source masks the ability of an animal to hear other sounds of importance which may also impact their fitness, such as sounds of predators or prey, environmental cues for navigation or homing, and conspecifics for mating, socializing or schooling. In Zone 4 the sound is still audible and may evoke a behavioural response (e.g. orientation, movement) or physiological response (e.g. stress hormones). The areas of Zones 1 and 2 are generally small (radii on the order of 50 – 5000 m for Zone 2), and thus only affect individuals of a population for short periods of time. The masking area (Zone 3) is much larger, with radii up to 100's of km for seismic surveys and exposures that may last for months. Thus Zone 3 is likely where the greatest effects on marine life occur. The significance of masking is difficult to quantify since the importance of communications for critical life functions are unknown in most cases, and we have limited ecological understanding of animals' ability to compensate for masking through adaptive strategies (Branstetter et al. 2016, Erbe et al. 2016).

The zone-view of the effects of noise does not accurately reflect the complexity of auditory injury or impairment and the choices animals make to accept sound exposure for other advantages such as feeding or mating (Ellison et al. 2012). When animals make the choice not to respond to noise, they can stay in an area where very long sound exposures result in auditory injury and impairment, and thus Zone 2 may be larger than Zone 4 (Hawkins and Popper 2017). Similarly, a rapid behavioral responses to sound can cause animals to rapidly leave an area, which could result in dangerously rapid depth changes

(Jepson et al. 2003, Blix et al. 2013) or entering an area that results in stranding (Cox et al. 2006); in this manner Zone 4 can become Zone 1.

Regulations that specify a maximum value for biologically relevant indicator are often imposed on human activities to minimize injury to marine mammals and other endangered marine life (Erbe 2013). Early marine sound mitigation regulations were based upon keeping the sound pressure level below the level associated with measured injuries to the hearing of marine life (NMFS 1995, NOAA 1998, FHWG 2008). Evidence has since demonstrated that the total sound exposure level and the peak sound pressure levels are better indicators of injury than the sound pressure level (Southall et al. 2007, Popper et al. 2014b). Peak sound pressure level is associated with immediate physiological or auditory injury from extremely high amplitude sounds that typically occur within very close proximity to a sound source. Injuries and impairment associated sound exposure level are due to long-term exposure to high intensity sounds. These injuries and impairments are far more likely to impact a greater number of individuals over a larger spatial area than might be expected from injury associated with peak sound pressure level. As noted above the area over which injury occurs are much smaller than the area over which effects from masking could occur.

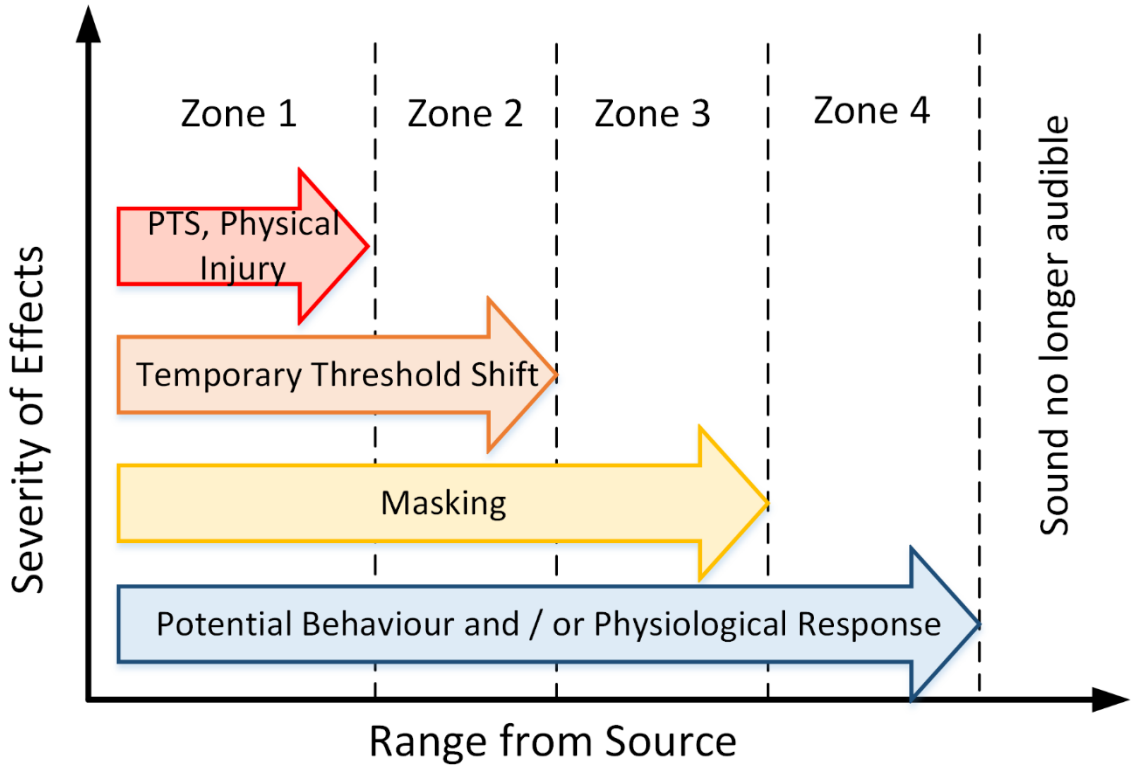

Figure 1-2. General principles of sound exposure. (after Dooling et al. (2015))

The sound exposure level (SEL) is a key acoustic metric considered in this thesis because it is the predictor of auditory injury and impairment. SEL is defined as 10 times the logarithm (base 10) of the integral of the squared sound pressure over some period of time, T, normalized by a reference squared pressure p_o^2 and reference time T_o:

$$L_{E,T} = 10 \log_{10} \left(\frac{1}{T_o p_o^2} \int_0^T p^2(t)\, dt \right). \qquad 1\text{-}1$$

where T_o is normally 1 second and p_o is 1 µPa, so that the units of $L_{E,T}$ are dB re 1 µPa²·s. In the far field of an acoustic source, pressure is equal to the particle motion (U), divided by the characteristic impedance of the fluid (ρc), and therefore the integral of $p^2(t)$ is proportional to the sound intensity (pU), which has units of W/m^2. If we integrate the sound intensity over time, we obtain energy, and therefore $L_{E,T}$ is used as a representation

of the sound energy in an acoustic event. By integrating over multiple events we can obtain the total energy of those events.

The equal energy hypothesis (Eldred et al. 1955) states that an equal amount of energy (i.e. the same SEL) will have the same impact on hearing regardless of how long it takes to accumulate; i.e. a 190 dB re 1 $\mu Pa^2 \cdot s$ SEL sound exposure will have the same effect whether the sound pressure level is 190 dB re 1 µPa for 1 s or 160 dB re 1 µPa for 1000 s. The equal energy hypothesis has proven to be a powerful approach for quantifying sound exposure, however, there are also well known limits to it's validity (Finneran 2015a). For instance, long periods between impulsive sounds allow some animals to partially recover hearing (Ward 1997), sounds below a certain threshold are often treated as 'effective quiet' and should not be accumulated (Stadler and Woodbury 2009), and for some animals sounds that are too short do not cause the same effects as longer but quieter sounds (Smith and R. Gilley 2008).

The fundamentals of hearing are the same for marine and terrestrial mammals in that sounds entering the inner ear are transformed into neuronal signals by hair cells on the basilar membrane. The stiffness and thickness of the membrane changes along its length which changes the frequency response of the hair cells from the membrane's base to its apex. Mammals hear sounds at different frequencies when the nerves associated with the hair cells that respond at those frequencies are stimulated. Noise induced hearing loss occurs when the hair cells or their connecting nerves are physiologically or physically impacted by loud sounds which leads to a shift in hearing thresholds. This can occur across a wide frequency range when exposed to a broadband impulse or only over a

narrower frequency range when exposed to an intense tonal signal. In cases of TTS the damage is recoverable, but more severe damage may lead to hair or nerve cell death and PTS (Le et al. 2017). Sounds below the threshold of effective quiet do not induce any physiological or neurological effects.

The fundamentals of hearing in fish and sea turtles are different than in mammals. The inner ears of all vertebrates contain otolith organs where bony respond with a lower amplitude and different phase to accelerations which allow the animals (including humans) to sense physical accelerations and gravity. In the case of fish, the otoliths are also sensitive to the acceleration from passing sound waves (Popper et al. 2014b). Fish hearing sensitivity is affected by the relationship between a fishes swimbladder and the inner ear. If the swimbladder is involved in hearing it acts as a transformer that converts the pressure fluctuations from sound waves into larger amplitude particle motions sensed by the otoliths which provides a higher sensitivity to sound (Sand and Hawkins 1973). Since there are many morphologies of swimbladders in different groups of fish, there is also a wide spectrum of hearing capabilities from groups that are only being sensitive to particle accelerations to groups that have low frequency hearing that is more sensitive than many marine mammals (as discussed below).

Hearing mechanisms in invertebrate marine life are more poorly understood. Decapod crustaceans have statocyst organs that allow the animals to sense acceleration and gravity in a manner similar to the otoliths in vertebrates. The statocysts are likely also sensitive to accelerations from sound waves, however, only at very high intensities (Popper et al. 2001). Some crustacean species also have chordontal organs that can

respond to movement of the appendages or exoskeleton which in turn may allow them to sense the substrate vibrations or particle accelerations associated with sound waves close to the source (Edmonds et al. 2016). Cephalods also have statocysts and sensory cells on their skins that are sensitive to particle acceleration (André et al. 2016, Samson et al. 2016).

Mammals, including marine mammals, respond differently to non-impulsive sources of human sound, such as ships, compared to impulsive sound sources such as pile driving and seismic airgun surveys (Southall et al. 2019b). For the purposes of noise-induced hearing loss, impulsive sources are characterized by being broadband, short (< 1 second) and having a high peak pressures and short rise times ([NIOSH] National Institute for Occupational Safety and Health 1998, Southall et al. 2019b). The hearing of mammals is more sensitive to the rapid variations of impulsive sound than non-impulsive sounds. The rate of impulses is also critical to their impacts – impulses that are 100 ms – 10 s apart cause more damage than those closer together than 100 ms, or farther apart than 30 s (Erdreich 1986, Henderson and Hamernik 1986). Impulses presented during high levels of non-impulsive sound tend to cause higher levels of injury than either the impulses or non-impulsive sound on their own (Hamernik et al. 1974, Henderson and Hamernik 1986). In the marine environment impulsive sounds include impact pile driving and seismic airgun arrays. Sonar pulses from Naval vessels, which stimulated extensive research into the effects of sound on marine life, are typically grouped with the non-impulsive sources due to their narrowband nature (NOAA 2001, NMFS 2018, Southall et al. 2019b), but were considered impulsive when reviewed by the European Union Task Group on Noise (Van der Graaf et al. 2012).

One of the differences in the effects of impulsive and non-impulsive sounds on hearing relates to how humans and other animals protect themselves from loud sounds. Terrestrial mammals have evolved mechanisms to protect their hearing from loud sound exposures, including tightening of the middle ear (Hung and Dallos 1972) and neural attenuation (Suga and Shimozawa 1974). Within the marine mammals we have some understanding of the hearing mechanisms of toothed whales (odontocetes), but virtually none about the large whales (mysticetes). Many odontocete species have a sophisticated 'automatic gain control' for detecting echoes in the presence of their outgoing echolocation pulses and those of other members of their group (Nachtigall and Supin 2008). They are able to learn to attenuate their hearing if a warning sound is received up to 30 seconds prior to a loud sound (Nachtigall et al. 2018). For all mammals if there is no warning of loud sounds the inner ear receives the full energy of impulsive sounds which leads to increased damage compared to non-impulsive sounds at the same energy (Akay 1978, Finneran 2015b). For terrestrial mammals impulses at a rate of 1 per second are particularly damaging since the acoustic reflex generally relaxes after 1 second, and all impulses arriving at the inner ear have maximum effect (Ward 1962, Buck et al. 1984, Danielson et al. 1991a).

The ability of an animal to hear a sound is an important component of understanding its possible effects. The frequencies that mammals are able to hear is related to the dimensions of the basilar membrane. Hearing sensitivity is measured using an audiogram that depicts the relationship of the lowest amplitude sound an animal can hear as a function of frequency. Figure 1-3 shows a number of fish and marine mammal audiograms. Gadiforms (e.g. cod) are examples of fish whose swim bladders involved in

their hearing which allows them to sense acoustic pressure at relatively low levels. Salmonids (salmon, trout) are examples of fish with less developed pressure sensitive hearing structures. Many other types of marine taxa (e.g. the squid and mud crab in Figure 1-3) have limited sensitivity to acoustic pressure and only sense sound very close to the source where the sound field also has a substantial particle motion component (Popper et al. 2018). The marine mammals have much more sensitive hearing than most other marine life (lower minimum values in Figure 1-3), and significant differences between the species groups. Many of the groups are less sensitive to frequencies below 200 Hz than the gadiforms and salmonids

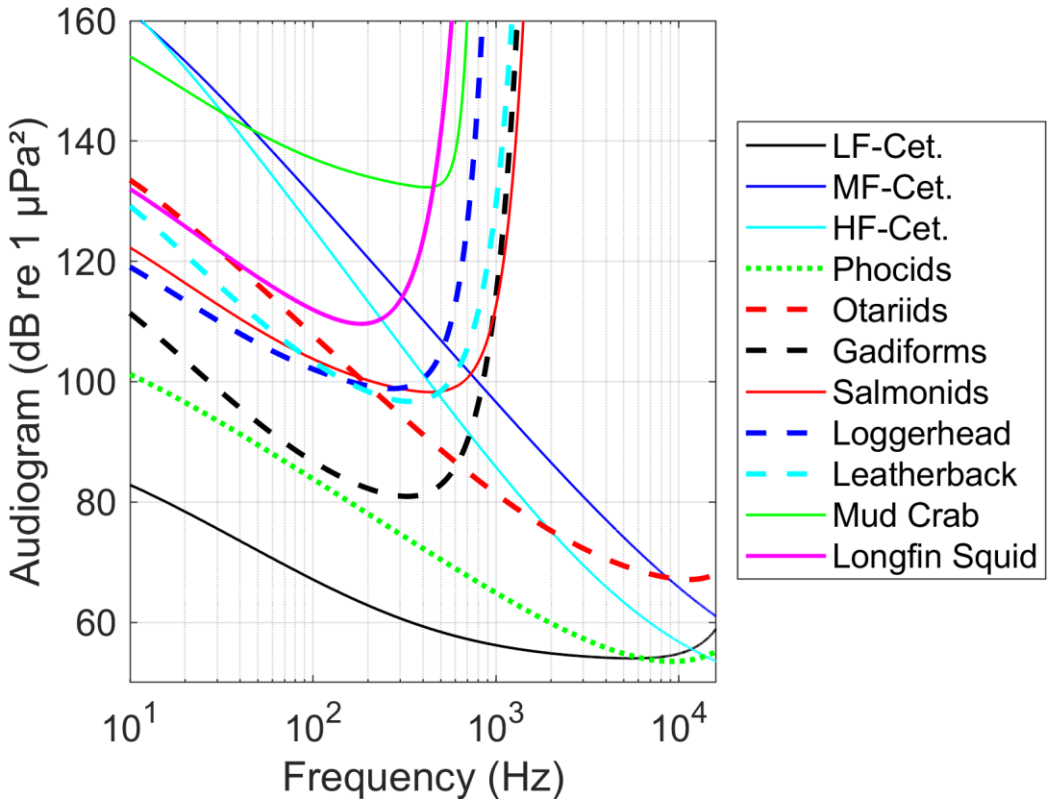

Figure 1-3. Examples of audiograms. References: Marine Mammals (LF-Cetaceans, MF-Cetaceans, HF-Cetaceans, Phocid and Otariid Seals): Southall et al. (2019b); Gadiforms and Salmonids - Ladich and Fay (2013); Loggerhead sea turtle - Martin et al. (2012b); Leatherback sea turtle – Eckert (2012); Mud crab - Hughes et al. (2014); Longfin Squid - Mooney et al. (2010).

The hearing sensitivity of an animal group is accounted for when computing the SEL by first applying an auditory frequency weighting function - for human hearing we use the 'A-weighting' (NIOSH 1998). The function is an inversion of the audiogram, normalized so that it has a gain of zero at the frequencies of peak sensitivity. Finneran (2016), analyzed existing audiogram data and other inputs to develop auditory weighting functions that represent our understanding of the hearing capabilities of marine mammals (Figure 1-4, the sixth group, sirenians, are not shown nor are the sensitivities of seals in-

air). In order to assess the significance of the auditory frequency weighted SEL, they must be compared to the appropriate thresholds (Tougaard et al. 2015). The auditory frequency weighting functions and numeric thresholds from Finneran (2016) that were incorporated into NMFS (2018) are contained in Table 1-1. The PTS thresholds non-impulsive and impulsive sounds are different, with the impulsive thresholds 13 – 18 dB below those for non-impulsive sounds. The audiograms and thresholds were subsequently published in Southall et al. (2019b), with additional updates to the names of the marine mammal hearing groups. The Southall et al. (2019b) group names are generally used throughout this thesis.

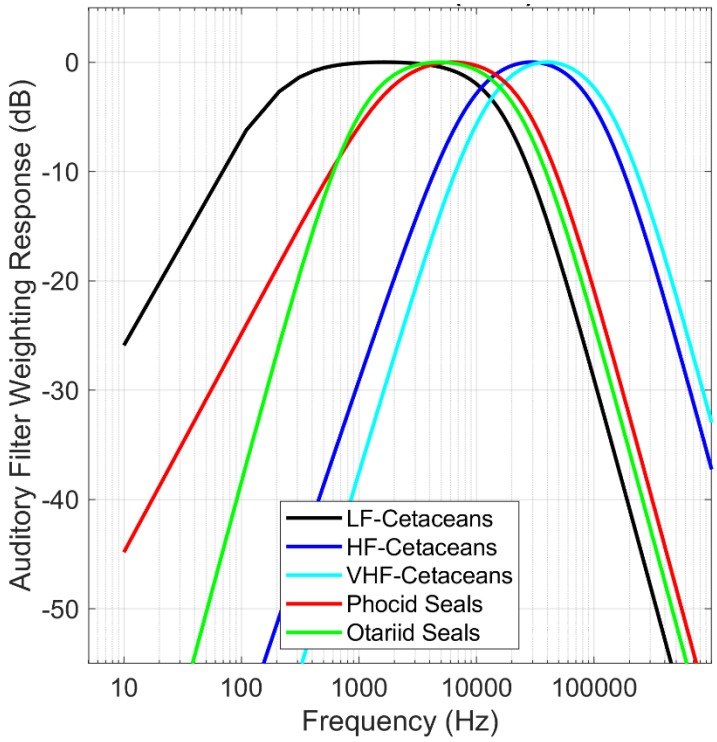

Figure 1-4. The Finneran (2016) marine mammal hearing group auditory weighting functions. Low frequency cetaceans include the large baleen whales (e.g. blue, fin and humpback whales). Mid-frequency cetaceans are the dolphins as well as sperm and beaked whales that whistle and echolocate in the band of ~1000 – 80000 Hz. High-frequency cetaceans are the dolphins, sperm whales (*kogia* spp) and porpoises that echolocate in the range of 120 kHz. Otariid seals are sea lions and fur seals, while phocid seals are considered 'true' seals. Equations for the curves are provided in Table 1-1.

Table 1-1. Summary of weighting function parameters and TTS/PTS thresholds. SEL thresholds are in dB re 1 µPa^2·s and peak sound pressure level thresholds are in dB re 1 µPa (Table AE-1 from NMFS (2018)). The SEL is accumulated over 24 hours. See Tougaard and Beedholm (2019) for an example of how to compute and apply the weighting functions. The MF group was renamed HF, and the HF group named VHF in Southall et al. (2019b).

$W(f) = C + 10\log_{10}\left\{\frac{(f/f_1)^{2a}}{\left[1+(f/f_1)^2\right]^a\left[1+(f/f_2)^2\right]^b}\right\}$						Non-impulsive		Impulse			
						TTS threshold	PTS threshold	TTS threshold		PTS threshold	
Group	*a*	*b*	f_1 (kHz)	f_2 (kHz)	*C* (dB)	SEL (weighted)	SEL (weighted)	SEL (weighted)	peak SPL (unweighted)	SEL (weighted)	peak SPL (unweighted)
LF	1	2	0.20	19	0.13	179	199	168	213	183	219
MF	1.6	2	8.8	110	1.20	178	198	170	224	185	230
HF	1.8	2	12	140	1.36	153	173	140	196	155	202
SI	1.8	2	4.3	25	2.62	186	206	175	220	190	226
OW	2	2	0.94	25	0.64	199	219	188	226	203	232
PW	1	2	1.9	30	0.75	181	201	170	212	185	218

Projects that are expected to generate sounds exceeding the PTS thresholds at required to mitigate possible effects on marine life. Project proponents use acoustic propagation modeling to estimate the isopleth distance where the 24-hour SEL exceeds the PTS threshold. They must visually and/or acoustically monitor the area around the activity and shut down the operation if a protected animal enters that area (Zone 1 in Figure 1-2). Since the impulsive thresholds are 13-18 dB lower than the thresholds for non-impulsive sounds, an accurate understanding of the nature of impulsive sounds, their attenuation with range from the source and their effects on hearing are important to properly mitigate the effects of offshore activities.

The thresholds shown in Table 1-1 are based on many extrapolations and expert opinions. Two important issues identified for research on marine mammals are 1) measuring the hearing of low frequency cetaceans and 2) determining the range from an

impulsive source at which the waveforms no longer have the characteristics that make them more damaging than a non-impulsive sound. More work is needed to improve our understanding of the effects of sound on fish and invertebrates. For these groups we need to develop auditory frequency weighting functions, determine the responses of different groups to human sounds, and understand the differences in response between impulsive and non-impulsive sounds. Thus, the study of human impulsive sources in real-world conditions is important for improving our ability to predict and mitigate injury to marine life from four human activities that occur worldwide – shipping, sonars and echosounders, seismic airgun surveys and impact pile driving for marine construction.

1.3. Questions Addressed by this Thesis.

This thesis analyzes data from impulsive and non-impulsive sound sources recorded in the open ocean in order to provide practical guidance on how to measure and quantify the SEL and assess the possible effects on marine life. The specific questions addressed are:

1. How do the unweighted and auditory frequency weighted SEL from seismic airgun surveys and impact pile driving change with distance from the source?
2. What are the recommended recording protocols for measuring the weighted SEL in terms of the hydrophone sensitivities, sampling rate and duty cycle. How does duty cycling affect the uncertainty in daily SEL estimates?
3. How do impulsive sounds transition to being non-impulsive for the purposes of accumulating SEL? Is there an objective measure that may be used to distinguish impulsive from non-impulsive sounds? Is there a practical threshold, similar to effective quiet, below which auditory injury or impairment does not need to be considered?

CHAPTER 2 BACKGROUND CONCEPTS

This Chapter introduces key terms, metrics, concepts and algorithms that are employed throughout the remainder of the thesis. For most applications noise is defined as any signal that interferes with a signal of interest, which implies noise is undesirable. From the point of view of a right whale, snapping shrimp, vessel and humpback whale sounds are noise, while other right whales and killer whale sounds are signal. To seismic exploration companies, airguns generate sounds of interest, while rain, wind and mammals are noise. To deal with this perception bias, the convention used throughout this thesis is the use of the 'sound' to describe acoustic perturbations generated by geologic, biologic or anthropogenic sources. 'Noise' is reserved for acoustic perturbations that interfere with detection of all sounds. Thus, noise includes acoustic perturbations generated by flow around a hydrophone, movement of a hydrophone, contact of a hydrophone by sediment or animals as well as self-noise of a hydrophone-recorder system.

2.1. ACOUSTIC METRICS

2.1.1. Basic Metrics

This thesis uses the symbols and definitions for acoustic metrics from ISO standard 18405 (ISO 2017a). An important element of the standard is the distinction between field quantities, such as sound pressure, and *level* quantities that are 10 times the logarithm of the field quantity, i.e. sound pressure *level*.

Definitions of the metrics employed in this thesis are provided in Table 2-1. The most important metrics employed in this analysis are:

- peak sound pressure level ($L_{p,pk}$) (note that the term peak SPL is deprecated).
- sound pressure level over an averaging duration T ($L_{p,T}$), which may be referred to as the SPL;
- sound exposure level over some period T ($L_{E,T}$), which may be referred to as the SEL; and
- weighted sound exposure levels ($L_{E,W,T}$) where 'W' is a frequency band or frequency weighting function. The frequency bands employed are the decidecade bands (see Section 2.1.2) and the marine mammal functional hearing group auditory frequency filters.
- Kurtosis which is a measure of the impulsiveness of a time series.

Table 2-1. Definition of acoustic metrics used in this thesis.

Metric	Definition	Units
Peak Sound Pressure Level ($L_{p,pk}$)	Ten times the logarithm of the ratio of the maximum instantaneous sound pressure level in a stated frequency band attained by an acoustic pressure signal, $p(t)$ to the reference value, p_0^2 (normally 1 µPa^2) $10\log_{10}\left(\frac{1}{p_o^2}\max(p^2(t))\right)$ Note that $L_{p,pk}$ is a poor indicator of a sound's loudness because the peak signal duration is often very short. The sound exposure level is a better indicator of loudness.	dB re 1 µPa²
Peak-to-peak sound pressure level ($L_{p,pk\text{-}pk}$)	Ten times the logarithm of the ratio of the difference between the maximum and minimum instantaneous sound pressure values in a stated frequency band over the duration of a signal of interest $p(t)$ to the reference value, p_0^2, (normally 1 µPa^2): $10\log_{10}\left\{\frac{\left[\max\left(p(t)\right)-\min\left(p(t)\right)\right]^2}{p_0^2}\right\}$	dB re 1 µPa²
Sound pressure level (SPL or L_p, $L_{p,T}$)	Ten times the logarithm of the ratio of the mean-square pressure level in a stated frequency band over a time window (T) containing the acoustic event to a reference value, p_0^2: (normally 1 µPa^2) $10\log_{10}\left(\frac{1}{p_o^2}\int_0^T\frac{(p^2(t))}{T}dt\right)$	dB re 1 µPa²

Metric	Definition	Units
Sound exposure level (SEL, $L_{E,T}$)	The sound exposure level is ten times the logarithm of the ratio of the time-integral of the squared pressure over the analysis duration (T), to the reference time T_0 (normally 1 s) and reference square pressure value p_0^2 (normally 1 µPa^2) $L_{E,T} = 10\log_{10}\left(\frac{1}{T_0 p_o^2}\int_0^T p^2(t)\,dt\right)$ where T_0 is a reference time interval of 1 s. The SEL represents the total acoustic energy received at some location during an acoustic event.	dB re 1 µPa^2·s
Weighted sound exposure level ($L_{E,W,T}$)	The sound exposure level computed over a time window T using a frequency weighted spectrum: $L_{E,W,T} = 10\log_{10}\left(\frac{1}{T_0 p_o^2}\sum_{t_{FFT}=0}^{T}\int_0^{f_s/2} W(f)S_t(f)df\right)$ where $W(f)$ is the frequency dependent auditory filter function and $S_t(f)$ is the power spectral density of $p(t)$ over a period of 't_{FFT}' seconds. The total period 'T' is normally divided into equal sized blocks of duration 't_{FFT}'.	dB re 1 µPa^2·s
Mean-square sound pressure spectral density level, $L_{p,f,t}$	Ten times the logarithm of the ratio of the distribution as a function of non-negative frequency of the mean-square sound pressure per unit bandwidth of a sound having a continuous spectrum, to the reference square pressure value p_0^2 (normally 1 µPa^2) : $10\log_{10}\left(S(f)^2 \Big/ p_0^2\right)$	dB re 1 µPa^2/Hz
Kurtosis, β	The fourth moment of a time series divided by the square of the second moment: $\beta = \frac{\mu_4}{\mu_2^2}$.; $\mu_2 = \frac{1}{t_2 - t_1}\sum_{t_1}^{t_2}[p(t) - \bar{p}]^2$; $\mu_4 = \frac{1}{t_2 - t_1}\sum_{t_1}^{t_2}[p(t) - \bar{p}]^4$,	Dimensionless
Skewness, γ	The third moment of a time series divided by the second moment to the power of 3/2. $\gamma = \frac{1}{t_2 - t_1}\sum_{t_1}^{t_2}[p(t) - \bar{p}]^3 \Big/ \left(\frac{1}{t_2 - t_1}\sum_{t_1}^{t_2}[p(t) - \bar{p}]^2\right)^{3/2}$	Dimensionless
Crest Factor	Difference, in dB, between the peak sound pressure level and the sound pressure level averaged over some specified period of time.	dB

Metric	Definition	Units
Harris Impulse Factor	Difference between the Impulse-time weighted SPL and slow-time weighted SPL (see Harris (1998), (IEC 2004))	dB

2.1.2. Metrics Related to Frequency

The distribution of a sound's power with frequency is described by its spectrum which is the absolute value of the Fourier transform of the sound's time series. The sound spectrum is split into of adjacent frequency bands whose width depends on the duration of the time series input to the Fourier transform (there are many excellent texts on Fourier Analysis; here I suggest Au and Hastings 2008 Principles of Marine Bioacoustics, Chapter 6, since this text also has chapters on hearing, use and production of sound by marine life and other background information relevant to the thesis subject matter.). When using 1-second of input data, the spectrum has 1 Hz wide bands, which yields an estimate of the power spectral density level of the sound (Welch 1967). It is common to overlap the data input to successive Fourier transforms by 50%, then average 120 of the resulting spectra to obtain the per-minute average power spectral density. These values directly compare to the Wenz curves, which represent typical deep ocean sound levels (Figure 2-1, (Wenz 1962)). Wenz averaged spectra over 200 seconds, and to be strictly comparable current projects should use the same duration, however, it has become common practice to use 1-minute durations since the results are very similar and many long-term autonomous recording programs have continuous data blocks shorter than 200 seconds.

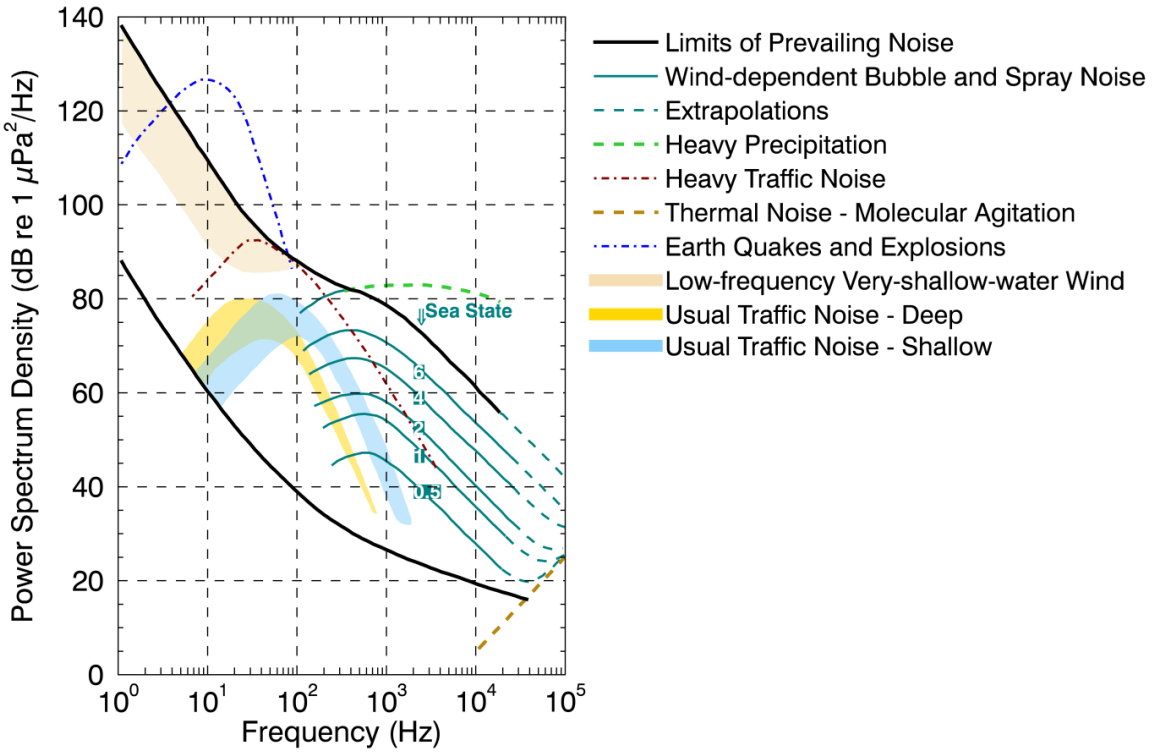

Figure 2-1. Wenz curves (NRC 2003), adapted from Wenz (1962), describing power spectral density levels of marine ambient sound from weather, wind, geologic activity, and commercial shipping.

In general mammals perceive exponential increases in frequency rather than linear increases (Scharf 1970, Saunders et al. 1979). Therefore, splitting the spectrum into 1 Hz bands is not representative of how mammals perceive sound; rather analyzing a sound spectrum with bands that increase exponentially in size gives data that are more meaningful. In underwater acoustics, a spectrum is commonly split into bands that are $1/10^{\text{th}}$ of a decade where each decade represents a 10-fold increase in frequency. The centre frequency of the ith decidecade band, $f_c(i)$, is defined as

$$f_c(i) = 10^{i/10}, \tag{2-1}$$

and the low (f_{lo}) and high (f_{hi}) frequency limits of the ith decidecade-band are defined as:

$$f_{lo} = f_c(i) \cdot 10^{-1/20} \text{ and } f_{hi} = f_c(i) \cdot 10^{1/20} . \quad (2\text{-}2)$$

This definition is the same as the ANSI definition for 1/3-octave-bands (base 10) (ISO 2017a, ANSI S1.1-1994 R2004). The decidecade bands become wider with increasing frequency, and on a logarithmic scale the bands appear equally spaced (Figure 2-2). The decidecade band limits and centre frequencies from 10 to 250000 Hz are contained in Table 2-2.

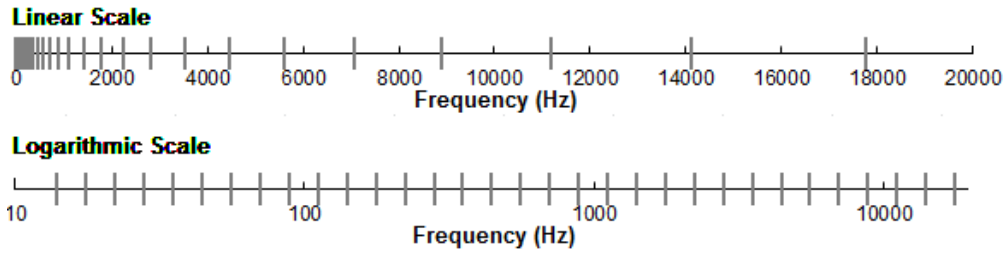

Figure 2-2. Decidecade bands shown on a linear frequency scale (top) and on a logarithmic scale (bottom).

Table 2-2. Decidecade low, centre, high and nominal centre frequencies from 10 to 250000 Hz.

Lower bound (Hz)	Centre frequency (Hz)	Upper bound (Hz)	Nominal centre frequency
8.91	10	11.22	10 Hz
11.22	12.59	14.13	12.5 Hz
14.13	15.85	17.78	16 Hz
17.78	19.95	22.39	20 Hz
22.39	25.12	28.18	25 Hz
28.18	31.62	35.48	32 Hz
35.48	39.81	44.67	40 Hz
44.67	50.12	56.23	50 Hz
56.23	63.10	70.79	63 Hz

Lower bound (Hz)	Centre frequency (Hz)	Upper bound (Hz)	Nominal centre frequency
70.79	79.43	89.13	80 Hz
89.13	100	112.2	100 Hz
112.2	125.9	141.3	125 Hz
141.3	158.5	177.8	160 Hz
177.8	199.5	223.9	200 Hz
223.9	251.2	281.8	250 Hz
281.8	316.2	354.8	315 Hz
354.8	398.1	446.7	400 Hz
446.7	501.2	562.3	500 Hz
562.3	631.0	707.9	630 Hz
707.9	794.3	891.3	800 Hz
891.3	1000	1122	1 kHz
1122	1259	1413	1.25 kHz
1413	1585	1778	1.6 kHz
1778	1995	2239	2 kHz
2239	2512	2818	2.5 kHz
2818	3162	3548	3.15 kHz
3548	3981	4467	4 kHz
4467	5012	5623	5 kHz
5623	6310	7079	6.3 kHz
7079	7943	8913	8 kHz
8913	10000	11220	10 kHz
11220	12589	14125	12.5 kHz
14125	15844	17783	16 kHz
17783	19953	22387	20 kHz
22387	25119	28184	25 kHz
28184	31623	35481	31.5 kHz
35481	39811	44668	40 kHz
44668	50119	56234	50 kHz
56234	63096	70795	63 kHz
70795	79433	89125	80 kHz
89125	100000	112202	100 kHz
112202	125893	141254	125 kHz

Lower bound (Hz)	Centre frequency (Hz)	Upper bound (Hz)	Nominal centre frequency
141254	158489	177828	160 kHz
177828	199526	223872	200 kHz
223872	251189	281838	250 kHz

The sound pressure level in the ith decidecade-band $L_{p,ddec\ i,T}$ is computed from the power spectrum $S(f)$ between f_{lo} and f_{hi}:

$$L_{p,ddec\ i,T} = 10\log_{10}\left(\frac{1}{T}\int_{f_{lo}}^{f_{hi}} S(f)df/p_o^2\right) \qquad 2\text{-}3$$

where T is the duration of time used to compute the power spectrum $S(f)$. Summing the decidecade band sound pressure level of all the decidecade bands yields the broadband sound pressure level:

$$Broadband\ SPL = 10\log_{10}\sum_i 10^{L_{p,ddec\ i,T}/10}. \qquad 2\text{-}4$$

The SPL in a band is equal to the average power spectral density level plus $10\cdot\log_{10}$(bandwidth):

$$L_{P,f2-f1,T} = \bar{L}_{p,f2-f1,T} + 10\log_{10}(f2 - f1). \qquad 2\text{-}5$$

For example, the SPL from a 10000 Hz bandwidth is 40 dB higher than the average spectral density in that band. We observe this effect often when comparing decidecade band levels that increase or remain flat as frequency increases while the power spectral density in the same frequency range decreases rapidly (e.g. Figure 2-3).

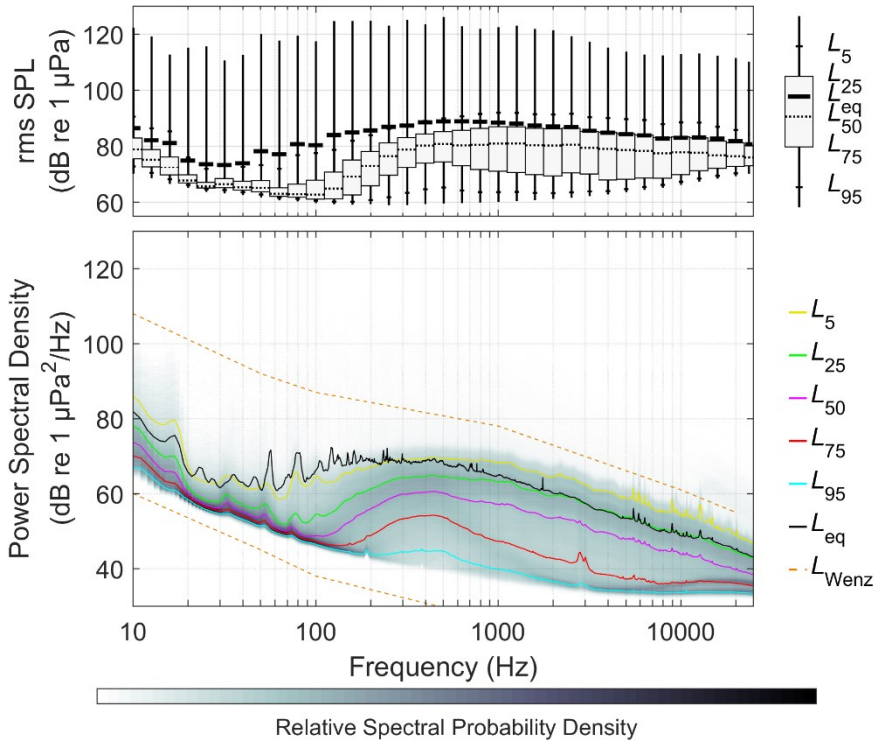

Figure 2-3. Comparison of decidecade band levels (top) to the power spectral density levels (bottom) from a one week recording in a sheltered bay off Nova Scotia in February 2013. The figures include representations of the exceedance percentiles, i.e., L_5 is the sound level exceeded by 5% of the data. L_{Wenz} are the limits of prevailing noise from (Wenz 1962).

2.2. Acoustic Propagation Effects

A key question in the study of underwater sound is the nature of the sound that is received some distance from its source. Understanding and modeling sound propagation in the ocean is a complex topic that is the subject of numerous textbooks (e.g. Kinsler et al. 2000, Jensen et al. 2011) and the subject of active research at centers around the globe, including Dalhousie. This section provides a descriptive overview of key sound propagation concepts for readers unfamiliar with the subject. These concepts are integral to interpreting the transformation of the sounds emitted by a source to those received some distance away. The sounds are transformed by 1) geometric spreading and

dispersion, 2) reflection, scattering and absorption at the seabed and surface, 3) refraction due to changes in sound speed and 4) absorption in sea water. These concepts are introduced in this section.

As a general rule, higher frequencies are more affected by propagation effects and travel shorter distances than low frequencies. At one extreme, the echolocation clicks of porpoise at 130 kHz only travel 500 m before becoming inaudible (Au et al. 1999). At the other extreme, sounds from fin whales (20 Hz) and low frequency energy from seismic airguns (5-100 Hz) can be detected thousands of kilometers away under the right conditions (Nieukirk et al. 2012)

Geometric Spreading Losses: Sound levels from an omnidirectional point source in the water column are reduced with range, a process known as *geometric spreading*. Before the sound emanating from the point source reaches the seabed or sea surface boundaries, the waves propagate spherically. In this case, the received levels at a recorder located a distance R from the source are $20\log_{10}R$ dB lower than the levels measured at 1 m from the source. Once the waves interact with the sea surface and seabed, spreading is limited to the cylinder formed by the surface and seabed with a lower range-dependent decay of $10\log_{10}R$ dB. Water depth is a key factor in predicting sound levels. Spherical and cylindrical spreading factors provide limits for quick assessment of the expected levels from a given source (Jensen et al. 2011). In shallow waters (<200 m) after the sound has travelled several water depths by cylindrical spreading, the sound enters the 'mode-stripping' region where higher order modes of the propagating sound no longer travel efficiently and the change in sound levels with range is approximately $15\log_{10}R$

(Ainslie et al. 2014a). Over longer ranges in shallow water, dispersion causes the time of arrival of sounds to spread as different frequencies and modes arrive at different times. For very shallow waters sound can not propagate at all if the water depth is less than a quarter of a wavelength (Urick 1983).

Absorption, Reflection and Scattering at the sea surface and seabed: If geometric spreading were the only factor governing sound attenuation in water, sound levels in shallow waters would almost always be higher than those in deep waters at the same range from the source. However, in shallow water the sound interacts more often with the seabed and sea surface than sound travelling in deep waters and these interactions reflect, absorb and scatter the sounds. The sea surface is a pressure release boundary, which means that pressure at the surface must be zero. As a result, the sound must be completely reflected at the surface and have the opposite phase as the incident sound so that the sum of the two sounds at the surface is zero. At the seabed there are many possible types of interactions depending on the composition of the bottom. Soft silt and clay bottoms absorb sound, sand and gravel bottoms tend to reflect sound like a partially reflective mirror, and some hard yet elastic bottoms such as limestone reflect the sound but also absorb some of the energy by converting the pressure waves to shear waves that propagate perpendicular to the original sound wave. In the Arctic the ice cover is also an elastic boundary layer that reflects and absorbs sound through shear conversion.

The angle of reflection equals the angle of incidence which is measured from the perpendicular to the surface. The effective perpendicular to the surface depends on the similarity of the sound's wavelength to the roughness of the surface. As the frequency

goes up the wavelength decreases and smaller changes in the surface shape become important. When the wavelength is equal to or smaller than the undulations in the seabed and sea surface the sound to reflects in random directions, which is also referred to as scattering. This effect reduces the sound that arrives at a receiver at longer ranges in shallow water. Thus, predicting the sound levels that propagate over several water depths requires a knowledge of the bottom shape and composition, the surface roughness and the sound's wavelength.

Refraction due to sound speed changes: As a rule of thumb, sound is 'lazy': It wants to travel at the slowest possible speed. When the sound speed changes with depth, which it almost always does, the sound refracts toward the depth with the lowest sound speed, which can result in sound being trapped in a 'duct' and travelling very long distances with minimal attenuation. Conversely, in conditions where the sound speed decreases with depth, sound is refracted towards the seabed and may not reach an intended receiver. The sound speed is a function of the temperature, salinity and pressure (depth). Colder and fresher water has a lower sound speed and conversely warmer and saltier water has a higher sound speed. As the water depth increases the pressure increases the water density slightly, which increases the sound speed (Jensen et al. 2011). These effects combine with environmental forces such as solar heating, wind mixing, and currents to constantly affect the sound speed in the upper 500 m of the water column which has daily variations around typical seasonal means (Figure 2-4). The ability of a minimum in the sound speed profile to 'trap' sound depends on the magnitude of the sound speed change at the minimum, the vertical height of the minimum and the sound's wavelength. Ducts must be several times larger than the wavelength for effective trapping

of sound (Etter 1996). A corollary of this effect is that higher frequencies are refracted more readily by sound speed changes than lower frequencies that have longer wavelengths. It is also possible for the sound speed to change with horizontal location, which leads to three-dimensional refraction of sound, however, this is far less common than refraction due to sound speed changes with depth.

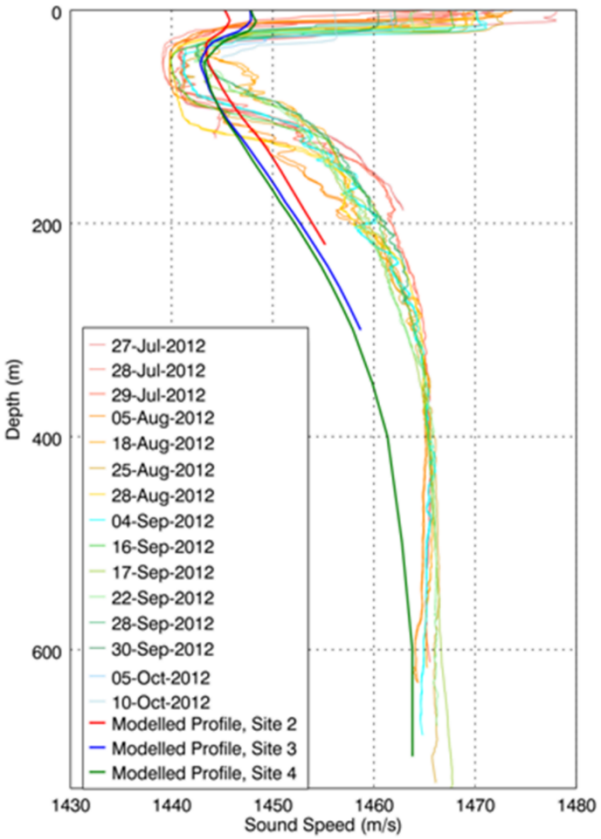

Figure 2-4. Example of seasonal sound speed profiles from (Teague et al. 1990)(Modelled Profiles) and actual sound speed profiles measured in situ in Baffin Bay.

Absorption by sea water: Acoustic energy is attenuated by molecular absorption in seawater. The volumetric sound absorption is quantified by an attenuation coefficient, expressed in units of decibels per kilometer (dB/km). Absorption depends on the sound's

frequency and the water's temperature, salinity, acidity, and pressure. In general, the absorption coefficient increases with the square of the frequency (i.e., low frequencies are less affected). The absorption of acoustic wave energy has a noticeable effect (>0.05 dB/km) at frequencies above 1 kHz. For example, at 10 kHz the absorption loss over 10 km distance can exceed 10 dB, as computed according to the formulae of François and Garrison (1982a, b), Ainslie and McColm (1998) or using the TEOS-10 software suite (http://www.teos-10.org/).

A note on source levels: Most analysis of sound propagation assumes that the source of sound can be represented as an infinitesimally small point, and its source level documented as the level 1 m from that point. This approximation is reasonable for small high frequency sources such as echosounders and acoustic current Doppler profilers, however, it is not accurate for two sources of interest in this thesis, seismic airgun arrays that have a spatial extent of ~100 m^2, and impact piles that are a line source spanning the height of the water column. Modeling the sound level from an airgun is performed by computing the received level far from the airgun array by computing the contribution of each airgun's bubbles as they grow and collapse, then back-propagating to determine an effective point source pressure and energy level (MacGillivray 2006). This value is called a source factor, which has units of μPa^2m^2. The source factor is higher than the actual sound levels close to the array. These methods work well for low frequencies (<500 Hz), however at high frequencies statistical approximations are in development (MacGillivray, per comms, 2017). For impact piles, various methods to accurately model and propagate the source factor are being developed (Lippert et al. 2016) and detailed results of actual measured levels as a function of range are required to validate the approaches.

2.3. Fundamentals of Analysis of Passive Acoustic Monitoring Data

Chapters 3-6 of this thesis involve the analysis of passive acoustic monitoring (PAM) data, i.e. data stored over periods of weeks to months by an autonomous data logger. This section provides:

1. An overview of acoustic data logger operation and how to use this information to convert the recordings into calibrated pressure time series.
2. Methods for converting the calibrated pressure times series into sound pressure level and sound exposure level values.
3. Methods for converting the calibrated pressure time series into power spectra, power spectral density levels, and decidecade sound pressure and sound exposure levels.
4. Methods for computing auditory frequency weighted sound exposure levels.

2.3.1. Calibrated Pressure Time Series

Information in this section is adapted from material written by the thesis author for the ADEON project (https://adeon.unh.edu) and is used with permission.

2.3.1.1. Functional Blocks of Passive Acoustic Data Recorders

Figure 2-5 is a functional block diagram of a passive acoustic data recorder. A description of each component in the analog section is provided in the sub-sections below.

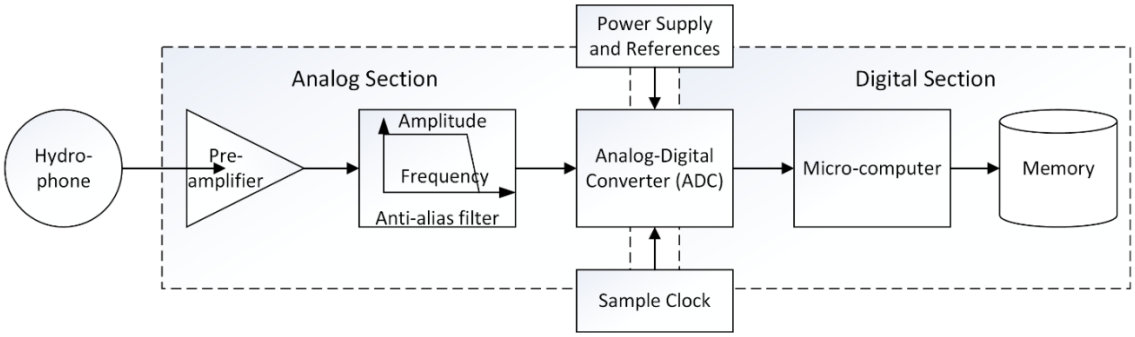

Figure 2-5. Block diagram of a passive acoustic data recorder.

2.3.1.2. Hydrophones

Hydrophones are the transducers that convert pressure fluctuations in the water to an electrical signal. The transducers are normally piezo-electric ceramics that generates a variable capacitance in response to the pressure fluctuations. Most hydrophones include a preamplifier that converts the charge to a voltage or current that is transmitted to the analog section of the recorder. For hydrophones with built-in preamplifiers with voltage outputs, the voltage sensitivity is specified in units of volts per Pascal (M_v in V/Pa) or as a sensitivity level in decibels relative to 1 V/µPa (dB re 1 V/µPa). For hydrophones that use current signaling, the current sensitivity shall be specified in units of amperes per Pascal (M_I in A/Pa).

The absolute sensitivity varies slightly between hydrophones, even within the same production batch. Similarly, the sensitivity changes with frequency. Hydrophones should

be purchased with a *measured* calibration curve supplied by the vendor. For accurate quantification of sound levels, the calibration curve must be included in the analysis of sound levels.

The sensitivity of the ceramic element impacts the overall self-noise of the hydrophone. The hydrophone preamplifier's input referred noise should be specified as an equivalent sound pressure level (SPL) in the water through the ceramic element's sensitivity. The greater the sensitivity of the ceramic element, the lower the hydrophone's self-noise for the same preamp input referred noise.

Hydrophones have a range of amplitudes over which their output is linearly related to the input pressure. Extreme care must be employed if the hydrophone is used outside of its linear range.

2.3.1.2.1. Hydrophone Movement and Data Below 10 Hz

Hydrophones build-up charge due to the static pressure caused by changes in depth that is discharged through the preamplifier's input impedance. If the hydrophone's output is AC-coupled to the recorder's input, there is a charge time for the AC coupling during power up. For hydrophones and recorders with good low-frequency response (i.e., below 10 Hz), the input impedance is very high, and the charge and discharge times can be seconds long, during which time the hydrophone output should be discarded. Similarly any hydrophone depth changes will produce hydrophone outputs that are not caused by an acoustic wave. Using the hydrostatic equation, $p = \rho g z$, a 1 cm change in depth is 101 Pa change in pressure, or ~160 dB re 1 µPa (assuming a density of 1030 kg/m^3). Hydrophone movement must be minimized for effective passive acoustic monitoring.

Data below 10 Hz from most passive acoustic recordings should not be used without special consideration due to large uncertainties caused by hydrophone movement, noise from flow around the hydrophone and uncertainty in the hydrophone calibration at those frequencies. In cases where high amplitude signals are present below 10 Hz that are not of interest to the analysis it is recommended that a 10 Hz high pass filter be applied to the data before performing further analysis.

2.3.1.3. Preamplifiers

The preamplifier can be integrated into the hydrophone, or there may be a separate preamplifier that is part of the recorder. Preamplifiers can be used to:

- Buffer the sensing element from the input to the ADC.
- Amplify hydrophone signals before analog-to-digital conversion if the dynamic range of the ADC is smaller than that of the hydrophone.
- Force analog-to-digital input to exceed the maximum range of the ADC, so that the ADC reaches its maximum output before the hydrophone becomes non-linear.

The frequency response and gain of the preamplifier is required for converting the input voltage to pressure.

2.3.1.4. Analog-to-Digital Converters and Anti-Aliasing Filters

Analog-to-Digital Converters (ADC) create a digital representation of the real-world analog signal. They represent the continuously varying analog signal with the closest value from a discrete 'stair-case' of levels that they may generate. They are characterized by:

- The sampling rate (i.e., how many times per second the analog input is converted to a digital representation). By the Nyquist theorem, the maximum frequency that is accurately represented by the digital data is one-half the sampling rate. Frequencies above the Nyquist frequency must be filtered from the analog input signal prior to digitization, otherwise they will 'alias' into lower frequencies and the digital signal will not be an accurate representation of the original analog input.
- Maximum input voltage.
- Bit depth (i.e., the number of 'bits' of digital resolution the ADC generates). The larger the number of bits for the same maximum input voltage, the smaller the distance between the discrete levels that the ADC can represent. Thus, a higher bit depth means better representation of the data (higher resolution).

The two main types of ADCs used in digital recorders are Successive Approximation Register (SAR) and Sigma-Delta:

- SAR ADCs tend to be used for medium to high resolution applications at sample rates up to 5 MHz. They are usually a lower power option than Sigma-Delta converters for the same resolution and sample rate; however, they require external anti-aliasing filters.
- Sigma Delta ADCs use an over sampling technique whereby they sample the input with a 1-bit ADC at a very high sample rate and then digitally filter and decimate to provide an output at a lower sample rate and a higher bit width. The primary

advantage of a Sigma Delta ADC is that the analog anti-aliasing requirements are greatly relaxed due to the high input sample rate.

For an ideal ADC, the number of bits in the output word places a limit on the noise floor of the converter. However, recorders with output word size greater than 16 bits, the system self-noise is usually greater than the quantization noise of an ideal ADC with that word size. Specifying an ADC with 18 or 24 bits does not necessary guarantee better system performance. An output word size may need to be specified if the processing requires a specific word length.

2.3.1.5. Computing a Calibrated Pressure Time series

To convert the digital values (DV) in the WAV files to acoustic pressure units, the following must be accounted for:

- Digital sensitivity (M_{ADC_D}) of the ADC, which depends on the bit depth N_{bit} (=16 or 24): $M_{ADC\_D} = 1/2^{N_{\text{bit}}}$. Unit: dimensionless.
- Voltage range of the ADC (V_{ADC}) = V_{max}-V_{min} where V_{min} is the minimum voltage the ADC can convert, and V_{max} is the maximum voltage the ADC can convert. Unit: 1 V.
- Gain of the hydrophone preamplifiers is G. Unit: 1 V/V.
- Voltage sensitivity of the hydrophone is M_v. Unit: 1 V/Pa. (Voltage sensitivity is often expressed in units of 1 V/µPa because the reference sound pressure in underwater acoustics is 1 µPa.).

Passive acoustic recorder data is stored as a digital file, typically .wav format which contains N_{bit}-long signed binary words. The maximum value of the digital words is V_{max} which has a digital value of 2^{Nbit-1} because one bit is reserved for the sign of the number. Thus, the input value to the ADC, in volts, for a digital value of DV is

$$V_{ADC\ in} = DV \cdot {}^{V_{max}}/_{2^{N_{bit}-1}}. \qquad 2\text{-}6$$

The preamplifier gain G is an amplification applied to the hydrophone signal before the ADC. This gain is the ratio of the output voltage to the input voltage: $G = V_{out}/V_{in}$, where V_{in} is the input voltage to the amplifier from the hydrophone and V_{out} is the output voltage from the amplifier. The voltage at the ADC is pre-amplified. Thus, to determine the voltage output by the hydrophone, $V_{ADC\ in}$ must be divided by G:

$$V_{HP\ out} = V_{ADC\ in}/G \qquad 2\text{-}7$$

To obtain the pressure value we need to apply the hydrophone sensitivity which is the ratio of the hydrophone output voltage to the input acoustic pressure. The sensitivity is customarily given as a sensitivity level in decibels relative to 1 V/µPa, which results in a negative number. The sensitivity depends on frequency, but it is usually approximately constant over a nominal bandwidth. The nominal sensitivity is usually provided by the manufacturer based on factory calibration, for example a sensitivity level of $M_{v,dB} = -165$ dB re 1 V/µPa. A less negative sensitivity corresponds to a more sensitive hydrophone. For example, a hydrophone with a sensitivity of −165 dB re 1 V/µPa is more sensitive than one with −180 dB re 1 V/µPa. The sensitivity level is converted to a voltage sensitivity as $M_v = 10^{M_{V.dB}/20}$ V/µPa, which is $5.623 \cdot 10^{-9}$ for a sensitivity level of -165 dB re 1V/µPa. Dividing $V_{HP\ out}$ by M_v and combining with the previous steps gives the pressure times series (Equation 2-8)

$$p(t) = \frac{DV \cdot V_{max}}{G \cdot M_v \cdot 2^{N_{bit}-1}}\ \mu\text{Pa} \qquad 2\text{-}8$$

2.3.2. Sound Pressure Level and Sound Exposure Level

The instantaneous sound pressure level is the 10 times the logarithm base 10 of the square of the pressure time series divided by a reference pressure, p_o, squared (Equation 2-9).

$$SPL = L_p = 10 * \log_{10} \frac{p(t)^2}{p_o^2} \text{ dB re 1 µPa} \qquad 2\text{-}9$$

As defined in Table 2-1, the peak sound pressure level is the maximum value of L_p over an interval of time. The peak-to-peak sound pressure level is 10 times the logarithm base 10 of the maximum minus the minimum value over an interval of time.

SPL as defined above is rarely used in practice except as the peak sound pressure level. Instead, SPL or L_p is the root mean square sound pressure level over a duration T, as shown in Table 2-1. The SEL is obtained by dividing by a reference duration of 1 second rather than the integration time *T*. Thus, the SEL is equal to the SPL plus $10 \cdot \log_{10}$(duration): $L_{E,T} = L_{p,T} + 10 \log_{10} T$. To convert from a daily SEL to an average daily SPL we subtract $10 \cdot \log_{10}$(86400 seconds) = 49.4 dB.

2.3.3. Obtaining Calibrated Spectra

Many of the operations we wish to perform on passive acoustic data occur in the frequency domain. Therefore, it is important to be able to convert a calibrated pressure time series into calibrated spectra and to verify that the energy was preserved. The information that follows is intended to be a brief refresher of the mechanics of spectral analysis – a proper text or course on spectral analysis is recommended for anyone intending to perform spectral analysis on acoustic data. This refresher uses MATLAB functions and its treatment of arrays where the first element is index 1.

The spectrum of a time series *p(t)* is given by it's fast Fourier transform (FFT). When using the MATLAB FFT, the result needs to be divided by the square root of the number of points in the time series to normalize to the correct unit of μPa:

```
Spectrum = fft(p) / sqrt(length(p)); % uPa; complex number
```

The power spectrum is more commonly used, which is the absolute value of the square of the spectrum:

```
powerSpectrum = abs(spectrum .* spectrum);  %uPa^2
```

Each element of the power spectrum vector contains the energy for the frequency bin, where the first bin is centered at frequency zero (DC), and the other bins are centered at a frequency of ((i-1) * F_s / length(*p(t)*)), up to a length(*p(t)*)/2 which has the energy at the Nyquist frequency of $F_s/2$ (where F_s is the sampling frequency). Above this bin the spectrum is mirrored. Because of this mirroring the bins above length(*p(t)*)/2 may be discarded as long as the energy in bins 2:length(*p(t)*)/2 is doubled.

```
powerSpectrumSingleSided = powerSpectrum(1:Fs/2+1);
powerSpectrumSingleSided(2:Fs/2) = 2 * powerSpectrumSingleSided(2:Fs/2)
```

To verify that the operation was performed correctly check the energy:

```
sum(p .* p) = sum(powerSpectrumSingleSided)
```

The power spectral density typically reported for long-term acoustic data is the power spectrum computed for 1 Hz bins, i.e., using 1 second of data in the FFT. Recall that the power spectrum level, or the power spectral density level, are obtained by taking $10 \cdot \log_{10}$ of the power spectrum or power spectral density.

When performing FFTs as shown above, energy from one spectral bin will 'leak' into adjacent bins. In many cases spectral leakage is not important, however, if there is a strong signal at one frequency it will elevate the power spectrum in neighbouring frequency bins. This effect is especially confounding when the extra energy is at or near zero frequency. As discussed above, small movement of the hydrophone can generate very large low frequency signals. Spectral leakage can be minimized by applying a window function to the time series before taking the fast Fourier transform. Common windows, arranged in order of effectiveness at reducing leakage from least to most, are: Hamming, Tukey, Hann and Blackmann-Harris. The Hann window is recommended for most acoustic data analysis because it is simple to implement, effective at sidelobe suppression and leakage suppression and a standard that most computing packages (e.g. MATLAB, R, Python, SciLab) provide and reviewers accept (Heinzel et al. 2002).

When using a window function in MATLAB, for instance win = hanning(F_s), it is important to note that the window is not energy balanced which will reduced the power spectral values. To balance the energy: 1) compute the sum of the squares of the window coefficients; 2) divide the number of points in the window by the sum of the squares of the coefficients obtained at step (1); 3) multiply each of the window coefficients by the square-root of the value obtained at step (2). When applying windows, it is essential to use an overlap-and-save method to ensure that each part of the time series is equally weighted (e.g. Welch 1967).

2.3.4. Computing Decidecades from Calibrated Spectra

Decidecades are computed from power spectra (i.e. the linear representation rather than the level representation) by summing the spectral bins associated with the frequencies of the decidecade (see Table 2-2). A minimum FFT size of $F_s/2$ is recommended to have at least one whole spectral bin in each of the decidecades starting at 10 Hz. The power from the spectral bins at the edges of the decidecades must be divided between the two adjacent decidecades. For instance, the 10 Hz decidecade is from 8.91 to 11.22 Hz – the overlap of this band with the frequency axis of a 1 Hz resolution FFT is shown in Figure 2-6. Figure 2-6 also shows the frequency coverage of each FFT bin – i.e. the 9 Hz bin covers from 8.5 to 9.5 Hz. To obtain the 10 Hz decidecade we sum:

(9.5 – 8.91) * PS(9 Hz) + PS(10 Hz) + (11.22 – 10.5) * PS(11 Hz)

Where PS(9 Hz) is the power spectrum at the 9 Hz bin, etc.

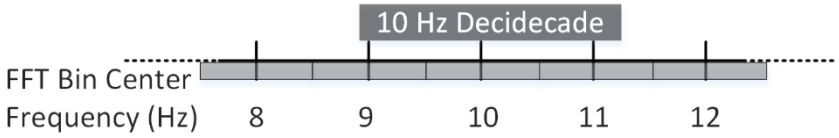

Figure 2-6. Overlap of the 10 Hz decidecade frequency band on a 1 Hz resolution frequency axis.

2.3.5. Computing Auditory Weighted SEL

There are three methods that may be used to compute the auditory weighted SEL – by direct summing of the weighted spectrum, by summing of the weighted decidecades, or by summing the energy of a filtered time series. All three methods require a function that generates the weighting coefficients using the equation and parameters from Table

AE-1 of NMFS (2018) shown here in Table 1-1. Example software for this section is provided in Section 2.3.6.

To apply weightings to a power spectrum, the coefficients are computed for the centre frequencies of the FFT that was used, then multiplied by the power spectrum and summed. When applying weightings to decidecades, the coefficients are computed for the centre frequency of each decidecade, then the multiplied by the decidecade spectra and summed. In most cases the weightings are performed on relatively short data samples, such as a 1-second or 1-minute power spectra or decidecades. To obtain the daily SEL the short-term SEL are summed in linear units then converted to a level presentation for analysts or comparison to the TTS and PTS thresholds.

In some cases, it is desirable to have an auditory frequency weighted time series, for example if there is a requirement to compute impulsive metrics of an auditory frequency weighted signal. An arbitrary magnitude finite impulse response (FIR) filter is recommended for this application (see Section 2.3.6.3). When using this method, the original calibrated time series is FIR filtered, then the filtered time series samples are squared, summed, and divided by the number of samples per second to obtain the SEL.

The three methods produce almost identical results (Figure 2-7). The decidecade method is the most versatile since it can be applied to data that has been compressed previously to decidecade SPL or SEL. Because of the coarse frequency resolution of decidecades that method produces biased values, especially when the data contains substantial low frequency energy which the auditory frequency weighting function is removing (e.g. Figure 2-7). The filter method appears to have not removed quite enough

low frequency energy when using the low-frequency auditory frequency weighting derived filter, likely because the filter was not able to follow the shape of the weighting function precisely for the sharp low-frequency roll-off. Given that the auditory frequency weighting functions are a synthesis of a broad range of audiograms from multiple individuals and species (see Southall et al (2019)), this small error is not considered important. To ensure the results are repeatable between sample rates, the same relative number of points in the FIR filter should be employed – i.e., always generate the filters using the sample rate as the number of points in the filter.

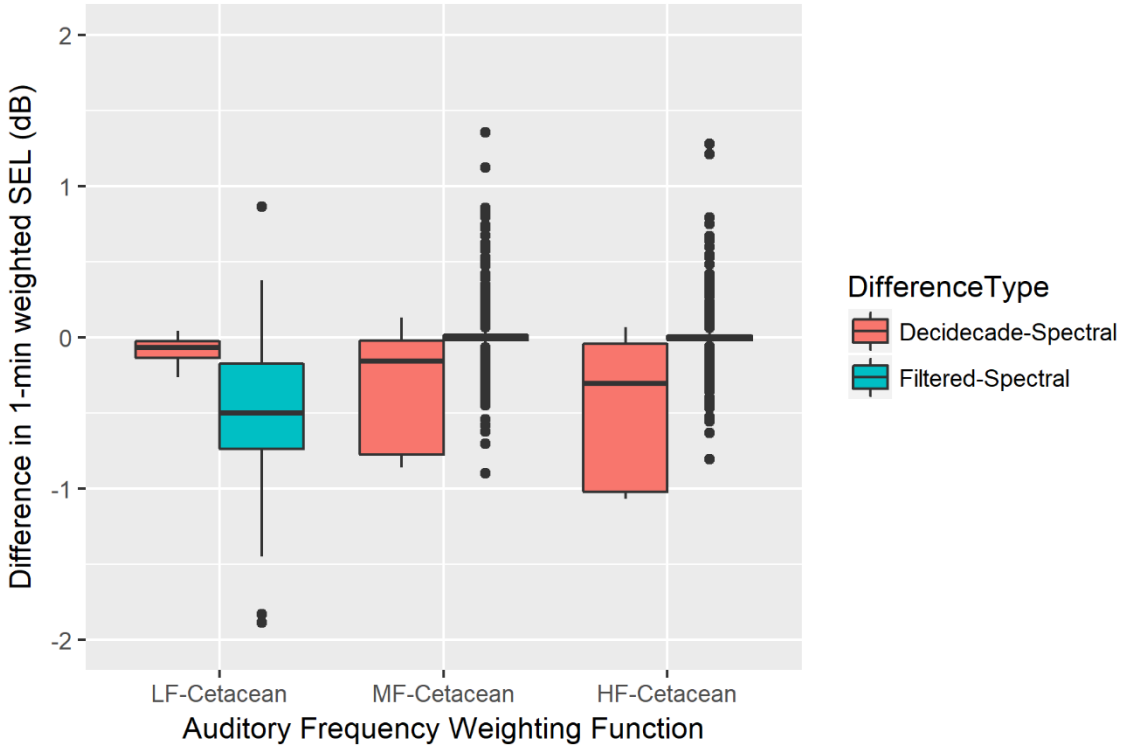

Figure 2-7. Comparison of methods for estimating auditory frequency weighted SEL Comparison shows the decidecade vs spectral methods, as well as the filtering vs spectral methods for the low, mid, and high-frequency cetacean auditory frequency weighting functions applied to the real-world data analyzed in Chapter 6.

2.3.6. Supporting Information – Code Samples

This section contains MATLAB software for methods discussed in this Chapter.

2.3.6.1. Computing the Auditory Frequency Weighting Functions:

```
function [mWeighting] = NMFS2018MWeighting(freq, a, b, f1, f2, C)
       %computes the NMFS 2018 M-weights for the input freq based on the
       %parameters provided from table AE-1 of NMFS 2018. Freq is the
       %frequency that the weighting function is calculated at; value is
       %returned in linear space.
       fByF1 = freq / f1;
       numerator = power(fByF1,2*a);

       denom1 = 1 + fByF1*fByF1;
       denom1 = power(denom1, a);
       fByF2 = freq / f2;
       denom2 = 1 + fByF2*fByF2;
       denom2 = power(denom2, b);
       denom = denom1 * denom2;

       mWeighting = C + 10*log10(numerator/denom);
       mWeighting = power(10, mWeighting / 10);
end

function [ mWeighting ] = getMWeighting( mammalGroup, freq, groupName )
       %% Frequency is in Hz
       % mammalGroup: NMFS2018 - you can implement older ones if needed
       %Weighting group: LFC, MFC, HFC, OTA, PHO
       switch groupName
           case 'NMFS2018'
               switch mammalGroup
                   case 'LFC'
                       a = 1.0;
                       b = 2;
                       f1 = 200;
                       f2 = 19000;
                       C = 0.13;
                       K = 179;
                   case 'MFC'
                       a = 1.6;
                       b = 2;
                       f1 = 8800;
                       f2 = 110000;
                       C = 1.2;
                       K = 177;
                   case 'HFC'
                       a = 1.8;
                       b = 2;
                       f1 = 12000;
                       f2 = 140000;
                       C = 1.36;
                       K = 152;
                   case 'PHO'
                       a = 1.0;
                       b = 2;
                       f1 = 1900;
                       f2 = 30000;
```

```
                    C = 0.75;
                    K = 180;
                case 'OTA'
                    a = 2.0;
                    b = 2;
                    f1 = 940;
                    f2 = 25000;
                    C = 0.64;
                    K = 198;

                otherwise
                    mWeighting = -1000;
                    return;
            end
        end
        mWeighting = NMFS2018MWeighting(freq, a, b, f1, f2, C);
end
```

2.3.6.2. Computing Auditory Frequency Weighted SEL using the Spectrum or Decidecades

The MATLAB processing to obtain one-minute SELs using power spectral density or decidedades is shown below:

```
    nFFTs = 60 * 2 - 1;  % 50% overlap, but can't overlap last buffer
    step = fs/2;
    specSPL = zeros(nWeights, 1);
    toSPL = zeros(nWeights, 1);
    window = hanning(fs);
    weight = sqrt(sum(window.*window)/(fs));
    window = window / weight;

    for ff = 1:nFFTs
        start = 1 + (ff-1)*step;
        last = start + fs - 1;
        dat = readData(start:last);
        psd = fft(dat .* window) / sqrt(fs);
        psd(2:step) = sqrt(2) * psd(2:step);
        psd = psd(1:step+1);
        psdAbs = abs(psd .* psd);
        dDecs = getThirdOctaveBands(psdAbs, lastTO, toTable, 1);
        for (w=1:nWeights)
            filtSpec = psdAbs .* specWeights(w, :)';
            specSPL(w) = specSPL(w) + sum(filtSpec);
            tobSpec = TOBs .* toWeights(w, :)';
            toSPL(w) = toSPL(w) + sum(tobSpec);
        end
    end
   % normalize to the get 1-minute SPL
    toSPL = toSPL / (fs*nFFTs);
    specSPL = specSPL / (fs*nFFTs);
    for w = 1:nWeights
        % convert to dB and add 10log10(60) to get 1-min SEL
        specSELs(w, counter) = 10*log10(specSPL(w)) + 10*log10(60);
        toSELs(w, counter) = 10*log10(toSPL(w)) + 10*log10(60);
```

```
end
```

2.3.6.3. Computing Auditory Frequency Weighted Time Series

The coefficients for the filter can easily be generated in MATLAB as follows:

```
NfilterPoints = Fs;
freqs = linspace(0, Fs/2, 1000);
response = zeros(size(freqs));
for p = 1:length(response)
    response(p) = getNMFS2018Weighting(mammalGroup, freqs(p), 'NMFS2018');
end
response = sqrt(response);  % because the filtering is done on
        % voltage data not power data.
freqs = freqs / (Fs/2);
d = fdesign.arbmag('N,F,A',NfilterPoints, freqs, response);
Hd = design(d,'freqsamp');
```

where *getNMFS2018Weighting* is a wrapper function for *NFMS2018MWeighting* that looks up the parameter values of Table 1-1 based on the auditory frequency weighting functional group name. Note that because of filter start-up length the time series input to the filter needs to be buffered and overlapped:

```
[readData] = getCalibratedData(FileName, fs,
    Tstart, Tend, readSamples, startSample);
readLen = size(readData, 1);
if startSample == 1
   bufferData(2*NfiltPts+1:readLen+2*NfiltPts) = readData;
    % mirror the data at the start of file:
   for (i=1:2*NfilterPoints)
      bufferData(i) = readData(2*NfilterPoints+1-i);
   end
else
   bufferData(1:2*NfilterPoints) = overlapBuffer;
   bufferData(2*NfilterPoints+1:2*NfilterPoints+readLen) = readData;
end
overlapBuffer = readData(readLen-2*NfilterPoints+1 : readLen);
filtData = fftfilt(Hd.numerator, bufferData);
% note that the start time of the filtered data is now the read
  % starttime - NfilterPoints/fs
analysisTS = filtData(NfilterPoints+1 : NfilterPoints+dataPts);
```

CHAPTER 3 CHARACTERISTICS OF SEISMIC SURVEY PULSES AND THE AMBIENT SOUNDSCAPE IN BAFFIN BAY AND MELVILLE BAY, WEST GREENLAND

This chapter contains the paper Martin et al. (2017), which was submitted to the Journal of the Acoustical Society of America in August 2016 and published December 2017. The material for this Chapter was the result of a large project conducted by JASCO Applied Sciences for Shell Global Solutions. The author contributions were:

- Bruce Martin was the project manager and primary investigator.
- Koen Broker was the project lead for Shell, assisted with the study design, and provided suggestions and reviews that strengthened the JASA article.
- Jeff MacDonnell assisted with the fieldwork and data analysis for the Shell project.
- Marie-Noel Matthews performed the acoustic propagation modeling for the analysis for Shell and was an important resource during discussions of model-measured comparisons.

The impulse detection and seismic correlation analysis algorithms used to extract the seismic pulses was written by Bruce Martin as part of JASCO's PAMLab software suite. Bruce is the original author of the software; it is now maintained by Briand Gaudet and Bruce Martin. The MATLAB software used to generate many of the figures in this Chapter was originally written by Bruce and is now maintained by Bruce and Christopher Whitt. The data preparation and statistical analysis for the effects of depth, analysis window duration, and frequency content was all performed by Bruce Martin, as were the ambient analysis for Baffin Bay and Melville Bay (Not included here). A companion

article lead by Heloise Frouin-Mouy discusses the marine mammal presence determined from these data sets (Frouin-Mouy et al. 2017).

Note that Tables 3-4 to 3-8 as well as Figures 3-16 to 3-27 are S-1 to S-5 and S-1 to S-12, respectively in the JASA Manuscript. These Tables and Figures appear as Supporting Information for this Chapter.

Title: Characteristics of seismic survey pulses and the ambient soundscape in Baffin Bay and Melville Bay, West Greenland

S. Bruce Martin[1], Marie-Noël R. Matthews, and Jeff T. MacDonnell[2]

JASCO Applied Sciences (Canada) Ltd.

32 Troop Avenue, Suite 202,

Dartmouth, Nova Scotia, Canada, B3B 1Z1

bruce.martin@jasco.com

Koen Bröker[3]

Shell Global Solutions International B.V.

Lange Kleiweg 40

2288GK Rijswijk

The Netherlands

Running Title: Soundscape of Baffin and Melville Bay

Date Submitted: 28 Aug 2016

---

[1] Also at Dalhousie University, Department of Oceanography, 1355 Oxford Street, PO BOX 15000,Halifax, Nova Scotia Canada, B3H 4R2

[2] Currently at Acoustic Data Analysis Center, P.O. Box 99000, Stn Forces Halifax, NS B3K 5X5

[3] Also at Groningen Institute for Evolutionary Life Sciences, University of Groningen, Nijenborgh 7, 9747AG Groningen, The Netherlands

ABSTRACT

In 2012 a seismic survey campaign involving four vessels was conducted in Baffin Bay, west Greenland. Long-distance (150 km) pre-survey acoustic modeling was performed in accordance with regulatory requirements. Four acoustic recorders, three with hydrophones at 100, 200, and 400 m depths, measured ambient and anthropogenic sound during the survey. Additional recordings without the surveys were made from September 2013 to September 2014. The results show that 1) the soundscape of Baffin Bay is typical for open ocean environments and Melville Bay's soundscape is dominated by glacial ice sounds; 2) there are distinct multipath arrivals of seismic pulses 40 km from the array; 3) seismic sound levels vary little as a function of depth; 4) high fidelity pre-survey acoustic propagation modeling produced reliable results; 5) the daily SEL did not exceed regulatory thresholds and were different using Southall et al. (2007) or NMFS weightings; 6) fluctuations of SPL with range were better described by additive models than linear regression; and 7) the survey increased the 1-min SPL by 28 dB, with most of the energy below 100 Hz; energy in the 16000 Hz octave band was 20 dB above the ambient background 6 km from the source.

PACS Numbers: 43.30.Ma, 43.30.Nb, 43.30.Pc, 43.80.Nd
Keywords: seismic airgun; ambient noise; SPL; Baffin Bay; Melville Bay; SEL

3.1. INTRODUCTION

In 2010, five petroleum exploration license blocks were awarded in Baffin Bay, west Greenland. Some of these blocks have considerable overlap with narwhal protection areas and are proximal to the Melville Bay Nature Reserve (Figure 3-1). As part of the environmental permitting process for seismic surveys in Greenland, the Danish Centre for

Environment and Energy (DCE) issued Environmental Impact Assessment requirements that included acoustic modeling and monitoring guidelines (Kyhn et al. 2011). These guidelines defined many of the responsible practices with respect to marine mammals and seismic surveys that were subsequently described by (Nowacek et al. 2013). The main mitigation measures in these guidelines are 1) establishing the radius of exclusion zones with high-fidelity acoustic modeling; 2) visually and/or acoustically monitoring exclusion zones to minimize auditory injury to marine mammals; and 3) turning off active sources when mammals are detected in exclusion zones. The DCE guidelines (Kyhn et al. 2011) apply the dual criteria recommended by Southall et al. (2007): a maximum peak sound pressure level (SPL) and a 24-hour sound exposure level (SEL) limit. Seismic surveys are usually performed using arrays of airguns spread over an area on the order of 100 m^2 and are therefore not point sources. The range from an airgun array where the peak sound pressure level criterion of 230 dB re 1 µPa for cetaceans is exceeded (if at all) is at most on the order of tens of meters, indeed comparable to the size of the airgun array itself (Caldwell and Dragoset 2000, Gisiner 2016). Thus, the criterion of concern for defining exclusion zones is the 24-hour SEL. The 24-hour SEL thresholds recommended in Southall et al. (2007) are weighted for the hearing bands of mammal groups; the SEL criterion is typically exceeded at ranges from the airgun array on the order of hundreds of meters (Tashmukhambetov et al. 2008, Breitzke and Bohlen 2010, Matthews 2012b). It is widely accepted that applying mitigation zones based on these thresholds minimizes the risk of injuring marine mammals (Gordon et al. 2003, Wartzok et al. 2003, Southall et al. 2007, Nowacek et al. 2013).

Seismic airgun pulses can be perceptible above the background ocean sound at distances in the order of hundreds of kilometers (Bohnenstiehl et al. 2012, MacGillivray et al. 2014, Blackwell et al. 2015) and even farther if the energy propagates in a deep sound channel (Thode et al. 2010, Nieukirk et al. 2012, Blackwell et al. 2015). At ranges between the injury exclusion zones and the limits of perception for seismic sound, animals may experience temporary threshold shift (TTS), behavioral disturbance, and masking effects (Gordon et al. 2003, Wartzok et al. 2003, Southall et al. 2007, Nowacek et al. 2013). The sound levels that induce behavioral responses from marine mammals cover a wide range of sound pressure and sound exposure levels and are dependent on factors such as the type of activity an animal was engaged in when exposed to the sound (Richardson et al. 1986, Wartzok et al. 2003, Ellison et al. 2012, Robertson et al. 2013). It is extremely difficult, therefore, to establish relevant metrics and appropriate thresholds to minimize behavioral effects (Southall et al. 2007, Kyhn et al. 2011, Finneran and Jenkins 2012, Wood et al. 2012, Wisniewska et al. 2014). Behavioral response studies aim to develop dose-behavioral response relationships reflecting the range of sound levels required to elicit a response within a population (Kastelein et al. 2013a) or the magnitude of response as a function of the stimulus (Kastelein et al. 2013b). The sound levels that have been reported to start eliciting behavioral responses range between 100 and 180 dB re 1 µPa SPL (Finneran and Jenkins 2012, Wood et al. 2012, Shannon et al. 2016, Carroll et al. 2017). The SPL depends on the averaging time used, which can lead to a range of possible values for the same pulse depending how the pulse length is determined (Madsen 2005). It is important to document the variability in the pulse length and SPL with in situ data.

Man-made sound has the potential to mask ecologically relevant sounds, especially when the frequency bands of the sound sources overlap. Sounds that are ecologically relevant to marine animals include conspecific calls, predator and prey sounds, natural sounds used for orientation, and echolocation calls from odontocetes (Clark et al. 2009). Seismic airgun arrays emit high-intensity low-frequency sound impulses with peak frequencies of near 50 Hz (Dragoset 1990, Caldwell and Dragoset 2000). They are expected to have minimal impacts on marine mammals, such as odontocetes, that have limited hearing sensitivity at these low frequencies (NRC 2005, Southall et al. 2007, NMFS 2018). However, Goold and Fish (1998) report frequencies of up to 8 kHz above the ambient background at a distance of 8 km from a 2120 in^3 seismic array in 50–100 m deep water, Madsen et al. (2006a) report measured per-pulse SPLs in the 10 kHz 1/3-octave-band greater than 110 dB at a range of 1.4 km from a 2590 in^3 seismic array in deep waters in the Gulf of Mexico, and Hermannsen et al. (2015) show energy above 10 kHz from single airguns at a range of 1300 m in 15 m deep water.

In summer 2011, license holders submitted four seismic survey applications to the DCE. As part of the Environmental Impact Assessment process, each proponent's acoustic modeling methods and results (Matthews 2012a) were reviewed by the DCE, and the cumulative effects of all surveys were assessed. To reduce the risk of hearing injury to marine life DCE required the proponent's to determine the radius around the vessel where permanent hearing threshold shift was predicted based on the recommendations of Southall et al. (2007) (Kyhn et al. 2011). A behavioural disturbance radius was estimated based upon an SPL threshold of 150 dB re 1 µPa in 2012 and 140 dB re 1 µPa in 2013 (Matthews 2012b, Matthews 2013). Guidance for effects on fish for

the project were disturbance at an SPL of 150 dB re 1 µPa and possible injury at a sound exposure level of 187 dB re 1 $\mu Pa^2 \cdot s$ ([FHWG] Fisheries Hydroacoustic Working Group 2008). The DCE report identified various data gaps, such as 1) limited documentation of the propagation of seismic airgun pulses around Greenland; 2) limited ambient sound data for Baffin Bay and Melville Bay; 3) limited knowledge of the variation in seismic array sound levels as a function of depth; 4) uncertainty about the importance of high-fidelity inputs for acoustic models (e.g., temperature/salinity profiles, bottom contours, and the sub-bottom geo-acoustic structure); and 5) the temporal and spatial variation of marine mammal distribution in Baffin Bay and Melville Bay (Wisniewska et al. 2014). Comparing measured and modeled sound propagation as a function of depth was noted as especially important, since cold fresh water from melting glaciers creates a strong sound speed minimum at 30–80 m depth, which is expected to trap and propagate low-frequency sounds for long distances in the sound duct.

To address these data gaps, we conducted a multi-year acoustic monitoring program. As part of Shell's seismic survey in the license areas, three vertical array moorings with hydrophones at three measurement depths were deployed in summer 2012 (Figure 3-1, also see Section 3.2.1). We also deployed one bottom-mounted autonomous recorder in Melville Bay from mid-August to mid-September 2012. During August and September 2012, two seismic source vessels conducted a 3-D seismic survey with 3480 in^3 airgun arrays near the vertical arrays, including two passes within 110 m slant range of the top hydrophones. The modeled broadside zero-to-peak sound pressure source level of the arrays was 247.3 dB re 1 µPa with a modeled per-pulse sound exposure level of 227.8 dB re 1 $\mu Pa^2 \cdot s$ (Matthews 2012b). Five recorders were deployed in September

2013 to study the summer ambient soundscape and to characterize a lower-energy shallow-hazards seismic survey conducted with a 140 in^3 array (modeled broadside zero-to-peak sound pressure source level of the array was 239.3 dB re 1 μPa with a modeled per-pulse sound exposure level of 214.5 dB re 1 $\mu Pa^2 \cdot s$) (Matthews 2013). Two recorders with hydrophones at mid-water column depth were deployed overwinter from 29 Sep 2013 to 6 Sep 2014 to capture the soundscape over a full year (see Section II.A).

Here we report on the new knowledge derived from the monitoring program through an analysis of the license block and Melville Bay recordings. We present 1) propagation of seismic pulses in Baffin Bay; 2) an overview of ambient sound characteristics, total sound levels, and spectral content associated with seismic pulses in Baffin and Melville Bay; 3) variation in seismic airgun sound levels as a function of depth; 4) a comparison of modeled and measured sound levels at ranges up to 65 km from the source; 5) cumulative sound exposure levels; 6) a comparison of different SPL metrics for predictions of ranges to behavioral disturbance of marine mammals; and 7) the measured spectral content of the pulses as a function of range to the seismic source. Due to the large amounts of data collected in this project, we have provided figures and tables that illustrate points on additional recorder channels in the Supporting Information section. The data from this project also generated extensive new information on the seasonal presence of marine mammals in Baffin Bay, which is reported in Frouin-Mouy et al. (2017).

3.2. METHODS

This section describes the autonomous recorder deployments and the methods used for analyzing the data and acoustic propagation modeling. With respect to acoustic terminology, this manuscript uses the terms recommended in ISO (2017a). Specifically, sound pressure level is 10 times the base-10 logarithm of the mean squared pressure summed over a specified time window and is abbreviated as SPL or $L_{\text{p,duration rms}}$ where 'p' stands for pressure and 'duration' is the averaging window length. The maximum of the pressure signal, in dB re 1 μPa, is referred to as peak sound pressure level or $L_{\text{p,pk}}$. The 1/3-octave-band used in this analysis followed the 1/10th decade (decidecade) definition of 1/3-octaves.

3.2.1. Recorders and Deployments

Autonomous Multichannel Acoustic Recorders (AMARs, JASCO Applied Sciences) were deployed at Stations BB1–BB4 (Figure 3-1, Table 3-4) between 29 Jul and 2 Oct 2012. Stations BB1–BB3 were bottom-mounted vertical arrays (Figure 3-2), with hydrophones at 100, 200, and 400 m water depths. The recording depths were chosen as a compromise between the expected propagation paths (see Section II.C), water column coverage, and eliminating interference with the seismic arrays. At these three stations, the top hydrophone (100 m depth) sampled continuously at 64 kHz to record seismic airgun pulses and marine mammal calls. The two lower hydrophones (200 and 400 m depth) sampled continuously at 8 kHz, primarily to record seismic airgun pulses. All three hydrophones were sampled by the same AMAR. The 8 kHz sample rate for the lower hydrophones was chosen to maximize the recording duration within the memory capacity of the system (1.792 TB). We chose not to duty cycle these recordings so that

the recordings would contain complete overpasses of the seismic vessel at all depths. Station BB3 was located within 3 km of pre-survey modeling Site 3 (Matthews 2012b) to permit comparisons between the measured and modeled data (Figure 3-1). At Station BB4, located within Melville Bay, an AMAR was deployed at the seabed (130 m) with a single omnidirectional hydrophone sampling at 64 kHz.

AMARs were deployed at Stations BB5–BB9 (Figure 3-1, Table 3-4) between 31 Aug and 30 Sep 2013. These systems were fitted with GTI-M8E-V35 hydrophones which, due to the shorter monitoring period that allowed for higher sampling rates, alternated between sampling rates of 64 and 375 kHz. The hydrophones were positioned between 300–500 m, in each case near mid-water column for the chosen locations (Table 3-4). To collect a year-long dataset without seismic activity, AMARs were deployed at Stations BB6 and BB10 from late September 2013 to early September 2014 (Figure 3-1, Table 3-4). Each year-long AMAR was fitted with a GTI-M8E-V35 dB omnidirectional hydrophone and cycled between 64 and 375 kHz, as well as periods of sleep. The details of hydrophone sampling configurations and sensitivities are given in Table 3-5 and Table 3-6.

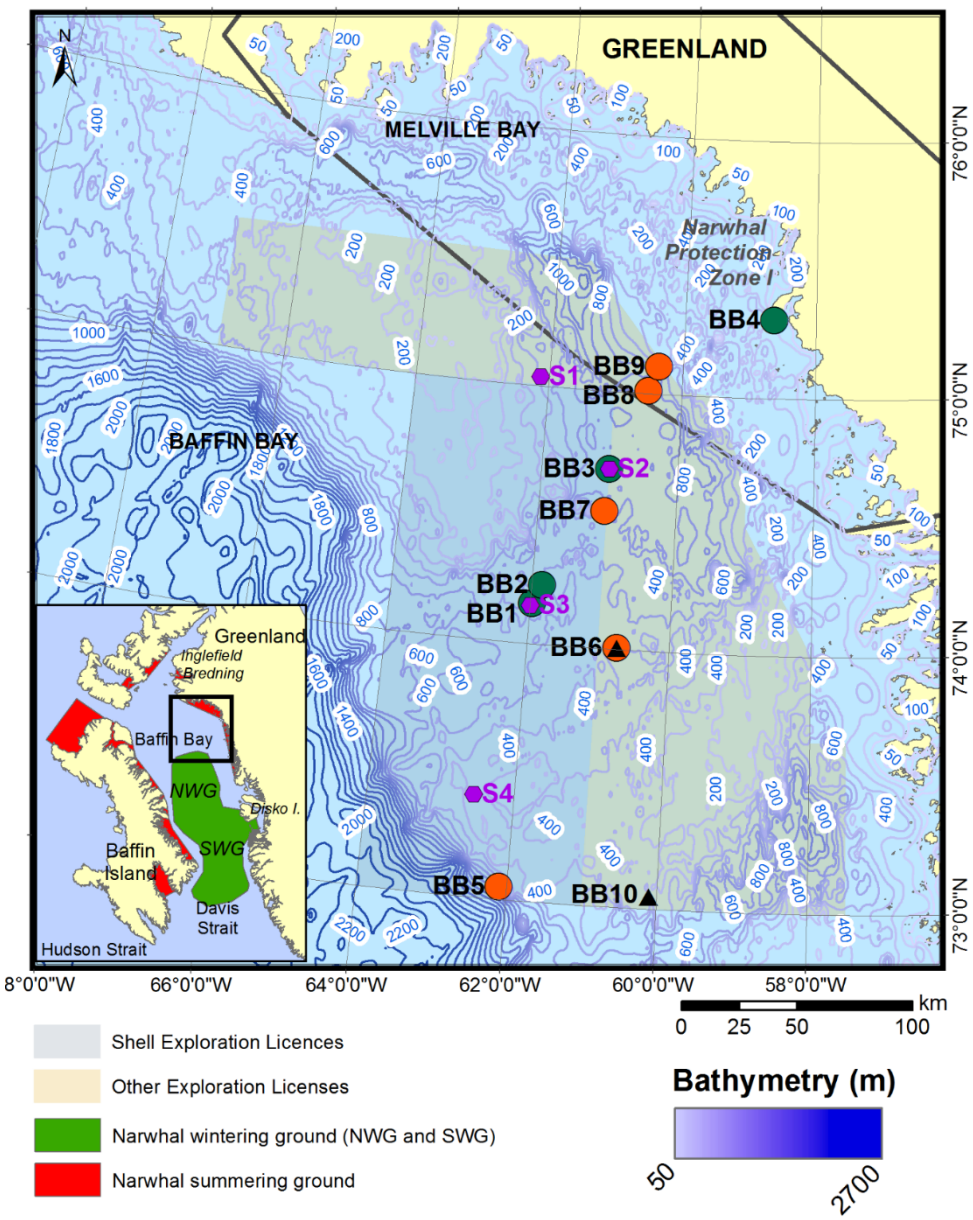

Figure 3-1. Baffin Bay recorder stations in summer 2012 (green circles/darker gray), summer 2013 (orange circles/light gray), and overwinter 2013–2014 (black triangles), as well as pre-survey modeling locations (purple hexagons). Narwhal protection area data from Kyhn et al. (2011).

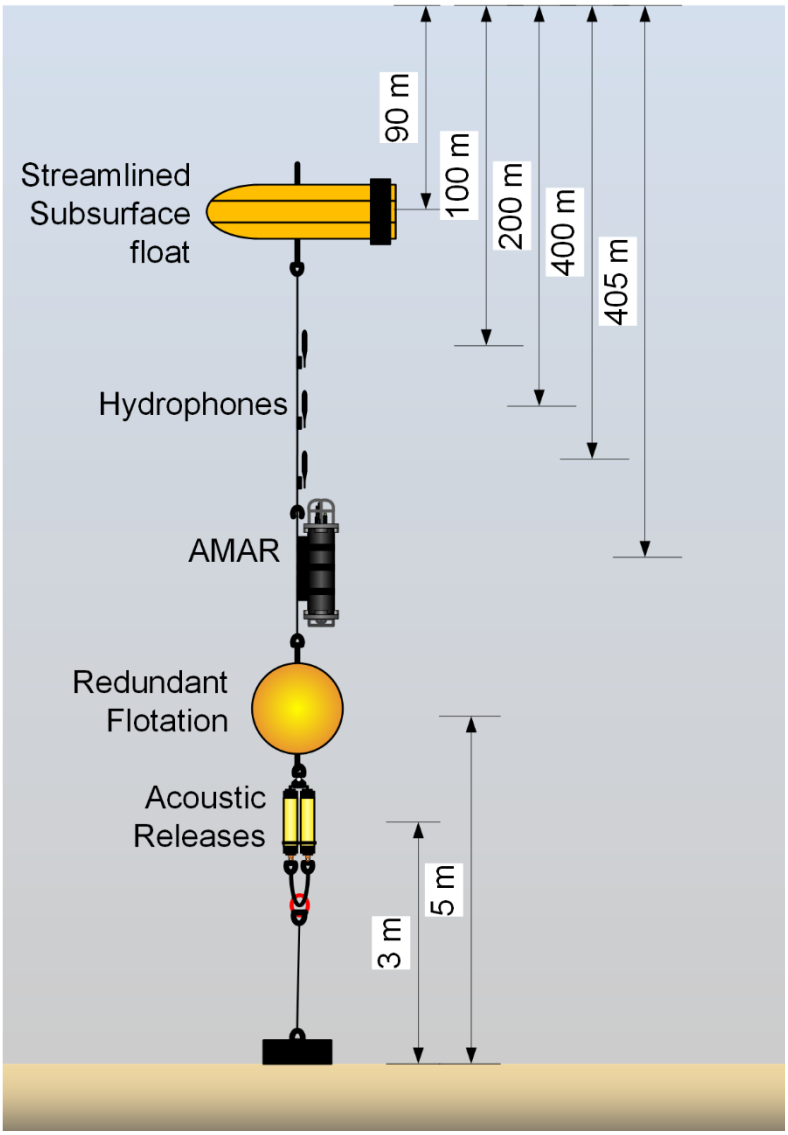

Figure 3-2. Overview of the mooring configuration used in 2012. The bottom hydrophone was located at ~ 400 m water depth with the recorder located ~5 m below it. The other hydrophones were located at 200 and 100 m depth. The streamlined sub-surface float was at 90 m depth.

3.2.2. Acoustic Data Analysis

Acoustic data were quantified using three standard metrics: peak sound pressure level, sound exposure level (SEL), and sound pressure level (SPL) (see for example Madsen, 2005 for definitions of these metrics). The broadband SPL, as well as the SPL,

in each 1/3-octave-band were computed. The metrics were computed for each minute of data to characterize the total sound levels and separately for each detected seismic pulse to characterize the short impulses. The one-minute decidecade SPLs were converted to decidecade SELs by adding $10*\log_{10}(60 \text{ seconds})$ and combined to assess the frequency-weighted sound levels (Southall *et al.*, 2007) or to compute the sound levels in octave bands so seismic sound levels could be discussed as a function of frequency. The 1 Hz power spectral densities averaged over 1 minute were computed and are presented in the Section III.A and the Supplementary Information as long term spectrograms, percentile levels, and spectral probability densities (see Merchant *et al.*, 2015 for a discussion of these methods).

Our analysis used exceedance percentile levels to quantify the distribution of recorded sound levels. Following standard acoustical terminology, the *n*th percentile level (L_n) is the level (i.e., power spectral density level, SPL, or SEL) exceeded by *n*% of the data. L_{max} is the maximum recorded sound level. L_{mean} is the linear arithmetic mean of the sound power, which can differ substantially from the median sound level $L_{50.}$ The exceedance percentiles are often presented as statistical sound levels using box-and-whisker plots (e.g., Figure 3-5). In such plots, the bottom and top of the 'box' are defined by the 75th and 25th percentile sound levels respectively, and a line through the middle of the box shows the median level. Whisker lines extending above and below the box show the total range of measured data, with short hash marks to indicate the 95th and 5th percentiles. The mean (L_{mean}) value is shown with a separate line across the plot.

Seismic survey pulses were identified using a variation on the Teager-Kaiser (TK) energy detector (Kandia and Stylianou 2006). The detector created an 'energy' time

series as the square root of the sum of the squared pressure signal over a period of 0.03 s. A detection was determined to have occurred when the square of this time series (sample X_i) was greater than the product of its neighbors by a chosen threshold (Equation 3-1).

$$X_i^2 - X_{i-1} * X_{i+1} > T \qquad 3\text{-}1$$

The pulse limits were defined by searching for the maximum energy in the neighborhood of each detection. Two versions of the detector were implemented for this study. The first version used the 90% energy duration method of analyzing man-made impulsive sounds (T_{90} SPL, e.g. Blackwell et al. 2004, Thode et al. 2010) by searching over a 7 s window and finding the period that contained 90% of the energy (7 s was required due to the extensive multi-path arrivals, see Figure 3-7 and Figure 3-8). The second version limited the duration of the impulse to the approximate integration time of mammalian hearing (Madsen 2005, Tougaard et al. 2015) by searching over a 0.5 s time window centered on the TK-detection and finding the 0.125 s period with the maximum energy. Multi-path arrivals from a single airgun pulse were separated into distinct impulses for analysis when we used the second approach. We chose the 0.125 s window based on Tougaard et al. (2015) and because it is also the standard used in terrestrial sound level meters for fast-time weighting (ANSI S1.4-1983 R2006) and hence will be simpler for other teams to replicate in the future. The results of these two approaches were compared with the total 1 min sound levels computed from the same time periods.

The data were pre-conditioned using a 10 Hz high-pass digital filter to remove very low-frequency electrical noise caused by an improper power supply to the current-loop circuits of the hydrophones. The finite impulse response filter was designed with the MATLAB (The Mathworks Inc, Natick Ma) *Filter and Window Design Application*, with

a 7 Hz stop frequency, a 10 Hz pass frequency, and 60 dB of stopband attenuation using the 'Kaiser Window' design option. The filter had 77342 points, and it did not substantially affect the measured signal levels above 10 Hz. Analysis of seismic pulses received 40 km from the source before the electrical noise began (5–6 Aug) showed up to a 0.2 dB difference in the per-pulse SPL and SEL, and up to a 1.5 dB difference in the peak sound pressure level. Processing of the wav file recordings was performed using the PAMlab software suite (JASCO Applied Sciences). Post processing of the PAMlab outputs and plot generation was performed using custom MATLAB scripts.

3.2.3. Seismic Source and Acoustic Propagation Modeling

Acoustic propagation modeling was a four-part process: 1) modeling of the airgun source; 2) modeling per-pulse sound exposure level propagation loss using a range-dependent parabolic equation model, 3) combining the source level and propagation loss to estimate the per-pulse SEL at the water volume around the source, and 4) converting the per-pulse SEL to SPL. The first two steps were performed at individual decidecade centre frequencies between 10 and 2000 Hz, and the contributions of each band were summed during the final step. We used the Airgun Array Source Model (AASM, JASCO Applied Sciences) to estimate the source signature of each airgun in the array by simulating the physics of bubble expansion and interactions with adjacent bubbles. The frequency dependent source level and beam pattern of the array were estimated by convolving the signatures of the individual airguns taking into account the geometry of the array (MacGillivray 2006, Matthews and MacGillivray 2013). The Marine Operations Noise Model (MONM, JASCO Applied Sciences) was used to perform parabolic equation propagation loss modeling. MONM is based on the U.S. Navy's Range-

dependent Acoustic Model (Collins 1993), modified to use complex density to approximate shear wave conversion energy loss at the seafloor (MacGillivray 2006, MacGillivray and Chapman 2012, Matthews and MacGillivray 2013).

Propagation loss estimates are affected by the bathymetry, water column sound speed profile, and acoustic properties of the seabed (Jensen et al. 2011). Pre-survey modeling (Matthews 2012b) was performed using sound speed profiles from the Generalized Digital Environmental Model (GDEM) database (Teague et al. 1990), bathymetry from the SRTM 30 data set (Rodríguez et al. 2005), and a five-layer seabed geo-acoustic profile based on available literature (Table 3-7). The sound speed profile in this area has a strong sound speed minimum at ~60 m depth because of cold fresher water lying over warmer more saline water (e.g., Figure 3-18). Therefore, we expected that sound would refract towards the sound speed minimum and that there would be higher sound levels at 100 m recording depth compared to the lower recording depths (see Sabra *et al.*, 2016 for an introduction to long range underwater sound propagation). Due to the width of the measured sound duct (~15 m/s change from 30 to 100 m depth) the measured sound levels at higher frequencies maybe slightly less than could have been measured at 60 m at long ranges.

Per-pulse SELs were converted to T_{90} SPLs using a range-dependent estimate of the pulse length. The pulse length was estimated by generating a synthetic pressure waveform for the airgun array through a Fourier synthesis of the waveform. The vertically and azimuthally directional starting field for the sound propagation model was generated in 1-Hz frequency bins from 10–2000 Hz, based on the source signature computed by AASM and the relative position of each array element. The propagated

sound field was summed across frequency, and then an inverse Fourier transform was performed to obtain the modeled waveform. The pulse length was obtained from the modeled waveform to produce a per-pulse SEL to SPL conversion factor. During the pre-survey modeling, two conversion factors were estimated, one eastward from Station BB1 and the other westward from BB1. For the post-survey analysis, a conversion factor along bearing of 030º (northeast) from Station BB1, towards BB3, was computed.

During data analysis, the measured and modeled sound levels were compared. Further modeling was performed to investigate if the differences between the measured and modeled sound levels could be reduced by increasing the frequency resolution of the modeling, running the model with the measured sound speed profiles, or using the bathymetry measured by the seismic vessels.

3.2.4. 2012 and 2013 Greenland Seismic Surveys

Seismic surveys were conducted in the Shell-operated license areas in 2012 and 2013. The 2012 3-D survey was conducted by the *Polarcus Amani* and *Polarcus Samur* from 2 Aug to 15 Oct. In that year, each vessel towed two 3480 in^3 seismic arrays (Figure 3-17). The arrays on each ship were operated alternately so that the average sounding rate per ship was 10–12 s. The median survey speed was 2.25 m/s, or 8.1 km/h. The vessels operated independently throughout the survey. The ships occasionally operated in the same area on parallel acquisition lines, separated in time by a 4 h delay (32 km separation). Approximately 228,000 pulses from the *Amani* and 220,000 from the *Samur* were recorded. The median ranges of the *Amani* to Stations BB1, BB3, and BB4 were 42, 106, and 124 km, respectively (Table 3-1, Figure 3-16). The median ranges to the *Samur* were 36, 62, and 105 km, respectively. The vessel tracks that passed closest to

Station BB1 on 4 Sep and BB3 on 18 Sep are examined. Station BB2 measurements were similar to BB1, so only BB1 is analyzed in detail.

Two other seismic surveys occurred in summer 2012 in Baffin Bay. ConocoPhillips, DONG Energy, and Nunaoil jointly conducted a 2-D survey from 25 Aug to 24 Sep in the license area north of the Shell license area. This survey's closest point of approach was ~40 km to Station BB3 and 120 km to BB4. Maersk Oil conducted a 3-D survey from 6 Aug to 1 Oct in the license area southeast of the Shell license area. This survey's closest point of approach was 100 km to Station BB1 and at least 200 km from BB4 (Wisniewska et al. 2014).

From 15 Sep to 8 Oct 2013 the *Fugro Discovery* conducted a localized shallow-hazards survey for Shell Oil using a 140 in^3 array (Figure 3-16, Table 3-4). Shallow hazards surveys detect features that may impact proposed oil and gas operations such as gas vents, abnormal pressure zones, and fault lines. Here we present the data from Station BB6 as an example of measurements that were 40 or more kilometers from the shallow-hazards survey, and BB7 as an example of recordings within the region of the survey. The two summer data sets with seismic surveys are compared with the year-long data from Stations BB6 and BB10.

Table 3-1. Minimum, median, and maximum distances from the *Amani* and *Samur* to Stations BB1, BB3, and BB4 (Figure 3-1) in summer 2012.

Ranges from survey vessel to station	Minimum distance (km)	Median distance (km)	Maximum distance (km)	Median daily closest point of approach (km)
Amani to:				
BB1	0.1	42	89	16
BB3	0.02	106	153	40
BB4	68	124	158	95
Samur to:				

Ranges from survey vessel to station	Minimum distance (km)	Median distance (km)	Maximum distance (km)	Median daily closest point of approach (km)
BB1	0.7	36	90	14
BB3	0.6	62	153	25
BB4	68	105	158	95

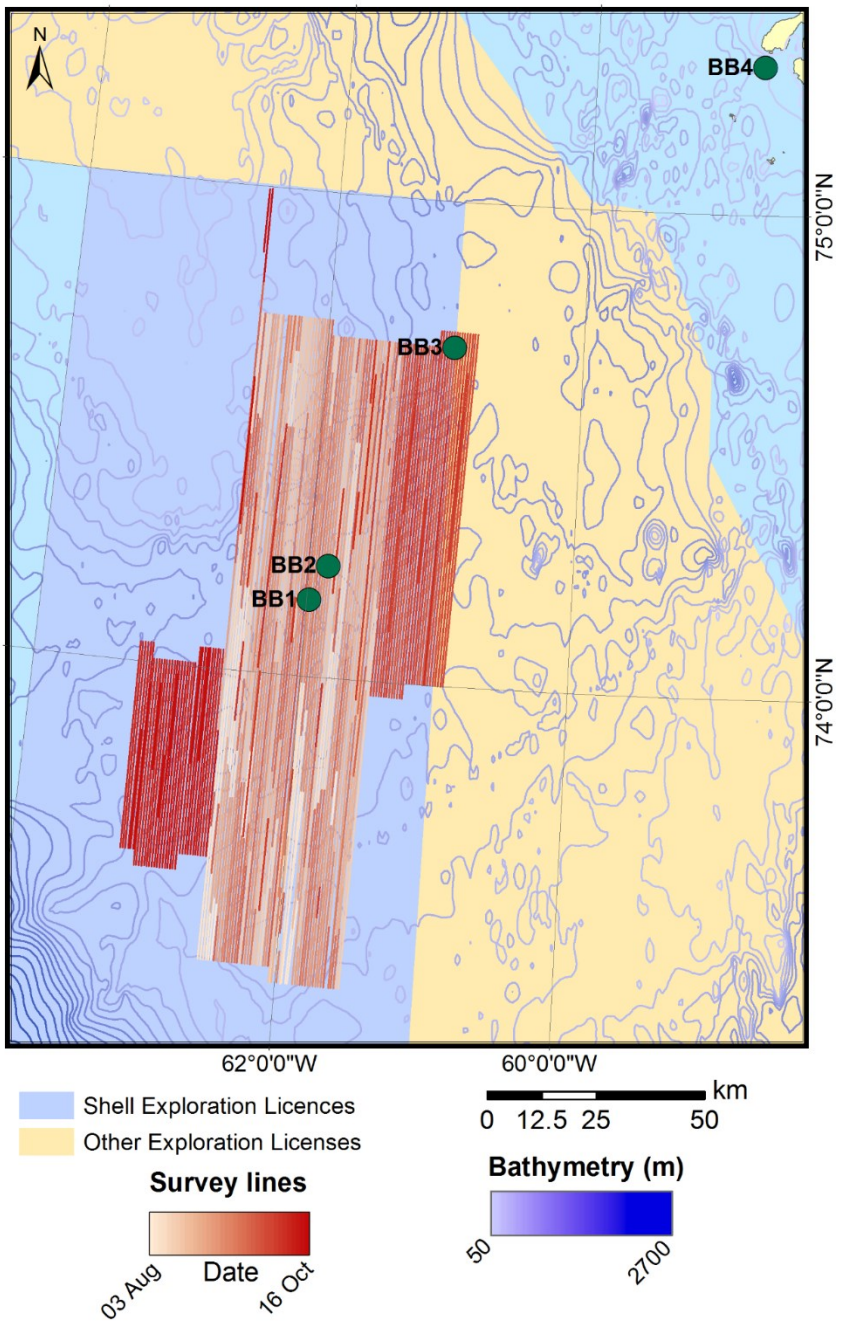

Figure 3-3. Survey lines of the *Amani* and *Samur* in summer 2012.

3.3. RESULTS AND DISCUSSION

3.3.1. Soundscapes of Baffin and Melville Bays

The various sets of acoustic data acquired during this project are characterized by different combinations of man-made and natural sounds (Figure 3-4): 1) the year-round recording at Station BB6 shows minimal man-made sounds; 2) the September 2013 recording at BB7 reveal few man-made sources until the start of the shallow hazards survey on 15 Sep; 3) the nearshore recordings in Melville Bay (BB4) from 2012 are dominated by glacial ice sounds; and 4) the BB1 recordings from 2012 prominently feature the 3-D seismic survey. When the seismic surveys started on 2 Aug 2012 and 15 Sep 2013, the average sound levels near the operations increased. The average 1-min SPL at Station BB1 was 106 dB re 1 µPa prior to 2 Aug 2012 and 134 dB re 1 µPa after that date, with most of the increase at frequencies below 100 Hz (Figure 3-4, Panel 4). The received sound levels at that station increased and decreased as the survey vessel approached and departed. Other stations (e.g., Station BB3, Figure 3-19) had similar results. The sounds from the surveys in the other license areas are not discernible in these figures.

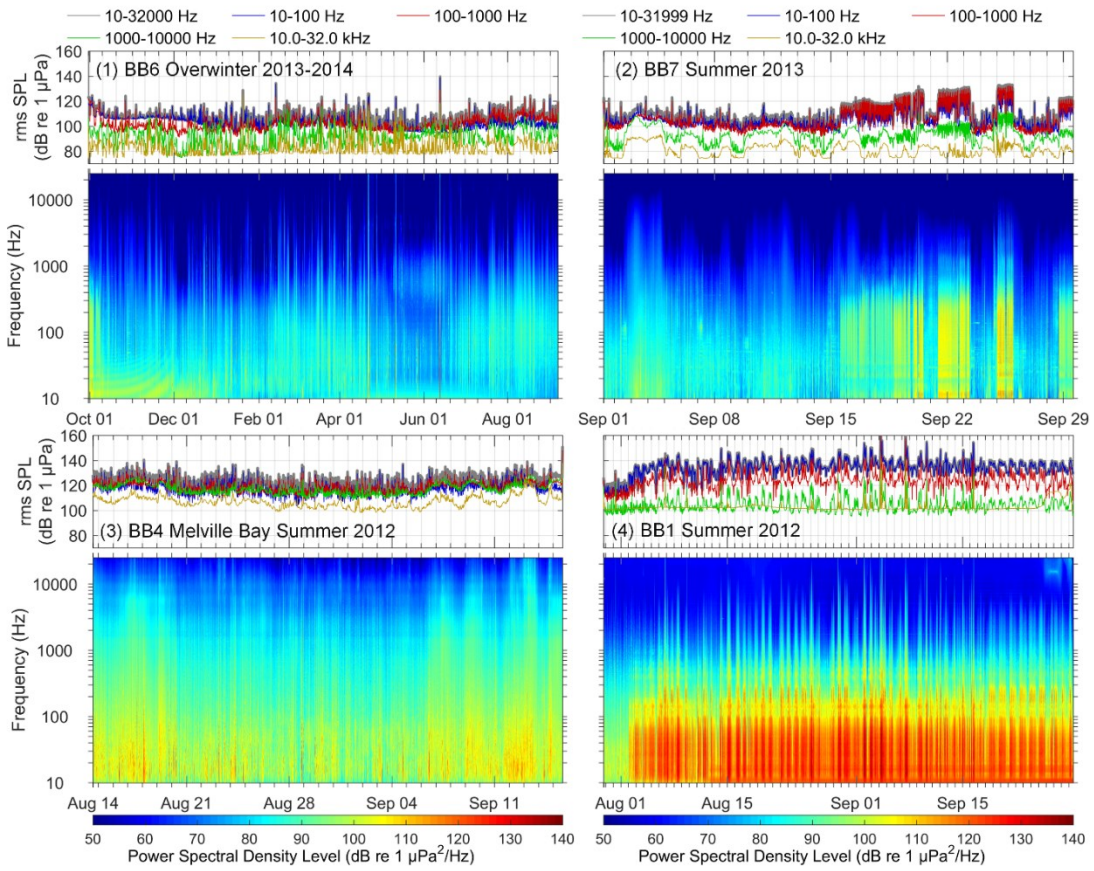

Figure 3-4. Summary of the received sound levels in Baffin Bay for four sound scenarios: 1) Station BB6 in overwinter 2013–2014 with minimal man-made sounds; 2) BB7 in summer 2013 at 3–100 km from a shallow hazards survey that started 15 Sep; 3) BB4 near glacial ice in Melville Bay in 2012; and 4) BB1 in summer 2012 at 0.1–90 km from the 3-D seismic survey that started 2 Aug. The bottom section of each figure shows long-term spectrograms and the top section corresponding band-level time series plots.

The summer 2012 stations were deployed 29 and 30 Jul and retrieved 29 Sep to 2 Oct (Table 3-4). Since the seismic survey started on 2 Aug, there were little data available from 2012 to assess the natural ambient soundscape in Baffin Bay. The summer 2013 and overwinter 2013–2014 recordings provide data for this purpose (Figure 3-5, Figure 3-19, Figure 3-21, Figure 3-23). Figure 3-5 shows the distribution of 1-min SPLs in four of these recordings. Broadband (10–32000 Hz) and four-decade bands are shown. The 10–100 Hz band normally contains sounds from natural and anthropogenic sources,

calls from the very large baleen whales, possible pseudo-noise from flow over hydrophones and cable strum. Large vessels, seismic surveys, baleen whales, as well as wind and wave action are the primary sources of sound in the 100–1000 Hz band. The 1000–10000 Hz band contained sounds from wind and wave action and potentially whistles from pilot whales and narwhals. The 10000–32000 Hz band contains energy from whistles, echolocation clicks, rain and high frequency man-made sources like echosounders and underwater communication modems (see Cato 2008, Hildebrand 2009 for a summary of ocean ambient noise).

Station BB6 is representative of ambient sound level measurements in Baffin Bay with a median SPL of 102 dB re 1 µPa in summer 2013 and 100 dB re 1 µPa overwinter 2013–2014 (Figure 3-5, Figure 3-21, Figure 3-23). There were few anthropogenic sound sources in this period, and no 3-D seismic surveys were conducted. The general shape of the spectra are similar to those reported from sonobuoy studies in 1981 (Leggat et al. 1981). The 100–1000 Hz band, driven by wind action, has the highest sound levels during summer. During winter, ice cover reduced the sound levels above 100 Hz from December to May (Figure 3-21, Figure 3-23) (see also Roth et al. 2012). Biologic sound sources were infrequent, with the exception of bearded seals (*Erignathus barbatus*) in May and June (Frouin-Mouy et al. 2017).

The sound spectra recorded at Station BB4 in Melville Bay were consistent with glacial ice melt. The median 1-min SPL was 116 dB re 1 µPa, 14 dB higher than the 102 dB re 1 µPa at Station BB7 in summer 2013 (Figure 3-5, Figure 3-20, Figure 3-23). The highest Melville Bay sound levels were in the 1000–10000 band, whereas in the data from other stations the 1000–10000 Hz band was much lower than the 100–1000 Hz and

10–100 Hz bands. Listening to the sound files from Station BB4 (e.g., the data represented in Figure 3-22) reveals many instances of ice cracking, as well as pops and hisses that are likely caused by air escaping from melting glacial ice (Pettit et al. 2015). This is reasonable given that this recording was made near the Greenland coast and its calving glaciers (Figure 3-1).

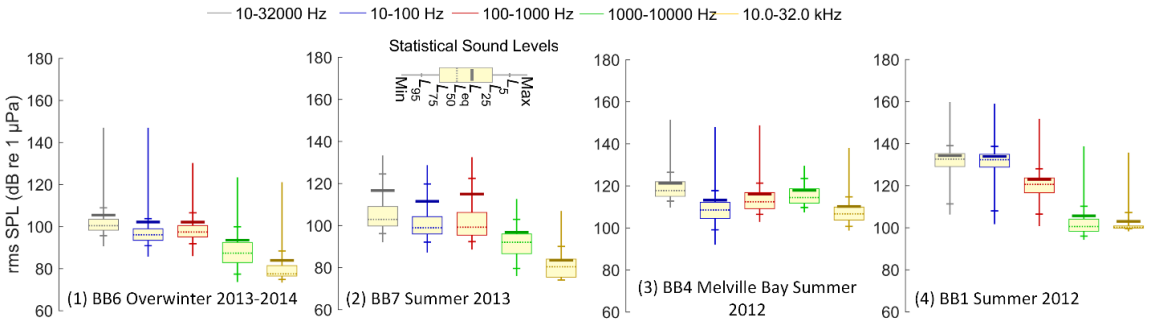

Figure 3-5. Comparison of the statistical received sound level distributions for the four sound scenarios in Figure 3-4 . From left to right the bands are 10–32000, 10–100, 100–1000, 1000–10000, and 10000–32000 Hz.

Seismic pulses were rarely detectable at Station BB4 (e.g. Figure 3-4), and the 1-min SPL was uncorrelated with the distance to the *Samur* and *Amani* (Figure 3-6, r^2 = 0.017, SE = 0.31). The periods with higher sound levels (e.g., 7–11 Sep, Figure 3-4) did not contain pulses originating from the seismic surveys in the adjacent lease areas either; instead, these periods contained more loud ice cracking events than the quieter periods.

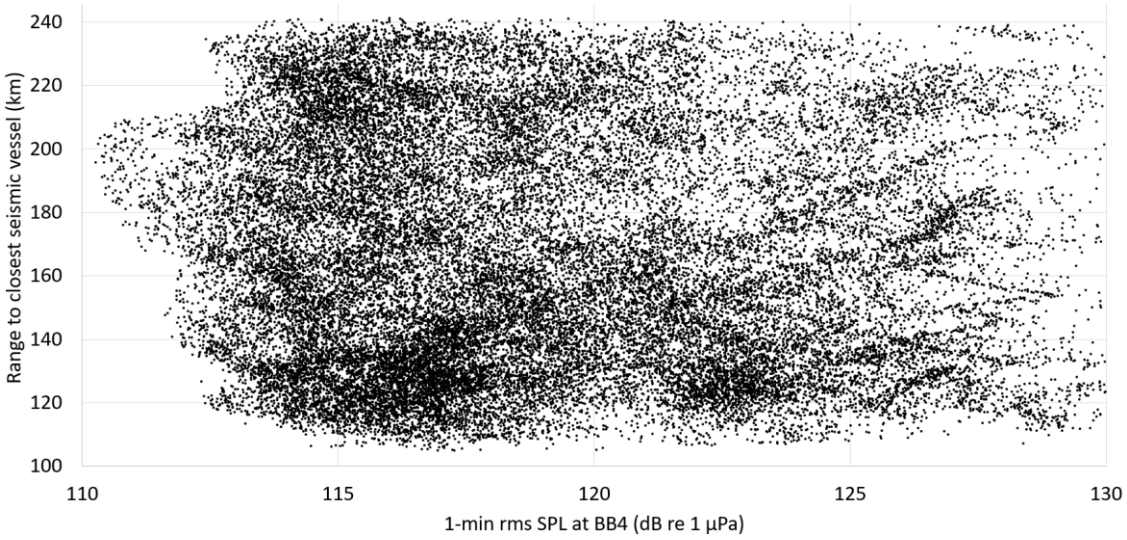

Figure 3-6. Ranges from Station BB4 to the Samur and Amani in summer 2012 and the 1-min SPL.

The octave-band 1-min SPLs at Station BB6 in September 2013 (Figure 3-23, Table 3-8) were used to establish a threshold where the seismic survey sounds would stand out against the ambient background sounds and begin masking other sounds in the same band as the received seismic energy (see Section 3.3.7). The data preceding the 2012 seismic survey were not used because the time period was quite short and the dynamic range of the 2012 ambient recordings was limited by the low sensitivity of the M8E−0dB hydrophones (see Table 3-6).

3.3.2. Nature of Seismic Airgun Pulses in Baffin Bay

The seismic pulses recorded in Baffin Bay showed very strong multipath arrivals for source-recorder ranges (or separations) of less than 40 km (Figure 3-7, Figure 3-8). The pattern of arrivals depended on the depth of the hydrophone, the water depth (770 m), and the range to the seismic vessel. At 100 m hydrophone depth Figure 3-7), the pulses arrived in pairs, where the first one was the upward traveling reflection from the seabed and the second was the downward traveling surface reflection. As the range to the

vessel increased, the time between the impulses in each pair decreased due to the reduced differences in path length. The number of pairs arriving at the hydrophone also increased with range. At the 400 m hydrophone (Figure 3-8), the path lengths between the bottom and surface reflections were the same; hence, the impulses were evenly spaced. Similar to the measurements at 100 m water depth, the number of impulses increased with the distance to the vessel. The additional impulses increased the 90% energy duration every time an additional propagation path became important (Figure 3-9). The duration decreased with range as the length of the propagation path shortened. At ~40 km from the source, the number of arrivals depended on many propagation variables (e.g., bathymetry, bottom scattering roughness, weather), and the pulse lengths ranged from 2 to 6 s (Figure 3-9).

Also, at ~ 40 km from the source, the received signal at 100 m depth began to exhibit a frequency upsweep pattern in the first 0.5–1 s of the pulse time series. This pattern became the dominant spectral feature at ranges greater than 40 km. These sweeps were the result of the sound being refracted into a low-velocity sound channel (Figure 3-18). Higher frequencies were refracted more steeply than the lower frequencies, resulting in a longer path length and thus later arrivals at higher frequencies. Upsweeps were faintly present at 200 m depth, but they were not detected at 400 m depth (Figure 3-8).

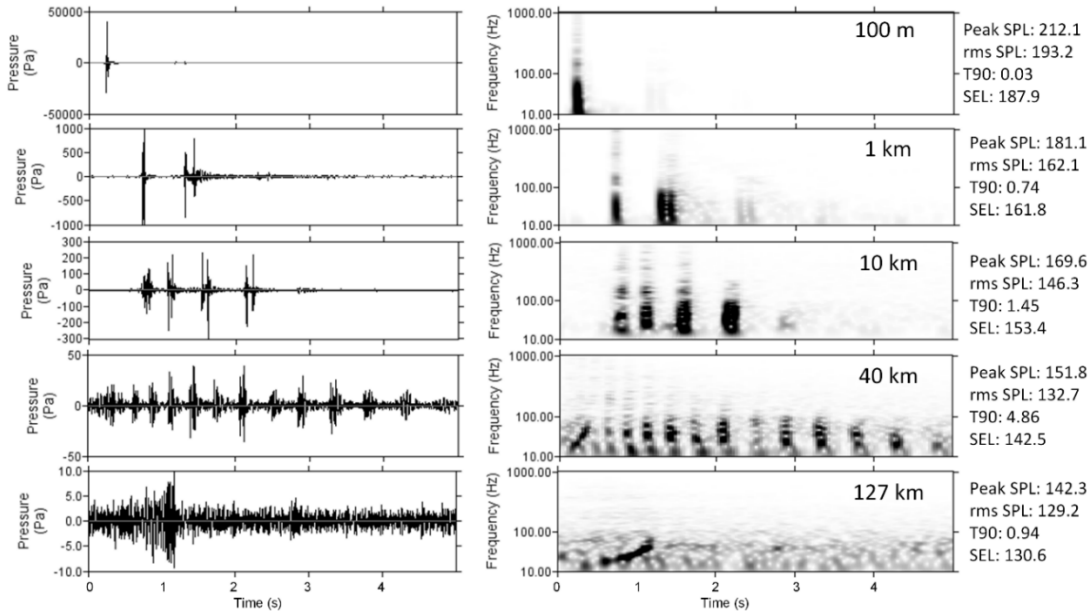

Figure 3-7. Shape of 3480 in^3 seismic array pulses at progressively longer ranges from Station BB3 in 770 m water depth at the 100 m deep hydrophone. All figures show 5 s of data. (Left) Time series waveforms, and (right) spectrograms (1 Hz resolution, 0.2 s of data per FFT (0.8 s zero-padding), 0.19 s overlap between FFTs, Hamming window). The SPL and SEL are for the T90 window durations shown.

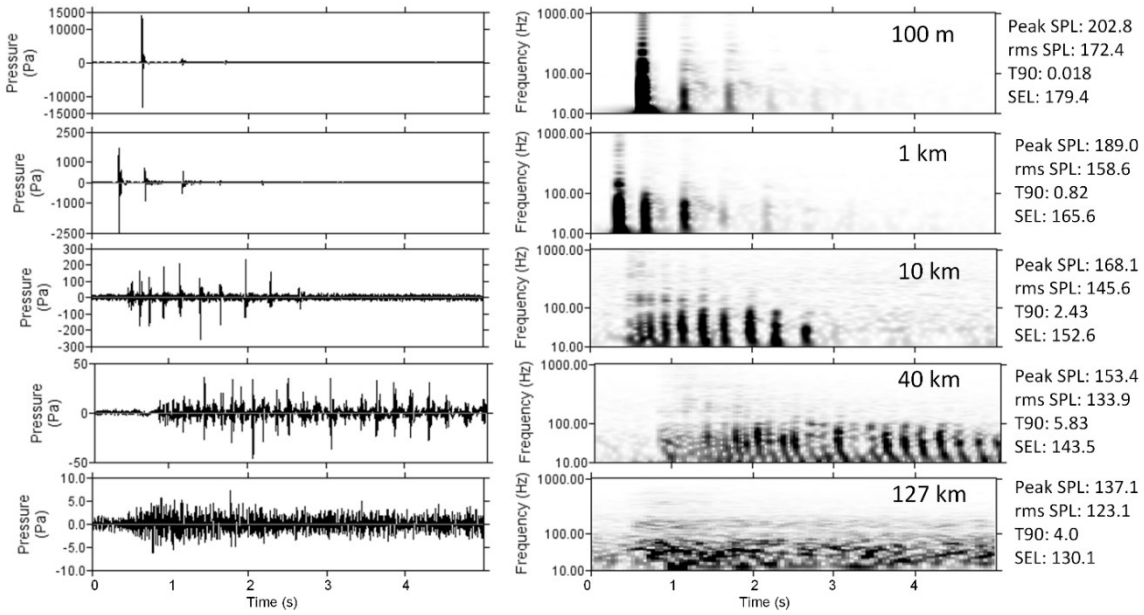

Figure 3-8. Shape of 3480 in^3 seismic array pulses at progressively longer ranges from Station BB3 in 770 m water depth at the 400 m deep hydrophone. These are the same pulses as shown in Figure 3-7 at 100 m depth. All figures show 5 s of data. (Left) Time series waveforms, and (right) spectrograms (1 Hz resolution, 0.2 s of data per FFT (0.8 s zero-padding), 0.19 s overlap between FFTs, Hamming window). The SPL and SEL are for the T_{90} window durations shown.

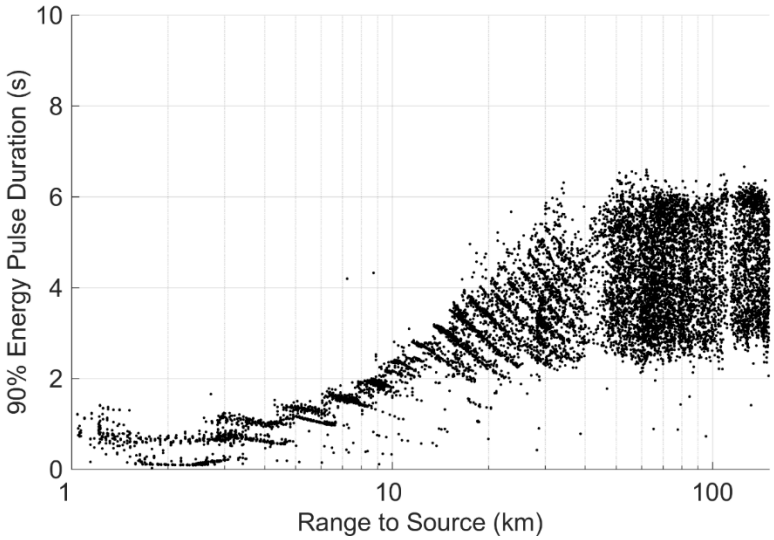

Figure 3-9. The 90% energy pulse duration compared to range for the data received at Station BB1 and BB3 on the 100 m deep hydrophones. Data were selected from 3.7 days when only a single seismic vessel was active. Ranges to the vessels were 1–150 km. For each minute of seismic activity, the five pulses with the highest energy were selected and plotted.

The pulses recorded in Baffin Bay had a different character than those reported from other deep-water measurements, in that the direct arrival and subsequent multipath arrivals in the recordings from Baffin Bay study had similar amplitudes (within 1–6 dB). These signal characteristics were sustained at ranges between 1 and 40 km, unlike those reported by Madsen et al. (2006a) from deep waters in the Gulf of Mexico where the first arrival had much higher levels than the multipath arrivals. The pulse structure was also different than the long reverberant pulses observed at intermediate ranges in deep water in the Lau Basin by Bohnenstiehl et al. (2012); however, the long range pulses (127 km) recorded at 400 m depth in Baffin Bay were similar to the Lau Basin pulses at comparable ranges (Figure 3-8).

The presence of many multipath arrivals in the present data suggests a smooth and flat seabed with a high reflection coefficient in the Baffin Bay project area. The Lau Basin region, by comparison, is a tectonic spreading zone with a very high sound speed bottom (primarily basalt with little surface sediment accumulation) that should be an excellent reflector. However, random seafloor deformations at the Lau Basin spreading zone scatter the higher frequencies so that only low frequencies propagate long distances. We note, by contrast to the deep-water propagation conditions in Baffin Bay and the Lau Basin, that seismic pulses received in shallow water areas (<100 m) are affected by shallow water filtering (Urick 1983), head waves from higher speed propagation in the substrate, and modal dispersion (Guerra et al. 2011, Guan et al. 2015).

3.3.3. Cumulative Sound Exposure and Predictions of Ranges to Radii for Auditory Injury of Marine Mammals

As discussed in the introduction to this chapter, recent regulatory frameworks for assessing and mitigating the effects of sound on marine life (Southall et al. 2007, Popper et al. 2014b, NMFS 2018) use two criteria to assess the risk of auditory injury: peak sound pressure level and cumulative SEL. For airgun arrays, the peak sound pressure level drops below the injury threshold level for marine mammals at a range of tens of meters. The cumulative SEL drops below the suggested regulatory sound levels for injury at ranges of hundreds of meters to 1 km +. This is the zone that must be monitored for protection of marine mammals (Matthews 2012b), especially for stationary receptors. Thus, an analysis of the cumulative SEL metric using the Greenland data may be instructive for future regulatory discussions.

The radius around the source where the measurements suggest possible auditory injury to marine mammals depends on which set of thresholds and auditory weighting functions are used. The *Guidelines to Environmental Impact Assessment of Seismic Activities in Greenland Waters* (Kyhn et al. 2011) mandates the M-weightings and thresholds recommended in (Southall et al. 2007). In the intervening period between the project and present, new approaches have been proposed by the National Ocean and Atmosphere Administration (NOAA) for the United States (NOAA 2013, NOAA 2015, NMFS 2016). Each approach proposed different auditory weighting methods and thresholds for auditory injury and behavioral disturbance. To estimate the ranges when the cumulative SEL exceeded the thresholds, we computed the frequency-weighted daily SEL at Stations BB1 and BB3 and plotted them against the closest point of approach of the seismic vessels for that day (Figure 3-10, using the Southall et al. (2007), (and NMFS

2016) recommendations). The Southall et al. (2007) weighting functions and thresholds predict potential hearing damage for pinnipeds at ranges of 600 m from the array and that low-frequency cetaceans could be injured at very close ranges (<100 m, Figure 3-10). The NMFS Technical Guidance (NMFS 2016) weighting functions and thresholds predict that the acoustic energy from this survey could injure high-frequency cetaceans at ranges of less than 500 m (Figure 3-10). On eight days when the seismic vessels' closest points of approach to the stations were greater than 10 km, the measured exposure levels exceeded the high-frequency cetacean threshold. Our review of these events showed that seismic sounds were present; however, additional energy from the close passage of other vessels increased the sound levels in the high-frequency weighted cetacean SEL for those days. The vessels were likely the seismic support vessel running ahead of the seismic vessels to ensure there are no obstructions that could affect the seismic arrays. The NMFS Technical Guidance threshold for exposure of high-frequency cetaceans to non-impulsive sounds is 173 dB re 1 $\mu Pa^2 \cdot s$; these exposures do not exceed the threshold. The data were included as 'seismic' by the automated processing since detection was performed on unweighted data and the weighting applied to the impulses after detection. These results highlight the need for continued research into the appropriate auditory weighting functions for marine species, the effects of sound on marine life, methods of data analysis, and thresholds that will minimize impacts.

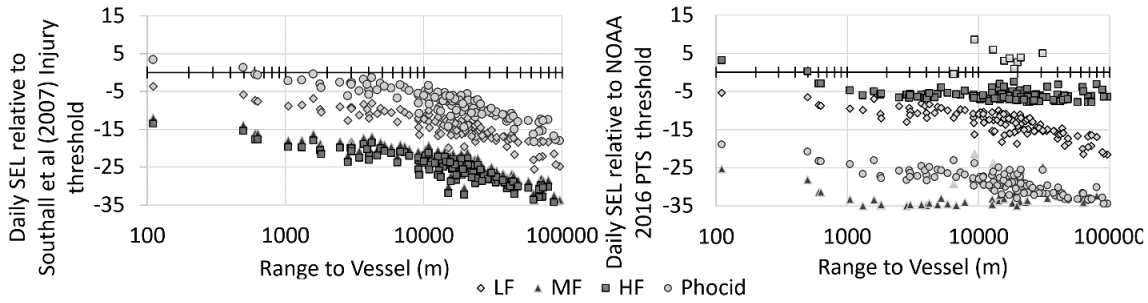

Figure 3-10. Exceedance of frequency-weighted daily SEL compared to injury metrics versus the closest range to either seismic vessel for the 100 m hydrophone at Station BB1. (Left) Southall et al. (2007) injury threshold. (Right) NMFS Technical Guidance (2016) permanent threshold shift (PTS). Positive values exceed the thresholds. Frequency band abbreviations: LF – low-frequency cetacean auditory weighting; MF - medium-frequency cetacean auditory weighting; HF - high-frequency cetacean auditory weighting; Pinniped - pinniped weighting from Southall et al. (2007) and the phocid weighting from NMFS Technical Guidance (2016). The light-gray shaded high-frequency data also contained energy from the close passage of vessel and hence are comparable to the threshold of 173 dB re 1 $\mu Pa^2 \cdot s$ rather than 155 dB re 1 $\mu Pa^2 \cdot s$, and hence do not constitute an exceedance of the thresholds.

3.3.4. Depth Dependence of Seismic Pulse Energy

DCE's review of the possible effects of seismic surveys on marine life raised the question of variation in the received levels as a function of depth (Wisniewska et al. 2014); therefore, our study recorded acoustic signals at 100, 200, and 400 m below the sea surface. We found that the SPL, per-pulse SEL, and 24-hour SEL showed only minor variations in the received sound levels as a function of depth in Baffin Bay. Figure 3-7 and Figure 3-8 show that the received sounds at ranges beyond 40 km from the source at a 100 m depth contained a low-frequency upsweep that was not present at 200 and 400 m depth, as described in the Section III.B. In the longest-range case (127 km), the SPL at 100 m depth was 6 dB higher than at 400 m; however, the pulse was also 4 times shorter at 100 m, which resulted in the same SEL at both depths.

At close ranges (0–3 km) there were differences with depth in the received signals that depended on the multipath reflections arriving at different times and the vertical

beam pattern of the seismic array (Figure 3-11). The airgun array pulse originates almost at the surface and propagates outwards, arriving at the 100 m deep hydrophone first, then the 200 m and 400 m deep hydrophones. The pulse then reflects off the seabed and the reflected pulses arrive at the hydrophones in the opposite order – 400 m, then 200 m and last at the 100 m. The pattern reversed again for the subsequent surface reflection (Figure 3-11). Seismic arrays concentrate sound in the vertical direction with an angular beam width that depends on frequency (Figure 3-24). As the vessel approached within 1 km of the recording station, the deepest hydrophone 'entered' the beam first, and therefore as the vessel approached the received sound level at 400 m depth rose before the levels at the 200 and 100 m depths (Figure 3-11). At the closest point of approach, all three hydrophones were almost entirely in the main lobe of the seismic array, so that the 100 m deep hydrophone had the highest sound levels since it was closest to the array and had the lowest geometric spreading loss.

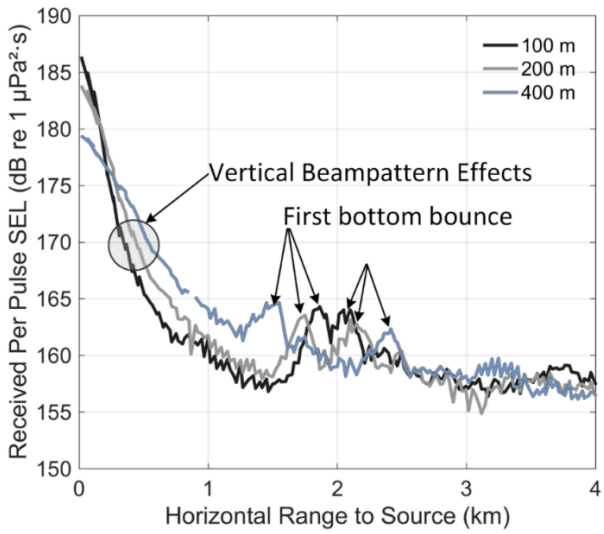

Figure 3-11. Per-pulse SEL for 125 ms impulses detected at Station BB3 hydrophones from the 3480 in^3 seismic source as it passed the station on 18 Sep 2012. Differences in received sound levels were primarily within the first 3 km from the source.

The daily SEL integrates the received exposure levels over a 24-hour period and provides a macroscopic assessment of the sound levels as a function of depth. The SELs were virtually identical at all depths, except when the source passed directly over the receivers. The single pulse SELs at the closest point of approach differed by 7 dB between the 100 and 400 m recordings on 18 Sept 2012 (Figure 3-11), yet the daily SELs only differed by 2 dB (Figure 3-12). The frequency content at all depths was also virtually identical (not shown). We conclude that for the purposes of assessing the possibility of auditory injury or behavioral disturbance to marine mammals, the sound levels as a function of depth can be treated as uniform for the conditions in Baffin Bay.

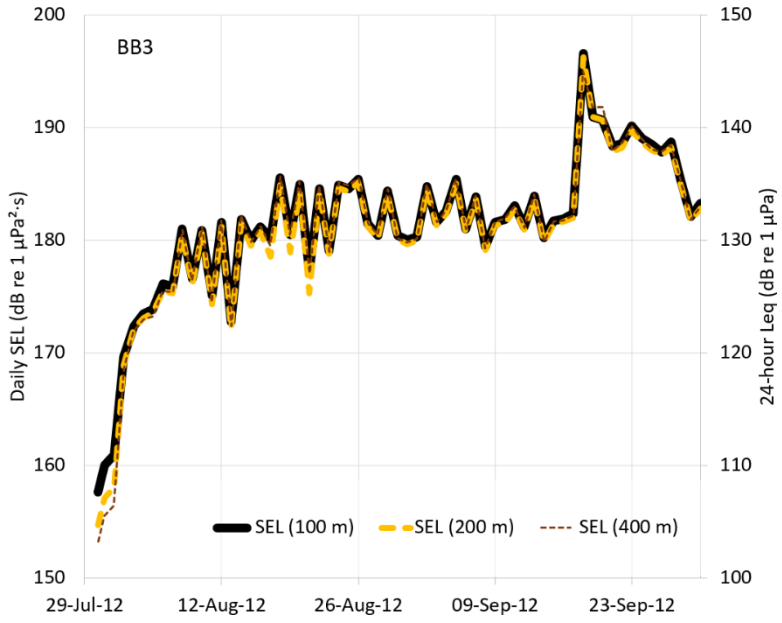

Figure 3-12. Daily SEL at Station BB3 for the entire recording period at each hydrophone depth. Differences in SEL between depths were only measured before the seismic program started and when the source passed directly over the receivers. Stations BB1 and BB2 produced similar results.

3.3.5. Verification of Propagation Modeling Results with Actual Environmental Inputs

A knowledge gap identified during the pre-survey modeling effort (Wisniewska *et al.*, 2014) was the poor understanding of the dependence of acoustic propagation model results on the accuracy of the environmental inputs, since there was little high-fidelity data available for Baffin Bay to base such an analysis on. The acoustic measurements collected as the seismic surveys passed Stations BB1 and BB3 enable us to directly compare the environmental parameters used for the pre-survey acoustic modeling (Matthews 2012b). The acoustic propagation model was re-run with the source at the vessel's closest point of approach to Station BB1 along the radial from BB1 to BB2 and BB3 (Figure 3-1). The measured per-pulse fixed window SPL as the ship approached Station BB1, as well as the simultaneous measurements at BB2 and BB3, were compared to the pre- and post-survey modeled SPLs. The SPLs were computed by applying a range-dependent conversion factor to the SELs modeled by MONM. The conversion factor was computed by running a full waveform version of MONM and computing the pulse duration as a function of range. The pre-survey modeled levels were 3–7 dB higher than the measured values at ranges greater than 500 m (Figure 3-13, left). Using the measured sound speed profile did not improve the error substantially. The results were improved (Figure 3-13, right) by recalculating the conversion factor. The full waveform model was re-run using the bathymetry measured by the seismic survey vessels along the line from Stations BB1 to BB3 and the measured sound speed profile (Figure 3-25, Figure 3-18). The pre-season conversion factor had been computed along two radials, one

from Station BB1 east and the other west. By using the more accurate conversion factor, the error reduced to 0–4 dB, even 65 km from the source.

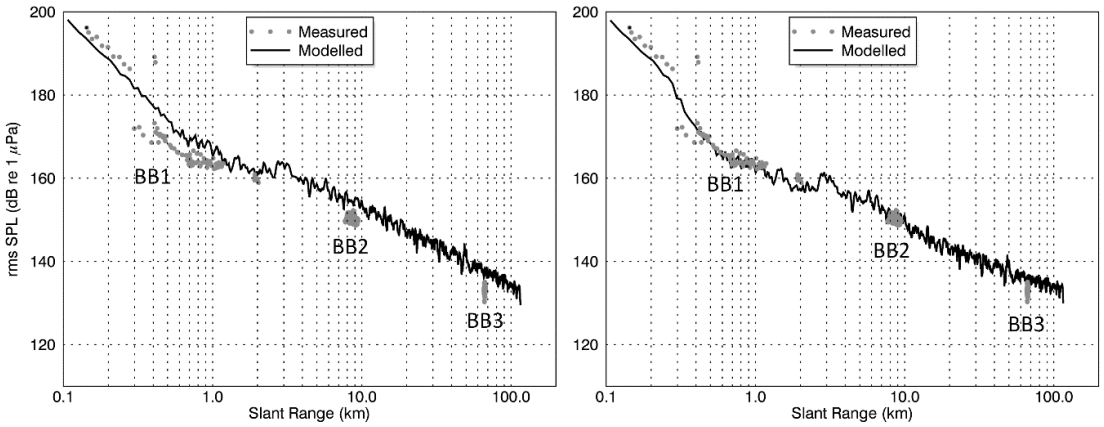

Figure 3-13. Comparison of the per pulse fixed window SPL at Stations BB1 to BB3 on 4 Sep 2012 as the *Amani* passed over the hydrophones at BB1 with the modeled outputs (left) using the pre-survey sound-speed profile, bathymetry, and SEL-SPL conversion radials, and (right) using the measured sound-speed profile, bathymetry, and SEL-SPL conversion radial from BB1 to BB3.

3.3.6. Approaches for Computing SPL

The first regulatory guidance for limiting effects of sound on marine mammals used the per-pulse SPL as the threshold metric for both behavioral disturbance and injury (NMFS and NOAA1995). Subsequent research has concluded that dual thresholds for the peak sound pressure level and weighted sound exposure levels are appropriate for limiting injury from sound (Southall *et al.* (2007), Popper et al (2014), NMFS 2018), however no direction has emerged for behavioral disturbance. Madsen (2005) clearly articulates the issues with variable length windows when calculating an impulsive SPL. Here we provide results from the long-term and long-range Baffin Bay dataset that supports Madsen's assertion. We demonstrate that if SPL must be used, any fixed window duration is preferable to a variable length window (e.g. the 90% energy

duration). We then show how this result supports Tougaard et al (2015) argument that it is essential that the metric used to establish a regulatory threshold be the same one that is used to measure compliance.

Measuring the peak and average sound levels is inherent in any study of the response of marine life to sound stimuli. In addition to the behavioral state of animals, the wide variability within and between the responses of individual animals makes it difficult to understand what elements of the sound are eliciting a response (Ellison et al. 2012, Southall et al. 2019a). It may be the similarity of a sound to predator calls, frequency content, absolute level, duration, the onset of the sound, rise time, perceived distance to the source, perceived motion of the source, or other cues not yet discovered (Wartzok et al. 2003, [NRC] National Research Council 2005, Nowacek et al. 2007, Southall et al. 2007, Gedamke et al. 2011, Ellison and Frankel 2012, Pirotta et al. 2012, Risch et al. 2012, Deruiter et al. 2013, Goldbogen et al. 2013, Popper et al. 2014b, Miller et al. 2015). Early studies of the effects of impulsive sound on marine life measured the SPL over a time window that includes 90% of the pulse energy (Blackwell *et al.*, 2004; Thode *et al.*, 2010). Madsen (2005) and Madsen *et al.* (2006) advocate computing the SPL over a maximum window of 100–200 ms, the presumed integration time range of the hearing system for most mammals, including all marine mammals that have been tested.

We compared how the peak sound pressure level and the SPL changed as the seismic source approached the recorders. The SPL was computed three ways: with a 125 ms fixed window, a 1-min fixed window, and a variable window that included 90% of the pulse energy. The 125 ms window has been shown to be near the time span over which mammalian ears integrate sound, and it applies to both terrestrial and marine

mammals (Plomp and Bouman 1959, Johnson 1968, Kastelein et al. 2010). In particular, Tougaard *et al.* (2015) transpose measurements from 11 other studies to the signal level in a 125 ms 'leaky integrator' and demonstrate that the onset of disturbance using this integration time was 40–50 dB above the porpoise audiogram and closely followed the shape of the audiogram. We chose to use a fixed duration 125 ms fixed window since it is much easier to implement than the leaky integrator and has a maximum difference in calculated sound levels of 2 dB compared to the leaky integrator—a difference far smaller than the spread of SPL values associated with marine mammal disturbance (Tougaard *et al.*, 2015). The fixed window also has the advantage of estimating conservative sound levels for pulses with high initial amplitudes and long reverberant tails, such as those from seismic surveys and pile driving.

For this analysis, we choose 3.7 days of data from the 100 m deep hydrophones at Stations BB1 and BB3 during periods when only a single seismic vessel was active. Ranges to the vessels were 0.5–150 km. As expected, the results of all four methods of computing the SPL exhibited a common trend of increasing sound levels as a vessel approached the recorder (Figure 3-14). However, each of the metrics had different slopes as a function of range, and different degrees of variability in the instantaneous variance and the deflections of the smoothing curve. The variance of the individual measurements increased with decreasing integration time, but the smoothing curves had fewer deflections. With longer integration times, there was less variance in the individual measurements, but the smoothing curve showed larger deflections, providing better insight into the average change in propagation loss as function of range. The T_{90} SPL was closer to the 125 ms SPL at short ranges, and closer to the 1-min SPL at long ranges. We

expect that the variability depends on range, water depth, bottom shape, and bottom type. Therefore, the relationship between the T_{90} SPL will be more dependent on the environment than the peak sound pressure levels, 125 ms SPL and 1-min SPL, which is undesirable for a regulatory metric.

Given the variable nature of the attenuations, the data were fit with an additive model (mgcv::gam; Wood, 2004), which smoothly followed the changing sound level attenuation as a function of range (e.g., Figure 3-14 and Figure 3-11). The additive models were fit with 6–20 knots (e.g., gam(SPL ~ s(range, k=20))). These models had a lower Akaike Information Criterion (AIC) scores than linear models of the form (SPL ~ log10(range) + range) and provided a better representation of the data. We recommend the use of additive models for predicting sound exceedance isopleths for measurement programs where the attenuation changes with range (i.e., from spherical-like spreading to cylindrical-like spreading (Figure 3-11))

Additive models were generated for each averaging duration and used to compute the range where the peak SPL and SPL dropped below 120, 130, 140, 150, 160, 170, and 180 dB re 1 µPa (Table 3-2). The ranges to the isopleths were highly dependent on the integration times. For example, the 160-dB isopleth was 48 km for the 125 ms integration time, but 26.5 km using the 90-percent energy windows and 11.6 km for 1-minute integration. This result underscores the argument made in Tougaard *et al.* (2015) that measurements performed to assess compliance with a regulatory threshold must use the same metric that was used to establish that threshold. Regulatory directions and/or international standards should specify the signal analysis methods, as well as the thresholds to maximize consistency between localities and projects. Whenever possible

the methods must be simple for regulators and project teams to implement. The 125 ms SPL is attractive for assessing seismic sources because 1) the duration is well matched to the length of the peak energy of the pulse in many environments; 2) it is near the length of time that the ears of many species groups integrates sound; 3) it is the fast-time weight duration in many sound level meters; and 4) it was shown by Tougaard et al (2015) to be a good predictor of the sound level at which porpoise respond to sound. We also note that the use of broadband SPL to predict behavioral reactions will likely be revisited. Like the weighted sound exposure levels used to estimate the onset of permanent threshold shift (PTS) and temporary threshold shift (TTS), we expect that audiogram-weighted SPL are better predictors of behavioral reactions.

Table 3-2. Radii (km) to SPL isopleths predicted by mgcv::gam additive models for the sound levels (e.g. Figure 3-15) generated using 3.7 days of data from time periods when only one seismic array was active. <0.1 and >150 indicate that the result is outside the range where extrapolation is considered unreliable.

Isopleth SPL (dB re 1 µPa)	Peak sound pressure level	125 ms fixed window	T90 SPL	1-min SPL
180	1	<0.1	<0.1	<0.1
170	6	0.5	1.5	<0.1
160	13.8	6	3.4	<0.1
150	41.8	14.8	8.3	1.6
140	111.8	48.3	23.1	11
130	>150	>150	75.1	54.1
120	>150	>150	>150	>150

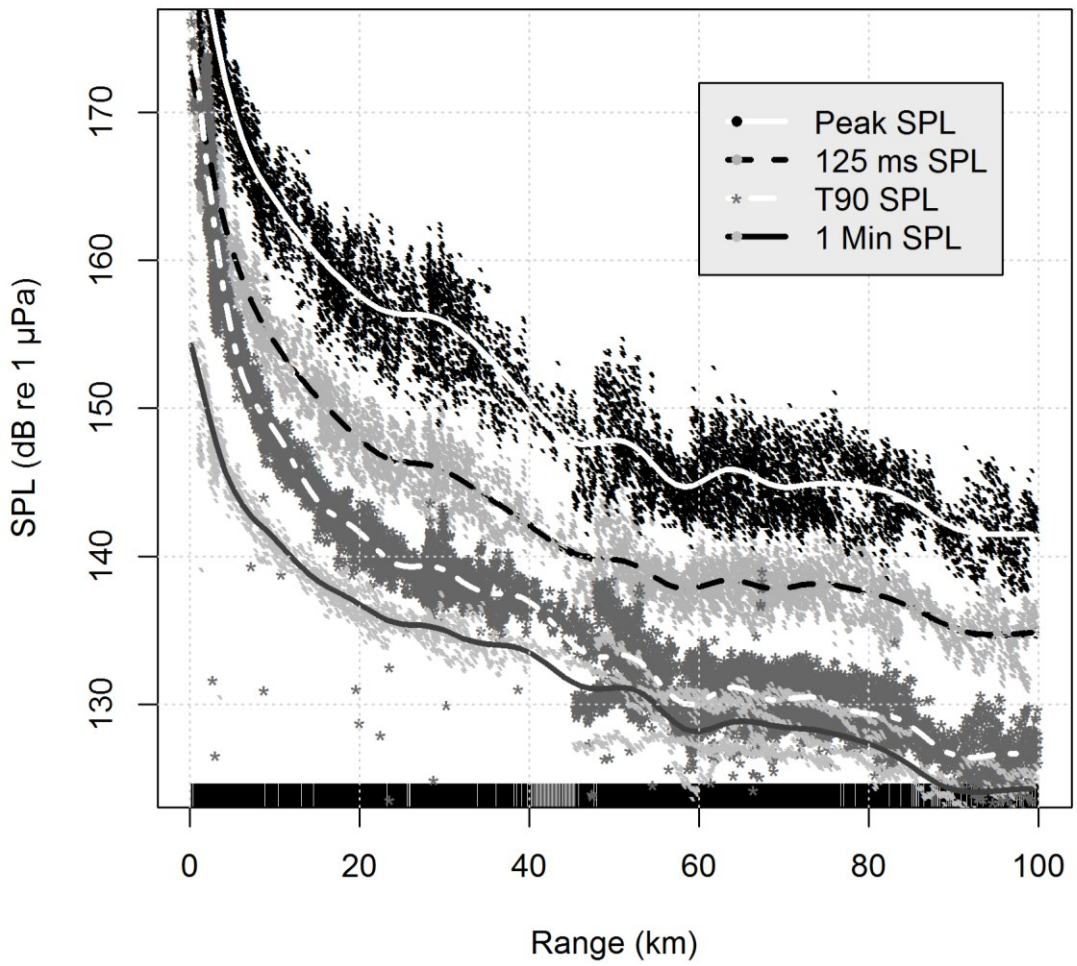

Figure 3-14. Analysis of the peak SPL and SPL computed using three different averaging durations as a function of range to the source vessel. 3.7 days of data from periods when only one ship was emitting are shown; the 100 m hydrophones were used in all cases.

3.3.7. Spectral Content of the Measured Data

We need to understand the spectral content of seismic pulses propagating over long distances to inform studies on the potential for seismic surveys to disturb marine mammals that communicate at frequencies above 1 kHz or to mask their communications or foraging calls (Goold and Fish, 1998; Madsen *et al.*, 2006; Hermannsen *et al.*, 2015). Masking is likely an important consideration of the effects of seismic sound on fish who use low amplitude low-frequency sound to synchronize mating (Nordeide and Kjellsby

1999, Dalen et al. 2007). The contributions of seismic survey sound below to the environment and hence to masking are better understood. The hydrophones at 100 m depth were sampled at 64 kHz; and the data thus provide information on the spectral content of seismic pulses up to 30 kHz over ranges of 0.1–150 km from the seismic source. For this investigation, we used the same 3.7 days of data that were selected for the SPL investigation (Section 3.3.6). The peak sound pressure level as well as the broadband SPL and SPL in 11 octave bands were plotted against the range to the seismic array. We computed the SPL using the 1-min (Figure 3-15), 125 ms (Figure 3-26), and 90% energy duration (Figure 3-27) window to help illustrate the differences between these metrics.

Additive models for the peak sound pressure level, SPL, and SPL in the octave bands from 16–16000 Hz were generated and used to determine where the SPL exceeded the median sound levels in the same band measured in September 2013 by 20 dB (Table 3-3). Twenty decibels was chosen as a general critical ratio for detectability of signals in noise at lower frequency bands across species groups (Au and Hastings 2008, Erbe 2008, Gaspard et al. 2012, Sills et al. 2014, Sills et al. 2015). Using the 1-min SPL as an indication of the average sound level from the seismic survey in Greenland waters, the range was 80 km for the 125 Hz band and decreased to 5.7 km for the 16 kHz octave band (Table 3-3). An assessment of masking effects between pulses (Guan et al. 2015) using a tool such as listening space reduction (Pine et al. 2018) is recommended. Note that the 16 kHz band integrated sound from 11 to 22 kHz; the large bandwidth increased the background levels compared to other bands, so that the noise floor of the recorder was reached at 6 km in this band (e.g., Figure 3-15). For the 16 kHz band, only up to 4 km was used to generate the additive models and predicted results would have been rejected

if the range exceed 8 km. For all other bands with predicted ranges less than 150 km, the models were only interpolated and not extrapolated.

We carefully reviewed the data collection, data analysis, and sound propagation effects to verify that these high-frequency measurements were real. We conducted a detailed review of the signal analysis software and verified that the high-frequency components were not an artefact of spectral leakage in the Fourier transforms. Because the multipath features of the signals measured at 100 m and 400 m depth were very similar (Figure 3-7, Figure 3-8), we are confident that the frequency content is similar throughout the water column, at least to 40 km from the source. Beyond 40 km, the high-frequency content measured on the 100 m deep hydrophones may be unrepresentative of the full water column. The hard and flat bottom conditions that we believe are responsible for the distinct multipath arrivals of the seismic pulses in Baffin Bay are also responsible in part for the long ranges where higher frequencies are still present. As noted in Section 3.2.3, the 100 m hydrophones were on the lower edge of the surface sound duct, so that the levels reported here are may be lower than would have been measured at 60 m.

Table 3-3. Range from the source (km) where the seismic pulse sound levels exceed the median one-minute SPL for Sept 2013 at station BB6 by 20 dB (Table 3-8). The range was limited to 150 km to avoid extrapolating beyond the measured data.

	Averaging duration		
	0.125-s SPL	90% energy duration SPL	1-min SPL
Peak SPL	89.3	91.8	97.9
SPL	>150	>150	>150
Octave bands:			
16 Hz	>150	>150	>150
31 Hz	>150	>150	>150
63 Hz	>150	>150	>150

	Averaging duration		
	0.125-s SPL	90% energy duration SPL	1-min SPL
125 Hz	145.5	117.3	77.9
250 Hz	102	56.6	44.7
500 Hz	86.8	41.4	32.5
1 kHz	21	27.5	17.4
2 kHz	17.5	21.5	13.5
4 kHz	16.4	16.9	10.6
8 kHz	12.4	11.6	9.4
16 kHz	6.1	6.8	5.7

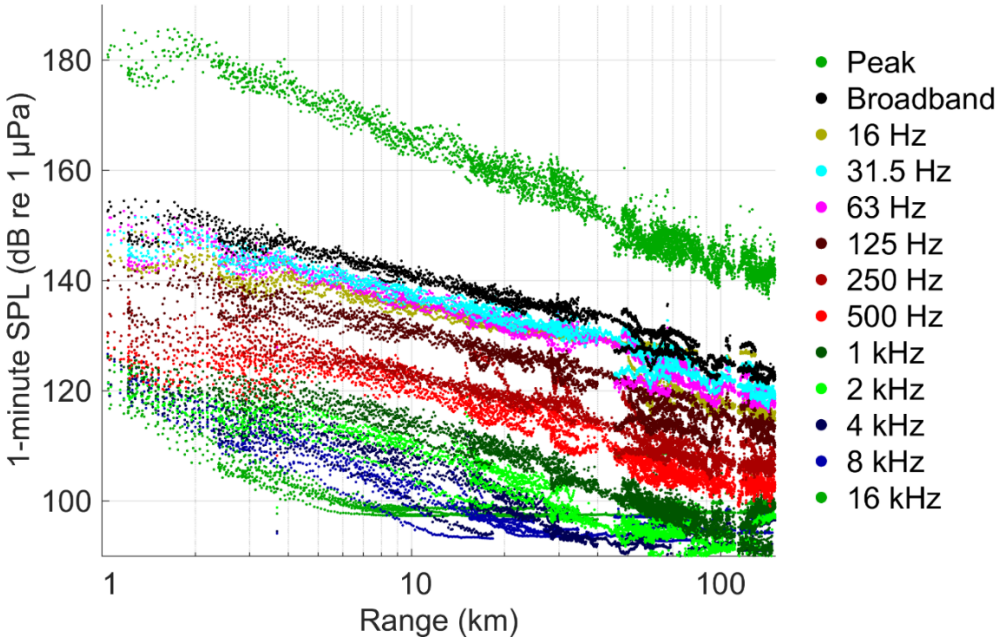

Figure 3-15. Received 1-min peak sound pressure level, broadband SPL, and octave-band SPLs (all in dB re 1 µPa) for ranges of 0.5–150 km during the 2012 Greenland survey. The 5400 min (3.7 days) of data shown are from periods when only one seismic survey source was emitting; the 100 m hydrophones at Stations BB1 and BB3 were used in all cases. To record the high seismic sound levels without saturating the hydrophone, low sensitivity hydrophones were employed. The system spectral noise floor was 58–63 dB re 1 µPa^2/Hz, or 98–103 dB re 1 µPa broadband in the 16 kHz octave band (see Table 3-8). The median ambient 16 kHz octave SPL in September 2013 was 77.9 dB re 1 µPa (Figure 3-21, Table 3-8).

3.4. SUMMARY AND CONCLUSIONS

The Baffin Bay recordings of seismic airgun and ambient sound levels in 600–770 m water depth were analyzed to understand the effects of a 3-D seismic survey on the acoustic environment. In 2012, data were recorded at three stations using vertical arrays with three hydrophones each; the top hydrophone at 100 m depth sampled at 64 kHz. A follow-on measurement of a shallow-hazards seismic program in 2013 and a year-long recording program overwinter in 2013–2014 showed that the soundscape in Baffin Bay is typical of open-ocean with little anthropogenic contribution to the soundscape. The August to September soundscape closer to shore in the Melville Bay nature sanctuary is loud and dominated by the sounds of melting glacial ice.

The seismic airgun sounds measured within 40 km of the source included up to 20 distinct multipath arrivals, far more than has been reported for seismic surveys in other deep-water environments. The pre-survey estimates of received sound levels were 3–7 dB higher than the levels measured for ranges of 0.5–65 km. The error between the measured and modelled sound levels decreased to 0–4 dB by using the sound speed profile, bathymetry, and modeling along the same radial as was measured.

When the vessel was closer to a station than 40 km, there was virtually no difference in the daily SEL as a function of depth; however, there were short-term variations in per-pulse SEL and SPL on the order of 6 dB. At ranges of 40 km from the seismic source, the difference in levels as a function of depth became notable. At 40 km, the per pulse SPL was generally below 140 dB re 1 µPa, which is well below the levels associated with risk of injury to marine life (see the Chapter Introduction). In the project area, the sound speed profile below 400 m is either iso-velocity or downward refracting.

Thus, measuring at the seabed would have provided similar information within 40 km of the source as we measured with the vertical arrays. For future monitoring projects in similar environments, we recommend collecting data at the seafloor only (assuming a downward refracting sound speed profile), which will allow for simpler moorings that are lower cost and easier to deploy and retrieve. These types of moorings have the added advantage of exhibiting lower levels of flow- induced pseudo-noise since most locations have little current at the seafloor.

The measured sound levels were compared to several proposed regulatory thresholds for auditory injury. Using the frequency weighting functions and thresholds recommended in Southall *et al.* (2007), which were incorporated into the *Guidelines to Environmental Impact Assessment of Seismic Activities in Greenland Waters,* we estimated the threshold of injury for low-frequency cetaceans at a range of <100 m and for phocids (seals) at a range of 600 m. These ranges agreed with the maximum expected ranges from the pre-survey modeling.

We noted that the SPL is a difficult metric to employ for regulatory thresholds since it depends on the integration time. We compared the SPL computed using two fixed window durations (125 ms and 1 min) with the SPL computed using 90% energy duration of the seismic pulses. The sound levels did not smoothly decrease as a function of range with any of the metrics and were best described using an additive model rather than a linear regression. We found that the integration time affects what information we extract from the data. Unsurprisingly, shorter integration times provide better information on the instantaneous variance in the signal, while longer integration times smooth the variance and reveal longer-term effects. The peak sound pressure level, 125 ms SPL, and 1-min

SPL curves tracked each other while the T_{90} SPL was closer to the 125 ms SPL at short range and close to the 1-min SPL at long range. Thus, the T_{90} SPL depends on the environment more strongly than the fixed integration windows and is not recommended for establishing regulatory thresholds. If the SPL must be used for characterizing the effects of sound on marine life, we suggest standardizing on the 125 ms window for seismic sources.

The Baffin Bay recordings confirm previous reports that seismic airgun sounds include energy up to at least 30 kHz. The SPL in the band used by dolphin species for social whistle communications (16 kHz octave band) were increased by 20 dB compared to the ambient levels measured in September 2013 at ranges of 6 km from the source vessels for all integration durations.

The collection and analysis of this dataset has produced a wealth of new information on the Baffin Bay environment and the variability of seismic array sound propagation. This study shows the importance of collecting systematic data during industrial operations when there are uncertainties in the possible effects of the activity on the acoustic environment. Future projects can extend this work by verifying the dependence of the multipath arrivals and high-frequency content on the bottom composition and depth, investigating the azimuthal characteristics of a seismic array, exploring the variation in sound levels with depth in different environments, and attempting to measure the behavioral reactions of marine life as a function of range to the seismic source.

3.5. ACKNOWLEDGEMENTS

The authors would like to thank Shell Global Solutions for making this data set available for publication and JASCO Applied Sciences for their support of the manuscript preparation. We also thank JASCO's engineering and field teams for developing and deploying the vertical moorings that successfully recorded this data set. Brad Boschetto (Shell International Exploration and Production) made helpful contributions to the initiation and execution of the project. Reviews by Mikhail Zykov, Roberto Racca, Peter van der Sman, David Barclay, and our anonymous reviewers contributed to the strength and readability of this manuscript. Finally, thanks to Karen Hiltz for her patient reviews and edits to the manuscript.

3.6. SUPPORTING INFORMATION

Table 3-4 Recorder deployment details for the summer 2012, summer 2013, and overwinter 2013–2014 acoustic monitoring programs in the Baffin Bay.

Recording period and station	Location	Recording period	Water depth (m)	Recording depths (m)
Summer 2012				
BB1	74.16N 61.98W	29 Jul 12 to 29 Sep 12	603	100, 200, 400
BB2	74.23N 61.85W	29 Jul 12 to 01 Oct 12	609	100, 200, 400
BB3	74.70N 61.01W	30 Jul 12 to 02 Oct 12	769	100, 200, 400
BB4	75.31N 58.64W	14 Aug 12 to 15 Sep 12	130	130
Summer 2013				
BB5	73.05N 62.10W	01 Sep 13 to 30 Sep 13	900	450
BB6	74.01N 60.74W	01 Sep 13 to 30 Sep 13	504	272
BB7	74.54N 61.04W	01 Sep 13 to 29 Sep 13	785	365
BB8	75.01N 60.50W	31 Aug 13 to 29 Sep 13	712	350
BB9	75.11N 60.36W	31 Aug 13 to 29 Sep 13	780	400
Overwinter 2013–2014				
BB6	73.05N 60.10W	30 Sep 13 to 04 Sep 14	1100	550

Recording period and station	Location	Recording period	Water depth (m)	Recording depths (m)
BB10	74.01N 60.74W	29 Sep 13 to 06 Sep 14	550	302

Table 3-5 Recorder configurations

Recording period and station	Recording depth	Sampling rate	Duty cycle	Hydrophone type
Summer 2012				
BB1	100	64000	Continuous	M8H-0dB
	200	8000	Continuous	M8H-0dB
	400	8000	Continuous	M8H-0dB
BB2	100	64000	Continuous	M8H-0dB
	200	8000	Continuous	M8H-0dB
	400	8000	Continuous	M8H-0dB
BB3	100	64000	Continuous	M8H-0dB
	200	8000	Continuous	M8H-0dB
	400	8000	Continuous	M8H-0dB
BB4	130	64000	Continuous	M8E-35dB
Summer 2013				
BB5	450	64000	8 min 35 s	M8E-35dB
		375000	43 s	M8E-35dB
BB6	272	64000	8 min 35 s	M8E-35dB
		375000	43 s	M8E-35dB
BB7	365	64000	8 min 35 s	M8E-35dB
		375000	43 s	M8E-35dB
BB8	350	64000	8 min 35 s	M8E-35dB
		375000	43 s	M8E-35dB
BB9	400	64000	8 min 35 s	M8E-35dB
		375000	43 s	M8E-35dB
Overwinter 2013–2014				M8E-35dB
BB6	550	64000	5 min 40 s	M8E-35dB
		375000	43 s	M8E-35dB
		Sleep	23 min 38 s	
BB10	302	64000	5 min 40 s	M8E-35dB
		375000	43 s	M8E-35dB

Recording period and station	Recording depth	Sampling rate	Duty cycle	Hydrophone type
		Sleep	23 min 38 s	

Table 3-6 Hydrophone sensitivity and noise data. The maximum frequency was limited by the anti-aliasing filter in the analog-to-digital converter at 0.47 of the sampling rate for the 64000 and 8000 kHz sampling rates, and by 3-pole analog filters for the 375000 kHz sampling rate. All hydrophones were individually calibrated with a G.R.A.S. 42-AA pistonphone calibrator before shipping to Greenland and on the vessel before deployment.

Hydrophone type	Nominal sensitivity (dBV/µPa)	Maximum measurable SPL (dB re 1 µPa)	Sampling rate	System spectral noise floor (dB re 1 μPa^2/Hz)	Broadband noise floor 16 kHz octave band (dB re 1 µPa)	Recording bandwidth (Hz)
M8E-35dB	−164	171	64000	28–33	68–73	10–30000
			375000	35–40	75–80	10–180000
M8H-0dB	−199	206	64000	58–63	98–103	10–30000
			8000	67–72	N/A	10–3750

Table 3-7. Geo-acoustic profile used during pre-season modeling of seismic pulse propagation in Baffin Bay (Matthews 2012b).

Depth below seafloor (m)	Density (g/cm^3)	Compressional sound speed (m/s)	Compressional attenuation (dB/λ)	Shear sound speed (m/s)	Shear attenuation (dB/λ)
0–20	1.77–1.80	1574–1600	0.90–1.05	305	4.02
20–160	1.80–1.97	1612–1777	1.05–0.88		
160–380	2.05–2.29	1819–2030	0.85–0.77		
380–500	2.44–2.55	2155–2250	0.70–0.64		
>500	2.55	2250	0.64		

Table 3-8. 25th, 50th (median), and 75th percentiles of the 1-min peak sound pressure levels, broadband SPLs, and octave band SPLs (all dB re 1 µPa) at Station BB7 (Figure 3-1) for 1–29 Sep 2013. A shallow hazards (40 in^3) seismic survey was active in the area and elevated the 25th percentile levels. The data collected prior to the seismic survey in 2012 could not be used because data were limited by hydrophone noise at 90–99 dB re 1 µPa in the bands above 1000 Hz.

Octave band centre frequency	Actual frequencies	1-min SPL (dB re 1 µPa)		
		75th percentile	Median	25th percentile
Peak	Peak	118.4	122.5	132.7
Broadband	9–28200 Hz	99.2	102.2	108.4
16	9–22 Hz	67.2	71.0	77.1
31.5	22–45 Hz	89.6	92.6	97.6
63	45–89 Hz	92.8	95.6	100.2
125	89–178 Hz	91.9	95.3	102.1
250	178–354 Hz	89.9	94.0	101.5
500	354–708 Hz	88.0	92.5	98.4
1000	708–1412 Hz	85.4	90.1	94.1
2000	1.4–2.8 kHz	81.3	87.0	91.1
4000	2.8–5.6 kHz	77.3	84.5	88.3
8000	5.6–11.2 kHz	74.4	81.3	85.3
16000	11.2–22.4 kHz	72.9	77.9	81.5
+22400 Hz	22.4–28.2 kHz	69.3	71.6	74.1

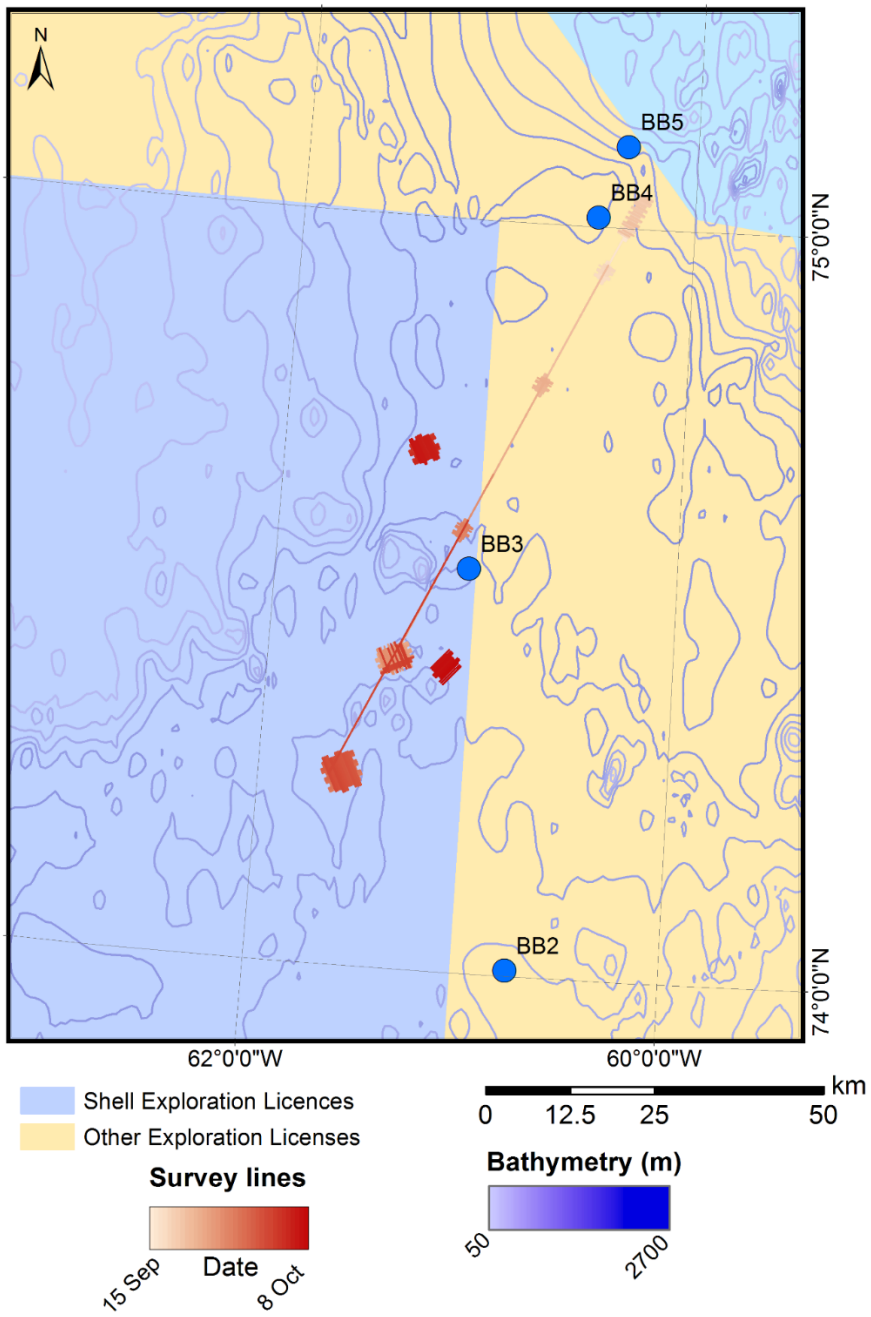

Figure 3-16. Survey tracks of the *Fugro Discovery* during the 2013 shallow-hazards seismic survey.

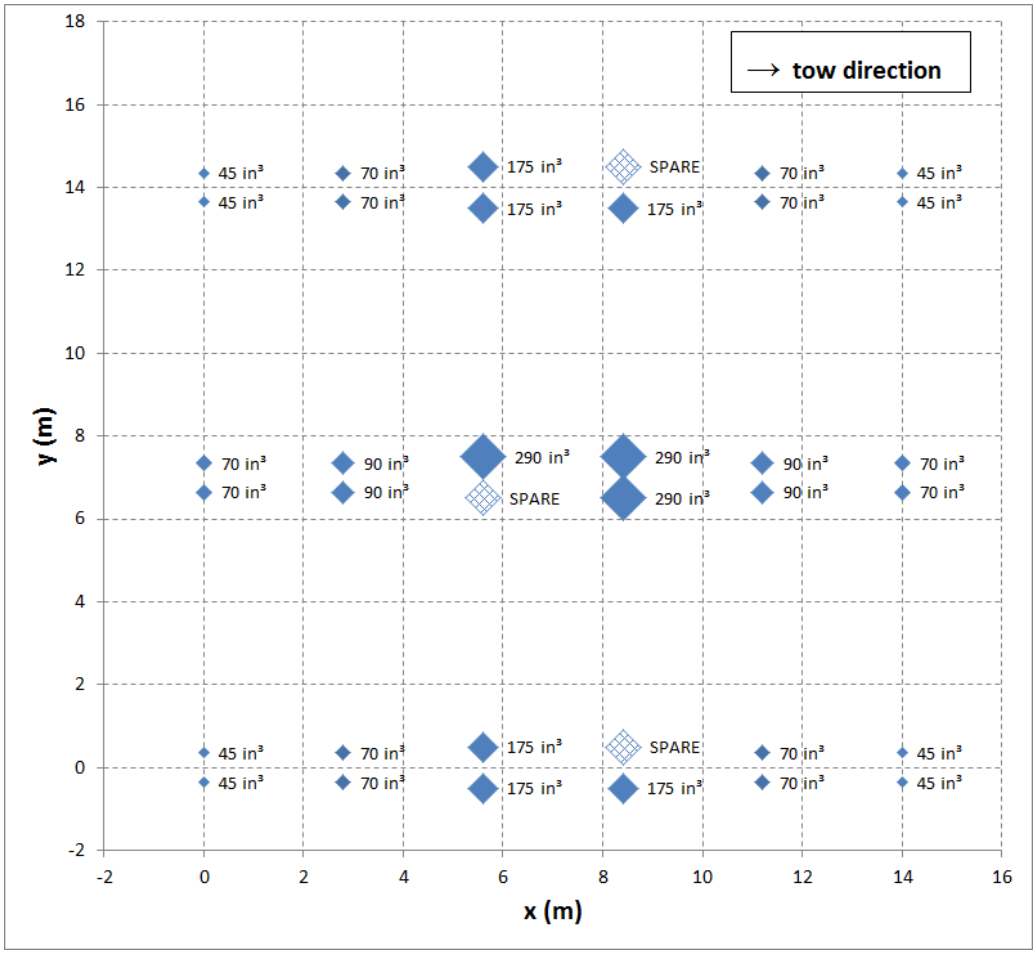

Figure 3-17. The 3480 in^3 seismic airgun array configuration employed by the *Amani* and *Samur* in Baffin Bay in summer 2012.

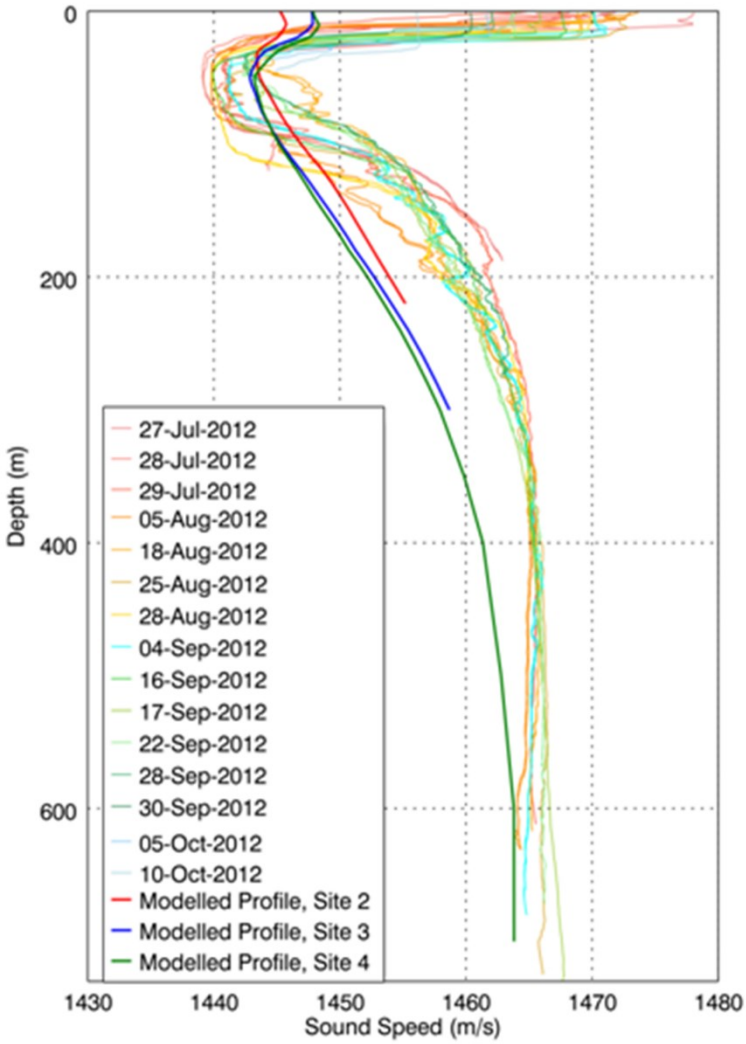

Figure 3-18. Sound speed profiles used for pre-season modeling compared to those measured in Baffin Bay in summer 2012.

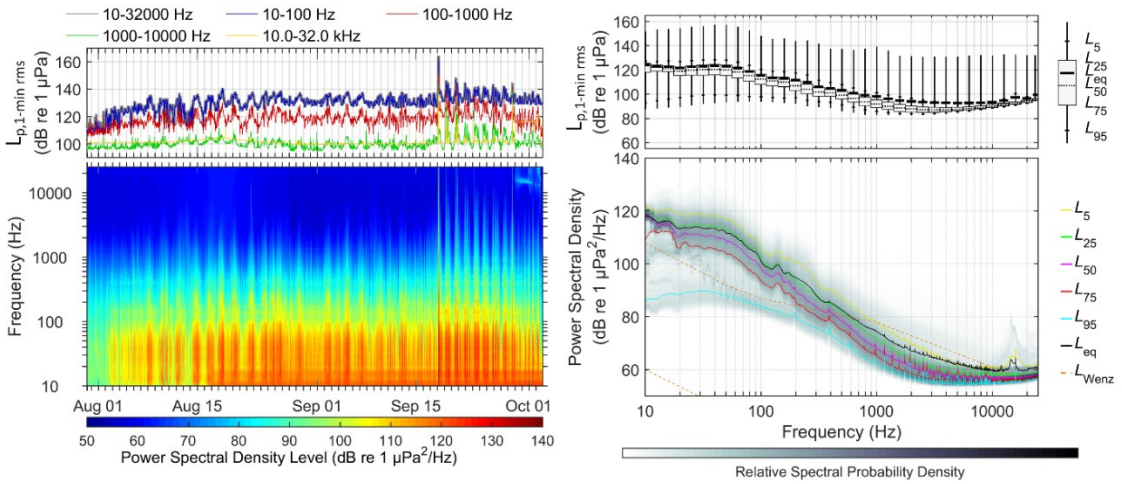

Figure 3-19. Summary of the received sound levels for the 100 m deep hydrophone at Station BB3 during summer 2012. (Bottom left) Long-term spectrogram and (top left) band-level plot. (Bottom right) Power spectral density exceedance curves and spectral probability density (top right) with 1/3-octave SPL distributions. The spectral noise floor for the low-sensitivity M8E-0dB hydrophones was ~ 53 dB re 1 µPa²/Hz. The 95th percentile represents the power spectral density before the survey started (30 Jul to 2 Aug 2012). Note that ConocoPhillips, DONG Energy, and Nunaoil jointly conducted a 2-D survey from 25 Aug to 24 Sep in the license area north of the Shell license area. Maersk Oil conducted a 3-D survey from 6 Aug to 1 Oct in the license area east of the Shell license area.

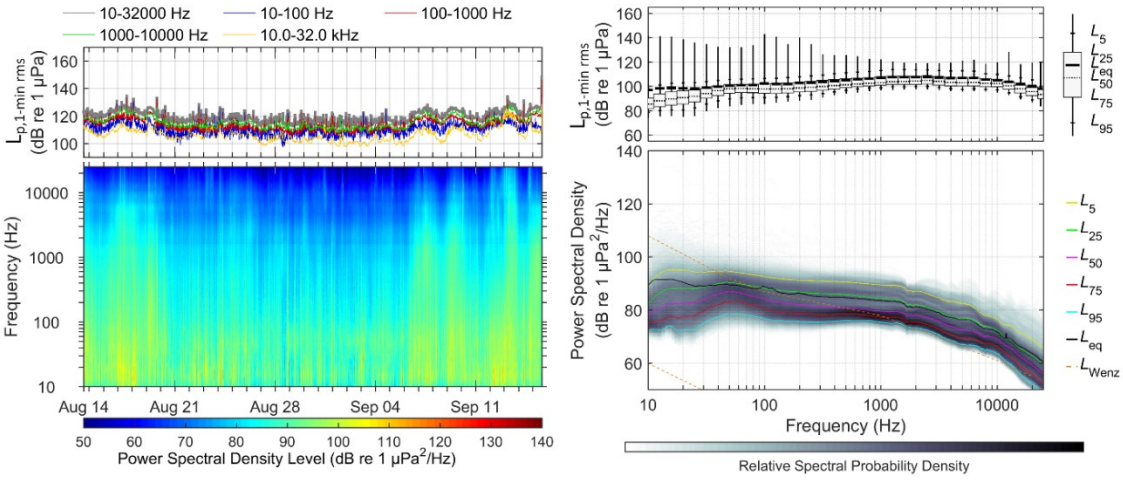

Figure 3-20. Summary of the received sound levels in Melville Bay at Station BB4 during summer 2012. (Bottom left) Long-term spectrogram and (top left) band-level plot. (Bottom right) Power spectral density exceedance curves and spectral probability density (top right) with 1/3-octave SPL distributions.

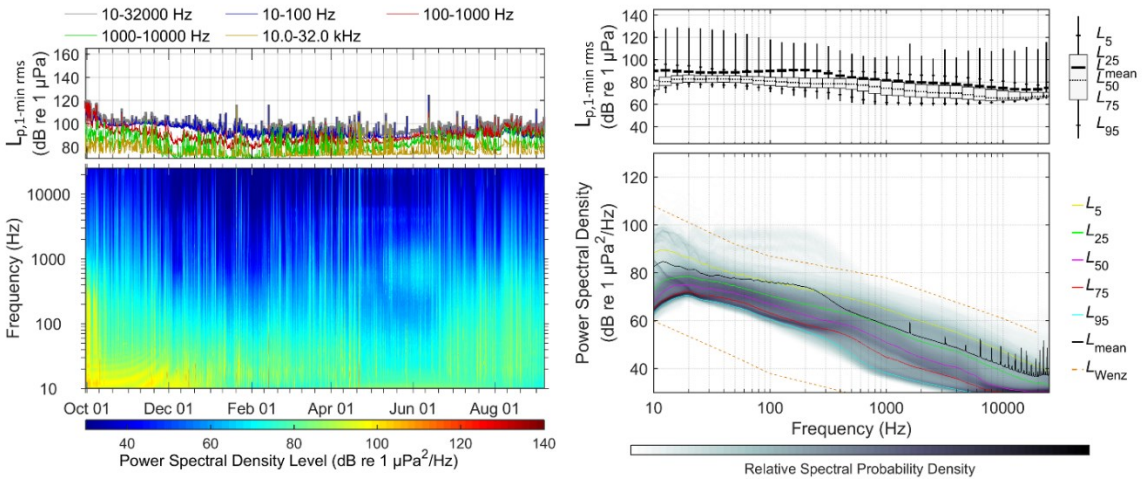

Figure 3-21. Summary of the received sound levels at Station BB6 overwinter, deployed September 2013 to September 2014 at approximately mid-water column in 550 m of water. (Bottom left) Long-term spectrogram and (top left) band-level plot. (Bottom right) Power spectral density exceedance curves and spectral probability density (top right) with 1/3-octave SPL distributions. Bearded seal calls increased the sound levels from 300–2000 Hz in May and June.

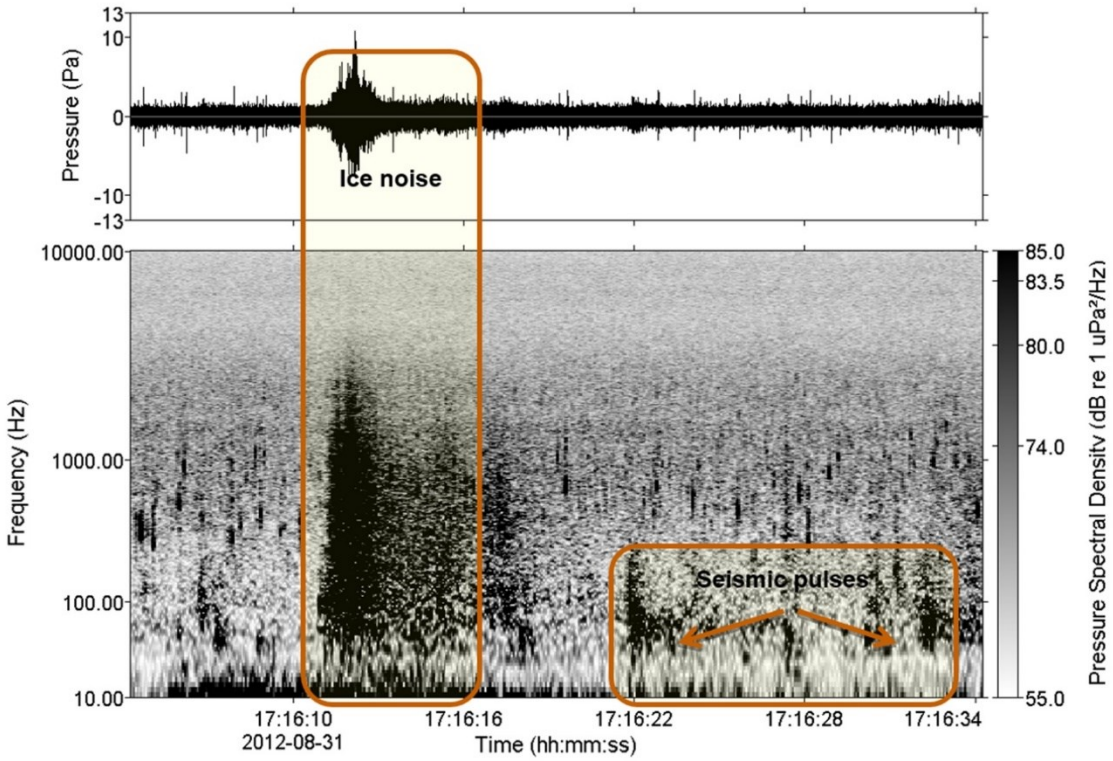

Figure 3-22. Sample data from Station BB4 on 31 Aug 2012 dominated by ice noise such as the large impulse at 17:16:11, and smaller pops and hisses from air escaping from glacial ice. Low level seismic airgun pulses are also present at 17:16:22 and 17:16:33 in the 50–150 Hz range. (32 768 pt FFT, 12 800 data pts, 6400 pt advance, Hamming window.)

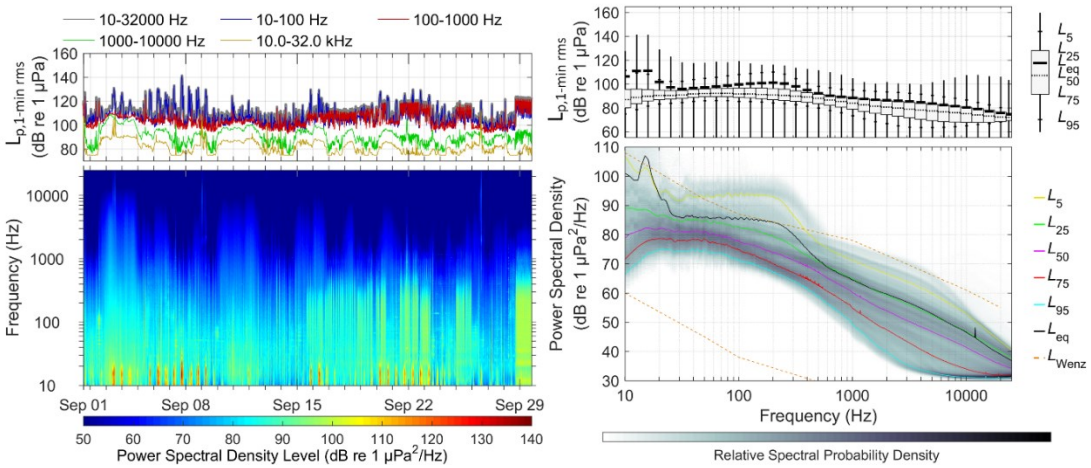

Figure 3-23. Summary of the received sound levels for mid-water column hydrophone at Station BB6 during summer 2013. (Bottom left) Long-term spectrogram and (top left) band-level plot. (Bottom right) Power spectral density exceedance curves and spectral probability density (top right) with 1/3-octave SPL distributions.

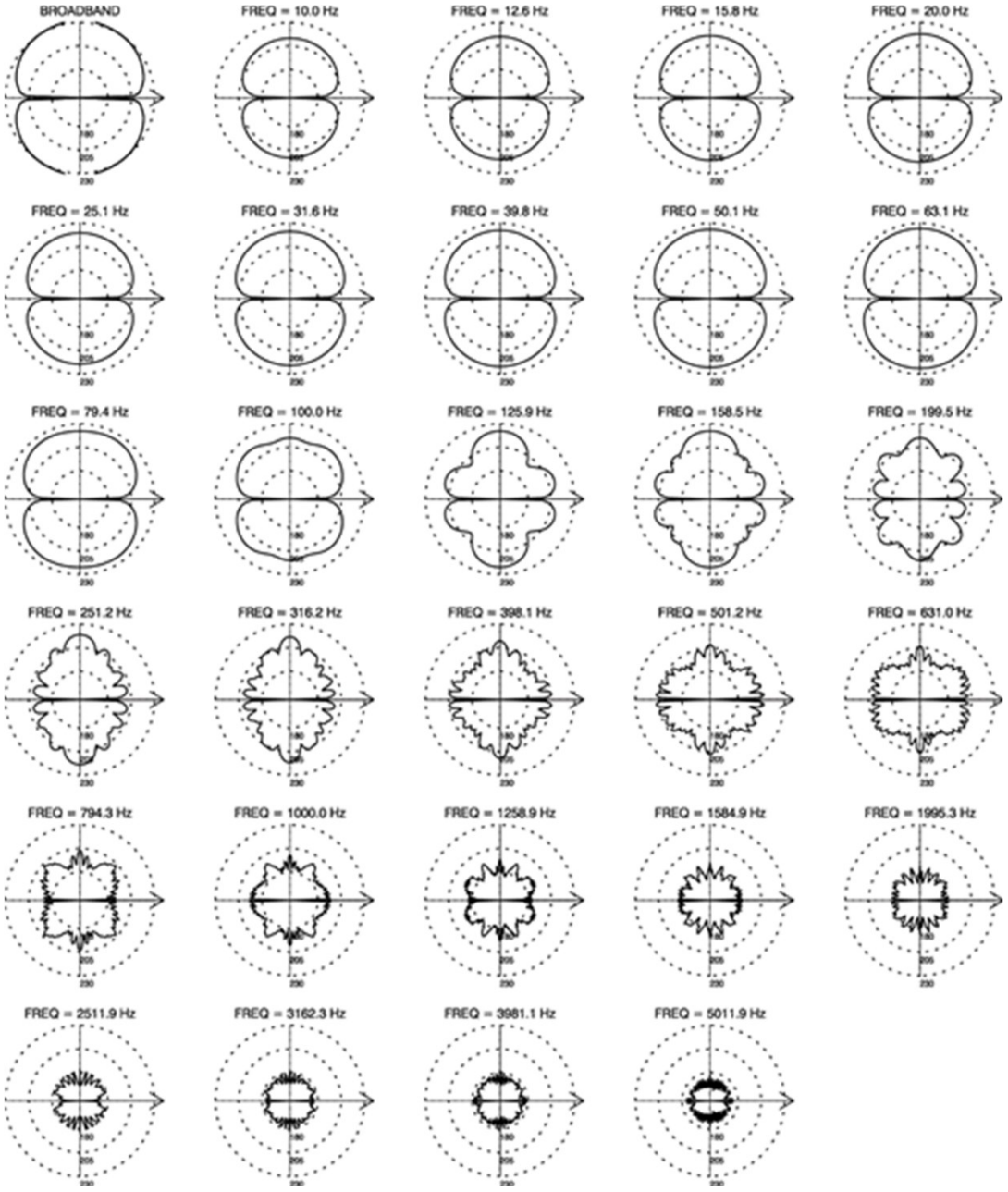

Figure 3-24. Modeled vertical beam pattern in the endfire direction of the 3480 in^3 airgun array used in Baffin Bay in 2012. The arrow represents the front of the array (Figure 3-17). Each figure shows the beampattern is a different decidecade center frequency. Each dotted ring is 10 dB in relative output energy.

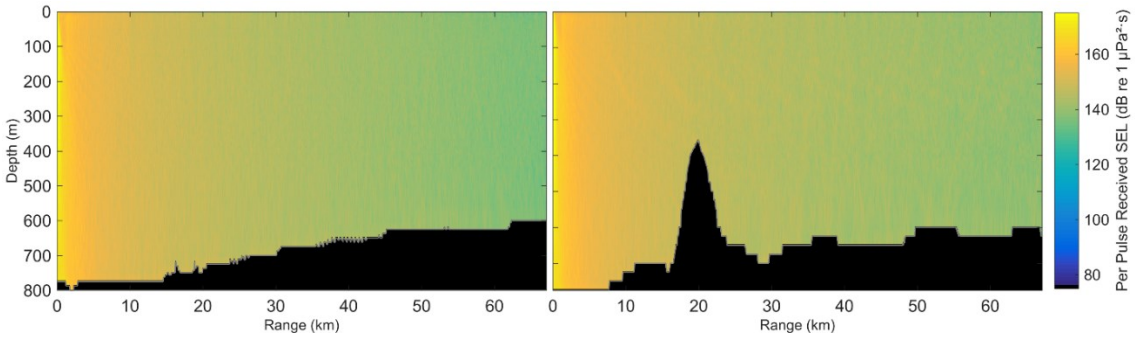

Figure 3-25. Differences in bathymetric profile from the (left) multibeam sonar and (right) SRTM-30 data set for a line from Station BB3 (left hand side of each panel) towards BB1 (right hand side of each panel).

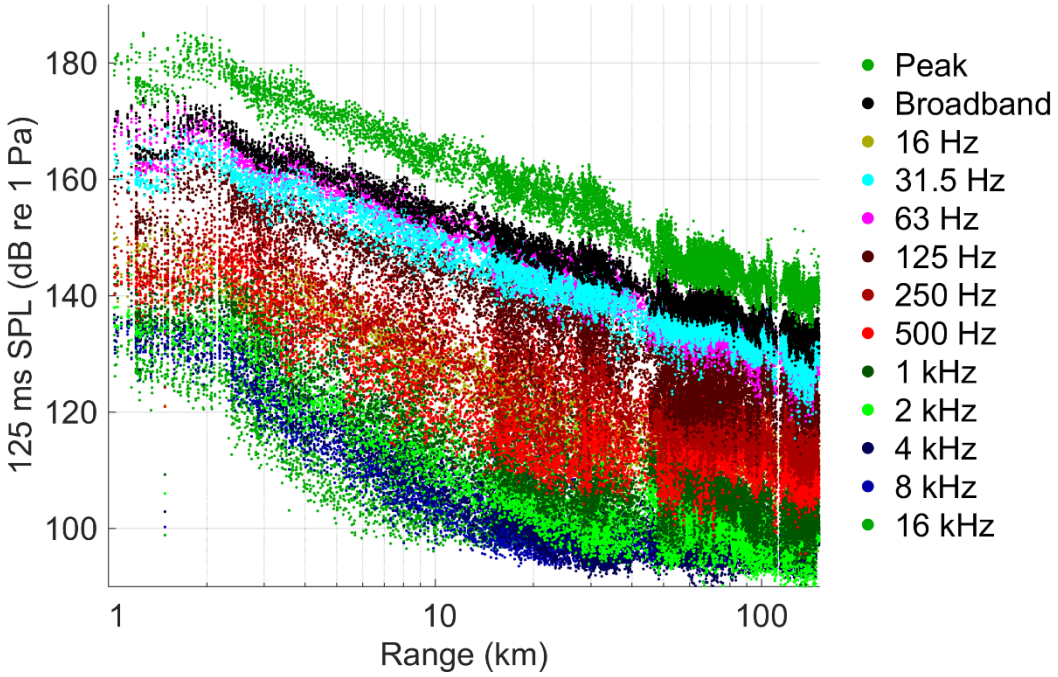

Figure 3-26. Received 125 ms peak SPL, broadband SPL, and octave-band SPLs (all in dB re 1 µPa) for ranges of 0–150 km during the 2012 Greenland survey, showing 3.7 days of data from periods when only one ship was emitting. The 100 m hydrophones at Stations BB1 and BB3 were used in all cases. Only the three detected impulses with the highest SPL per minute are shown for clarity.

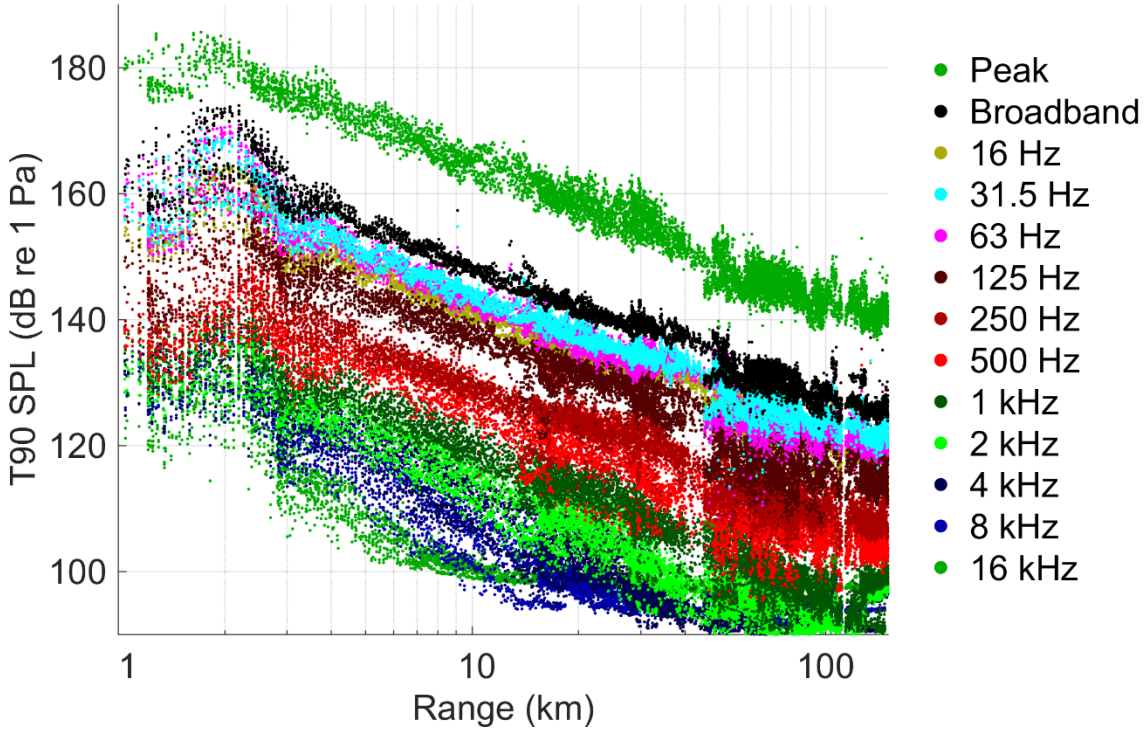

Figure 3-27. Received 90% pulse energy duration peak sound pressure level, broadband SPL, and octave-band SPLs (all in dB re 1 µPa) for ranges of 0.5–150 km during the 2012 Greenland survey, showing 3.7 days of data from periods when only one ship was emitting. The 100 m hydrophones at Stations BB1 and BB3 were used in all cases. Only the three detected impulses with the highest SPL per minute are shown for clarity.

CHAPTER 4 ANALYSIS OF THE DEPENDENCE OF MARINE PILE DRIVING SOUND LEVELS ON STRIKE ENERGY, PILE PENETRATION AND PROPAGATION EFFECTS USING A LINEAR MIXED MODEL BASED ON DAMPED CYLINDRICAL SPREADING

This chapter contains a paper submitted to the Journal of the Acoustical Society of America in December 2018. The material shown here is the revision submitted 25 Feb 2019. The data for this chapter came from a project to measure the biologic effects isopleths during the construction of the Block Island Wind Farm. Tetra Tech Inc was hired by Deep Water Wind to perform the full environmental monitoring program. Tetra Tech subcontracted JASCO for the acoustic monitoring. Bruce Martin was the project manager and primary investigator for JASCO. Jeff MacDonnell was part of the field team and assisted with the original analysis of the data, during which we identified that unexplained factors were affecting the biologic effects isopleths.

I used the data for a BIOL5062 'Data analysis for Biologists' term project in the fall of 2016 where the comparison of bootstrapping to the increased intercept was initially performed. In the Winter term of 2017 the data was reanalyzed using linear and additive mixed models as part of a STATS5062 'Data Analysis' term project. In both term projects the coefficient of geometric spreading with range and linear spreading with range were model coefficients. An early draft manuscript based on that analysis was reviewed by Michael Ainslie, who pointed out the Lippert et al. (2018) damped cylindrical spreading (DCS) model that had just been published. This model has a number of merits including recognizing that piles are distributed, cylindrical sound sources and that the coefficient for linear range spreading is proportional to the number of reflections. In the fall of 2017 I had experimented with a similar construct without good results and saw the

merits of this approach. The analysis was re-performed to compare the original model with the DCS and the manuscript updated to focus on comparing the models. Subsequently I decided to drop the original model and only report on the DCS model's results. The reviewer comments from JASA suggested focusing on acoustic propagation effects and elaborating on the pile penetration and strike energy analsyis, which is what is contained in this Chapter.

The impulse detection algorithm and SEL analysis used to quantify the pile driving impulses were written by Bruce Martin as part of JASCO's PAMLab software suite. Bruce is the original author of the software; it is now maintained by Briand Gaudet and Bruce Martin. The data preparation, statistical analysis and manuscript preparation were all performed by Bruce Martin.

Note that Tables 4-7 – 4-10 as well as Figures 4-9 – 4-15 are S-1 to S-4 and S-1 to S-7, respectively in the JASA Manuscript. These Tables and Figures appear as Supporting Information for this Chapter.

Title: *Analysis of the dependence of marine pile driving sound levels on strike energy, pile penetration and propagation effects using a linear mixed model based on damped cylindrical spreading*

S. Bruce Martin*[4]

Dalhousie University, Department of Oceanography, 1355 Oxford Street, PO BOX 15000, Halifax, Nova Scotia Canada, B3H 4R2

Email: bruce.martin@jasco.com

Running Title: Variability of sound from pile driving

Date Submitted: 31 Dec 2018

Resubmitted 1 March 2019

[4] Also at JASCO Applied Sciences Canada, Suite 202, 32 Troop Avenue, Dartmouth NS, B3B 1Z1.

ABSTRACT

Acoustic recordings were made during the installation of four offshore wind turbines at the Block Island Wind Farm, USA. The turbine foundations have four legs inclined inwards in a pyramidal configuration. Four bottom mounted recorders measured received sound levels at distances of 541–9067 m during 24 pile driving events. Linear mixed models based on damped cylindrical spreading were used to analyze the data. The model's random effects coefficients represented useful information about variability in the acoustic propagation conditions. The received sound levels were dependent on the angle between pile and seabed, strike energy, and pile penetration. Deeper pile penetrations increased sound levels in a frequency dependent manner. The estimated area around the piles where auditory injury and disturbance to marine life could occur were not circular and changed by almost an order of magnitude between the lowest and highest sound level cases. This study extends earlier results showing a linear relationship between the peak SPL and per-strike SEL. Recommendations are made for how to collect and analyze pile driving data. The results will inform regulatory mitigations of the effects of pile driving sound on marine life and contribute to developing improved pile driving source models.

AIP Codes: Bioacoustic Effects, Acoustic Noise Measurement, Impulse Noise
PACS Code: 43.30 Nb
Keywords: Isopleth; Pile Driving; Block Island Wind Farm; Strike Energy; Pile Penetration

4.1. INTRODUCTION

Offshore wind farms are being installed around the world to provide a sustainable source of electricity. In waters up to 50 m deep, wind turbines are normally secured to the

seabed using impact pile driving which generates intense impulses of sound that may disturb marine life 70 km from their source (Bailey et al. 2010). This sound could have significant ecological effects on marine life. The sounds are often studied during the installation of wind farms (e.g. Madsen et al. 2006b, Betke 2008, Matuschek and Betke 2009, Bailey et al. 2010, Brandt et al. 2011, Dähne et al. 2013, Wilkes and Gavrilov 2017). The studies have identified effects including fish mortality at close ranges to the pile driving, as well as temporary threshold shift in fish hearing (Halvorsen et al. 2011, Halvorsen et al. 2012b, Casper et al. 2013, Casper et al. 2017a). Harbor porpoise have been shown to avoid pile driving at distances of 20 km or longer (Dähne et al. 2013, Tougaard et al. 2014) and exposure to intense impulsive sound can induce temporary threshold shifts in marine mammals (e.g., Finneran et al. 2002, Lucke et al. 2009, Finneran et al. 2011, Kastelein et al. 2017). Over the past two decades, American regulatory thresholds to minimize harm have been proposed for marine mammals (NOAA 1995, Southall et al. 2007, NOAA 2013, NOAA 2015, NMFS 2018, Southall et al. 2019b) as well as fishes, turtles, and marine invertebrates (FHWG 2008, Popper et al. 2014a). Erbe (2013) and Lucke et al. (2014) document underwater sound regulations developed in many other jurisdictions. Despite the extensive studies and recent adoption of regulations, many questions remain about the properties of pile-driving sounds and their impacts on different marine taxa.

When an impact hammer strikes the top of a pile, the Poisson effect creates a compressional deformation that propagates down the pile as a band of increased diameter at speeds on the order of 5000 m/s. When the deformation enters the water, it creates an acoustic pressure wave that propagates at the sound speed in water, approximately 1500

m/s. The difference in sound speed between the metal pile and the water creates a Mach cone angled 15–19 degrees from the axis of the pile (Dahl 2015, MacGillivray 2018a). The Mach cone acts as a continuous line source of sound instead of a point source. Sophisticated methods are required to predict and accurately measure the sound signatures, especially within three water depths of the pile (Reinhall and Dahl 2011, Ainslie et al. 2014b). At distances greater than three water depths the received sound exposure level (SEL) is expected to follow Equation (4-1)

$$L_E(R) = constant - (A \log_{10} R + BR) \quad (4\text{-}1)$$

where R is the range from pile to receiver in meters, the constant is the regression's intercept term that fits the data, A is in the range of 10 – 20, and B arises from multiple reflections of the sound from the seabed and surface (Zampolli et al. 2013, Ainslie et al. 2014b, Lippert et al. 2018). The propagation parameters A and B depend on the bottom composition, the water column sound speed profile as well as the surface and seabed roughness. Equation (4-1) is a simple model that does not consider variations in bathymetry and bottom composition, however, it is useful for developing a conceptual understanding of pile driving sound propagation, and as a framework for regression analysis of measured data (Ainslie et al. 2014b, Lippert et al. 2018).

It is important to note that the constant in Equation (4-1) is not a source factor but does depend on project specific conditions such as the hammer strike energy, the coupling of the hammer energy into the pile, and the damping of pile vibrations by the sediment surrounding the embedded end of the pile (MacGillivray 2014, Lippert et al. 2016). Previous measurements of the relationship between radiated sound levels and strike energy found a 10 dB increase in peak-to-peak sound pressure level for a 6 dB

increase in strike energy (Bailey et al. 2010), or a 12 dB increase in peak-to-peak sound pressure level and an 8 dB increase in SEL for a 10 dB increase in strike energy (Robinson et al. 2007). The peak sound pressure level attenuates more quickly with range than SEL due to dispersive effects in shallow water as well as interactions with the sea-surface and seabed which scatters high frequencies. Therefore, recordings at different ranges likely would have changed the measured relationship between strike energy and peak-to-peak sound pressure levels (Lippert et al. 2015).

The Block Island Wind Farm is the first offshore wind farm installed in the United States. It is located ~6 km from Block Island, Rhode Island. The farm has five 6 MW turbines. Each turbine is mounted on four-leg-jacket foundations pinned to the seabed with ~60 m long, 1.52 m diameter piles that were driven in three sections. The foundation legs were identified as A1, A2, B1 and B2, while the piles sections were identified as P1, P2, and P3. The piles were aligned with the cardinal points of the compass and inclined ~19-degrees inwards so that the foundation is like a pyramid. The leg inclination of ~19 degrees is similar to the Mach cone angle, so that the Mach cone on the outside of the pile should propagate with fewer bottom and surface interactions than the cone inside the pile. This suggests that the acoustic propagation losses could have a directional component. A similar pile configuration was measured by Bailey et al. (2010) where significantly different peak-to-peak sound pressure levels were measured on one side of the pile compared to the other. Bailey et al. (2010) propose that this could be due to different tidal conditions or bathymetry effects, and suggest that a long-term static recording program at multiple ranges from multiple piles would be needed to determine the cause of these differences. Wilkes and Gavrilov (2017) modeled and measured inclined (raked) piles in

shallow water (7 m) and confirmed that there is directional variability in the received sound levels.

The Block Island project's incident harassment authorization (https://bit.ly/2PyxSXB) and United States Army Corps of Engineers permit (https://bit.ly/2PCn0rC) included acoustic thresholds for biological effects of sound on marine life and estimates of the distance from the piles that sound levels were above the thresholds (Table 4-1). A conceptual line drawn on a map that joins points with equal sound levels is called an isopleth. The project team was required to maintain a visual watch for marine mammals within the 600 m Level A isopleth and to shut down piling if a mammal was present. The isopleth distances estimated during the permitting process (Table 4-1) were based on the Practical Spreading Model (NOAA 2012) which does not include any location specific information that would affect sound propagation. As a result, the monitoring conditions in Block Island Wind Farm permit required a systematic sound source characterization study. The study included short and long-term components. The short-term study used real-time acoustic measurements from a vessel as well as sound levels measured at 4 or 5 ranges using bottom mounted recorders. The recorders were retrieved each evening, the data downloaded and analyzed by linear regression (using Equation 4-1) to estimate isopleth radii that were assumed to be circular. Twelve pile sections were analyzed during the short-term monitoring from 30 Aug – 18 Sept 2015. The long-term study used bottom mounted recorders to measure ambient sound levels and pile driving of 24 pile sections in September and October 2015.

Table 4-1. Permitted sound level isopleths for impact pile driving at the Block Island Wind Farm (see https://bit.ly/2PyxSXB and https://bit.ly/2PCn0rC). The distances were estimated by NMFS assuming an attenuation of $15 \cdot \log_{10}$(Range). For the 187 dB re 1 $\mu Pa^2 \cdot s$ $L_{E,24h}$ isopleth, a source factor of 219 dB re 1 $\mu Pa^2 m^2$ and a pile driving time of 27000 seconds was assumed (NOAA Formal ESA Section 7 Consultation for Deepwater Wind, 30 Jan 2014, Table 9 (https://bit.ly/2Q7P5Gw)). The actual number of strikes ranged from 1960 (26 Oct) to 7812 (18 Sep).

Sound level threshold	Maximum radius (m)
206 dB re 1 µPa $L_{p,pk}$ (Fish Injury)	7
180 dB re 1 µPa $L_{p,}$ (Level A Marine Mammal Harassment)	600
166 dB re 1 µPa L_p (sea turtle disturbance)	3,414
160 dB re 1 µPa L_p (Marine Mammal Level B disturbance)	7,000
150 dB re 1 µPa L_p (Fish Disturbance)	39,810
187 dB re 1 $\mu Pa^2 \cdot s$ $L_{E,24h}$ (Fish Injury)	116,591

Martin et al. (2016) investigated methods for rapidly computing the pile driving sound regulatory isopleths using the short- and long-term data. The study compared three methods. The first two methods were straightforward. The first method fit the data to Equation 4-1), and the second method applied the Practical Spreading Model (NOAA 2012) at three different ranges. The third method was a measured-modeled fit between the collected data and an ensemble of acoustic propagation models. For the measured-modeled fit, the pile was assumed to be a point source (to simplify the analysis) and a range of possible seabed geoacoustic properties were modeled. A minimum least squared fit was then performed to select the geoacoustic properties and source factor that minimized the difference between the data and model. All three types of analysis were applied to single pile driving events and produced an unsatisfactorily wide range of isopleth distances when compared across events and methods. For example, the methods produced ranges to the 160 dB re 1 µPa sound pressure level isopleth between 3457 m and 7454 m for the same pile driving event (Martin et al. 2016). As an example of

variability between events, the 160 dB re 1 μPa isopleth for the first segments of the four legs of Foundation 3 were between 2011 and 4578 m (measured Aug 30 – Sep 2, 2015).

Three questions arose from these analyses of the Block Island data: 1) what is the source of the large variability in sound levels between pile driving events?; 2) how does the variability affect the dimensions of biological effects isopleths?; and 3) given this variability exists, how should acoustic measurements and analysis be performed to accurately determine the radius around a piling event where the sound may affect marine life?

This study analyzes the received sound levels from 24 pile sections using a linear mixed model. The model included range, the angle between the pile and seabed, the strike energy and pile penetration as fixed effects and allowed propagation variations due to pile-to-recorder bathymetry, bottom properties and the sound speed profile to be represented by random effects. This structure separated the propagation effects from variability in the source sound levels. The model was used to predict the ranges to the sound isopleths. Two methods of estimating the isopleth prediction intervals were investigated. The paper is organized as follows. Section 4.2 describes the acoustic measurements and data analysis methods. Section 4.3 provides an overview of the measured pile driving sound levels, the linear model parameters, and the isopleth distances predicted by the model. Section 4.4 discusses the isopleth distances and their variability, compares the current and previous results and makes recommendations for future pile measurements and analysis.

The Supporting Information (section 4.6) provides: 1) details of the recorder configurations and locations; 2) details of the Teager-Kaiser impulse detector; 3) pile

locations and the 24 pile driving events analyzed; 4) typical data from all recorders for a single pile; 5) measured sound speed profiles; 6) examples of the pile driving logs; 7) further details on the performance of the linear models; 8) isopleth radii for the Block Island Wind Farm pile driving using a wide selection of regulatory thresholds; and 9) the outline for '***R***'-code to perform the linear mixed modeling and prediction interval estimation.

4.2. METHODS

4.2.1. Acoustic Measurements

Continuous acoustic measurements sampled at 64 kHz were made using AMAR acoustic recorders (JASCO Applied Sciences) located at the seabed at four ranges from the wind turbine foundations (Figure 4-1). The sound intensity spreads throughout the water column and usually decreases at a rate between $1/R$ ($10 \cdot \log_{10} R$) and $1/R^2$ ($20 \cdot \log_{10} R$) (where R is the distance between the pile and receiver; Ainslie et al. 2014b). Since the intensity changes as the logarithm of the distance, the measurement locations were also spaced approximately logarithmically. The prediction intervals of linear models are smallest if the prediction range is inside the measured range. Therefore, it is desirable to put the recorder closest to the pile inside the shortest expected isopleth distance, and the farthest recorder outside the longest expected isopleth. The closest distance the recorders were permitted, for safety and logistical reasons, was 500 m. Since it was logistically impractical to deploy and retrieve recorders more than 10 km from the measurement site (the Fish Disturbance isopleth was 40 km, see Table 4-1), the longest range was selected to be 9000 m and therefore recorders were placed at nominal ranges of

500, 1500, 4500, and 9000 m from Foundation 3 (Figure 4-1). The combination of pile driving events as well as recorder and pile locations resulted in 16 measurement ranges, of which 10 were approximately evenly distributed between 541 and 2550 m, three were around 4800 m, and three were near 9000 m.

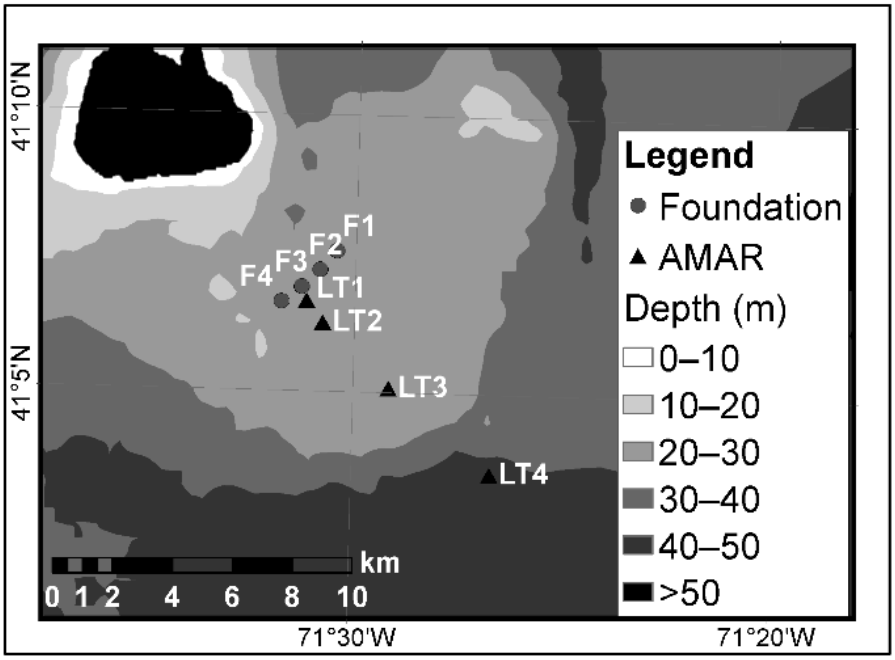

Figure 4-1. Location of the four Block Island Wind Farm foundations (F1-4) monitored in this study and the recorder locations (LT1-4). Foundation F5 (not shown) was completed during the short-term monitoring phase of the project.

Data from 80 pile and recorder combinations were analyzed spread across the four recorders and 24-piling events. Each pile leg (A1, A2, B1, and B2) was measured six times. All three pile sections were measured at Foundation F1 as well as Foundation F2, section 1; Foundation F3, section 2; and Foundation F4, section 3.

4.2.2. Acoustic Data Analysis

Data was provided by the pile driving contractor for the strike energy for every piling blow and the number of strikes required to penetrate each 30 cm of sediment. To

determine how sound levels varied with strike energy and pile penetration, the sound levels for each pile impulse were required. The impulses were extracted from the raw acoustic data using a Teager-Kaiser (Kandia and Stylianou 2006) energy detector with an averaging window set to 31 ms. For a subset of the pile strikes, the detector identified multi-path arrivals after the main impulse. To automatically remove these unwanted detections, they were grouped using K-means clustering with three clusters for 1) spurious high amplitude events, 2) the main group of events, and 3) the low amplitude multi-path arrivals (custom Python software (The Python Software Foundation, www.python.org, V3.5.2) using the package 'pyclustering' V0.6.6.). The multi-path arrival cluster was set to have a mean SEL at least 12 dB below the main arrival group. Any events with higher SEL were included in the analysis.

For each impulse, the 0.125 s time window containing the highest squared pressure was selected for computing the peak sound pressure level ($L_{p,pk}$), sound pressure level (SPL, $L_{p,rms.0.125s}$), per-pulse sound exposure level (SEL, $L_{E,0.125s}$) as well as the SEL in each decidecade band from 10–25000 Hz ($L_{E,0.125s,ddec}$)(terminology and metrics from ISO 2017a are used in this analysis). The fixed time window was selected to generate stable and reproducible SPL estimates. The duration of 0.125 s was chosen to be approximately as long as marine mammal auditory integration times (see Erbe et al. 2016 for a discussion of auditory integration times). This duration was a good match to the duration of the received pulses – 75% of the pulses had a 90% energy duration less than 0.125 seconds. This window duration was also chosen because the 0.125 s duration leaky integrator ($L_{eq\text{-}fast}$) has been shown to be well suited to the study of the effects of sound on marine mammals (Tougaard et al. 2015). $L_{eq\text{-}fast}$ is the fast-time weighted root-mean-

square sound pressure level defined for sound level meters (ANSI S1.4-1983 R2006) that time-weights the received impulse so that the centre 0.125 sec of sound as well as the following ~0.5 seconds are summed in a manner similar to the measured response of human hearing (Tougaard and Beedholm 2019). For this study a 0.125 s fixed window rather than $L_{\text{eq-fast}}$ was used since it is simpler to compute and therefore simpler to adopt as a recommended approach for analyzing pile driving data. The fixed window duration SPL is always greater than $L_{\text{eq-fast}}$; it is 2 dB higher than $L_{\text{eq-fast}}$ at 0.125 second duration for the actual pulse, and 4 dB higher for a 0.0625 second pulse (to verify this evaluate Equation (1) of Tougaard et al. 2015 for a range of actual pulse durations). Thus, the fixed window duration is conservative in that it computes higher sound pressure levels for short pulses that are closer to the 90% duration SPLs but does not excessively attenuate the SPL for longer pulses.

The Technical Guidance on effects of sound on marine mammals from the United States National Marine Fisheries Service recommends the peak sound pressure level and auditory frequency weighted sound exposure level (SEL) as indicators of possible auditory injury or impairment (NMFS 2018, Southall et al. 2019b). Therefore, we have also computed auditory frequency weighted SEL from the 0.125 second window decidecade data. To verify that energy was not missed, the total SEL over the period of each pile driving event computed from the continuous data stream (which includes energy not associated with the impulses) was compared to the total SEL from just the detected impulses. The continuous SEL was within 1-2 dB of the energy contained in the impulses, even at the longest-range recorder (9067 m). The differences were smaller for the weighted SEL than the total SEL. The 10 Hz and above decidecades were summed to

provide the broadband per-strike SEL ($L_{E,0.125s}$). The per-strike SEL were summed to obtain the per-pile SEL.

4.2.3. Linear Regressions

Regression analysis modeled the measured data so that estimates of the sound levels anywhere near the pile could be computed as a function of location and pile driving parameters. Additional predictor variables to describe the pile driving source were: the strike energy, the pile penetration versus strike number, as well as the angle between the pile and the seabed along the line between each pile and recorder. The strike energy and pile penetration logs were provided by the construction contractor Weeks via Tetra Tech and Deepwater Wind. The logs were digitized and time-aligned with the strike detection data. A measure of pile angle was needed. The foundation legs were oriented north-south/east-west, and recorders were deployed along a line extending to the south-east from Foundation F3 (Figure 4-1). Two analysis variables, $\theta_{MC\text{-}R}$ (Mach cone – recorder angle) and θ_{graze} (grazing angle for the Mach cone with the seabed) were created. $\theta_{MC\text{-}R}$ has a value of zero when the pile is inclined away from the recorder and a value of 180 when the pile is inclined towards the recorder. These correspond to the minimum and maximum values of θ_{graze}, which are in the range of +/- 15 degrees. We also knew that changes in the propagation conditions would need to be accounted for since there were changes in the sound speed profile during the measurement period as well as a wide variety of wind and wave states that affected surface scattering.

The structure of linear model (Equation 4-2) is an extension of the damped cylindrical spreading (DCS) model proposed by Lippert et al. (2018) who observed that sound from pile driving must have a geometric attenuation of $10 \cdot \log_{10}(R)$, where R is the

range in meters from pile to recorder, as well as an attenuation that depends on the number of interactions with the seabed and surface.

$$RL = RL_0 + \mathrm{A} \cdot \mathrm{SE} + \mathrm{B} \cdot \mathrm{PP} + C\left(\frac{R}{2H\cot(\theta_{graze})}\right) - (10\log_{10} R + \alpha(f)R) \quad (4\text{-}2)$$

The linear attenuation term is proportional to the range divided by $2H\cot(\theta_{graze})$ where H is the water depth; this term represents the number of interactions with the seabed and surface. The DCS model was extended by adding a strike energy term, *SE*, a pile penetration into the sediment term, *PP*, and a term to account for sound absorption by seawater, $\alpha(f)R$. The $10\cdot\log_{10}(R)$ and $\alpha(f)R$ terms are fixed effects that were accounted for by adding their values to the measured received levels before performing the linear regressions. The response variable in Equation (4-2), *RL*, could be any acoustic metric. Table 4-2 describes the predictor variables. The grazing angle in the DCS model varies with pile inclination and the minimum value was not known a priori. Therefore, the minimum pile inclination was determined as an additional fit parameter for the model. We assumed that the pile legs were inclined inwards 19 degrees, then searched over the range of 0-10 degrees (in 0.1degree increments) for the grazing angle that minimized the AIC for the model fit. The angle was 5.1 for the unweighted SEL and SPL fits, 5.5 for the low-frequency cetacean auditory frequency weighted per-strike SEL and 6.4 for the peak sound pressure level as well as the mid- and high- frequency cetacean auditory frequency weighted SEL fits. A constant value of 5.5 was employed for this analysis. Both the linear strike energy and pile penetration as well as logarithm of those values were evaluated as covariates.

Equation (4-2) is missing terms that account for variability in the propagation conditions such as different sound speed profiles, pile-receiver bathymetry and bottom composition, sea state as well as changes in water depth due to tides. Using an advanced numerical propagation model as the basis for Equation (4-2) rather than damped cylindrical spreading from Lippert et al. (2018) would account for these factors as was previously performed by Wilkes and Gavrilov (2017). However, such a model is much more difficult to use for regressions with measured data and less intuitive for understanding the regression results. Instead, these factors may be investigated by using the random effects term of a linear mixed model. Random effects models group the measured observations based on data parameters and estimate an intercept offset coefficient for that group, so that the remaining linear coefficients better represent their underlying variability in the data. If the propagation effects are unimportant then a linear mixed model will not substantially improve the model goodness-of-fit compared to a standard linear model. Goodness-of-fit can be evaluated with the Akaike Information Criteria (AIC) and plots of residuals versus predictors (among many other methods). By comparing the goodness-of-fit with different random effects predictor variables the type of propagation dependence was determined. The random effects evaluated were: 1) date only (8 cases), which would indicate that sound speed profile was the most important effect; 2) the recording location (4 cases) which would indicate coarse bathymetry was an important effect; 3) pile-recorder path (16 cases), which would indicate that the bathymetry and bottom composition were the most important effect; 4) the pile ID (24 cases) which would indicate that a time specific effect was most important (such as surface scattering); and 5) each pile event and recorder location as independent effects

(80 cases) which would indicate all effects are important. Linear modelling was performed in the '***R***' programming language using the packages 'nlme' for linear mixed modeling (Pinheiro et al. 2017), 'MASS' for standard linear modeling (Venables and Ripley 2002) and 'robustlmm' for robust linear mixed modeling (Koller 2016). Robust mixed effects modeling was used to determine if outliers or heterogeneity affected the model results.

Data from all recorders were used in the linear regressions for peak SPL, SPL, low-frequency-cetacean, otariid and phocid auditory frequency weighted SEL. Data from the recorders at ranges longer than 5000 m were not used for the mid- and high-frequency cetacean auditory frequency weighted SEL because the signal to noise ratio at the longer ranges was too low.

Table 4-2. Predictor variables for the pile driving linear mixed models.

Parameter	Meaning
RL	**Received Level**: any of the measured sound metrics ($L_{p,pk}$, $L_{p,rms,0.125s,}$ $L_{E,24h}$, and five $L_{E,24h,W}$ for the NMFS marine mammal auditory function weighted SEL (NMFS 2018).
RL_0	This is the intercept from the linear model in the same units as RL.
R	**Range** from the pile in meters
SE	**Strike Energy** from pile driving logs in kilojoules
PP	**Pile Penetration Depth** in meters – range 0 to 60 m.
θ_{graze}	**Mach Cone-Grazing Angle:** angle between the Mach Cone and the seabed.
$\theta_{MC \cdot R}$	**Mach Cone-Recorder Angle:** Angle between the recorder and pile, rotated so that if the Mach cone was headed directly at the recorder, the angle was 0. For pile-recorder geometries where the Mach cone was directed downwards at the seabed, the value was 180 degrees.
H	**Water depth** at the recorder, in meters.

Parameter	Meaning
α(f)	**Absorption:** seawater absorption term (e.g.François and Garrison 1982b). Fixed values were used for each metric: 0 dB/km for $L_{p,0.125s,}$ $L_{p,pk}$, $L_{E,0.125s,}$ and $L_{E,0.125s,LF}$; 0.25 dB/km for $L_{E,0.125s,OTA}$ and $L_{E,0.125s,PHO;}$ 1 dB/km for $L_{E,0.125s,MF}$ and $L_{E,0.125s,HF.}$ This term was included in the model to separate the known sea water absorption effects from the unknown effect of reflections from the seabed and sea-surface which was modeled using $C{\cdot}R/(2H\cot(\theta_{graze}))$. These values of absorption were chosen as representative of the frequencies with the most energy from the source in the passband of the auditory weighting functions.

4.2.4. Determining Isopleth Prediction Intervals

Since the estimated isopleths are the product of a statistical fit it is important to determine the prediction interval of the models, and hence the maximum predicted isopleth distances. For linear mixed models the recommended method of estimating prediction intervals is bootstrapping the model, which means running the model with a subset of the available data multiple times to test the range of predicted values. For each bootstrap run, 24 piles were selected randomly from the list, with replacement (i.e. the same pile could be selected more than once). For each pile, a 1:20 decimated strike data set was used, where the starting sample for the decimation was randomly selected between 1 and 20. Each of the bootstrap models were used to predict the received sound level for three strike energies and pile penetrations (2.5th, 50th, and 97.5th exceedance levels of all strikes measured), range (25 m step size), and $\theta_{MC\text{-}R}$ (2 degrees step size). This data array was searched to find the median isopleth ranges, as well as the 2.5% and 97.5% prediction intervals. To be conservative the predictions were made using the overall population fixed effects and ignored the random effects since future measurements could be made along any radial and day. One thousand bootstrap runs were performed for each acoustic metric. For predicting the daily SEL metrics it was necessary to select the number of strikes to model. We assumed 8000 strikes were

assumed to occur since the day with the highest number of strikes was Sept 19 with 7812. For the daily SEL radii estimation we assumed that all strikes had the same per-strike SEL for three cases – the 2.5th, 50th (median) and 97.5th percentiles from the bootstrapped model.

The bootstrapping method of estimating prediction intervals for linear mixed models is computationally intensive for large data sets and requires a moderate computer programming capability. A faster and simpler method is desirable, especially for sound source characterizations that must report results within 24 hours of data collection. Therefore, a second method was evaluated. A single linear mixed model run was performed using all the data, and the difference between the measured and modeled data were computed, using only the population fixed effects (again ignoring the random effects to be conservative). The predicted sound levels were then increased by the 97.5th percentile of the differences (i.e. the residuals), and the range to the isopleths computed using the offset predictions. This method is referred to as the 'increase intercept' method since it effectively adds the offset to the intercept (RL_0) term of the linear models.

4.3. RESULTS

4.3.1. Measured Sound Levels

The measured sound levels generally decreased with range from the piles, but also depended on the grazing angle (Figure 4-2). For each pile the sound levels were approximately normally distributed about their mean values, however, the mean values changed with grazing angle which resulted in multiple protuberances in the sound level violin plots (Figure 4-2, top) and up to 15 dB differences in the total SEL per pile (Figure

4-2, bottom). For example, consider the data at a range of 4618 m, which are from the four legs of pile section 3 at Foundation 4 measured at recorder LT3 (see Table 4-9). The 7856 detected impulses had two clusters of per-strike peak sound pressure levels (Figure 4-2, top). The range of measured per-pile SEL at 4618 m was 172-182 dB re 1 $\mu Pa^2 \cdot s$ (Figure 4-2, bottom). The pile grazing angles as well as variations in propagation conditions, hammer energy, pile penetration into the sediment and the total number of strikes per pile also influenced these sound levels. Detailed measurements from recorder LT1 for piling at Foundation 3, section 2, leg B2 are shown in Figure 4-3 (541 m range – the closest range measured). The sound levels rose in steps because of changes in strike energy and rose steadily throughout the pile driving as the pile penetrated deeper into the sediment (Figure 4-3, A, B). The total pile SEL (L_E) increased rapidly during the first 200-300 strikes, but then increased more slowly throughout the remainder of the pile driving (Figure 4-3, B). The energy was concentrated in the 100–800 Hz band (Figure 4-3, C).

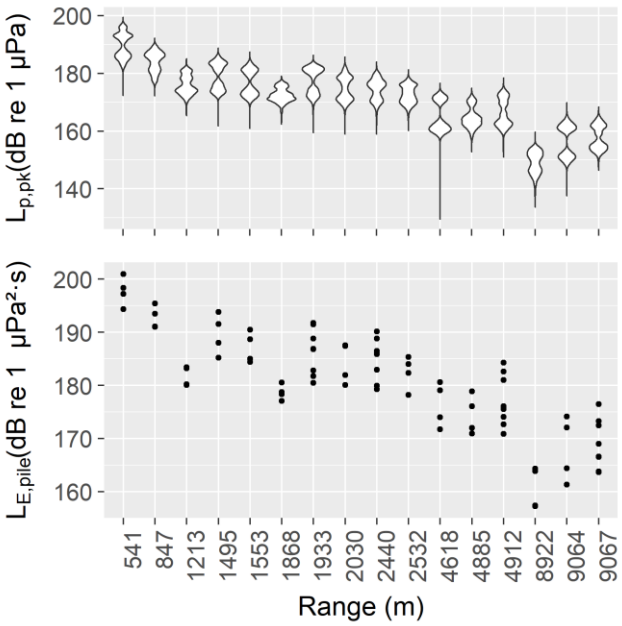

Figure 4-2. Distribution of received sound levels vs measurement range for all detected impact pile driving impulses (range not to scale). (Top) Violin plots of peak sound pressure levels. The different protuberances in each of the distributions correspond to different $\theta_{MC\text{-}R}$ affecting the received sound levels. (Bottom) the per-pile SEL; each dot corresponds to a full measurement made at the range shown on the X-axis.

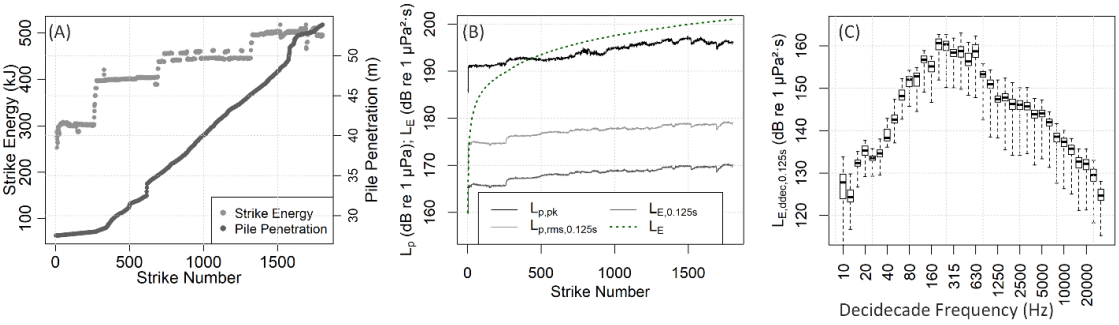

Figure 4-3. Sound levels measured 541 m from the pile during installation of Foundation 3, pile section 2, leg B2 (F3P2B2): (A) Strike Energy and Pile Penetration; (B) Time series of $L_{p,pk}$, $L_{p,rms,0.125\ s}$, $L_{E,0.125s}$ as well as the accumulation of the total pile L_E. (C) distribution of $L_{E,0.125\ s,ddec.}$ The mean background decidecade SEL (0.125 s integration time) was below 120 dB re 1 µPa²·s for all bands and are not shown.

4.3.2. Linear Model of the Measured Sound Levels

The linear and robust mixed models were both superior to the simple linear model in accounting for the dependencies in the data. The linear mixed model and the robust

linear mixed model had similar residual structures, prediction parameters and hence similar performance. The linear mixed modeling approach was selected for further analysis and the bootstrapping analysis of the prediction intervals because each pass of the model was much faster than the robust version.

A wide variety of model definitions were evaluated before selecting the final form for further evaluation. Table 4-3 shows the model definition and AIC for four combinations of predictor variables and the five possible random effects. The model that is linear in strike energy and linear in pile penetration had a much lower AIC than any of the models that included the logarithm of those variables. The Pile ID + recorder ID random effect greatly reduced the AIC and was selected as the best model. This random effect represents each combination of date, time of day and pile-to-recorder path as a unique structure. The random effects are adjustments to the model's intercept term. All random effects coefficients had a magnitude of less than 6 dB, and 75% of them were below 3 dB. The distribution of the random effects as a function of acoustic metric response variable, date, $\theta_{MC\text{-}R}$ and pile-recorder radial are shown in Figure 4-4. The linear mixed model coefficients and standard deviations determine by the bootstrapping analysis are shown in

. The standard linear model estimated pile penetration and strike energy coefficients were within 10% of the values found for the linear mixed model but with higher standard deviations.

Table 4-3. Akaike Information Criterion for different linear mixed model definitions and random effects for the low frequency cetacean auditory frequency weighted per-strike sound exposure levels (LF SEL, Southall et al. (2019b)). The covariate abbreviations are: R – range, SE – strike energy, PP – pile penetration, Q – $R/(2H\cot(\theta_{graze}))$ where H is the water depth. A, B, and C are the model fit parameters. The intercept term is assumed and not explicitly included.

Model Definition	Random Effect (number of unique effects)	AIC
LF SEL ~ $10\cdot\log_{10}(R) + \alpha(f)\cdot R + A\cdot SE + B\cdot PP + C\cdot Q$	Pile ID + recorder (80)	297646
LF SEL ~ $10\cdot\log_{10}(R) + \alpha(f)\cdot R + A\cdot SE + B\cdot\log_{10}(PP) + C\cdot Q$	Pile ID + recorder (80)	302824
LF SEL ~ $10\cdot\log_{10}(R) + \alpha(f)\cdot R + A\cdot\log_{10}(SE) + B\cdot PP + C\cdot Q$	Pile ID + recorder (80)	308575
LF SEL ~ $10\cdot\log_{10}(R) + \alpha(f)\cdot R + A\cdot\log_{10}(SE) + B\cdot\log_{10}(PP) + C\cdot Q$	Pile ID + recorder (80)	317243
LF SEL ~ $10\cdot\log_{10}(R) + \alpha(f)\cdot R + A\cdot SE + B\cdot PP + C\cdot Q$	Range (16)	453917
LF SEL ~ $10\cdot\log_{10}(R) + \alpha(f)\cdot R + A\cdot SE + B\cdot PP + C\cdot Q$	Recorder (4)	464884
LF SEL ~ $10\cdot\log_{10}(R) + \alpha(f)\cdot R + A\cdot SE + B\cdot PP + C\cdot Q$	Pile ID (24)	476348
LF SEL ~ $10\cdot\log_{10}(R) + \alpha(f)\cdot R + A\cdot SE + B\cdot PP + C\cdot Q$	Date (8)	503789

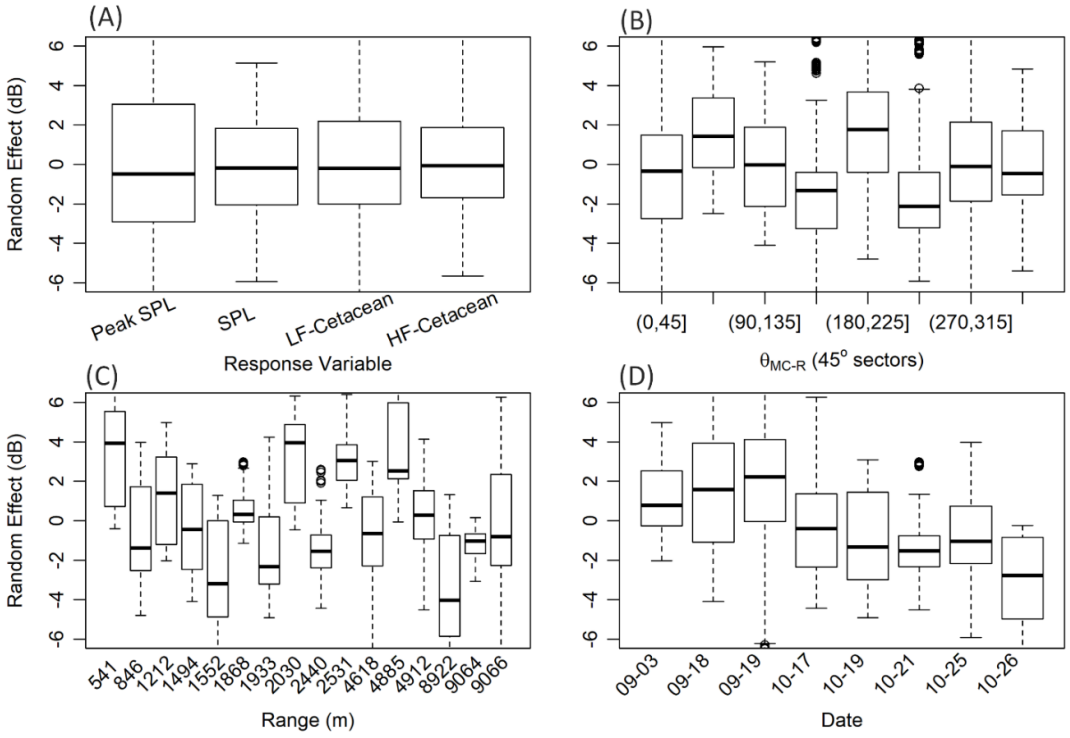

Figure 4-4. Distribution of the random effect intercept coefficients. The data was obtained by running the model for four Response Variables; for each Response Variable the model was run 10 times, with a random selection of $1/10^{th}$ of the complete data set.

Table 4-4. Mean (standard deviation) coefficients for the DCS-based linear mixed model (A, B and C in Equation 4-2). The standard deviations were obtained using 1000 boot-strapping model runs where each run used 5% of the dataset. LF, HF, VHF, OTA and PHO refer to the Southall et al. (2019b) low, high and very high frequency cetacean as well as otariid and phocid marine mammal hearing groups. 8000 strikes were used for computing the daily SELs. Q is $\frac{R}{2H\,cot(\theta_{graze})}$

Sound Metric	Intercept (dB)	A·Strike Energy (dB/kJ)	B·Pile Penetration (dB/m)	C·Q (dB/reflection)
$L_{p,pk}$	208. (0.56)	0.0101 (0.0011)	0.0565 (0.012)	-0.357 (0.015)
$L_{p,rms}$	195 (0.48)	0.0120 (0.0010)	0.0276 (0.0088)	-0.304 (0.012)
$L_{E,0.125s}$	186 (0.46)	0.0120 (0.0010)	0.0278 (0.0092)	-0.305 (0.012)
$L_{E,0.125s,LF}$	184 (0.48)	0.0118 (0.0010)	0.0451 (0.0089)	-0.318 (0.013)
$L_{E,0.125s,OTA}$	173 (0.52)	0.0101 (0.0010)	0.0888 (0.0084)	-0.323 (0.018)
$L_{E,0.125s,PHO}$	174 (0.51)	0.0108 (0.0009)	0.0792 (0.0082)	-0.313 (0.015)
$L_{E,0.125s,HF}$	159 (0.62)	0.0101 (0.0012)	0.0779 (0.012)	-0.267 (0.017)
$L_{E,0.125s,VHF}$	155 (0.69)	0.0099 (0.0012)	0.0732 (0.014)	-0.279 (0.018)

The interactions of the model terms are difficult to visualize from Table 4-4. Figure 4-5 provides predictions of the low-frequency cetacean auditory frequency weighted SEL for bearings of 0-360 degrees and for the 16 ranges measured during the long-term program. The predictions are overlaid with the per-strike $L_{E,0.125s,LF}$ from all measurements. The 1/cot(θ_{graze}) dependence of the DCS model is evident in Figure 4-5. When the pile was inclined toward the recorder (180 degrees), the sound levels were attenuated more rapidly with range compared to orientations where the piles were inclined away from the recorders (0 & 360 degrees). The median hammer strike energy and pile penetrations were used for the median predictions in Figure 4-5, while the 2.5th and 97.5th percentiles of the strike energies and pile penetrations were used for the dashed prediction intervals in Figure 4-5.

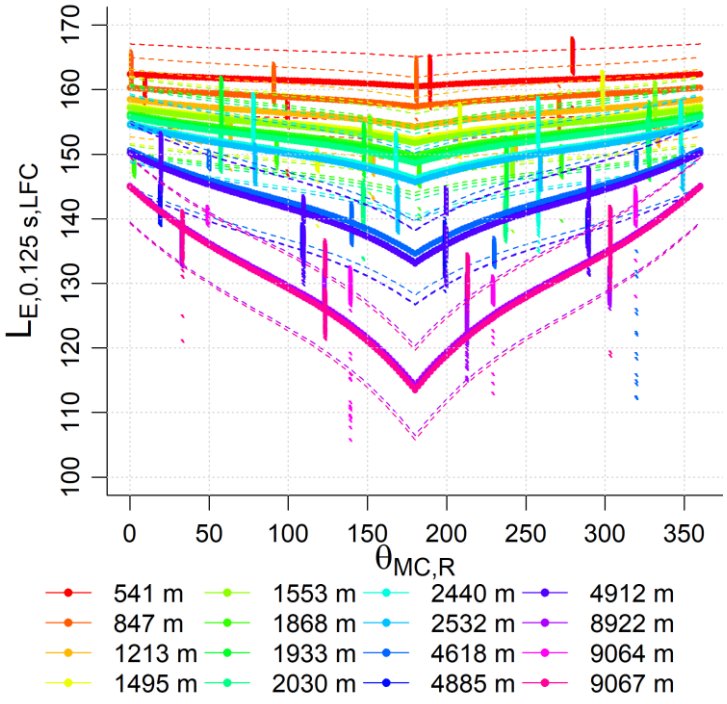

Figure 4-5. Measured and modelled $L_{E,0.125s,LF}$ (dB re 1 μPa²·s) versus the mach-cone recorder angle ($\theta_{MC\text{-}R}$) for all data collected during the long-term monitoring program at Block Island. Solid lines show the median predicted $L_{E,0.125s,LF}$ (from the 1000 bootstrapping model runs) for the 16 measurement ranges at the median hammer strike energy and pile penetrations using the coefficients in Table 4-4. The dashed lines are the 95% prediction interval (2.5^{th} – 97.5^{th} percentiles of 1000 bootstrapping runs). The complete set of all measured $L_{E,0.125s,LF}$ are overlaid, adjusted by the per-pile random effects coefficients.

4.4. Discussion

This analysis of the Block Island Wind Farm long-term data using a linear mixed model identified two types of variability that affected the received sound levels 540 – 9100 m from the impact pile driving: 1) variability in the source factor – i.e. the emitted sound levels depended on the strike energy and pile penetration; and 2) variability in the propagation conditions which included the inclination of the pile, source-receiver path

effects, and date/time related effects. The results are informative for the development of pile driving acoustic propagation models, and for determining how to establish sound level isopleths for the monitoring of marine life during future offshore pile driving to install wind turbines. The results are also useful for extending the range of validity of the empirical peak sound pressure level versus SEL relationship proposed by Lippert et al. (2015).

4.4.1. Variability in Sound Levels

The long-term data from monitoring of the Block Island Wind Farm provided enough data to evaluate a novel method of analyzing pile driving sound levels: the use of a linear mixed model based on damped cylindrical spreading (Lippert et al. 2018). The random effect in the linear mixed model was designed as an offset to a standard linear model's intercept term that could serve as a pile-to-recorder correction to the propagation loss for each pile-driving event. Thus, the linear model provided information about the acoustic propagation variability and changes in the source factor because of changes in the pile driving conditions – specifically the strike energy and pile penetration.

The coefficients for strike energy varied by sound metric (Table 4-4). The coefficient for strike energy was slightly smaller for metrics where the data has more high frequency dependence (e.g. the peak sound pressure level and the high frequency cetacean weighted SEL). The strike energy term serves to increase the model intercept term (Equation 4-2) by 0.01 – 0.012 dB/kJ. The mixture of linear and logarithmic units was unexpected, but this combination was strongly preferred by the AIC and was therefore selected as the best model. Since the minimum and maximum strike energy were 74 kJ and 684 kJ, the predicted sound levels increased up to 6.5 dB because of

changes in the strike energy which will substantially increase the biological effects isopleths. For comparison, Robinson et al. (2007) measured the ramp up of pile driving energy from 80-800 kJ over 800 strikes and found an increase in broadband SEL of 8 dB and the peak-to-peak sound pressure level increased 10-12 dB (i.e. the maximum peak sound pressure level to compressional peak sound pressure level). The model coefficients found here are very similar: a 8.6 dB increase in SEL and a 7.2 dB increase in peak sound pressure level (nominally a 13.2 dB increase in peak-to-peak sound pressure level) for the range of strike energies measured by Robinson et al. (2007). The Robinson et al. (2007) results did not separate possible effects of pile penetration from the strike energy increases.

The model indicated that sound levels rose as the pile penetrated the sediment for all metrics. The pile penetration coefficient was higher for the metrics that depend on high frequency content, including L_{pk}, and the otariid, phocid, high- and very high-frequency cetacean auditory frequency weighted SEL (Table 4-4). The maximum penetration of the piles at the Block Island Wind Farm was 60 m, so the effective increase in the intercept term ranged from ~1.5 dB for $L_{p,rms}$, and $L_{E,\ 24h}$; ~3 dB for $L_{p,pk}$ and $L_{E,24h,LF}$; and up to 5 dB for $L_{E,24h,HF}$, $L_{E,24h,VHF}$, $L_{E,24h,OTA}$, and $L_{E,24h,PHO}$. MacGillivray (2014) reported that measured sound levels at frequencies above 600 Hz were higher than predicted by a pile sound source model that agreed very well with measurements below 600 Hz. The possible sources of mismatch were identified as an incorrect spectrum in the source forcing function, or excitation of higher order vibration modes in the pile. The increase in sound levels at higher frequencies with penetration found here supports the idea that higher order vibrations are being excited in the piles, since both the free length

of the pile and how tightly the bottom is held will affect the frequency and amplitude of those vibrations. The pile penetration results are useful for several purposes. First, the higher-frequency weighted SEL have substantial energy contributions starting at ~ 2kHz (NMFS 2018) which is higher than the 2-3 kHz that is the top frequency for most pile driving source models (Lippert et al. 2016). The current results should inform the development of improved high frequency modeling capabilities so that accurate estimates of the possible effects of pile driving on pinnipeds and odontocetes may be performed. Note that those are the marine mammal species groups most likely to be found in the shallow waters where pile driving occurs. Second, the variation in sound levels with pile penetration changes the isopleths during the pile driving, even if the strike energy remains unchanged. Variable isopleths are discussed in Section 4.4.2.

The range and directional variability in received levels were modeled in Equation (4-2) by the fixed $10 \cdot \log_{10}(R) + \alpha(f) \cdot R$ term, the damped cylindrical spreading term, $C \cdot R/(2H\cot(\theta_{graze}))$, and the random effects. The largest source of variability in the sound levels measured at Block Island was the inclination angle between the pile and the seabed in the direction of the receiver. This was also noted during finite element modeling and measurement of raked (inclined) piles by Wilkes and Gavrilov (2017). When the pile is inclined towards the receiver there are more interactions with the surface and seabed which attenuates the received sound levels. The coefficient of the reflection term in the DCS model was approximately −0.3 dB/reflection (Table 4-4

). To understand this term, for the average conditions at the Block Island project site (25 m water depth), there were 2 seabed reflections per kilometer (reflections/km) when the pile was inclined away from the recorder, 7 reflections/km for directions where the pile appears to be vertical, and 13 reflections/km when the pile was inclined towards the recorder (assuming no refractive effects). Thus, the attenuation varied from 0.6 dB/km to 3.9 dB/km (slightly more for the peak sound pressure level). The results from Wilkes and Gavrilov (2017) showed differences in received SEL of 15 dB as a function of angle at a range of 1.3-1.5 km. Their measurements were made in 6.5-7 m of water,

and hence there would be 3-4 times more reflections per km than we encountered at Block Island and hence higher attenuations. Thus both the current measurement and Wilkes and Gavrilov (2017) agree with the DCS model. The implication of these results is that future modeling and measurements of inclined piles for regulatory compliance must consider the orientation of the piles and its effects on the biological isopleths.

The random effects corrections of the linear mixed model represented useful information about the function of the model and the acoustic propagation conditions. Random effect corrections did not depend on the Response Variable (Figure 4-4, A), as expected for correct functioning of the model. The boxplots of the random effects corrections vs angle between the Mach cone and recorder ($\theta_{MC\text{-}R}$) do not overlap at some angles (Figure 4-4, B), which suggests there may still be an angular dependence that is not fully accounted for in the model, perhaps due to the use of a fixed value for θ_{graze} rather than a value that depended on the pile location and / or the analysis metric. The boxplots of random effects coefficients vs range, where range is a proxy for the pile-to-recorder path, are highly non-overlapping (Figure 4-4, C), meaning there are different propagation effects along these paths that do not depend on time and are likely due to small-scale bathymetry and sediment composition differences. These types of variations due to small changes in propagation conditions were predicted by the Monte Carlo simulations of Lippert and Estorff (2014). The random effects corrections plotted against date show two clusters – the first three in September have mean corrections above zero, and the five in October have corrections below zero (Figure 4-4, D). This view of the random effects appears to have detected changes in the sound speed profile which was upward refracting in September and iso-velocity in October.

4.4.2. Effects of Sound Level Variability on Isopleths

The linear mixed model was developed to understand the variability in the measured sound levels, which provided insights into changes in the effective source factor as well as propagation conditions. Linear models of sound levels vs range from human activities are created to estimate the biological effects isopleth distances. In the present study we estimated the median isopleths and their variability due to the known effects as well as the prediction interval of the models. The median isopleths measured during the long-term monitoring of the Block Island Wind Farm installation were lower than the pre-construction estimates for all biological effects' thresholds and propagation directions (the 206 dB re 1 µPa $L_{p,pk}$ and 207 dB re 1 µPa $L_{p,0.125\,s}$ could not be extrapolated from the measurements without extending the regressions too far from the minimum measurement distance of 541 m). In some cases, the models indicated that for directions where the pile was inclined away from receiver, the sound levels could exceed the permitted distances. This occurred for the sea turtle behavioural disturbance and marine mammal level B harassment thresholds at ranges longer than permitted when the strike energies where high and the piles were near refusal (i.e. at full penetration depth, see Table 4-1 and Table 4-5).

The sources of variability result in isopleth distances that are neither symmetric nor constant (e.g. Figure 4-6). They depend on pile driving parameters that change over the duration of the piling, and on random fluctuations in the piling and propagation conditions. The directional effect is measured in dB/reflection. The effects on regulatory radii are more exaggerated for isopleths that have longer ranges with fewer seabed and surface interactions (see Figure 4-6 and Table 4-5). It is worth noting that the directional

effect measured here for inclined piles may also be recreated to some extent by steep bathymetry – changes in water depth from shallow to deep water will decrease attenuation, and from deep to shallow will increase attenuation. The effect of the strike energy and pile penetration on the isopleth distances are fixed effects that are predictable, however, their effects are compounded by the directional effect. Figure 4-6 demonstrates this using the prediction interval from the model – the distance doubled for a pile inclined towards the recorder but went up by almost a factor of four for a pile inclined away from the recorder. The effect is demonstrated in Figure 4-7 that shows the sea turtle disturbance isopleth of 166 dB re 1 μPa $L_{p,rms}$ as it evolved over one piling event – pile F3P2B2 on 18 Sep 2015 (also shown in Figure 4-3). During this piling event the strike energy increased from 308 kJ to 518 kJ, and the pile penetration increased from 28 m to 54 m. The isopleth distances doubled when the pile was inclined away from the recorder but only increased by ~40% when the pile was inclined towards the recorder. These results show the importance of including accurate treatment of the strike energy and pile penetration in acoustic propagation modeling of pile driving. Cushioning materials between the hammer and pile head are also a key component of accurate modeling of how strike energy converts to radiated energy (MacGillivray 2014).

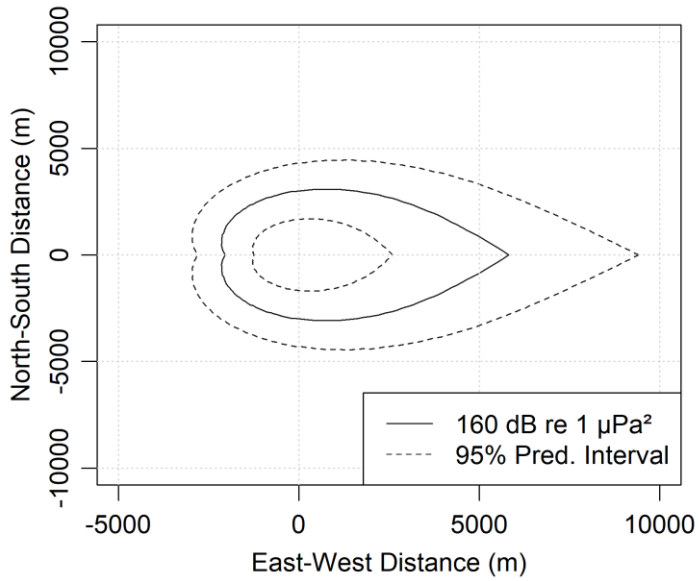

Figure 4-6. Bootstrapped predictions of the Block Island Wind Farm isopleths of biological effects for the 160 dB re 1 µPa² $L_{p,0.125\,s}$ isopleth (see Table 4-1) with 2.5 and 97.5% prediction intervals. The isopleths are non-circular because of the directional sound propagation effects with the inclined piles. Zero degrees in Figure 4-5 is to the right in this figure.

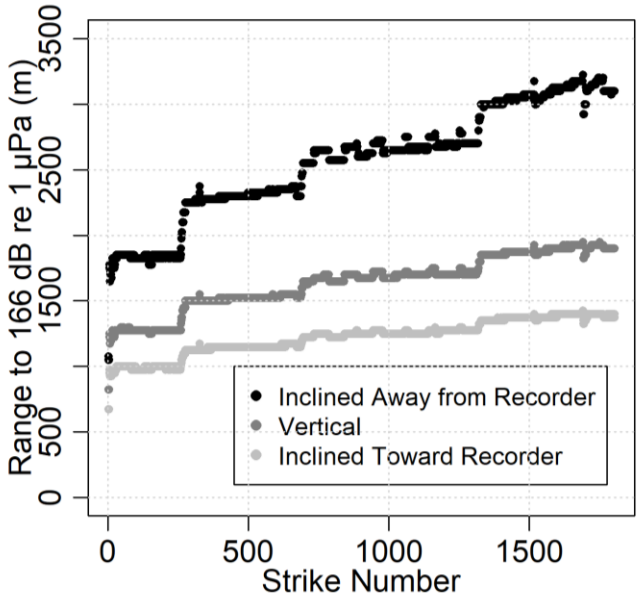

Figure 4-7. Estimate of the range to the sea turtle disturbance sound pressure level (166 dB re 1 µPa) using the actual strike energies and pile penetrations from pile F3P2B2 on 18 Sep 2015. Strike energy and pile penetration are shown in Figure 4-3.

Table 4-5. Example isopleths (m) using the BIWF data and the DCS-based model for selected biological effects thresholds from NMFS and NOAA (1995), Popper et al. (2014b), and Southall et al. (2019b). Ranges are shown for three conditions: 1) the loudest case – the pile inclined away from the recorder with 97.5th percentile of the hammer energy and penetration depth; 2) the median case of a vertical pile and the median hammer energy; and 3) the quietest case – the pile inclined towards the recorder with 2.5th percentile of the hammer energy and pile penetration. The bold number at the centre of each box is the median range. The lower-left and upper-right numbers are the lower and upper prediction intervals (2.5th and 97.5th percentiles, respectively), obtained by bootstrapping the linear mixed effects model 1000 times for each of the acoustic metrics and predicting the sound levels at each range steps of 25 m.

Isopleth Metric	Regulatory threshold	Pile Inclined away from recorder with 644 kJ hammer energy & 56 m pile penetration	Vertical pile with 392 kJ hammer energy & 38 m pile penetration	Inclined toward recorder with 74 kJ hammer energy & 8 m pile penetration
Fish unweighted potential mortal injury[1]	210 dB re 1 µPa²·s $L_{E,24h}$	350 **<250*** <250*	300 **<250*** <250*	275 **<250*** <250*
Fish unweighted recoverable injury[1]	203 dB re 1 µPa²·s $L_{E,24h}$	1450 **600** <250*	1050 **500** <250*	825 **400** <250*
LF weighted PTS[2]	183 dB re 1 µPa²·s $L_{E,24\,h,LF}$	14700 **10075** 5200	6025 **4475** 2775	3800 **2900** 1900
Marine mammal level B take[3]	160 dB re 1 µPa $L_{p,0.125\,s}$	9425 **5800** 2575	4325 **3025** 1675	2825 **2075** 1250
VHF weighted PTS[2]	155 dB re 1 µPa²·s $L_{E,24\,h,VHF}$	7575 **5425** 2925	4725 **3525** 2100	3400 **2575** 1625

[1] Popper et al. (2014b) Table 7.3
[2] Southall et al. (2019b).
[3](NMFS and NOAA 1995)
* Because the shortest measurement range was 541 m, it was not appropriate to extrapolate the regressions closer to the pile than 250 m.

The results above show the importance of determining the prediction interval for linear models of pile driving sound levels when estimating the biologic effects isopleths. A quick but accurate method of determining the maximum distance is desired. The bootstrapping and increased intercept methods of estimating the maximum isopleth distance are compared in Table 4-6. Both methods produced the same median isopleth

distance for all three cases and all three metrics. The maximum isopleth distances differed by at most 2% between methods. The increased intercept method is recommended for most applications due to ease of computation.

Table 4-6. Comparing methods of determining the isopleth distance prediction interval. Method 1: 1000 bootstrapped model runs. Method 2: perform a single linear mixed model run, then increase the intercept term of so that 97.5% of the measured data points are below the prediction line. Bold values in the bottom left of each cell are the median isopleths. The value in the top right-hand corner of each cell is the 97.5th percentile prediction interval maximum.

Isopleth Metric	Regulatory threshold	Prediction Interval Modeling method	Pile Inclined away from recorder with 644 kJ hammer energy & 56 m pile penetration	Vertical pile with 392 kJ hammer energy & 38 m pile penetration	Inclined toward recorder with 74 kJ hammer energy & 8 m pile penetration
Turtle disturbance	166 dB re 1 µPa $L_{p,\,0.125\,s}$	Bootstrapping	4625 **2325**	2525 **1525**	1775 **1150**
		Increase Intercept	4675 **2325**	2575 **1525**	1800 **1150**
Marine mammal level B take	160 dB re 1 µPa $L_{p,0.125\,s}$	Bootstrapping	9425 **5800**	4325 **3025**	2825 **2075**
		Increase Intercept	9600 **5800**	4375 **3025**	2850 **2075**
Fish disturbance	150 dB re 1 µPa $L_{p,0.125\,s}$	Bootstrapping	>20000 **15550**	8000 **6300**	4925 **3925**
		Increase Intercept	>20000 **15550**	7950 **6300**	4875 **3925**

4.4.3. Relationship between Peak Sound Pressure Level and Sound Exposure Level

Lippert et al. (2015) discussed the difficulties in modeling the peak (and peak-to-peak) sound pressure level due to scattering from the rough seabed and surface. The SEL however, is relatively straight-forward to model and numerous accurate methods exist (for frequencies below 2 kHz, Lippert et al. 2016). In Lippert et al. (2015) they demonstrate that there is a linear relationship between the peak-to-peak sound pressure

level and the SEL using data from three North Sea piling operations in water depths of 27-40 meters. The linear relation is given in Equation 4-3).

$$L_{p,pk} = A \cdot L_{E,0.125s} + B \ . \quad (4\text{-}3)$$

It is desirable to know if the relationship holds for the Block Island data. The coefficient values obtained by Lippert et al. (2015) were A~1.4 and B~-40 dB. In the present study $L_{p,pk}$ was used instead of $L_{p,pk\text{-}pk}$ since the regulatory threshold for fish uses the $L_{p,pk}$ metric (Table 4-1). When the L_E was restricted to the same range of values as measured by Lippert et al. (2015) (155-170 dB re 1 μPa²·s) the model coefficients from Equation 4-3) were A=1.37 and B=-32 (Figure 4-8). This is excellent agreement with the previous results, noting that $L_{p,pk\text{-}pk}$ will be approximately 6 dB greater than $L_{p,pk}$ and hence the intercept term B reported here should be ~6 dB greater than reported by Lippert et al. (2015). For the full range of per-strike L_E measured at Block Island Wind Farm, as slightly different parameter set was obtained with A=1.13 and B=2. The similarity of the results with such different parameters, particularly the term 'B', is a reminder that model parameters that look largely different can produce similar results. Thus the Lippert et al. (2015) peak sound pressure level – vs – SEL relationship holds over a wider range of SELs than was previously demonstrated. In the present results, data from all bearings were included in Figure 4-8, and therefore we have effectively fit data over a wide range of $R/(2H\cot(\theta_{graze}))$ where the variations were in R and θ_{graze} but easily could have been due to changes in depth (H). Thus, the relationship likely holds over a wide range of water depths.

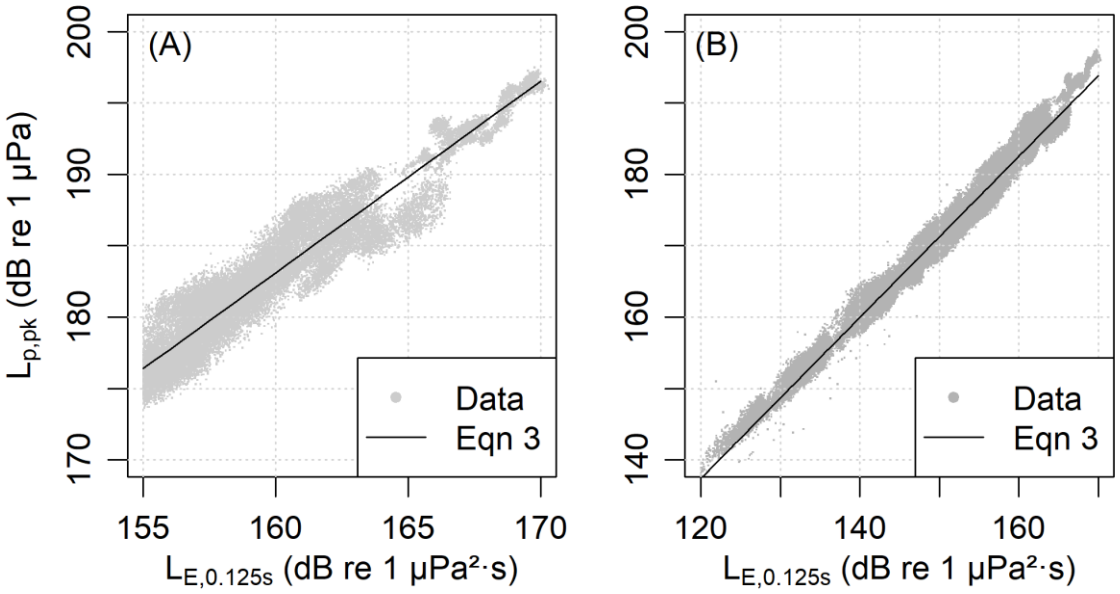

Figure 4-8. Per-strike SEL ($L_{E,0.125s}$) vs peak sound pressure level ($L_{p,pk}$) and regression curves. (A) restricting the L_E to the range reported in Lippert et al. (2015). (B) The full $L_{E,0.125s}$ range measured at Block Island Wind Farm.

4.4.4. Recommendations for Recording and Analyzing Pile Driving Biological Effects Isopleths

Accurate measurement of the distances from pile driving over where biological effects are possible requires careful attention to detail. For data collection:

1) Perform numerical acoustic modelling to estimate the biologic effects isopleths. Assume at least a +/-3 dB variability in source factor to estimate the possible range of radii.

2) Place one recorder at or near the shortest expected isopleth distance, and another at or beyond the furthest isopleth distance you wish to estimate. Confidence intervals are much larger outside the range span measured.

3) Use at least three recorders, however four are highly recommended when the range span of interest is larger than 1–2 km.

4) Logarithmically space recorders in range in as straight a line from the pile as possible.

5) Place all recorders at the same depth where possible; being in a straight line is more important.

6) For water depths less than 50 m, a single hydrophone on the bottom will suffice in most conditions. For deeper waters with complex propagation conditions a second hydrophone in the water column may be needed – the acoustic propagation modelling will help inform this choice.

7) For inclined piles, monitor along the radial with the pile inclined away from the recorders.

With respect to data analysis:

1) Process all events with a fixed window duration; 0.125 s is recommended.

2) Use a systematic, repeatable method to remove outliers and false alarms from the data.

3) For single radial measurements, fit the data to an equation of the form $RL = constant - 10\log_{10}R + \frac{B \cdot R}{2H \cot \theta_{graze}}$ where B should be negative (Lippert et al. 2018)

4) For multiple pile or radial measurements use a linear mixed model, where the random effect is the recorder-pile combination.

5) Estimate and include the prediction intervals by determining an offset for the model's RL_0 term that results 97.5% of the measured data being less than the model fit.

6) During detailed post analysis include the hammer strike energy and pile penetration data as co-variates if they are available.

For analysis of a single piling event, the linear models will produce the same result whether their input is a single mean value for the acoustic metrics, or the value for each individual impulse. In these cases, computing the one-minute peak sound pressure level and sound exposure levels is simpler and will generate equivalent results. The one-minute method should not be used for sound pressure level metrics.

4.5. ACKNOWLEDGEMENTS

The author would like to thank Deepwater Wind / Block Island Wind Farm for making this data set available for publication and JASCO Applied Sciences for support preparation of this manuscript. Thanks to JASCO's engineering department and field teams for developing and deploying the moorings that successfully recorded this data set. The logistics and field work components were arranged and supported by Tetra Tech Inc and performed from the F/V *Heather Lynn*. Thanks to Robert Mills, David Zeddies and Jeff MacDonnell of JASCO for assistance with the original data analysis for Block Island Wind Farm that was the starting point for this analysis. Thanks to Joanna Mills-Flemming for assistance with setting up and understanding the operation of linear mixed models and robust linear mixed models. Sound speed profile data were supplied by Tetra Tech Inc.

Thanks to Michael Ainslie for his reviews of early versions of the manuscript, in particular for pointing out the newly published (Lippert et al. 2018) that became an integral part of this analysis.

Thanks to the anonymous reviewers of the original manuscript who challenged me to generalize the discussion and provide more insights into the pile penetration and strike energy results.

4.6. SUPPORTING INFORMATION

4.6.1. Recorders

Autonomous Multichannel Acoustic Recorders (AMARs, JASCO Applied Sciences) were deployed at Stations LT1-LT4 from 1 September – 1 November 2015 Table 4-7. The mooring configuration is shown in Figure 4-9.

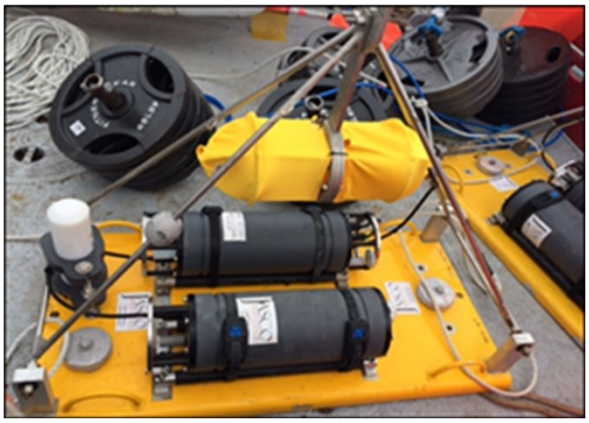

Figure 4-9. Recorder configuration on bottom plates with hydrophones mounted ~0.5m above the seabed. The upper cylinder is the recorder, the lower cylinder is a 48-D-cell alkaline battery pack.

The recorders sampled continuously at 64 kHz using GTI-M8E-0dB hydrophones (-200 dB re 1 V/µPa nominal sensitivity) which measures a maximum peak-to-peak pressure of 202 dB re 1 µPa. The hydrophones were calibrated in the laboratory prior to

deployment using a G.R.A.S. 42-AC pistonphone calibrator, as well as on the ship deck prior to deployment. AMAR268 at Station LT4 during the second deployment had a second hydrophone with 35 dB of preamplifier gain to monitor the ambient soundscape between piling sessions.

Table 4-7. BIWF long-term recorder locations. Two deployments were performed with a retrieval and servicing of the recorders between monitoring sessions.

StartDate	EndDate	AMAR	Station	Latitude	Longitude	depth
1-Sep-15	20-Sep-15	AMAR205	LT1	41.10997	-71.51983	25
1-Sep-15	20-Sep-15	AMAR216	LT2	41.10318	-71.51205	26
19-Sep-15	20-Sep-15	AMAR207	LT3	41.08473	-71.48648	23
1-Sep-15	20-Sep-15	AMAR224	LT4	41.05993	-71.44663	43
14-Oct-15	1-Nov-15	AMAR214	LT1	41.11064	-71.51905	25
14-Oct-15	1-Nov-15	AMAR176	LT2	41.10407	-71.5125	26
14-Oct-15	1-Nov-15	AMAR223	LT3	41.0847	-71.4857	23
14-Oct-15	1-Nov-15	AMAR268	LT4	41.05934	-71.44476	43

4.6.2. Pile Locations and Pile Driving Dates Analyzed

Table 4-8 contains the location of the four foundations measured during the long-term program. Table 4-9 identifies the piles measured along with key pile driving parameters.

Table 4-8. Foundation Locations

Foundation	Latitude	Longitude
F1	41.12572	-71.5076
F2	41.11994	-71.514
F3	41.11474	-71.5212
F4	41.1102	-71.5291

Table 4-9. Summary of the piles analyzed

Foundation	Pile Type	Leg	Date	Start Time (EDT)	End Time (EDT)	Total Blows	Max Strike	Total Energy (MN•m)
F1	P1	A1	2015-09-19	13:00	13:37	1295	212	188
F1	P1	A2	2015-09-19	15:10	15:53	1364	176	178
F1	P1	B1	2015-09-19	8:28	12:40	1110	175	125
F1	P1	B2	2015-09-19	13:56	14:44	1471	173	206
F1	P2	A1	2015-10-17	13:37	14:11	1095	495	462
F1	P2	A2	2015-10-17	12:39	13:25	1289	469	502
F1	P2	B1	2015-10-17	14:17	14:49	1043	496	429
F1	P2	B2	2015-10-17	11:39	12:32	1295	412	450
F1	P3	A1	2015-10-21	10:16	11:09	1957	612	1119
F1	P3	A2	2015-10-21	9:10	10:10	2020	600	1144
F1	P3	B1	2015-10-19	16:25	17:15	1685	647	969
F1	P3	B2	2015-10-19	15:05	16:10	2010	652	1206
F2	P1	A1	2015-09-03	11:13	11:41	766	101	60.9
F2	P1	A2	2015-09-03	9:55	10:22	741	101	57.8
F2	P1	B1	2015-09-03	14:40	15:15	906	171	88.8
F2	P1	B2	2015-09-03	16:49	17:17	733	102	57
F3	P2	A1	2015-09-18	10:01	10:49	1639	327	483
F3	P2	A2	2015-09-18	14:17	15:08	1767	318	522
F3	P2	B1	2015-09-18	8:36	9:38	2128	522	957
F3	P2	B2	2015-09-18	12:52	13:58	2278	518	969
F4	P3	A1	2015-10-26	8:13	9:11	1960	572	855
F4	P3	A2	2015-10-25	16:37	17:46	2515	445	600
F4	P3	B1	2015-10-25	14:18	15:06	1669	465	584
F4	P3	B2	2015-10-25	15:23	16:16	1712	539	679

4.6.3. Teager-Kaiser Energy Detector

The Teager-Kaiser (TK) detector operated on the calibrated time series from each hydrophone. The time series data was squared and summed over a 31 ms window, then divided by the number of samples in the 31 ms window, and the square-root was taken. The 31 ms 'root-mean-square time series' was divided by its mean value for each two-second buffer of data and passed to the Teager-Kaiser (TK) operator (4-4) (Kaiser 1990, Kandia and Stylianou 2006).

$$TK(i) = \frac{X(i)^2}{X(i-1)X(i+1)} \qquad 4\text{-}4$$

The 31 ms duration was empirically selected to match the detector time-step to the typical length of the pile driving impulses. Normalizing the two-second buffer by its mean value allows us to use a fixed threshold that is independent of the absolute magnitude of the raw time series data. When the TK operator exceeds the detector threshold, set empirically to 25, a pile strike was detected. The processing then selected a 0.5 second window from the original time series centered on the impulse detection time and found the 0.125 second duration with the highest squared sound level. The peak SPL, SPL, SEL and 1/3-octave-band SELs were computed on the 0.125 s windows. The detector was configured with a 'lock-out' of 0.25 seconds after a strike was identified to minimize false alarms on multi-path arrivals. This detector was implemented in custom Java software (Oracle, Redwood Shores CA, V1.8) as part of the PAMlab tool suite (JASCO Applied Sciences, Halifax NS, V8.1).

4.6.4. Example Acoustic Measurements

Figure 4-10 is an example of all impulses detected by the TK detector for piling at Foundation 1, Section 1, leg B2 (F1P1B2) on 19 Sep 2015. The pile driving logs (see Section 4.6.6) indicate 1471 strikes were used. Figure 4-11 shows the same data after applying K-means clustering with 3 groups to separate the main arrivals, reflections, and occasional over-energy events (e.g. vessels or other local events). 1467 strikes were identified at a range of 2030 m, 1412 at 2531 m, 1543 at 4885 m, and 1467 at 8922 m.

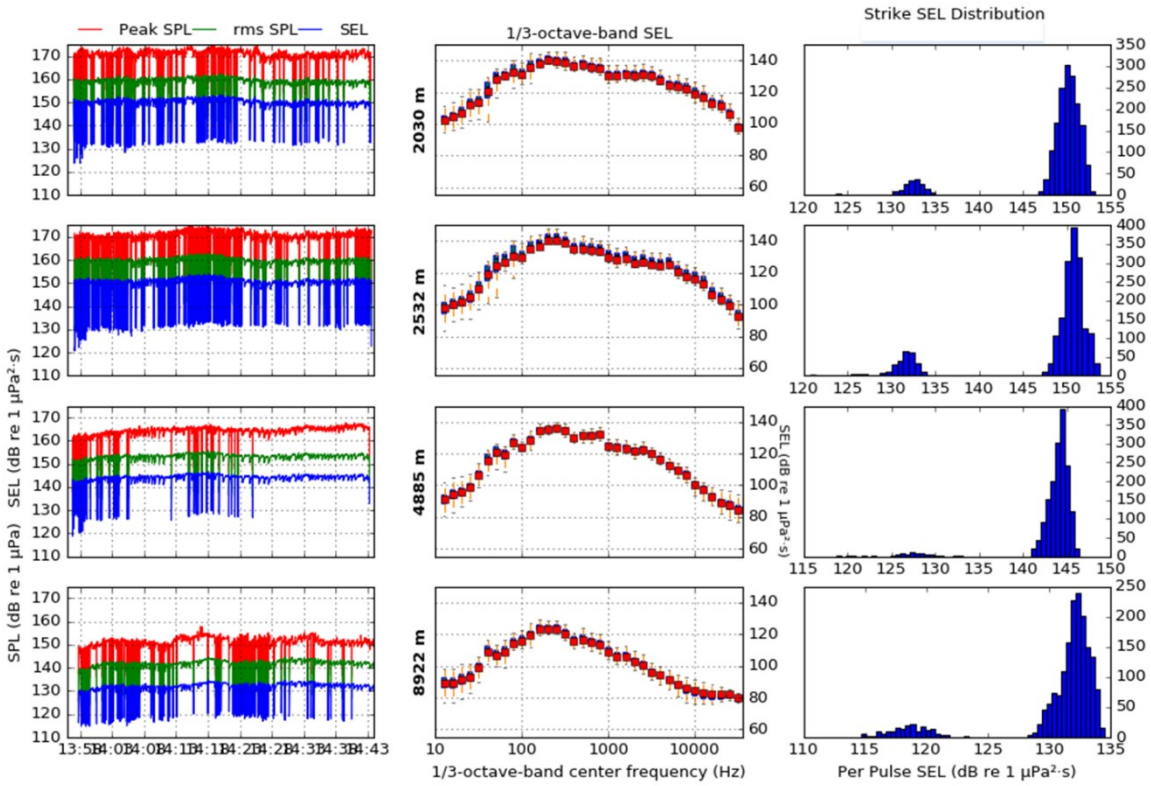

Figure 4-10. Example of the sound levels or the impulses identified by the TK detector for Pile Section 1, Leg B2, Foundation 1. (Left Column) peak SPL (red), 0.125 s SPL (green) and SEL (blue) for each detected strike. Middle column: distribution of decidecade-band SELs. Right hand column: distribution of per-strike SELs, showing a bimodal distribution where the large peaks are the main arrivals and the smaller peak are from detection of secondary multi-path arrivals.

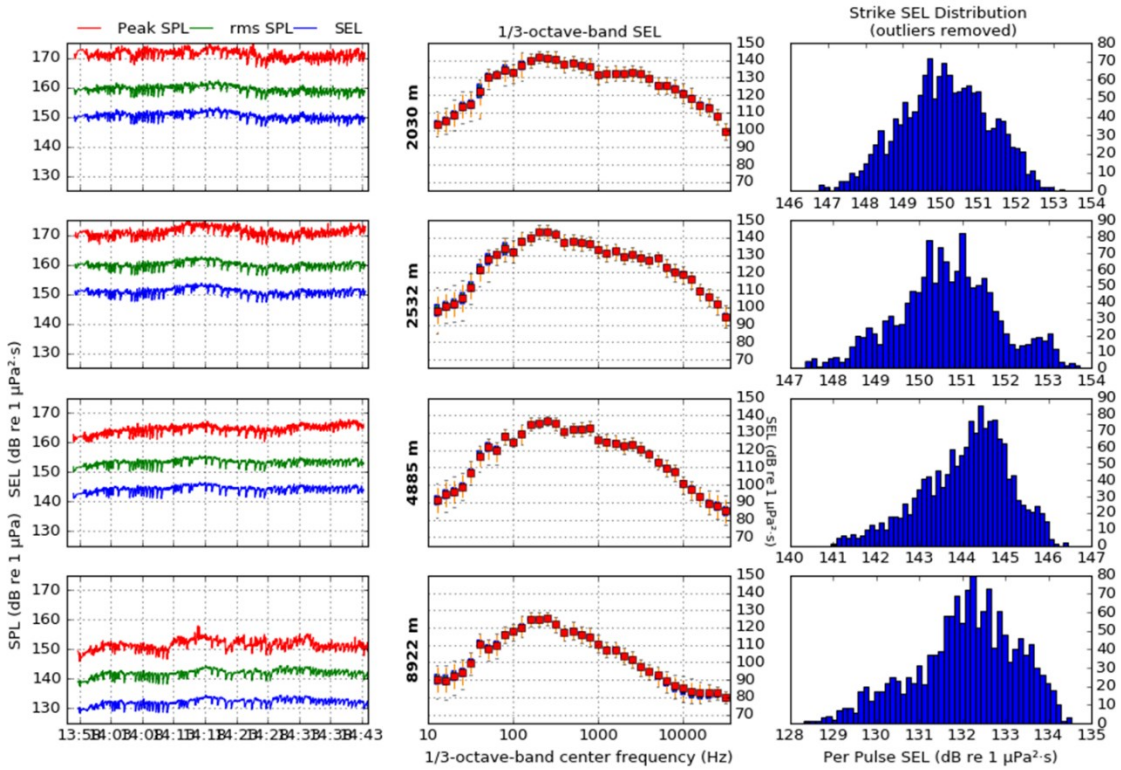

Figure 4-11. Example of the sound levels of the impulses identified by the TK detector for Pile Section 1, Leg B2, Foundation 1 after K-means clustering removed multipath arrivals. (Left Column) peak SPL (red), 0.125 s SPL (green) and SEL (blue) for each detected strike. Middle column: distribution of decidecade-band SELs. Right hand column: distribution of per-strike SELs showing approximately Gaussian distributions.

4.6.5. Sound Speed Profiles

Sound speed profiles collected during the long-term monitoring program are shown in

Figure 4-12. September was characterized by warm water on top of colder deep water.

October had a well-mixed iso-velocity structure.

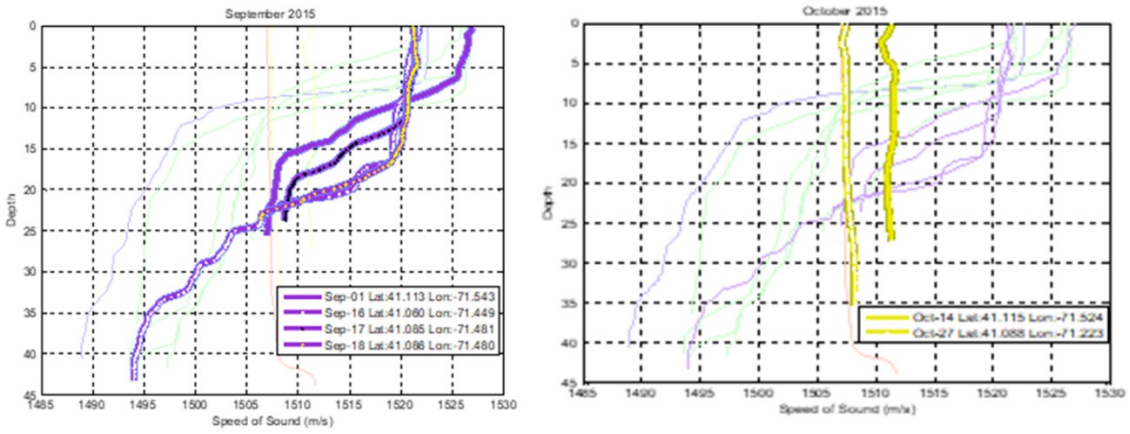

Figure 4-12 Sound speed profiles measured at the project site during pile driving operations. (Left) September 1, 16, 17 and 18, showing a downward refracting profile. (Right) October 14 and 27 showing an isovelocity profile. Data provided by Tetra Tech Inc.

4.6.6. Example Pile Driving Logs

Figure 4-13 provides an example of the pile driving stroke logs. Figure 4-14 provides an example of the penetration logs which record the progress of pile driving for every meter of penetration into the sediment. The depth-per-stroke was interpolated from the penetration file and merged with the stroke data.

MHC 21 - Strokedata List - MENCK Kaltenkirchen
WEEKS/MANSON - BLOCK ISLAND WIND FARM 1, J5
BIWF5 A1 - length - diameter
17.09.2015

date	time	stroke	blow rate 1/min	height mm	energy kJ	HP ham. bar	HP PP bar	oil flow l	oil temp °C	DP1 mbar	DP2 mbar	WP/ LP bar	WL bar
09/17/15	12:30:33	1	0	105	71	158	165	0	14	76	0	0	0
09/17/15	12:30:43	2	0	85	69	165	172	0	14	76	0	0	0
09/17/15	12:30:51	3	0	105	68	163	171	0	14	86	0	0	0
09/17/15	12:32:10	4	0	105	74	172	180	0	14	78	0	0	0
09/17/15	12:32:19	5	0	105	78	165	173	0	14	75	0	0	0
09/17/15	12:32:28	6	0	105	84	164	172	0	14	76	0	0	0
09/17/15	12:33:51	7	0	105	72	102	105	0	15	61	0	0	0
09/17/15	12:34:00	8	0	105	75	167	177	0	15	121	0	0	0
09/17/15	12:34:07	9	0	105	78	171	180	0	15	82	0	0	0

Figure 4-13. Example stroke data log file

MHC 21 - Penetration List - MENCK Kaltenkirchen
WEEKS/MANSON - BLOCK ISLAND WIND FARM 1, J5
BIWF5 A1 - length - diameter
17.09.2015

penetration [m]	blows/pen	av energy/bl [kJ]	energy/pen [kJ]	stroke
1.00	5	72.15	360.75	5
5.00	1	84.22	84.22	6
6.00	20	68.40	1368.00	26
7.00	43	74.29	3194.47	69
8.00	39	81.22	3167.58	108
9.00	64	74.51	4768.64	172
10.00	74	78.44	5804.56	246
11.00	104	78.16	8128.64	350
12.00	115	84.40	9706.00	465

Figure 4-14. Example penetration file

4.6.7. Model Performance, Random Effects and Residuals

The model definition was selected using the *AIC*, Equation (4-5),

$$AIC = 2N - 2 \cdot \ln(L) \tag{4-5}$$

where N is the number of covariates and L is the maximum likelihood of the model. The *AIC* compares the goodness of fit between models, with lower values being better. A difference of 2 between two model's *AIC* values is equivalent to a 1/*e* improvement in the likelihood of the model and thus a substantial improvement. To fully evaluate a model's performance the distribution of residuals and other measures need to be considered. Table 4-3 in the main text shows a selection of the *AIC* for different models and demonstrates the improvement of the goodness of fit using the linear strike energy and pile penetration as well as the unique pile – recorder combination as the random effect. Figure 4-15 shows the near normal distribution of the random effect amplitudes and

residuals for the best fit model. Along with Figure 4-4 these indicate that the model is performing well.

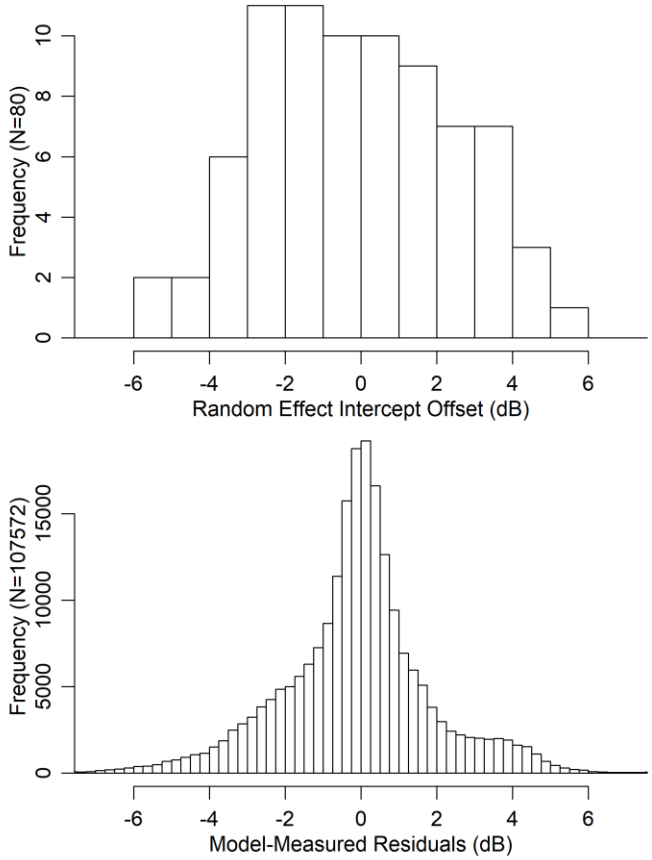

Figure 4-15. Distribution of Random Effect Intercept Offset values and residuals for the Low Frequency Cetacean SEL model.

4.6.8. Block Island Isopleths

Table 4-10. Estimated radii (m) using the DCS model for the biological effects isopleths applied to the Block Island Wind Farm (BIWF) construction and the NOAA 2016 marine mammal permanent threshold shift isopleths. Ranges are shown for three conditions: 1) the loudest case – the pile inclined away from the recorder with 97.5th percentile of the hammer energy (648 kJ); 2) the median case of a vertical pile and the median hammer energy; and 3) the quietest case – the pile inclined towards the recorder with 2.5th percentile of the hammer energy (74 kJ). The bold number at the centre of each box is the median range. The lower-left and upper-right numbers are the lower and upper prediction intervals (2.5th and 97.5th percentiles, respectively), obtained by bootstrapping the linear mixed effects model 1000 times for each of the acoustic metrics and predicting the sound levels at each range steps of 25 m.

Isopleth Metric	Regulatory threshold	Permitted radius (m)	Pile Inclined away from recorder with 644 kJ hammer energy & 56 m pile penetration	Vertical pile with 392 kJ hammer energy & 38 m pile penetration	Inclined toward recorder with 74 kJ hammer energy & 8 m pile penetration
Sound pressure level radii (m)					
Turtle physiological injury[1]	207 dB re 1 µPa $L_{p,0.125\ s}$	6	<250*	<250*	<250*
Fish physiological injury[1]	206 dB re 1 µPa $L_{p,pk}$	7	<250*	<250*	<250*
Marine mammal level A take[1]	180 dB re 1 µPa $L_{p,0.125\ s}$	600	350 **<250*** <250*	<250*	<250*
Turtle disturbance[1]	166 dB re 1 µPa $L_{p,0.125\ s}$	3414	4625 **2325** 800	2525 **1525** 675	1775 **1150** 550
Marine mammal level B take[1]	160 dB re 1 µPa $L_{p,0.125\ s}$	7000	9425 **5800** 2575	4325 **3025** 1675	2825 **2075** 1250
Fish disturbance[1]	150 dB re 1 µPa $L_{p,0.125\ s}$	39810	>20000 **15550** 9900	8000 **6300** 4450	4925 **3925** 2875
Fish Single Strike Mortal Injury[5]	183 dB re 1 re 1 µPa²·s L_E	Not Used for BIWF	<250*	<250*	<250*
Sound exposure radii (m) for 8000 strikes assuming constant strike energy and pile penetration					
Fish unweighted PTS[1,4]	187 dB re 1 µPa²·s $L_{E,24h}$	116591	12450 **8275** 4175	5350 **3900** 2375	3425 **2575** 1675
Fish unweighted potential mortal injury[3]	210 dB re 1 µPa²·s $L_{E,24h}$	Not used for BIWF	350 **<250*** <250*	300 **<250*** <250*	275 **<250*** <250*
Fish unweighted recoverable injury[3]	203 dB re 1 µPa²·s $L_{E,24h}$	Not used for BIWF	1450 **600** <250*	1050 **500** <250*	825 **400** <250*
Otariid Weighted PTS[2]	203 dB re 1 µPa²·s $L_{E,24\ h,OTA}$	Not used for BIWF	<250*	<250*	<250*
HF weighted PTS[2]	185 dB re 1 µPa²·s $L_{E,24\ h,MF}$	Not used for BIWF	300 **<250*** <250*	275 **<250*** <250*	250 **<250*** <250*
phocid weighted PTS[2]	185 dB re 1 µPa²·s $L_{E,24\ h,PHO}$	Not used for BIWF	4350 **2150** 625	2525 **1475** 525	1800 **1125** 450
LF weighted PTS[2]	183 dB re 1 µPa²·s $L_{E,24\ h,LF}$	Not used for BIWF	14700 **10075** 5200	6025 **4475** 2775	3800 **2900** 1900

Isopleth Metric	Regulatory threshold	Permitted radius (m)	Pile Inclined away from recorder with 644 kJ hammer energy & 56 m pile penetration	Vertical pile with 392 kJ hammer energy & 38 m pile penetration	Inclined toward recorder with 74 kJ hammer energy & 8 m pile penetration
VHF weighted PTS[2]	155 dB re 1 µPa²·s $L_{E,24\,h,VHF}$	Not used for BIWF	7575 **5425** 2925	4725 **3525** 2100	3400 **2575** 1625

[1]BIWF B/O.
[2]Southall et al (2019) marine mammal hearing group weightings and thresholds.
[3] Popper et al. (2014b) Table 7.3
[4] Popper et al. (2014b) set the temporary threshold shift isopleth for fish with swimbladders at >186 dB re 1 µPa²·s
[5]Casper et al. (2017a) found mortal injuries occurring for stripped bass exposed to 183 dB re 1 µPa²·s L_E
* Because the shortest measurement range was 541 m, it was not appropriate to extrapolate the regressions closer to the pile than 250 m.

4.6.9. Sample 'R' Code for Linear Mixed Models and Prediction Interval Estimation.

```
library(pracma)    # for cot(theta)
library(nlme)      # for the linear mixed models

# load your data file - it suggested columns in the data file are:
#    Pulse Time, peak SPL, SPL, range (from pile to recorder),
#       per pulse SEL & NOAA 2016 M-Weighted SELs, as well as the
#       per-pulse strike energy and pile penetration if available (unlikely for 24-hour analysis)
pd <- read.csv('datafile.csv', header=TRUE )

rawResponse = 'LFC'   # insert the name of the column from the datafile that you want to fit
responseVar = 'offsetResponse'    # this is the variable we will actually fit. see below ...
grazingAngleDegrees = 17    # this depends on your project's selection of pile materials, see Lippert et al 2018.
   # if you are modeling an inclined pile then the grazingAngle will depend on the pile-recorder geometry.
grazingAngleRadians = pi*grazingAngleDegrees/180

# add 10Log(R) to the raw data to get the offset data for modeling
pd[responseVar] = pd[rawResponse] + 10*log10(pd$range)

# compute the reflection term ... if your water depth is not constant with range, then you'll
# need to determine the average water depth between the pile and each recorder location, and
# insert it either into the datafile.csv or handle it here.
waterDepth = 25     # enter you water depth, in meters.
pd$reflects = pd$range / (2 * waterDepth * cot(grazingAngleRadians))

# create a categorical variable for use in the mixed modeling; this could be a recorder ID number
# or station name if they are already in datafile.csv. Here we simply turn the range into a factor.
pd$recorderId = as.factor(pd$range)
```

```
# run the model, here we assume that you do not have strike energy or pile penetration and
#    so that the number of reflections is the only predictor variable
dcsModel = lme('responseVar~reflects', random=~1|recorderId, data=pd, method="REML")
summary(dcsModel)

# now compute the predicted levels and store the residuals
pd$predictedLevels = predict(dcsModel, pd, level=c(0))
pd$level0Residuals = pd[responseVar] - pd$predictedLevels

# compute the vertical offset needed to incorporate 'predictInterval' percent of the measured
# data. 95% or 97.5% are recommended thresholds
predInterval = 0.975
offset = quantile(pd$level0Residuals, predInterval)

# determine the min and max range to extrapolate. The model is strictly valid only between the
# minimum and maximum ranges, however, it is often desirable to extrapolate to one half the
# minimum range and twice the maximum to cover a wider set of isopleth radii.  Do not
extrapolate
# by more than a factor of 2.
ranges = unique(pd$range)
minR = min(ranges) / 2
maxR = max(ranges) * 2
modelRanges = seq(from=minR, to=maxR, by=25)

# now predict the sound levels over the extrapolation space:
isoplethDF = data.frame(range=modelRanges, reflects = modelRanges /
(2*waterDepth*cot(grazingAngleRadians)))
predictedLevels = predict(dcsModel, isoplethDF, level=c(0))

# now we need to convert these levels back to the actual range dependent levels (remove
10log(R))
isoplethDF$predictedLevels = predictedLevels - 10*log10(isoplethDF$range)
# add the offset value to get the prediction interval sound level:
isoPlethDF$predictionIntervalLevels = isoplethDF$predictedLevels + offset

# store the results as a CSV file that contains the mean sound level and upper bound prediction
# interval as a function of range. You can then search this file to find the first range that is below
the
# regulatory isopleth threshold.
saveFrame = data.frame(modelRanges, isoplethDF$predictedLevels,
isoplethDF$predictionIntervalLevels)
colnames(saveFrame) = c('range', 'mean level', paste('L', predInterval, ' level', sep=''))
write.csv(saveFrame, paste(rawResponse, '_LME_verticalShiftBy_', predInterval,
'perc_Ranges.csv', sep=''))
```

CHAPTER 5 USING SOUND EXPOSURE LEVEL FOR THE ANALYSIS AND MANAGEMENT OF UNDERWATER SOUNDSCAPES

This chapter contains a manuscript submitted to the Journal of the Acoustical Society of America in January 2019, updated in February 2019 to address reviewer comments, and accepted in April 2019. The data in this chapter is drawn from a wide range of projects that I've been involved with at JASCO, with numerous staff who have assisted with the original data collection and analysis. The one-minute SPL and SEL computations were performed using software written by myself as part of the PAMLab software suite. Bruce is the original author of the software; it is now maintained by Briand Gaudet and Bruce Martin. The remaining analysis using the auto-correlation was conceived and implemented by Bruce Martin in '***R***'.

The co-author contributions are as follows:

- Corey Morris reviewed several versions of the draft manuscript before submission to JASA and posed questions that improved the work, most importantly the suggestion that I look for a manner of separating baseline soundscapes from those affected by human sources. Corey helped provide biological and ecological context for the analysis. Corey is also the PI for the project that contributed the Carson Canyon data.
- Koen Bröker is included both as the PI and data owner for the Shell Baffin Bay project, but also for identifying that the paper was not highlighting in the text that a 24-hour accumulation time for moving sources and receivers may not be appropriate.

- Caitlin O'Neill contributed the Resolute Bay data.

Note that Table Table 5-3 - Table 5-5 as well as Figure 5-7- Figure 5-13 are S-1 to S-3 and S-1 to S-7, respectively, in the JASA Manuscript. These Tables and Figures appear as Supporting Information for this Chapter.

Title: *Using Sound Exposure Level for the analysis and management of underwater soundscapes*

S. Bruce Martin*[5], Corey Morris[2], Koen Bröker [3#], Caitlin O'Neill[4]

[1]Dalhousie University, Department of Oceanography, 1355 Oxford Street, PO Box 15000, Halifax, Nova Scotia, Canada B3H 4R2

[2]Fisheries and Oceans Canada, Northwest Atlantic Fisheries Centre, PO Box 5667, 80 East White Hills Road, St. John's, Canada NL A1C 5X1

[3]Shell Global Solutions International B.V., Lange Kleiweg 40, 2288GK Rijswijk, The Netherlands

[4]Fisheries and Oceans Canada, Institute of Ocean Sciences, 9860 West Saanich Road, Sidney, BC, Canada V8L 4B2

Email: sbmartin@dal.ca

Running Title: SEL: A regulatory and soundscape metric

Date Submitted: 12 January 2019

---

* Also at JASCO Applied Sciences Canada, Suite 202, 32 Troop Avenue, Dartmouth NS, B3B 1Z1.
# Also at Groningen Institute for Evolutionary Life Sciences, University of Groningen, Nijenborgh 7, 9747AG Groningen, The Netherlands

ABSTRACT

The auditory frequency weighted daily sound exposure level (SEL) is used in many jurisdictions to assess possible injury to the hearing of marine life. Therefore, using daily SEL to describe soundscapes would provide baseline information about the environment using the same tools used to measure injury. Here, the daily SEL from twelve recordings with durations of 18 to 97 days are analyzed to: 1) identify natural soundscapes versus environments affected by human activity; 2) demonstrate how SEL accumulates from different types of sources; 3) show the effects of recorder duty cycling on daily SEL; 4) make recommendations on collecting data for daily SEL analysis; and 5) discuss the use of the daily SEL as an indicator of cumulative effects. The autocorrelation of the one-minute sound exposure is used to help identify soundscapes not affected by human activity. Human sound sources reduce the autocorrelation and add low-frequency energy to the soundscapes. To measure the daily SEL for all marine mammal auditory frequency weighting groups data should be sampled at 64 kHz or higher, for at least one minute out of every 30. The daily autocorrelation of the one-minute SEL provides a confidence interval for the daily SEL computed with duty-cycled data.

AIP Codes: 43.30.Nb, 43.50.Yn, 43.80.Nd

Keywords: Daily sound exposure level; Marine Soundscape; Anthropogenic Noise.

5.1. INTRODUCTION

Mankind's increasing use of the ocean for transportation, food and energy extraction has led to an increase in marine pollutants including sound. Studies of these activities demonstrate potentially negative impacts of our activities on marine life (Southall et al. 2019b). The effects of sounds on humans and animals can be visualized as

a series of four zones or concentric rings of diminishing impact around the sound source (e.g., Figure 1 in Dooling et al. 2015). In this model the highest level of impact occurs in Zone 1 from exposures that cause physical barotrauma or permanent hearing loss (e.g., Halvorsen et al. 2012a, Casper et al. 2017b), followed by temporary hearing loss in Zone 2 (see review in Finneran 2015c), then masking of important biological sounds used by animals in Zone 3 (Shannon et al. 2016), and finally in Zone 4 the sound levels elicit subtle behavioral or physiological stress responses (Rolland et al. 2012).

The zone-view of the effects of noise does not accurately reflect the complexity of auditory injury or impairment and the choices animals make to accept sound exposure for other advantages such as feeding or mating (Ellison et al. 2012). When animals make the choice not to respond to noise, they can stay in an area where very long sound exposures result in auditory injury and impairment, and thus Zone 2 may be larger than Zone 4 (Hawkins and Popper 2017). Similarly, behavioral reactions to sound can cause animals to rapidly leave an area, which could result in dangerously rapid depth changes (Jepson et al. 2003, Blix et al. 2013) or entering an area that results in stranding (Cox et al. 2006); in this manner Zone 4 becomes Zone 1.

As a general rule regulations impose a requirement on human ocean activities to predict the size of Zone 1, then ensure that no endangered or threatened animals are within that area (Erbe 2013). Regulations to reduce masking, disturbance, and behavioral responses are less common but may be applied for instance to whale watching boats (e.g. https://bit.ly/2zx03ye). As more studies of the effects of sound become available, it will be possible to manage the effects of a wider range of man-made sound to prevent behavioral changes that could affect feeding, navigating, mating, rearing of young, or the

harvesting of commercial fish stocks. The Population Consequences of Acoustic Disturbance (NRC 2005) and Population Consequences of Disturbance (King et al. 2015) models provide frameworks for understanding the sub-lethal effects of sound on marine populations (Costa et al. 2016).

Managing sound levels requires indicators that relate sound characteristics including amplitude to their effects on marine life. Sound exposure level, peak sound pressure level, and the sound pressure level are three amplitude metrics typically used to quantify sound in the environment. Early marine sound mitigation regulations were based on keeping sound pressure levels below the level associated with measured injuries to the hearing of marine mammals (NMFS and NOAA 1995, NOAA 1998). Evidence has since demonstrated that peak sound pressure level and sound exposure level are better predictors of injury for most groups of marine life (Southall et al. 2007, Popper et al. 2014b, Southall et al. 2019b). Peak sound pressure level is associated with immediate physiological injury to tissues (Halvorsen et al. 2012b). The sound pressure level varies with the averaging time, which makes it difficult to obtain repeatable values between research teams or methods, especially when analyzing the effects of impulsive sound sources (Madsen 2005, Hawkins et al. 2014). Sound exposure level is associated with fatigue injury through the equal energy hypothesis that states the effects on hearing are the same for the same total energy (Eldredge and Covell 1958). For example, a sound pressure level of 190 dB re 1 μPa^2 for 1 second or 160 dB re 1 μPa^2 for 1000 seconds both have an SEL of 190 dB re 1 $\mu Pa^2 \cdot s$ and are expected to have the same effect on hearing. The daily SEL metric has an additional advantage over the sound pressure level

of an acoustic event in that its duration is precisely defined. It is also simple to compute since it does not depend on detecting when a signal is present.

There are many research results that show the equal energy hypothesis does not represent the complexity of the effects of sound on hearing. It is well established that impulsive sounds affect hearing at lower sound exposure levels than non-impulsive sounds (Ward 1962, Akay 1978, Finneran 2015c). The temporal pattern of impulses also changes the effects of sound on hearing for the same total sound exposure level. In terrestrial mammals, including humans, 1 pulse per second has significantly greater impact that 10 pulses per second or 1 pulse every 10 seconds (Danielson et al. 1991a, Qiu et al. 2013b). Within the American regulations to protect marine life from human sounds, the dependence of hearing effects on sound's temporal patterns are reflected in different equal energy thresholds for non-impulsive and impulsive sounds (Popper et al. 2014b, NMFS 2018). More research is still required to understand how sound's characteristics besides the pressure amplitude and energy affect marine life. Particularly important are particle motion effects on fish and invertebrates and the temporal patterns of the sound on all marine taxa (Finneran 2015c, Hawkins and Popper 2017, Houser et al. 2017, Popper and Hawkins 2018).

The publication of the *Technical Guidance on Assessing the Effects of Anthropogenic Sound on Marine Mammal Hearing* (NMFS 2016) and a minor revision (NFMS 2018), have made the auditory frequency weighted sound exposure level, integrated over 24-hours, the primary metric for predicting and measuring the effects of human industrial sound on marine life. However, this metric is not well understood – there are few examples of typical SELs or how the SEL depends on movement of sources

and receivers, limited information on how to collect data for assessment of daily SEL, or results showing what additional information about the environment can be obtained by analyzing the daily SEL. This study addresses these data gaps through the analysis of twelve long-term data sets that provide examples of natural soundscapes and those affected by human activities. The temporal characteristics of human sound sources and natural environments are addressed in a separate study.

This manuscript is supported by extensive Supplementary Material that includes: why SEL is a measure of the received energy, how to compute SEL across multiple events, further information on auditory weighting functions, hydrophone and recorder self-noise data, Gamma random noise distributions that are similar to typical ocean noise distributions, statistical measures (mean, variance, skewness, kurtosis, Gamma fit, and autocorrelation durations) for each data set, and confidence intervals for duty cycled daily SELs.

5.2. METHODS

5.2.1. Data Sets

Twelve data sets from ten recording locations (Figure 5-1) were analyzed to provide an indication of the range of daily SEL, show how SEL accumulates from different sources, and provide examples of how different data collection techniques affect daily SEL. All recordings were performed using an AMAR G3 recorder (JASCO Applied Sciences) and either GeoSpectrum or HTI-99-HF hydrophones (Table 5-1). The data sets were selected to ensure that flow noise and other artefacts did not contribute to the daily SEL.

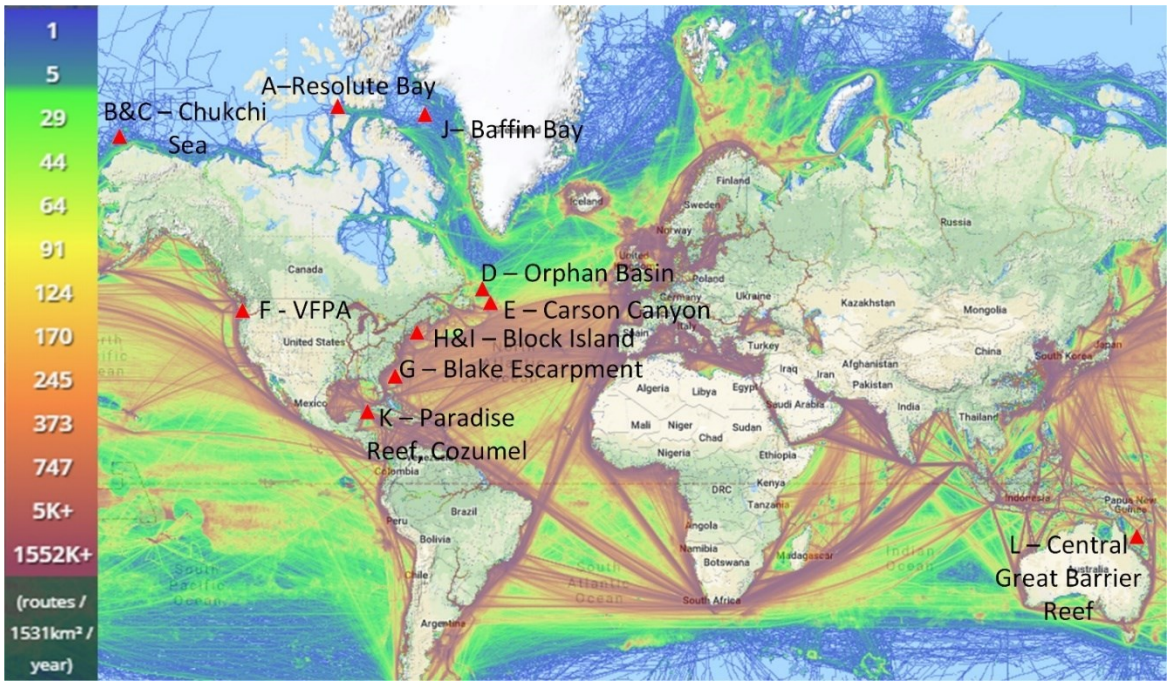

Figure 5-1. Recording locations whose data were used in this analysis. The underlay of the map is the 2017 marine traffic density as provided by www.marinetraffic.com.

Table 5-1. Acoustic recordings used in this study. System spectral noise floor values with a superscript 'R' indicates that the noise floor limit was from the recorder, the remainder of the limits are due to the hydrophones.

Location ID	Location name	Primary Sound Sources	Water depth (m)	Latitude (degrees North)	Longitude (degrees East)	Recording dates	Hydrophone type	Hydrophone sensitivity level (dB re 1V / µPa)	System spectral noise	Sample rate and duty cycle	10 Hz+ daily SEL noise floor (dB re 1 µPa²) *
A	Resolute Bay	Open ocean and small boats (16 Aug – 2 Oct); Ice + open water noise (3 Oct-2 Nov)	60	74.65	-94.84	16 Aug – 2 Nov 2014	M8E-V35dB	−165	32	2 min @ 96 kHz; 2 min sleep	128.2
B	Chukchi Sea, 2014	Open ocean	47	71.34	-163.1	6 Aug– 14 Oct 2014	M8E-V35dB	−165	34^{R}	13 min @ 16 kHz; 2 min @ 375 kHz	135^{R}
C	Chukchi Sea, 2015	Dynamic positioning from semi-submersible drill rig; location is 1 km from Chukchi 2014 site.	51	71.19	-163.5	25 Jul– 2 Oct 2015	M8E-V35dB	−165	32	64 kHz continuous	126.5
D	Orphan Basin	Open ocean (1 Apr – 24 May); seismic airgun survey (25 May – 30 Jun)	1282	48.73	-49.38	1 Apr – 30 Jun 2016	HTI-99-HF	−163	42	11 min @ 8 kHz; 1 min @ 250 kHz; 8 min sleep	142
E	Carson Canyon	Open ocean, fishing, seismic airgun survey	120	45.46	-48.79	4 Sep– 17 Oct 2016	M36-V35-100	−165	34^{R}	7 min @ 16 kHz; 1 min @ 375 kHz	135^{R}

Location ID	Location name	Primary Sound Sources	Water depth (m)	Latitude (degrees North)	Longitude (degrees East)	Recording dates	Hydrophone type	Hydrophone sensitivity level (dB re 1V / µPa)	System spectral noise	Sample rate and duty cycle	10 Hz+ daily SEL noise floor (dB re 1 µPa²) *
F	Vancouver-Fraser Port Authority	Recorded under the port of Vancouver's inbound shipping lane.	170	49.05	-123.3	1 Jan–7 Apr 2018	M36-V35-100	−165	32	128 kHz continuous	129.5
G	Blake Escarpment	Open ocean with some shipping	872	29.25	-78.35	15 Mar–9 Jun 2018	M36-V35-100	−165	34 R	16 min @ 8 kHz; 1 min @ 250 kHz; 4 min sleep	134 R
H	Block Island, 850 m from piling	Impact pile driving	26	41.11	-71.52	14 Oct–3 Nov 2015	M8E-V0dB	−200	53 R	64 kHz continuous	147 R
I	Block Island, 9100 m from piling	Impact pile driving	42	41.06	-71.45	14 Oct–3 Nov 2015	M8E-V35dB	−165	32	64 kHz continuous	126.5
J	Baffin Bay	Seismic airgun survey except first 2 days.	603	74.16	61.98	30 Jul–30 Sep 2012	M8E-V0dB	−200	56 R	64 kHz continuous	150 R
K	Paradise Reef	Coral Reef, 500 m from cruise ship pier; frequented by small tourist dive boats.	11	20.47	-86.98	15 Jul – 2 Sep 2017	M36-V35-100	−165	34 R	14 min @ 32 kHz; 1 min @ 375 kHz	135 R
L	Central Great Barrier Reef	Coral reef without human sources.	18	-18.8	147.5	27 Apr – 15 Jul 2013	M8E-V35dB	-164	34R	7 min @ 64 kHz; 2 min @ 375 kHz; 6 min sleep	135R

* Daily 10 Hz and above SEL noise floor is the spectral noise floor + $10*\log_{10}$(86400 sec/day) + $10*\log_{10}$(recorder bandwidth) – see Section 5.6.

5.2.2. Sound Exposure Level

The acoustic metrics and terminology employed in this analysis follow ISO Standard 18405 (ISO 2017a). The sound exposure level is a representation of sound energy that is defined as 10 dB times the logarithm (base 10) of the sound exposure, which is the integral of the squared sound pressure over some period of time, T, normalized by a reference squared pressure p_o^2 and reference time T_o (Equation 5-1)

$$L_{E,T} = 10\log_{10}\left(\frac{1}{T_0 p_o^2}\int_0^T p^2(t)\,dt\right) \text{ dB re 1 } \mu\text{Pa}^2\cdot\text{s} \quad (5\text{-}1)$$

T_o is normally 1 second and p_o is 1 µPa, so that the unit of $L_{E,T}$ are dB re 1 µPa²·s. The daily SEL is 49.4 dB higher than the arithmetic mean of the daily sound pressure level.

There are two pathways by which sound can affect hearing - intense, high amplitude sounds that damage hearing organs, or long-term exposure that causes temporary or permanent threshold shifts. The long-term exposures only affect hearing if the sounds are within an animal's hearing frequency range. Therefore, during SEL analysis recorded sounds are typically filtered by the animal's auditory frequency weighting function before integrating to obtain SEL. Weighted sound exposure and SEL are defined in Equation 5-2) and 5-3:

$$E_{p,W,T} = \sum_{n=0}^{N}\int_0^{f_s/2} W(f)S_t(f)df \text{ Pa}^2\cdot\text{s} \quad (5\text{-}2)$$

$$L_{E,W,T} = 10\log_{10}\left(\frac{E_{p,W,T}}{T_0 p_o^2}\right) \text{ dB re 1 } \mu\text{Pa}^2\cdot\text{s}, \quad (5\text{-}3)$$

where $W(f)$ is the auditory frequency weighting function and $S_t(f)$ is the power spectrum of the pressure time series over a period of 't' seconds. The total signal duration 'T' is

normally divided into 'N' equal sized blocks of duration 't' whose sound exposures are summed before taking $10\log_{10}$ to convert to the decibel representation.

Auditory frequency weighting functions and auditory injury thresholds have been defined for six groups of marine mammals: low-, high- and very high-frequency cetaceans, sirenians as well as otariid and phocid seals in water (Southall et al. 2019b; sirenians are not considered here). As a first approximation, the low-frequency auditory weighting function may be thought of as a 100 Hz high pass filter. Similarly, the phocid and otariid functions are ~4 kHz high pass filters, the high-frequency function is ~10 kHz high pass filter, and the very high-frequency function is ~20 kHz high pass filter. For this analysis, the full bandwidth SEL for the recordings is computed starting at the 10 Hz decidecade and is referred to as the '10+ Hz SEL' or the '10 Hz and above SEL'. The SEL that is applied under American regulations for marine life other than mammals is the 10+ Hz SEL (Equation 5-1). Research on the hearing of other marine animal groups is needed to define their auditory frequency weighting functions and exposure thresholds. Equation 5-2) may be applied to the power spectrum as shown, or it may be applied to the decidecade SEL for an event using the centre frequencies of the decidecades to compute the weighting (see Section 5.6 or Tougaard and Beedholm 2019).

5.2.3. Determining the Effects of Duty Cycling on SEL

Seven of the data sets used in this analysis were duty cycled between high and low sample rates (Table 5-1). The high sample rate data were essential for detecting the calls of high- and very high-frequency marine mammals, as well as for computing the weighted SEL for these groups. To estimate the weighted SEL from the duty-cycled data, we first computed the per-minute sound pressure level ($L_{p,1\ min}$) and per-minute

dedidecade sound pressure levels ($L_{p,ddec,1min}$) for the data from both sample rates. A one-minute duration was chosen since it is the shortest continuous duration used in this analysis (Table 5-1) and a common duration for estimating the sound pressure level (Ainslie et al. 2018). The measured data had missing sound pressure and decidecade sound pressure values due to the duty-cycling. These were estimated by linear interpolation of the linear data (i.e. $10^{Lp/(10\ \mathrm{dB})}$) on either side of the missing values. The linear decidecade sound pressures were weighted by the marine mammal auditory frequency weighting functions, then summed to obtain the weighted per-minute sound pressures, and those were summed to obtain the daily sound exposure at each sampling rate (Equation 5-4).

$$L_{E,W,24h} = 10\log_{10}\left(\sum_{t=0}^{t=1440\ min} 10^{L_{P,W,t}/10}\right) + 10\log_{10}(60\ sec/minute) \tag{5-4}$$

For each auditory frequency weighting function, the daily SEL was computed from all available data with enough bandwidth. The minimum sample rates were 8000 Hz for 10+ Hz and low-frequency cetacean weightings, 16000 Hz for otariid and phocid weightings, and 48000 Hz for high- and very high-frequency cetacean weightings. When data from more than one sample rate was available the data sets were merged in time before interpolating.

The low duty cycle for higher sample rates (Table 5-1) means that the daily SEL for the seals as well as the high- and very-high frequency cetaceans were extrapolated from only 4-10 percent of a day's data. To estimate the error from this extrapolation, the daily SEL were computed from the continuously sampled data sets (data sets C, F, H, I and J) with duty cycles simulated by decimating the data to 1 minute every 2, 3, 4, 5, 6, 8, 10,

12, 15, or 20 minutes. The errors were the full-bandwidth continuous daily SEL subtracted from the SEL calculated after decimating in time so that a negative value means the subsampled SEL was less than the actual SEL. For each decimation rate, the decimated daily SEL was computed for all starting points of the sub-sampling, which increased the sample size for estimating the effects of sub-sampling. For example, the Chukchi Sea 2015 data (data set C) had 67 full daily SEL, 134 daily SEL estimates at the 1:2 decimation rate, and 1340 at 1:20.

When using daily SEL computed from duty-cycled data it is useful to know the range of errors that could result from the duty cycling. Since the duty cycled SEL were computed by interpolating the available measurements, the accuracy of the daily SEL depends on how well the measurement made at some time '*T*' can be predicted from the previous measurement, for example *T*-20 minutes for the Orphan Basin data. It was expected that the error would be related to the decimated data's autocorrelation. The error in daily SEL obtained by subsampling each of the continuous data sets were plotted against the first autocorrelation time lag of the subsampled one-minute sound exposures (Equation 5-2) for that day. This corresponds to a lag of 2, 3, 4, 5, 6, 8, 10, 12, 15, or 20 minutes depending on the sub-sampling. The resulting distributions were characterized by their mean values and the 95% confidence intervals. We also tested how well the subsampled auto-correlation matched the auto-correlation of the original data. To assess the generality of these results, the same analysis was performed using Gamma-distributed random data rather than continuous data sets. The characteristics of the Gamma-random data are discussed in Section 5.6.5. Comparisons were made for the marine mammal auditory frequency weighting function weighted and 10+ Hz daily SEL.

5.3. RESULTS

5.3.1. Daily SEL Levels in the Data Sets

Figure 5-2 shows the daily SEL for data sets A-L (Figure 5-1, Table 5-1). Table 5-2 lists the mean daily SEL and standard deviations. The mean high- and very high-frequency auditory frequency weighted SEL were often self-noise limited for the data from Orphan Basin (D) and Baffin Bay (J). Figure 5-3 provides auto-correlations of the one-minute SEL from the full duration of each recording.

The data sets include natural soundscapes as well as soundscapes with different types of human activity. The Resolute Bay (A) and Chukchi 2014 data (B) are both Arctic recordings in water depths of 50-60 m. In Resolute Bay (A) during open water the daily SEL depends on the passage of small boats. After ice arrives the sound levels drop due to both the ice cover and less wind driven noise. In the Chukchi Sea 2014 during periods of low background sound levels (presumably periods of low winds) the 10+ Hz daily SEL dropped to 140–145 dB re 1 $\mu Pa^2 \cdot s$ and increased to 160 dB dB re 1 $\mu Pa^2 \cdot s$ during periods of high winds. Since the mean low-frequency cetacean auditory frequency weighted daily SEL were within 2.5 dB below the 10+ Hz SEL, at least half of the sound energy was above 100 Hz in this soundscape. The 10+ Hz, low-frequency, otariid, and phocid weighted SEL were highly auto-correlated for the 26 hours shown in Figure 5-3, which indicates that a slowly varying process was affecting the sound levels – i.e., wind and wave driven sound. In contrast, ice formation and movement in Resolute Bay data (A) increased the variability in the daily SEL and decorrelated the data within 30 minutes.

Blake Escarpment (data set I) and Orphan Basin (data set D) (Figures 7 and 8, Table 5-2) had similar mean low-frequency cetacean auditory frequency weighted SEL

that were also close to the low-frequency cetacean auditory frequency weighted levels in the Chukchi Sea in 2014. Both had maximum daily 10+ Hz SEL of 160 dB re 1 $\mu Pa^2 \cdot s$, except for 3 days at Blake Escarpment. At Blake Escarpment, the 10+ Hz SEL were 8.4 dB above the low-frequency cetacean auditory frequency weighted SEL, while in Orphan Basin, prior to the start of seismic surveys on 25 May 2016, the 10+ Hz SEL was only 2.9 dB above the low-frequency cetacean auditory frequency weighted SEL, like the Chukchi Sea in 2014. The autocorrelations of the Orphan Basin data remained high after 26 hours, like the results in the Chukchi, whereas the Blake Escarpment autocorrelation dropped below 0.1 within 30 minutes. The autocorrelation difference indicates that the primary source of sound changes on the scale of 30 minutes at Blake Escarpment. The differences between the 10+ Hz SEL and low-frequency cetacean auditory frequency weighted SEL were due to energy in the 10–100 Hz frequency band. This is the band with highest energies from heavy shipping (e.g. Wenz 1962, McDonald et al. 2006, Chapman and Price 2011), but it may also contain energy from animals (e.g., fishes and large whales), seismic surveys, or flow-induced noise around hydrophones. Manually reviewing the Blake Escarpment data showed that vessels frequently passed the recorder, but there were no other distinct sound sources when no vessels were present.

The Chukchi Sea 2015 exploratory drilling program (data set C) and Vancouver-Fraser Port Authority (data set F) data contain high levels of sound from vessels. The Chukchi Sea 2015 data were 1 km from exploratory oil and gas drilling and had a 10+ Hz and low-frequency cetacean auditory frequency weighted daily SEL 26 dB higher than the same site in 2014. At 16 km from the drilling activities, the average 10+ Hz daily SEL was 16 dB higher than in 2014 (not shown). Most of the sound was produced by

dynamic positioning systems whose energy is above 100 Hz, which can be seen by the small difference between the 10+ Hz and the low-frequency cetacean auditory frequency weighting function SEL. This difference was higher at the 16 km measurement site due to more sound from support vessels instead of the drilling platform. At the Vancouver-Fraser Port the mean 10+ Hz daily SEL was 14 dB above the Chukchi in 2014. The differences decreased with increasing frequency but were still ~7 dB for the high- and very high-frequency auditory frequency weighted SEL. The Carson Canyon data (data set E) also show the effects of vessel range on SEL. The project's fishing vessel operated for several days within 1–4 km of the recorder, but there was no obvious signal of its presence in the daily SEL results. A different fishing vessel passed directly over the recorder on 11 Sept and generated a daily SEL comparable to the drilling program in the 2015 Chukchi data (data set C) or near the Vancouver transit lanes (data set F).

Seismic surveys (Baffin Bay, Orphan Basin after 25 May, Carson Canyon on 22 Sep; data sets J, D, E respectively) increased the daily 10+ Hz SEL by 10–40 dB and the low-frequency cetacean auditory frequency weighted SEL increased by 0–30 dB depending on the closest daily range to the vessel. The shortest range recorded to a seismic array was 100 m which occurred in Baffin Bay on 4 Sept 2012 and generated a 10 Hz + daily SEL of 189 dB re 1 $\mu Pa^2 \cdot s$. In Baffin Bay (data set J), the airgun arrays were on average 40 km from the recorder (Martin et al. 2017). At Orphan Basin (data set D; after 25 May), the ranges to the recorder were unknown, but presumed to be longer than 200 km when the survey began, decreasing to ~20 km at the end of recording. In this recording, the 10+ Hz daily SEL values increased 10–30 dB from pre-seismic, and the low-frequency cetacean auditory frequency weighted SEL increased 0–20 dB. The otariid

and phocid auditory frequency weighted SEL did not increase due to the seismic pulse energy until several weeks into the survey when the range to the vessel decreased and the high-frequency signal strength increased, similar to the Baffin Bay results (Figure 5-2). The change in autocorrelation as a result of the seismic surveys can be seen in monthly plots (Figure 5-4).

The daily SEL at Block Island (H and I) were among the highest compared here, likely due to the large amounts of activity associated with the pile driving program (Table 5-2). The average daily SEL at the 9100 m location on days without piling were generally higher than at 850 m. At 9100 m vessels passing the recorder contributed a similar amount to the daily SEL as the pile driving (see also Figure 5-6). The impact pile driving increased the daily SEL by 10-25 dB at 850 m from the pile driving compared to the levels at 9100 m. The high- and very high-frequency marine mammal auditory frequency weighted SEL did not increase during pile driving at 9100 m due to the relatively high SEL that had already accumulated from the vessels. The 9100 m location was in 42 m of water and was farther from Block Island, so we presume it received more energy from shipping than the 850 m location.

Coral reef (K & L) soundscapes are substantially different from the other environments measured (Figure 5-2, Figure 5-3). The daily SEL in these locations was constant, with standard deviations less than 1 dB at the Great Barrier Reef and 1-3 dB at Paradise Reef. At both sites there is a peak in the auto-correlation of the 1-minute sound exposures at 24 hours due to the sonorous activity of many reef animals that are synchronized with the solar cycle. Few anthropogenic sounds were present in the Great Barrier Reef recording (L) which resulted in an auto-correlation of almost 1 after 24

hours. The Great Barrier Reef site is the only one where the low-frequency cetacean auditory function weighted SEL was not the highest weighted daily SEL. The Paradise Reef location was ~500 m from a cruise ship pier and frequented by many tourist dive boats. A total of 76 cruise ships visited the port during the recording period, with visits typically lasting 10 hours from ~08:30-18:30. This human activity elevated the daily SELs by 5-10 dB compared to the Great Barrier Reef, changed the auto-correlation structure, and resulted in the low-frequency cetacean auditory function weighted SEL being the highest weighted SEL on most days. The peak in the auto-correlation structure at 10 hours is a result of the vessels entering and leaving port. The peak at 24 hours is due to daily patterns in the vessel activity as well as from the soniferous animals on the reef. There is a notable peak in the high- and very high frequency auditory frequency weighted SEL on 27 July, 10 August, and 24 August which was caused by a 27 kHz echosounder. The very high frequency cetacean SEL exceeded the (Southall et al. 2019b) permanent threshold shift regulatory limit for continuous noise on those days. The echosounder has been linked to one of the cruise ships that was the only vessel in port on the 27th of July, and her only other port visits were 10 and 24 August. None of the other 16 unique cruise ships that visited the port appeared to have left their echosounders running.

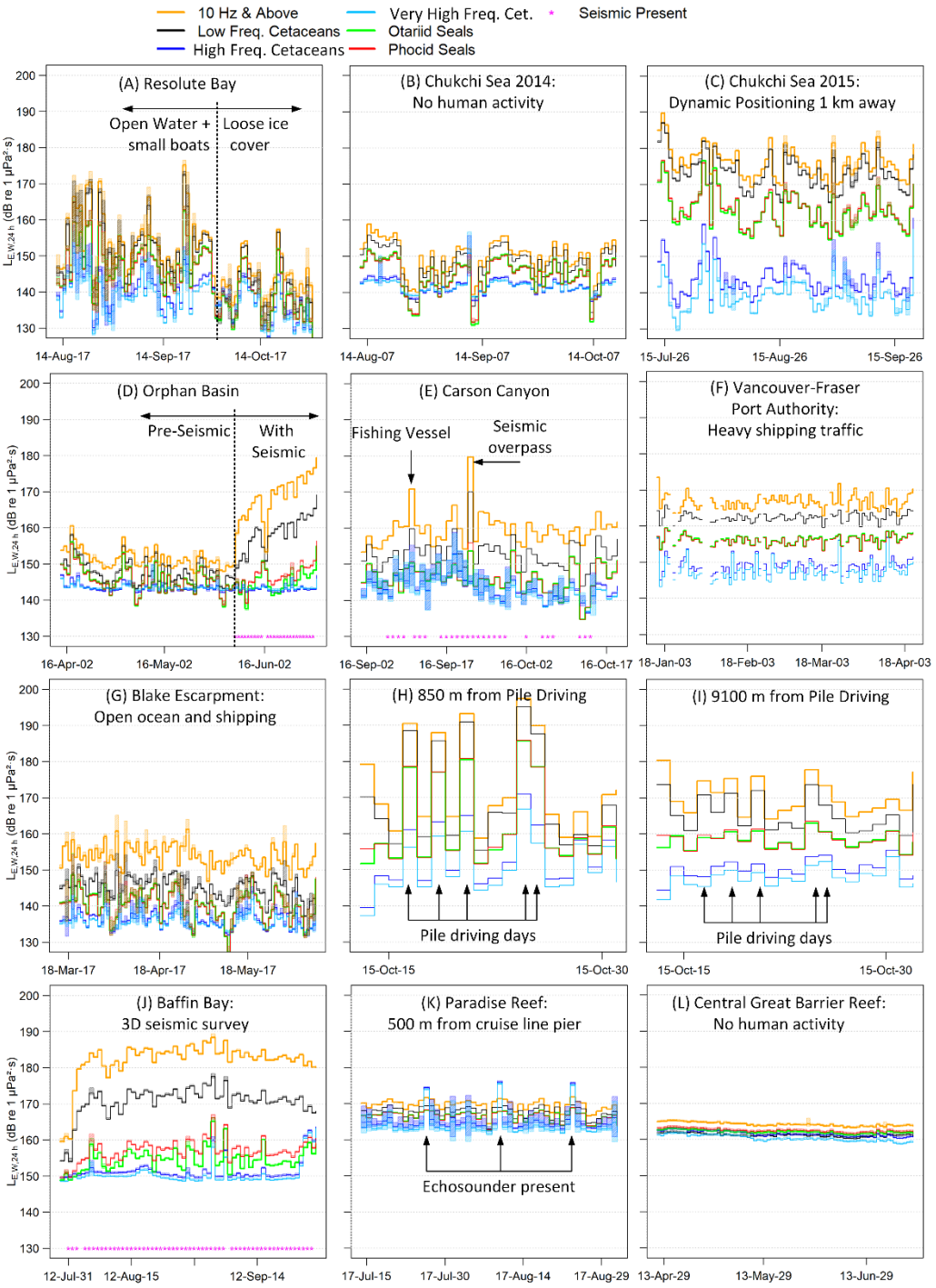

Figure 5-2. Daily weighted SEL for sites A-L (Table 5-1, Figure 5-1) with sound levels shown in Table 5-2. For each figure the 10+ Hz SEL is shown along with the five Southall et al. (2019b) marine mammal auditory frequency weighting functions. For the duty-cycled recordings (data sets A, B, D, E, G, K and L) the SEL was computed as described in Section II.C. The 95% confidence interval is shown by the shaded boxes around each days' weighted SELs.

Table 5-2. Arithmetic mean daily SEL (dB re 1 µPa²·s) and standard deviations (gray bracketed text) for data sets A-L (Figures 6 and 7). The Resolute Bay data (A) has been divided into open-water and small boats (16 Aug – 2 Oct) and with ice-cover (3 Oct – 2 Nov) periods. The Orphan Basin (D) data has been divided into pre-seismic (1 Apr to 24 May) and with-seismic (25 May to 30 Jun) periods.

Location ID	Location name	Data Description	10 Hz and above	Low-frequency Cetacean	High-Frequency Cetacean	Very High-Frequency Cetacean	Phocid Seals	Otariid Seals
A	Resolute Bay Aug - Sept	Open ocean	162.9 (8.2)	160.5 (8.0)	143.8 (4.9)	141.9 (4.8)	152.6 (6.3)	152.5 (6.3)
A	Resolute Bay Ice Covered (Oct-Nov)	Ice + open water noise	147.2 (5.7)	145.7 (6.7)	138.3 (5.1)	137.2 (4.9)	142.0 (6.1)	142.1 (6.3)
B	Chukchi Sea, 2014	Open ocean	151.8 (4.7)	150.0 (4.9)	142.3 (2.2)	142.1 (1.8)	146.4 (4.8)	146.6 (5.0)
C	Chukchi Sea, 2015	Dynamic positioning from semi-submersible drill rig	178.7 (4.4)	176.2 (4.6)	148.1 (4.4)	143.6 (4.1)	166.5 (4.9)	166.4 (5.1)
D	Orphan Basin – pre-seismic	Open ocean	152.5 (2.6)	149.4 (3.3)	143.5 (1.1)	143.5 (0.6)	147.0 (3.4)	147.3 (3.6)
D	Orphan Basin – with seismic	Seismic Survey getting closer to recorder with time.	172.2 (6.0)	161.2 (5.0)	142.7 (1.0)	142.8 (0.6)	148.2 (3.3)	146.6 (3.5)
E	Carson Canyon	Open ocean, fishing, seismic airgun survey	159.7 (4.8)	152.4 (4.4)	143.0 (3.0)	142.5 (2.9)	145.9 (3.9)	145.8 (3.8)
F	Vancouver-Fraser Port Authority	Port of Vancouver's inbound shipping lane.	167.2 (2.0)	162.6 (1.3)	149.9 (2.3)	148.7 (2.7)	156.3 (1.3)	156.4 (1.3)
G	Blake Escarpment	Open ocean with some shipping	154.8 (3.1)	146.2 (3.1)	137.6 (2.8)	136.5 (2.2)	141.8 (4.1)	141.9 (4.2)
H	Block Island, 850 m from piling	Impact pile driving	187.6 (13.1)	185.4 (13.6)	161.1 (8.4)	157.1 (7.6)	176.0 (11.6)	175.7 (11.7)
I	Block Island, 9100 m from piling	Impact pile driving	172.9 (4.9)	168.0 (4.8)	151.0 (2.6)	148.8 (2.8)	159.1 (2.4)	158.8 (2.7)
J	Baffin Bay	Seismic airgun survey except first 2 days.	183.5 (5.6)	171.8 (4.4)	153.0 (2.8)	152.0 (2.8)	158.0 (3.0)	156.0 (3.2)
K	Paradise Reef	Coral Reef, 500 m from cruise terminal; frequented by small tourist dive boats.	169.8 (1.5)	168.0 (1.5)	166.8 (2.8)	165.9 (2.9)	166.7 (1.3)	166.7 (1.3)
L	Central Great Barrier Reef	Coral reef without human sources.	164.2 (0.5)	161.2 (0.5)	161.6 (0.7)	160.4 (0.8)	162.5 (0.5)	162.1 (0.5)

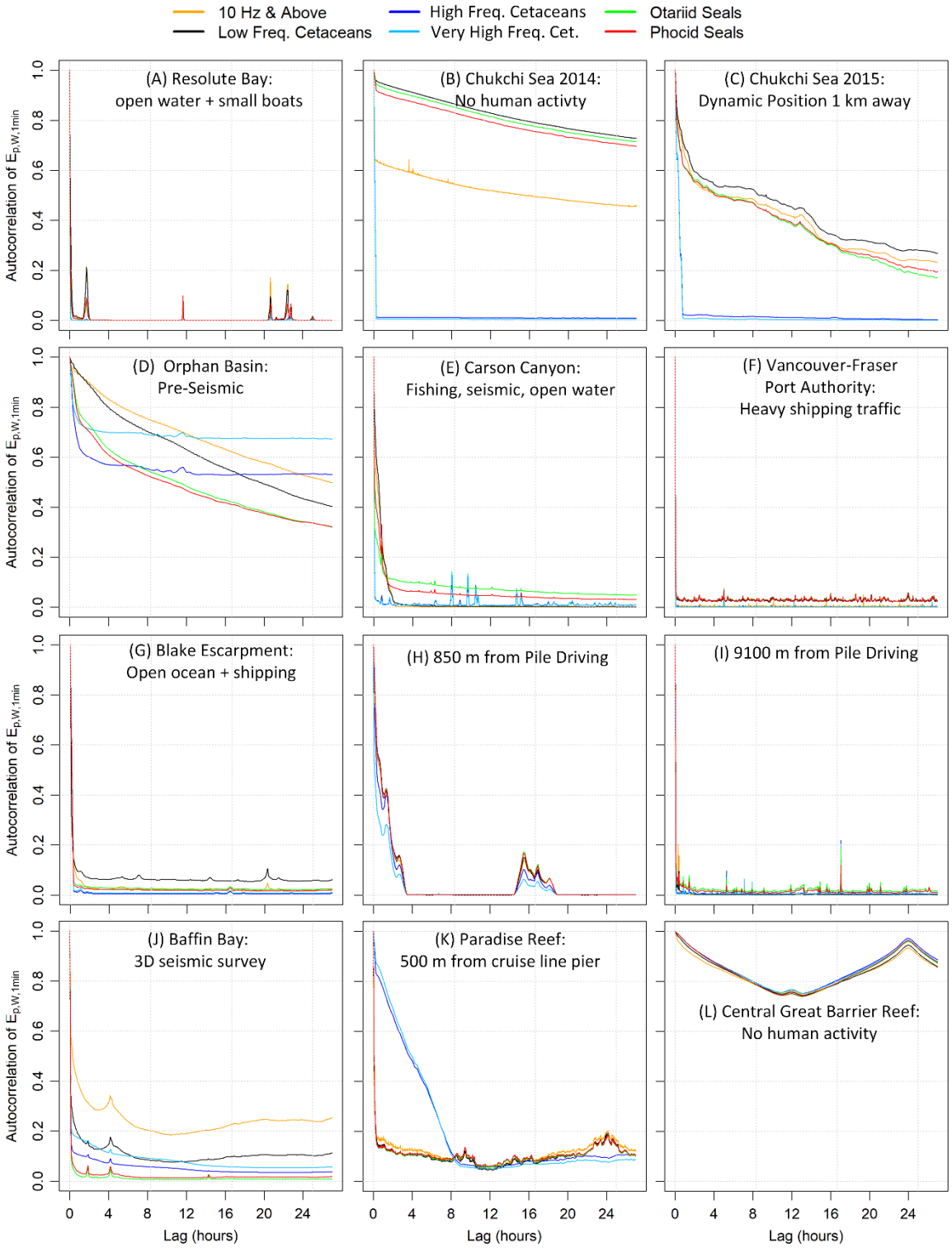

Figure 5-3. Autocorrelations of the one-minute sound exposure at sites A-L (Table 5-1, Figure 5-1). For each plot, the 10+ Hz data are shown along with the five Southall et al. (2019b) marine mammal auditory frequency weighting functions. For data sets that were divided into subsets in Table 5-2, only one subset is included in this figure.

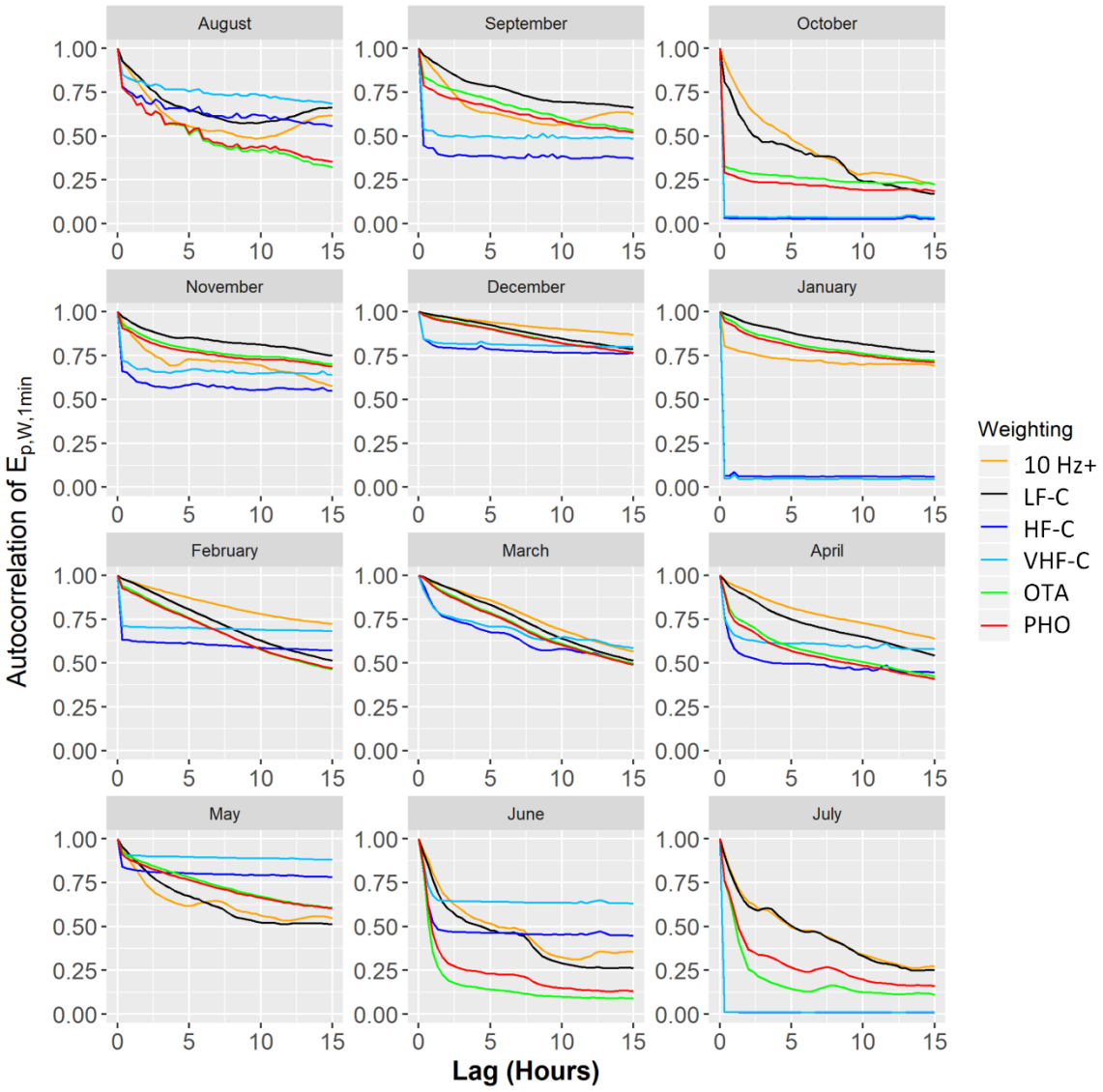

Figure 5-4. Example of the autocorrelation of each month's 1-minute auditory frequency weighted SEL for the Orphan Basin data. Top left is August 2015, bottom right is July 2016. August, September and part of October 2015 as well as part of May, and all of June and July 2016 had seismic survey activity in the area. The abbreviations for the weighting functions are The auditory frequency weighting functions shown are: 10 Hz+ – 10+ Hz (10 Hz and above); LF-C – low-frequency cetacean; HF-C – high-frequency cetaceans; VHF-C – very high-frequency cetaceans; PHO – Phocid seals; and OTA – otariid seals.

5.3.2. Accumulation of SEL

5.3.2.1. Case 1: Vessels and Seismic Surveys in Baffin Bay

Figure 5-5 shows twelve hours of data from the Baffin Bay data set (J) during which two seismic vessels passed by the recorder. SEL accumulated slowly while the first seismic vessel approached the recorder. At ~05:45, the seismic support vessel passed near the recorder; its propulsion sounds were the first sounds above the recorder noise floor for the high- and very high-frequency weighted daily SEL. The total SEL increased rapidly in the last kilometer as the per-pulse SEL increased by 20 dB. The remainder of the passage of the first vessel plus the entire passage of the second vessel only increased the 10+ Hz SEL by 2 dB. The weighted SEL increased by smaller amounts. The daily SEL did not increase for the remainder of the 24-hour period (not shown).

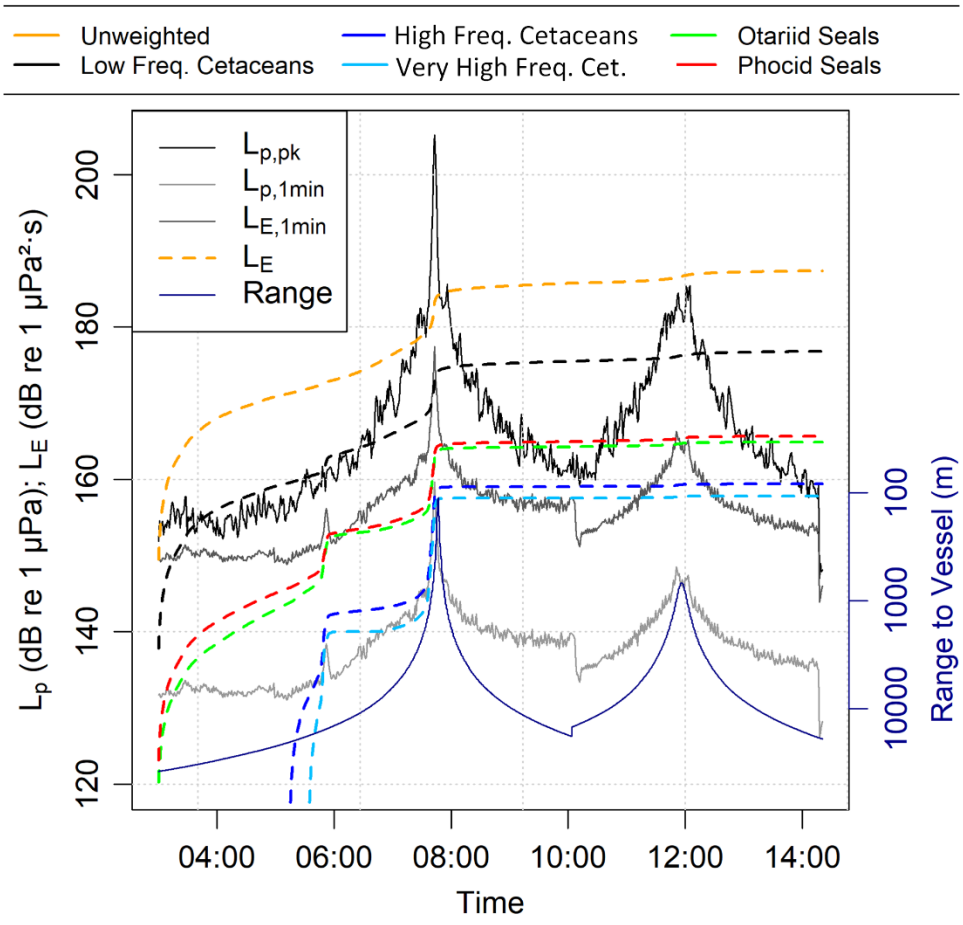

Figure 5-5. Accumulation of seismic survey SEL over a 12-hour period on 4 Sep 2012 during the overpass of two seismic source vessels in Baffin Bay (M). The 10+ Hz SEL increased from 184.5 dB re 1 µPa²·s after the first vessel passed at 07:50 to 186.7 dB re 1 µPa²·s at 12:00 when the second passed. For more on this data set see Martin et al. (2017).

5.3.2.2. Case 2: Accumulation of SEL near a Pile-Driving Construction Site

The daily SEL is the sum of the ambient sound from wind and waves, human activity and biologic sounds. The daily SEL at a receiver depends on the source level of each source and the attenuation of sounds with distance (Figure 5-6). The figure shows the accumulation of SEL on 25 Oct 2015 during pile driving at Block Island (H&I). At a range of 850 m from the piling (Figure 5-6(a)), a vessel passed the recorder at ~04:00, which increased SEL by 5–10 dB. Three bouts of impact piling began at 18:15. The first

bout increased the daily SEL by 10-25 dB, depending on the auditory frequency weighting. Between the vessel passage and the start of piling the daily SEL increased slowly, likely due to ambient background sound. The ambient sound did not increase the daily SEL after pile driving. At 9100 m from the pile driving location (Figure 5-6(b)), vessel passages at midnight and ~07:00 were the primary source of daily SEL. The first bout of pile driving did not add enough sound energy to the daily SEL to be discernible. The second and third bouts of pile driving only made a slight increase in the low-frequency cetacean auditory frequency weighted SEL.

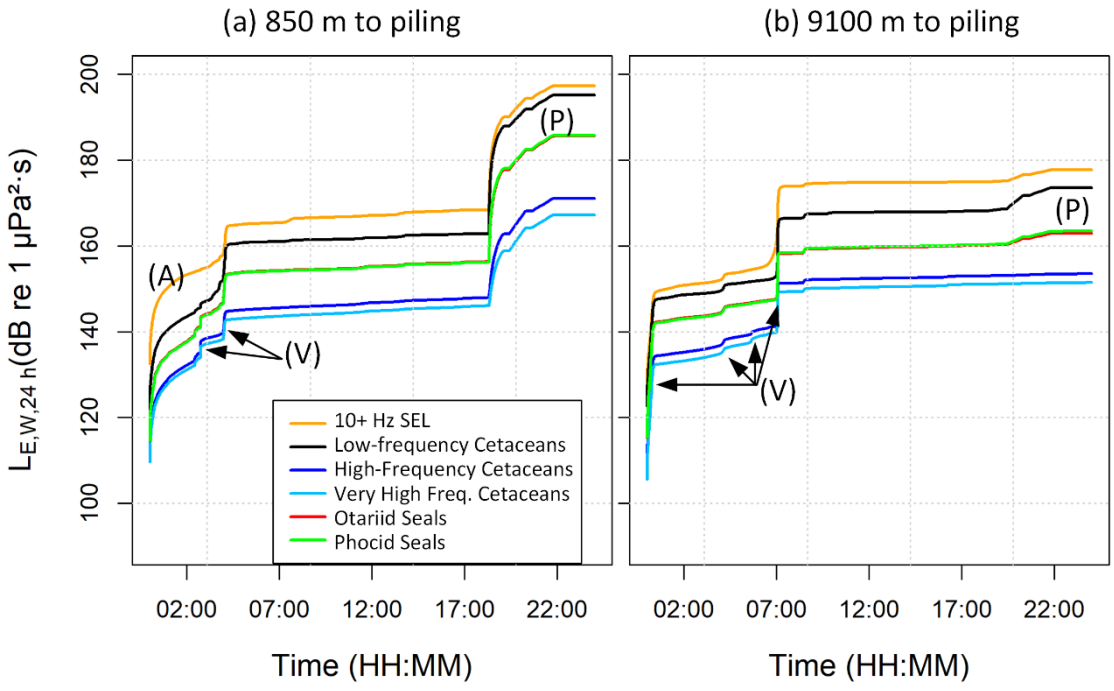

Figure 5-6. Comparison of the accumulation of SEL at a pile driving site over a 24-hour period at two ranges from pile driving on 25 Oct 2015 during construction of the Block Island Wind Farm, USA. The primary source of sound during large changes in SEL are annotated: (A)-Ambient, (V)-Vessel Passages; (P)-impact pile driving. (a) 850 m from the piling location. (b) 9100 m from the piling location.

5.3.3. Effects of Duty Cycles on SEL

Duty-cycling introduces an error in the daily SEL estimate whose mean value ranges from −1.7 to +1.1 dB. The error in estimated SEL increases with decreasing autocorrelation; the errors are more often underestimates of SEL rather than overestimates. The relationship between autocorrelation (at the first available time lag – i.e., 2, 3, 4, etc. minutes, as described in Section II.C) and SEL error was not linear and had a large range of error values for any one correlation value. Therefore the 95% confidence intervals were determined empirically from the measured data. To confirm that the behavior of the real data sets was predictable, the results were compared with Gamma-distributed random noise. The worst case 95% confidence interval for the error is ± 6 dB, both for the real data and simulations with Gamma-distributed random noise (see Section 5.6.7). As an example of the use of the confidence interval results, the range of SEL error for each day and auditory frequency weighting function were added to Figure 5-2 as shaded areas around the expected value

5.4. DISCUSSION

5.4.1. Accumulation of SEL from Stationary and Moving Sources and Implications for the Distance from a Source where Auditory Injury may Occur

An important property of SEL from human sound sources is that the relative movement of the source and receiver determines how SEL accumulates, which is clearly shown in Figures 10 and 11 as well as by the echosounder at Paradise Reef (Figure 5-2-K). The highest 10 Hz and above daily SEL of 193 dB re 1 $\mu Pa^2 \cdot s$ was recorded on 21 Oct 2015 at 850 m from the pile driving. This was 4 dB higher than the maximum

seismic daily SEL, even though the seismic vessel passed only 100 m from the recorder (Baffin Bay, 4 Sept 2012). This result underscores how moving sources like seismic and vessels mitigate accumulation of SEL compared to a stationary source like pile driving. A moving biologic receptor would similarly mitigate the accumulation of SEL from stationary sources as well as mobile ones. If we assume that most sensitive biologic receptors will move, even if just over distances of several hundred meters, then the closest point of approach (CPA) to the source will dominate the received SEL (as shown in Figure 5-5 and Figure 5-6 and by Monte Carlo simulations (Gedamke et al. 2011)). The duration of CPAs is typically on the order of minutes, and thus integration over a period of an hour will accumulate all of the energy from a moving human source that a biologic receptor would encounter. As noted in (Southall et al. 2019b), further investigation of appropriate SEL integration and rest times is required.

It is known that hearing begins to recover quickly after exposure to loud sounds (Hirsh and Ward 1952). For example porpoise recovered from 10 dB of TTS within an hour (Kastelein et al. 2012c). It is therefore reasonable to consider resetting SEL exposure an hour after CPA for moving human sources and / or moving biologic receivers. For non-impulsive sources of sound, such as dynamically positioned oil rigs or sea-floor production facilities, a different approach is required, which is acknowledged in NMFS (2018), although no specific advice is given. For this type of source the distance around the activity where one would expect animals to be affected, and likely excluded, is equal to the area where the average sound level is above the threshold of effective quiet (Ward et al. 1976a, Mooney et al. 2009, Kastelein et al. 2017, Martin and Lucke, this issue). There is some evidence for this effect in the detections of odontocetes 2 km

compared to 20 km from a mobile offshore drilling unit working in 2400 m of water off Nova Scotia (Martin et al. 2019). Further work in understanding effective quiet, hearing recovery, and appropriate accumulation times is required for all marine taxa.

5.4.2. Identifying Soundscapes Dominated by Wind and Wave Sounds

The data sets analyzed here demonstrate a range of effects that our use of the oceans has in changing soundscape experienced by marine life. Recordings such as Chukchi 2014 (B) and Orphan Basin pre-seismic (D) provide a baseline soundscape for the open ocean that is measurably different from the other environments. Similarly, the Great Barrier Reef is a baseline coral reef environment that contrasts with the measurements at Paradise Reef.

From the results we propose the following indicators to identify soundscapes that are unaffected by anthropogenic activity or intense biologic sound production: 1) the daily 10+ Hz SEL is below 160 dB re 1 $\mu Pa^2 \cdot s$, even in high winds; 2) the low-frequency cetacean auditory frequency weighted SEL is within 3 dB of the 10+ Hz SEL (i.e., at least half of the daily SEL is from frequencies above 100 Hz); and 3) the low-frequency cetacean auditory frequency weighted SEL has a correlation coefficient above 0.6 for time lags of at least 3 hours when computed with 1-minute SEL over periods of at least 1 month. For coral reefs, the proposed indicators are slightly different: 1) the daily 10+ Hz SEL is below 170 dB re 1 $\mu Pa^2 \cdot s$, even in high winds; and 2) the autocorrelations of all auditory frequency weighted one-minute SEL are above 0.75 at 24 hours lag when computed using at least 1 month of data. The duration over which the autocorrelations remain high indicates how isolated the soundscape is from variable sound sources,

usually of human origin. The details of the low-frequency cetacean auditory frequency weighting are not important for these results – rather the results depend on excluding energy between 10 and 100 Hz – which is the effect of the low-frequency cetacean weighting. We replicated these results using by computing SEL using only 100–20,000 Hz decidecades (Equation 5-3).

It is important to understand the properties of the long-term autocorrelation of the 1-minute sound exposure as a soundscape indicator. The autocorrelation of the sound exposure is defined in as the sum of the sound exposure (E_p) times the delayed version of itself, divided by the summed square (Equation 5).

$$R_{EE}(\tau) = \frac{\sum_{t=0}^{T-1} E_p(t)E_p(t-\tau)}{\sum_{t=0}^{T-1} E_p(t)E_p(t)} \quad (5\text{-}5)$$

This operation will always have a value of 1 when τ is 0. When τ is not zero, the autocorrelation measures the change in sound exposure for each value of τ. This operation is susceptible to being dominated by large amplitude values that overwhelm other patterns that may be in the data. For example, the echosounder at Paradise Reef (K) was only present 1 day in 14, yet the high- and very high-frequency weighted sound exposures are above 0.1 for 10 hours, the duration that the vessel was in port. This is also a property of the autocorrelation that also makes it useful as a soundscape descriptor – loud sources at random times reduce the autocorrelation and indicates human effects on the acoustic environment. At the same time, it is important to separate the data into periods that are dominated by identifiable sources before assessing the soundscapes during those periods individually. For this reason, we have divided the Orphan Basin data into pre-seismic and with seismic periods, and the Resolute Bay data into open water and

ice-covered periods (Table 5-2). In general, consider determining the autocorrelation on a month-by-month basis to look for long-term variability in a soundscape (e.g. Figure 5-4).

A few notes on how autocorrelation was used in this analysis are warranted. First, autocorrelation was performed on the sound exposure, rather than the sound exposure level (see Equation 5-2 and 5-3). The choice is essential so that the large range of exposure values can decorrelate the soundscape when sources like ships are present. When SEL is used the correlation coefficient remains near 1 for all data sets for lags of days. Second, the absolute values of the sound exposure are important, and therefore the data should not be de-meaned before performing the autocorrelation. For many other applications of autocorrelation this is not the case. As a result of this choice, autocorrelation coefficient values below zero will not occur. Finally, the data used for autocorrelation must be evenly spaced. For example, the Chukchi Sea 2014 data (B) has two minutes of data at the high sample rate, and 13 minutes at the low sample rate. All this data, when sorted in time, may be autocorrelated to determine the properties of the 10 Hz and above SEL or the low frequency cetacean auditory frequency weighted SEL. For the remaining weighted SEL only one minute of the two minutes of high sample rate data should be used.

5.4.3. Selecting Hardware and Duty Cycles for SEL Analysis.

The data sets analyzed illustrate two considerations when selecting recording equipment and determining the recording configuration: it is possible for the recording system noise floor to be higher than the TTS thresholds for high-frequency cetaceans, and the recording configuration may not support accurate assessment of the auditory frequency weighted SEL.

The recording system noise floor and sampling rate set the minimum daily SEL that can be measured, which may be higher than the Southall et al. (2019b) TTS thresholds from non-impulsive sound sources for very high frequency cetaceans of 153 dB re 1 $\mu Pa^2 \cdot s$ and the impulsive threshold of 140 dB re 1 $\mu Pa^2 \cdot s$ (see Tables 6 and 7 of Southall et al. 2019b). For hydrophone data acquisition systems, the spectral noise floor is the sum of noise from the analog-to-digital converter, hydrophone pre-amplifier, and hydrophone ceramic. Different hydrophone noise floors had a notable effect in the data sets analyzed. The Orphan Basin data (D) were computed from data sampled at 250,000 Hz using HTI-99-HF hydrophones, which resulted in an SEL noise floor of ~142 dB re 1 $\mu Pa^2 \cdot s$ (Table 5-1, Figure 5-2). The Blake Escarpment data (G) was also recorded at 250 kHz, but with the lower noise GeoSpectrum M36 hydrophone, so that the minimum high-frequency marine mammal daily SEL was ~134 dB re 1 $\mu Pa^2 \cdot s$ – which is visible as a lower noise floor in Figure 5-2. The Baffin Bay (L) and Block Island 850 m (H) configurations are typical of recordings made near high-intensity human activities such as pile driving and seismic surveys where low sensitivity hydrophones are needed to avoid saturation from the sound source. The low-sensitivity resulted in spectral density noise floor of 53 dB re 1 $\mu Pa^2/Hz$ which with 64 kHz sampling rate, the noise integrated to a daily minimum SEL of 150 dB re 1 $\mu Pa^2 \cdot s$.

Solutions for the noise floor limit are to reduce the bandwidth analyzed and/or only integrating for the period when the source is present. As discussed above 24 hours is the currently recommended duration but should be reconsidered as more data becomes available. With respect to the recording bandwidth, the main sounds of interest for the effects of man-made noise on marine life (pile driving, seismic arrays, vessels, and naval

sonar) are all dominated by frequencies below 10 kHz, with some energy reaching to 30 kHz and higher at short ranges (Simard et al. 2016, Martin et al. 2017, MacGillivray 2018b). Based on these frequencies and our understanding of the hearing bands of marine mammals as well as most fishes and invertebrates, recording programs concerned with quantifying SEL should analyze data sampled at ~64,000 Hz. This sampling rate results in a usable frequency band of ~30 kHz which captures the energy of most sound sources of interest; reaches the 0-dB attenuation range of the high-frequency cetacean auditory frequency weighting function, and the bandwidth is narrow enough that most recorders and hydrophones will not be self-noise limited. With respect to the daily SEL from human sources, a higher sample rate is only required to study the effects of sources such as echosounders and multibeam sonars. Recording programs whose objectives include detections of odontocete clicks also need to sample faster than 64,000 Hz.

The recording duty cycle is a system configuration parameter that affects the confidence interval of the daily SEL estimates. As the duty-cycle decreases the autocorrelation coefficient decreases and the daily SEL error increases – i.e. higher errors at 1 minute in 20 than 1 minute in 2 (see Section 5.6.7). When the duty cycle is less than 1 minute in 30 the decimated autocorrelation does not track the true autocorrelation reliably and SEL should not be computed from such data. When selecting a duty cycle, we recommend recording more often rather for longer periods if daily SEL is a desired output of the project. For example, recording for 1 minute every 6 minutes is much more useful than recording for 10 consecutive minutes per hour. This result is also true when determining the presence of mysticete whales using duty-cycled data (Thomisch et al. 2015). The minimum recording duration we recommend is 1 minute, however 30 seconds

would likely provide good data as well. We have also found that when cycling between multiple sample rates, selecting a total duty cycle that is an even number of minutes is preferred as it allows more options when downsampling before autocorrelation (e.g., the Chukchi Sea 2014 data discussed in Section IV.B). When recording data to measure SEL for regulatory compliance, continuous recording is strongly recommended.

5.4.4. Using the Daily SEL in Soundscape Management - Cumulative Effects Assessment

A goal of many environmental assessments is to understand how a proposed project will add to existing human activity and affect the animals in the area. When estimating the effects underwater sound from multiple human activities, Ellison et al. (2016) provide a method based on summing the SEL from each activity for simulated animals moving through the project area. This operation is difficult for locations with many existing sound sources whose movements and source factors are uncertain. Instead, long-term baseline measurements may be used to determine the existing daily SEL, to which SEL from the proposed activity may be added. It is also possible to use the difference between the daily SEL and accepted sound tolerance levels (e.g. the Southall et al. 2019b TTS thresholds) is such an indicator of how much additional sound may be added to the environment without risk of inducing TTS. This comparison has limitations since it accumulates sound that is likely below the threshold for effective quiet and could, for some recorder configurations include system noise. It is also limited since it does not account for healing of the hearing system between intermittent exposures and the temporal effects of sound patterns are not accounted for in this (or the equal-energy hypothesis in general, Hamernik et al. 2003). Regardless, it is still a useful ‘first-look’ at

the capacity of animals in the environment to be exposed to additional sound without hearing injury or impairment. Locations where the sound levels are elevated by non-impulsive sources (e.g. Chukchi Sea 2015, Vancouver-Fraser Port Authority) require special consideration if new impulsive sound sources may be added to the environment. At these locations the non-impulsive sound levels are high enough that low and high-frequency cetaceans are already past TTS for impulsive sounds before an impulsive source starts. Studies have shown that animals and humans become more susceptible to impulsive sounds when high levels of non-impulsive sound are already present (Henderson and Hamernik 1986, Ahroon et al. 1993, Kastelein et al. 2015). Examples of these situations include pile driving in a busy harbour, vertical seismic profiling to image newly drilled oil and gas wells, or the narrow beam of an echosounder below a passing ship.

5.5. ACKNOWLEDGEMENTS

The authors thank the following organizations for including their data sets in this analysis:

- Shell Global Solutions for the Chukchi Sea 2014 and 2015 as well as the Baffin Bay data;
- Deepwater Wind / Block Island Wind Farm for the Block Island data;
- The Atlantic Deepwater Ecosystem Observation Network (ADEON) for the Blake Escarpment data. Study concept, oversight, and funding were provided by the U.S. Department of the Interior, Bureau of Ocean Energy Management, Environmental Studies Program, Washington, DC under contract Number M16PC00003, in

partnership with other NOPP funding agencies. Funding for ship time was provided under separate contracts by ONR, Code 32.

- The Department of Fisheries and Oceans Canada, Newfoundland, for the Carson Canyon data set. This project was performed under a Contribution Agreement with the Environmental Studies Research Fund.
- The Resolute Bay data collection was supported by the Ocean Tracking Network through the Natural Sciences and Engineering Research Council of Canada with additional support from the Canadian Foundation for Innovation, and the Social Sciences and Humanities Research Council.
- JASCO Applied Sciences for the Paradise Reef data (in collaboration with Comisión Nacional de Áreas Naturales Protegidas (CONANP) and Arrecifes de Cozumel National Park), the Great Barrier Reef data (in collaboration with James Cook University), and Orphan Basin data (as part of a Contribution Agreement with the Environmental Studies Research Fund).

Thanks to the two anonymous reviewers whose comments improved the focus of this manuscript, and to Michael Ainslie and David Barclay for their constructive reviews of early versions of the manuscript. Thanks to all the JASCO Applied Sciences teams and vessel crews who participated in the data collection programs whose data was used in this manuscript. Finally, thanks to Karen Hiltz for her editorial review of the manuscript.

5.6. SUPPORTING INFORMATION

5.6.1. Why does SEL Represent Total Acoustic Energy?

In the far field of an acoustic source, pressure is equal to the particle motion (U), divided by the characteristic impedance of the fluid (ρc – density times the speed of sound).

$$U = {}^{P}/_{\rho c} \tag{5-6}$$

The intensity of an acoustic wave is defined as $I=PU$, and thus the integral of the pressure $p^2(t)$ is proportional to the sound intensity, which has units of W/m^2. If we integrate the sound intensity over time, we obtain energy, and therefore $L_{E,T}$ is used as a representation of the sound energy in an acoustic event. From the definition of SEL, a 10 dB increase in SEL occurs when 10 times more energy has been received.

5.6.2. What is the SEL from Multiple Acoustic Events?

By integrating over multiple events, we can obtain the total energy of those events. If the sound exposure level of each event is the same, then the total sound exposure level is simply $L_E = L_{E,1\ event} + 10\log_{10} N$, where N is the number of events. If the sound source is non-impulsive, such as a vessel or an oil and gas production platform, then the fundamental 'event' is the average sound exposure level over one second, which equals the daily sound pressure level. N is 86,400 seconds per day, so that the daily SEL is 49.4 dB greater than the average daily SPL.

5.6.3. Auditory Filters and Weighted Sound Exposure Levels

The ability of an animal to hear a sound must be considered when estimating the sound's possible effects. Hearing sensitivity is measured using an audiogram that plots

the threshold of hearing as a function of frequency. For human hearing we use the 'A-weighting' auditory weighting function to filter sounds before estimating its effects (NIOSH 1998). The filter is an inversion of the audiogram, normalized so that the filter has zero gain at the frequencies of peak sensitivity. Finneran (2016) and Southall et al. (2019b) analyzed existing audiogram data and other inputs to develop auditory weighting functions that represent our understanding of the hearing capabilities of six groups of marine mammals (Figure 5-7). The equations for these filters are given in Table AE-1 of NMFS (2016) and in Southall et al. (2019b). There is insufficient data to generate auditory filter functions for any other marine animal groups.

The auditory filters are applied to recorded acoustic data before accumulating the sound exposure levels when estimating the possible effects of human activities. For this analysis the weighted sound exposure level of a time period or event (such as a pile driving impulse) is determined from decidecade band sound exposure levels. The decidecade exposures are multiplied by the value of the weighting function at the decidecade centre frequency, and the total exposure is computed by summing across decidecades (Equation 5-7)

$$L_{E,ddec,T} = 10\log_{10}\left(\frac{1}{T_0 p_0^2}\sum_{ddec\ f_1}^{ddec\ f_2} S(f)\right) \tag{5-7}$$

$$L_{E,W,T} = 10\log_{10}\left[\sum_{i=ddec1}^{ddecN} W(i)10^{L_{E,ddec,T}/(10\ dB)}\right]$$

where $S(f)$ is the discrete Fourier transform of the 'T'-second long time series, '$ddec\ f_1$' and '$ddec\ f_2$' are the lower and upper frequency bins of the decidecade frequency band, respectively (ISO 2017a).

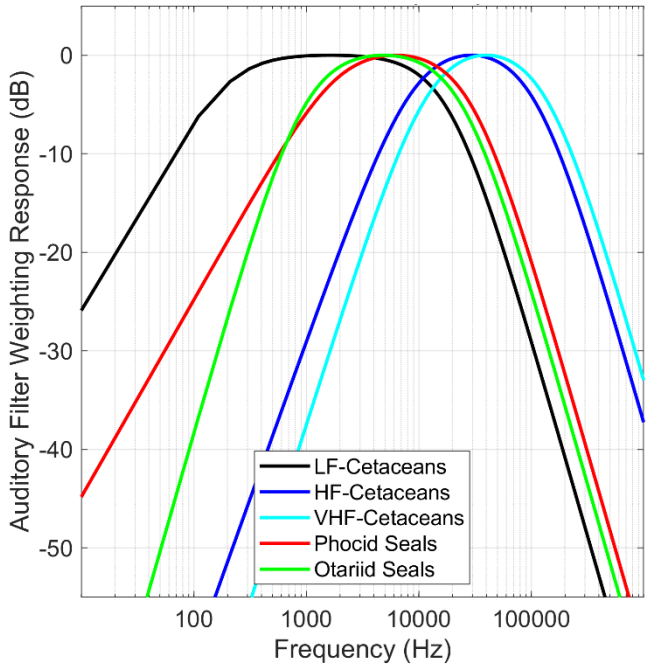

Figure 5-7. The (Southall et al. 2019b) marine mammal hearing group auditory weighting functions. Low-frequency cetaceans include the large baleen whales (e.g., blue, fin, and humpback whales). Mid-frequency cetaceans are the dolphins as well as sperm and beaked whales that echolocate in the ~1000–80000 Hz band. High-frequency cetaceans are the dolphins, sperm whales (*kogia* spp), and porpoises that echolocate in the120 kHz range. Otariid Seals are sea lions and fur seals, while phocid seals are considered 'true' seals. Southall et al. (2019b) renamed the mid-frequency cetaceans to high-frequency and high-frequency to very-high frequency.

5.6.4. Hydrophone Data Recorder Self-Noise

The noise profiles for the GTI M36-V35 and HTI-99-HF hydrophones are shown in Figure 5-8 and Figure 5-9 respectively. Hydrophone noise curves are often presented as the levels at two frequencies that are interpolated to find the overall noise level.

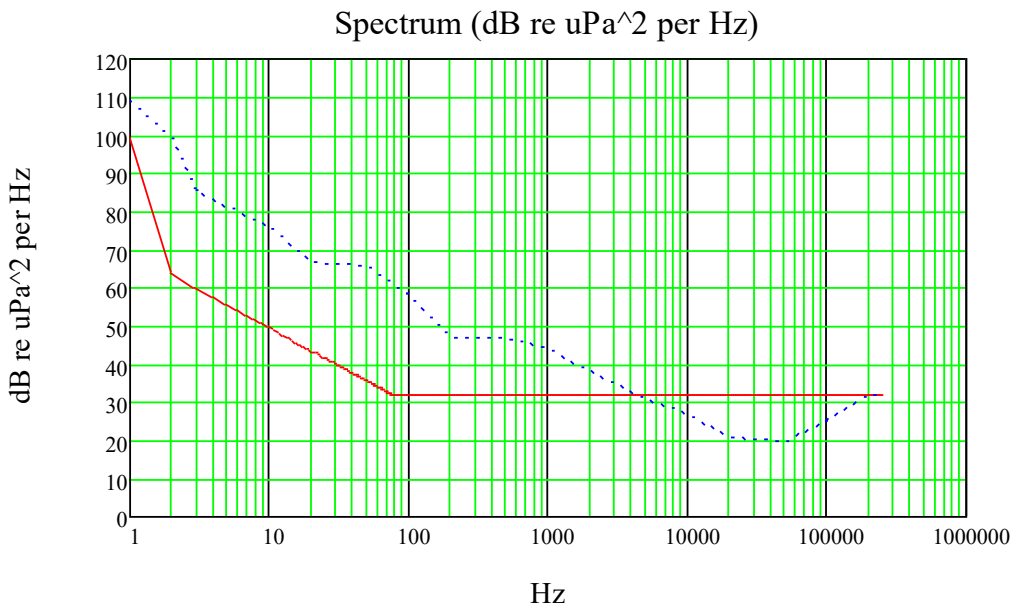

Figure 5-8. GeoSpectrum M36 hydrophone with 35 dB preamplifier spectral noise floor. The dashed blue line is the approximate sea-state 0 ambient noise floor (Wenz 1962).

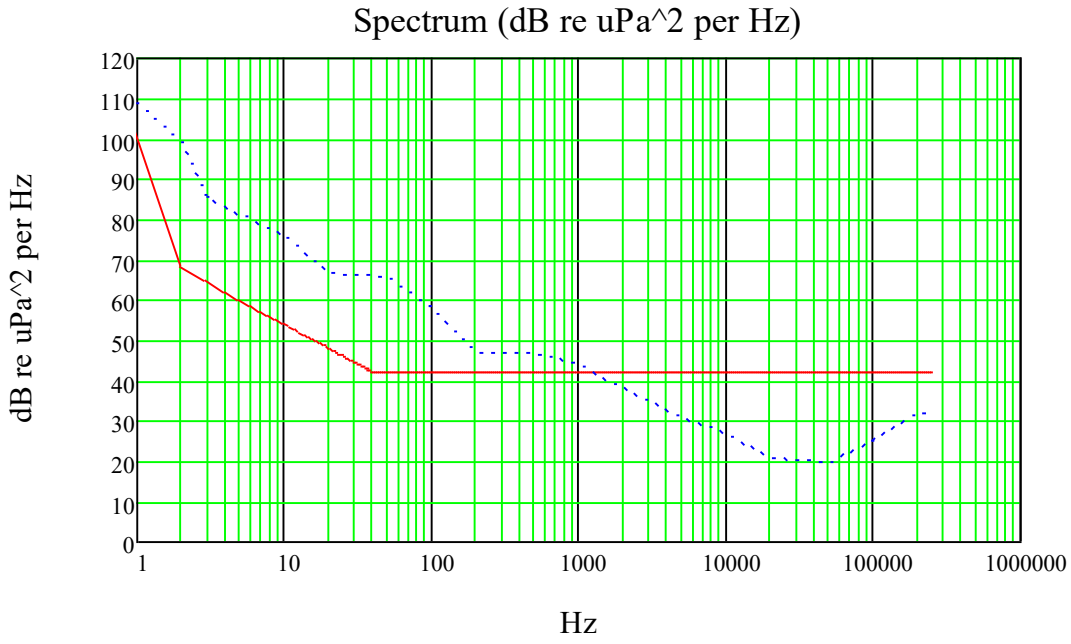

Figure 5-9. HTI-99-HF hydrophone with 35 dB preamplifier spectral noise floor. The dashed blue line is the approximate sea-state 0 ambient noise floor (Wenz 1962).

5.6.5. Gamma Distributed Random SELs

It is well known that typical sound pressure levels, and therefore sound exposure levels, have positive tails to their distributions and are approximately Gamma-distributed (e.g., Figure 5-10, Snyder (2007)). Therefore, when simulating the per-minute SELs seven Gamma-distributed data sets were created, each one 89 days long (equal to the Vancouver-Fraser Port Authority data set). The simulated Gamma parameters (Equation 5-8) are contained in Table 5-3. These parameterizations represent the distributions found in the actual data (Table 5-4). A base sound pressure level of 90 was added to each distribution.

$$f(x;k,\theta) = \frac{x^{k-1}e^{-x/\theta}}{\theta^k \Gamma(k)} \tag{5-8}$$

Table 5-3. Gamma-distributions used for simulating daily SEL errors due to duty cycling.

Shape (k)	Scale (θ)	PDF
1	1	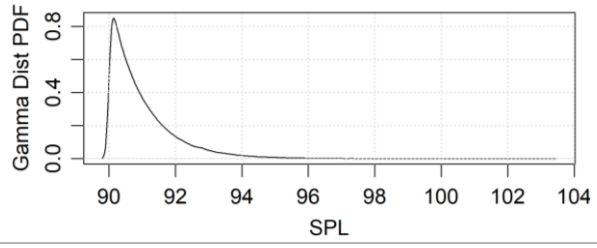
2	0.25	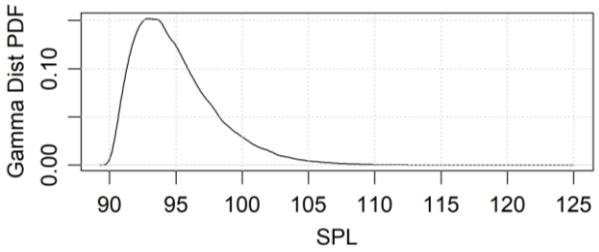
6	1	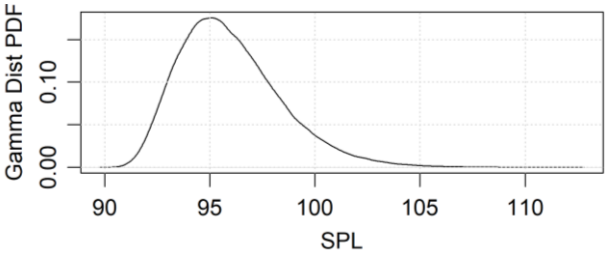

Shape (k)	Scale (θ)	PDF
4	0.5	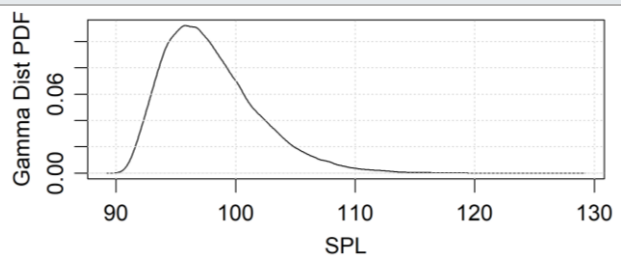
8	0.5	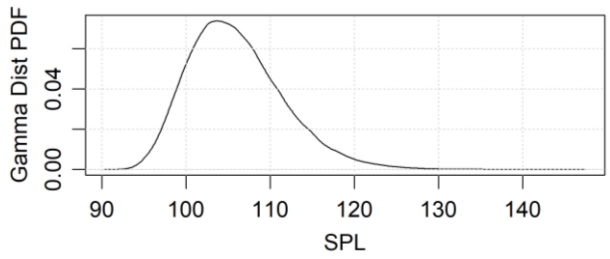
5	0.25	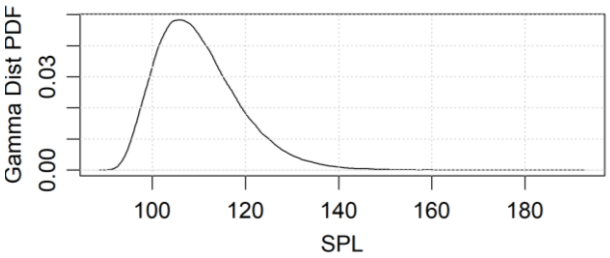
6	0.15	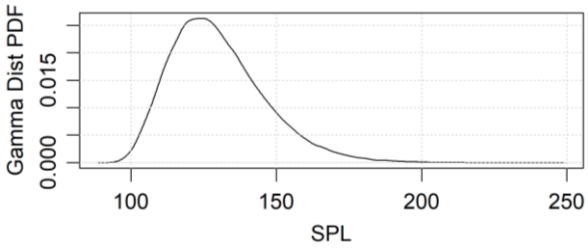

5.6.6. Statistical Measures for Each Dataset

The variance, skewness, and kurtosis for each dataset were computed from the 1-minute SEL values as indicators of how the data were distributed (Table 5-4). The skewness of a Gaussian is expected to be 0, and its kurtosis is expected to be 3. In most cases the data were non Gaussian and better described by the Gamma distribution (Table 5-4, Figure 5-10). The auto-correlation of the 1-minute SELs across each full recording duration was also computed. The correlation coefficient at a lag of 20 minutes is recorded

in Table 5-4 as an indication of our confidence in the interpolation of daily SEL. The dependence of the correlation coefficients on duty-cycling are shown in Figure 5-11. As the duty cycling increases the difference between the continuous auto-correlation (curves) and the duty-cycled auto-correlations (vertical lines and dots) increases, which indicates that duty-cycling should be no more than 1 minute in 30 in order to use the autocorrelation as a soundscape descriptor.

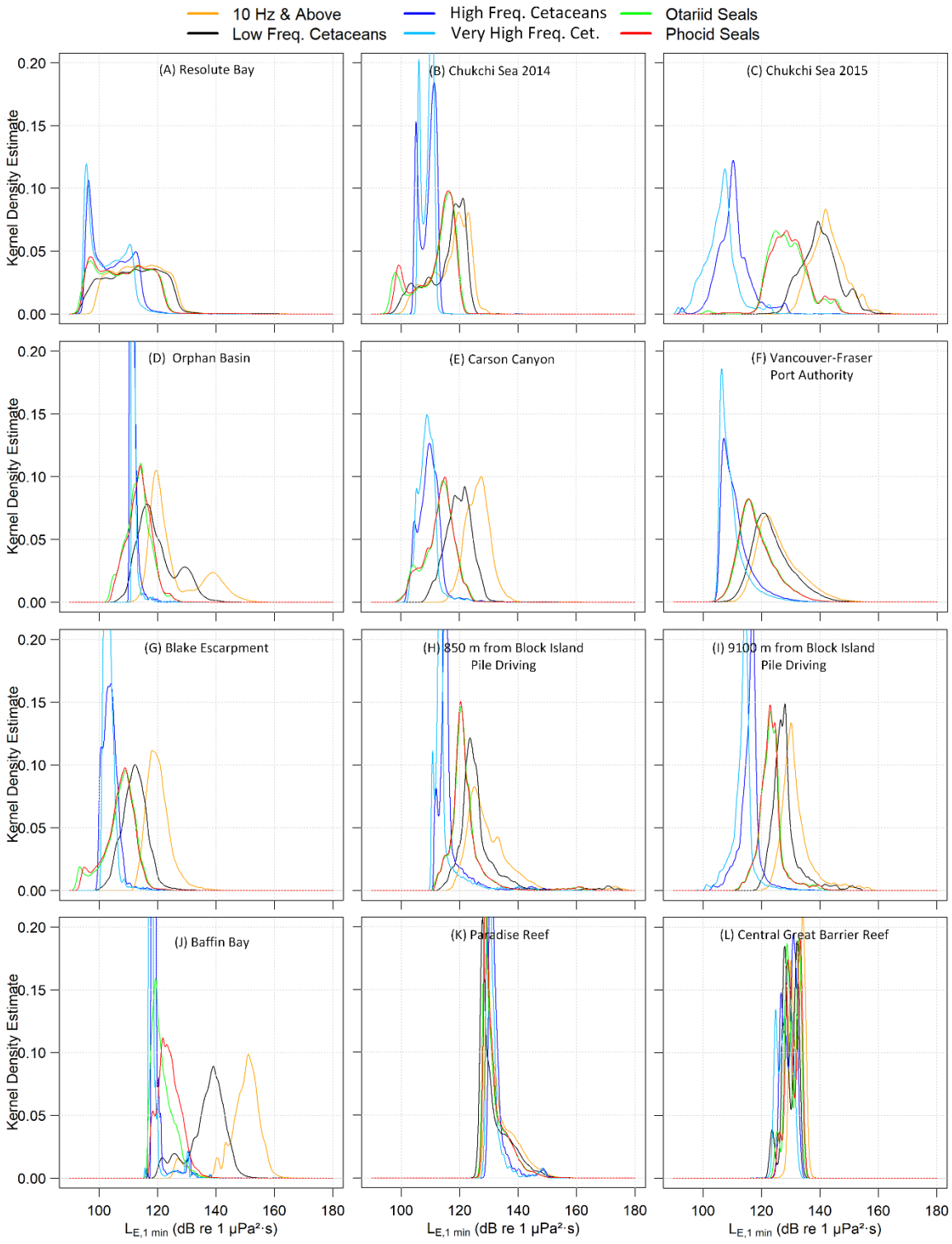

Figure 5-10. Kernel density estimates (i.e. empirical probability density functions) for the data sets.

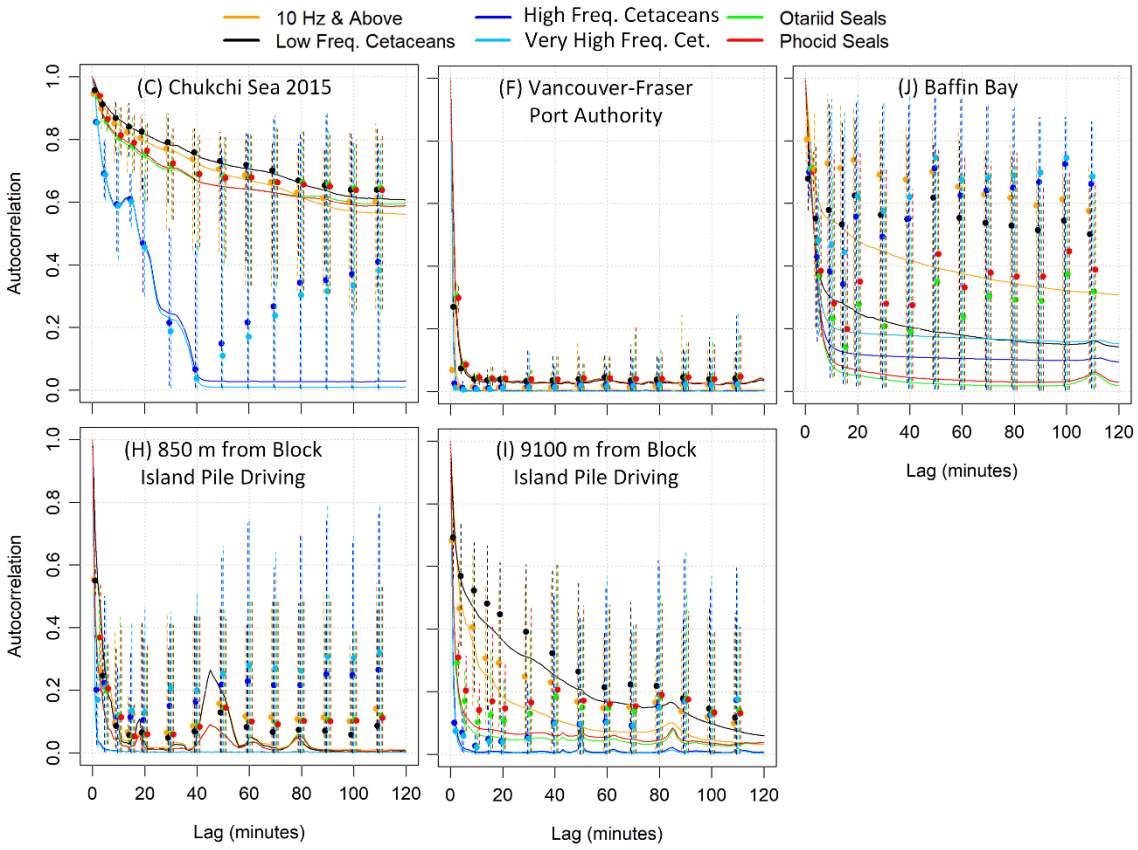

Figure 5-11. Autocorrelation comparisons. Curve show the auto-correlations for the continuous data sets analyzed. The dots and vertical dashed lines show the mean (dots) and range (vertical dashed lines) of the auto-correlations at the first time lag after decimating the continuous data to simulate duty-cycling.

Table 5-4. Statistical metrics for the datasets analysed. For each data set the metrics for each of the marine mammal weighting functions are provided: SEL – unweighted (10 Hz and above); LF-C – low frequency cetacean; HF-C – high-frequency cetaceans; VHF-C – very high frequency cetaceans; PHO – Phocid seals; OTA – otariid seals.

Weighting function	Variance	Skewness (Gaussian = 0)	Kurtosis (Gaussian = 3)	Best fit Gamma-shape (k)	Best fit Gamma scale (θ)	Autocorrelation at 20-minute lag
(A) Resolute Bay						
10 Hz+ SEL	69.6	0.3	3.2	2.4	0.2	0.2
LF-C	85.7	0.1	2.7	2.7	0.1	0.2
HF-C	43.2	0.4	2.4	1.3	0.1	0
VHF-C	38.7	0.5	2.5	1.3	0.2	0
PHO	72.2	0.2	2.3	1.9	0.1	0.1
OTA	75.7	0.1	2.2	1.9	0.1	0.1
(B) Chukchi 2014						
10 Hz+ SEL	40.2	-0.6	2.5	5.8	0.3	0.6
LF-C	44.1	-0.8	2.6	5.7	0.3	1
HF-C	7.4	-0.1	4.3	1.7	0.4	0.2
VHF-C	4.2	0.4	11.6	1.9	0.5	0.2
PHO	42.7	-0.8	2.4	2.1	0.1	1

Weighting function	Variance	Skewness (Gaussian = 0)	Kurtosis (Gaussian = 3)	Best fit Gamma-shape (k)	Best fit Gamma scale (θ)	Autocorrelation at 20-minute lag
OTA	47.8	-0.9	2.5	2	0.1	1
(C) Chukchi 2015						
10 Hz+ SEL	32.8	0.4	3.1	7.4	0.5	0.9
LF-C	38.7	0.2	2.9	10	0.5	0.9
HF-C	30.8	0.7	5.4	7.8	0.4	0.7
VHF-C	28	0.5	5.2	5.6	0.4	0.7
PHO	40.4	0.4	3.5	15.9	0.6	0.9
OTA	44.1	0.2	4.7	13.9	0.5	0.9
(D) Orphan Basin (all data)						
10 Hz+ SEL	78.9	1.1	2.9	2.8	0.2	1
LF-C	44.5	0.7	2.9	4.3	0.3	1
HF-C	1.7	4	30.2	1.6	1.2	0.8
VHF-C	0.8	6.7	69.4	1.7	2.3	0.8
PHO	16.9	0.2	3.4	4.1	0.4	0.9
OTA	17.9	0.2	3.5	4.3	0.4	0.9
(E) Carson Canyon						
10 Hz+ SEL	18.7	0.9	8.7	7.6	0.6	0.5
LF-C	20.7	0.4	5.7	6.4	0.5	0.6
HF-C	14	1.2	8	3.6	0.5	0
VHF-C	11.4	2	12.5	3.5	0.6	0
PHO	24.9	-0.2	3.3	7	0.5	0.4
OTA	26.2	-0.3	3.1	6.4	0.4	0.3
(F) Vancouver-Fraser Port Authority						
10 Hz+ SEL	52.9	0.9	3.9	6.8	0.4	0
LF-C	46.1	0.8	3.6	11.7	0.5	0
HF-C	25.7	1.7	6.8	2.6	0.3	0
VHF-C	21.3	2.1	9.1	2.5	0.4	0
PHO	37.9	0.9	3.9	7.9	0.5	0
OTA	37.7	0.8	4	8.9	0.5	0
(G) Blake Escarpment						
10 Hz+ SEL	16.5	1.2	5.9	4.8	0.5	0.5
LF-C	18.1	0.3	4.1	8.2	0.6	0.6
HF-C	7.5	2.1	14.7	2.2	0.5	0
VHF-C	4.5	3.5	28.1	2.3	0.8	0
PHO	26.4	-0.4	3.8	3.7	0.3	0
OTA	30	-0.6	3.8	3.2	0.2	0
(H) 850 m from Pile Driving at Block Island						
10 Hz+ SEL	77.9	2.4	11.6	3.2	0.2	0.6
LF-C	68.6	3.3	16.9	4.1	0.3	0.6
HF-C	28.7	3.6	18.3	2	0.4	0.5
VHF-C	24.7	3.5	17.7	1.8	0.4	0.4
PHO	50.1	3.4	18.5	3.5	0.3	0.6
OTA	49.8	3.4	18.2	3.7	0.3	0.6
(I) 9100 m from Pile Driving at Block Island						
10 Hz+ SEL	32.3	1.9	8.3	5.2	0.4	0
LF-C	26.9	2.2	10	5.5	0.5	0
HF-C	13.5	0.7	10.2	18.4	1.1	0
VHF-C	13.3	0.7	10.7	16.5	1	0
PHO	18.4	1.4	8.3	13.3	0.9	0
OTA	17.9	1.2	7.7	14.6	0.9	0
(J) Baffin Bay						
10 Hz+ SEL	60.5	−1	4.2	5.4	0.2	0.6
LF-C	39.7	−0.8	3.2	5.1	0.3	0.7
HF-C	8.3	3.6	16.4	2.6	0.8	0.4
VHF-C	8.6	3.7	16.9	2.6	0.8	0.6

Weighting function	Variance	Skewness (Gaussian = 0)	Kurtosis (Gaussian = 3)	Best fit Gamma-shape (k)	Best fit Gamma scale (θ)	Autocorrelation at 20-minute lag
PHO	14.3	0.6	3.7	3.3	0.4	0.2
OTA	13.1	1.2	5	2.8	0.5	0.1
(K) Paradise Reef						
10 Hz+ SEL	26.2	1.2	4	2.7	0.3	0.2
LF-C	26.2	1.3	4.2	2.8	0.4	0.2
HF-C	10.4	3.2	15.3	2.7	0.7	0.8
VHF-C	9.8	3.6	18.2	2.9	0.8	0.9
PHO	16.6	1.6	5.5	3.4	0.5	0.2
OTA	17.7	1.5	5.3	3.3	0.5	0.1
(L) Central Great Barrier Reef						
10 Hz+ SEL	4.2	-0.1	1.8	4.2	0.9	0.8
LF-C	6.9	-0.5	2.5	5.2	0.7	0.9
HF-C	4.6	-0.2	1.8	5.4	1	1
VHF-C	5.2	-0.2	2	5.7	0.9	1
PHO	5.5	-0.2	2	5.2	0.8	1
OTA	5.9	-0.3	2.2	5.2	0.8	1

5.6.7. Confidence Intervals of Estimated Daily SELs

Table 5-5. Confidence intervals and mean errors for daily SEL based on the 24-hour autocorrelation coefficient at the first lag time derived from the real data and simulated Gamma-distributed random data.

Auditory filter function and bound	Autocorrelation range at first time lag																			
	1–0.95	0.95–0.9	0.9–0.85	0.85–0.8	0.8–0.75	0.75–0.7	0.7–0.65	0.65–0.6	0.6–0.55	0.55–0.5	0.5–0.45	0.45–0.4	0.4–0.35	0.35–0.3	0.3–0.25	0.25–0.2	0.2–0.15	0.15–0.1	0.1–0.05	0.05–0
SEL lower	−0.18	−0.27	−0.41	−0.74	−0.97	−1.26	−1.31	−2.54	−3.7	−4.65	−5.59	−6.03	−7.31	−6.45	−6.05	−5.58	−5.89	−5.65	−4.9	−4.78
SEL upper	0.09	0.12	0.2	0.27	0.36	0.42	0.54	0.64	1	0.84	0.85	1.74	1.31	0.93	1.08	1.45	1.94	1.79	2.25	5.28
SEL mean	−0.06	−0.08	−0.1	−0.15	−0.16	−0.24	−0.29	−0.44	−0.5	−0.7	−0.76	−0.99	−1.31	−1.31	−1.48	−1.5	−1.7	−1.54	−1.23	0.47
LF-C lower	−0.14	−0.26	−0.41	−0.83	−1.06	−1.26	−1.84	−1.91	−4.91	−3.87	−5.4	−6.37	−5	−5.35	−4.78	−3.95	−4.1	−3.5	−3.16	−3.22
LF-C upper	0.08	0.12	0.19	0.2	0.32	0.49	0.55	0.62	0.69	0.9	0.87	1.56	1.31	1.6	1.06	1.24	1.77	1.68	2.05	3.84
LF-C mean	−0.03	−0.06	−0.08	−0.13	−0.18	−0.22	−0.31	−0.33	−0.62	−0.63	−0.76	−0.9	−0.95	−1.17	−1.13	−1.19	−1.11	−0.85	−0.44	0.87
HF-C lower	−0.16	−0.51	−0.99	−1.16	−1.28	−2.5	−3.85	−3.32	−4.21	−4.55	−5.52	−5.59	−5.71	−5.76	−5.74	−5.22	−5.28	−5.38	−4.52	−4.52
HF-C upper	0.08	0.14	0.18	0.23	0.25	0.34	0.64	0.56	0.67	0.8	1.08	0.68	1.04	1.42	1.26	1.75	1.76	1.75	2.08	5.4
HF-C mean	−0.05	−0.1	−0.14	−0.19	−0.24	−0.31	−0.49	−0.44	−0.7	−0.74	−1.1	−1.16	−1.36	−1.48	−1.5	−1.47	−1.52	−1.34	−0.89	0.82
VHF-C lower	−0.17	−0.57	−0.92	−1.02	−1.92	−3.91	−4.05	−5.37	−5.67	−6.13	−5.34	−5.01	−6.6	−7.38	−6.42	−6.59	−6.85	−5.94	−5.82	−5.11
VHF-C upper	0.08	0.14	0.23	0.27	0.25	0.31	0.58	0.5	0.72	0.58	1.1	0.99	0.76	1.39	1.45	1.59	1.61	1.67	2.27	6.03
VHF-C mean	−0.05	−0.12	−0.16	−0.17	−0.27	−0.39	−0.45	−0.73	−0.82	−1.06	−1.14	−1.2	−1.51	−1.86	−1.65	−1.75	−1.78	−1.63	−1.16	0.7
OTA lower	−0.14	−0.33	−0.67	−0.89	−1.18	−1.46	−1.56	−2.32	−3.16	−3.69	−4.11	−4.36	−4.1	−4.27	−3.47	−3.59	−3.34	−3.09	−2.69	−4.87
OTA upper	0.08	0.13	0.18	0.26	0.31	0.43	0.59	0.62	0.53	0.53	0.84	0.93	1.25	1.31	1.55	1.66	1.62	1.83	2	4.08
OTA mean	−0.04	−0.09	−0.11	−0.16	−0.18	−0.28	−0.29	−0.49	−0.63	−0.67	−0.92	−0.91	−0.96	−1.12	−1.01	−1.08	−0.92	−0.62	−0.21	1.11
PHO lower	−0.14	−0.31	−0.59	−0.81	−1.29	−1.3	−1.5	−2.08	−2.48	−4.69	−4.04	−4.52	−4.18	−4.19	−3.47	−3.54	−3.44	−3.14	−2.72	−4.14
PHO upper	0.07	0.13	0.16	0.23	0.37	0.49	0.53	0.79	0.48	0.62	0.83	1.5	0.87	1.09	1.33	1.86	1.71	1.77	1.97	3.98
PHO mean	−0.04	−0.08	−0.1	−0.13	−0.2	−0.22	−0.31	−0.46	−0.54	−0.71	−0.84	−0.91	−1.06	−1.09	−1	−1.03	−0.96	−0.65	−0.24	1.08
Simulated SEL lower	−0.18	−0.27	−0.41	−0.74	−0.97	−1.26	−1.31	−2.54	−3.7	−4.65	−5.59	−6.03	−7.31	−6.45	−6.05	−5.58	−5.89	−5.65	−4.9	−4.78
Simulated SEL upper	0.09	0.12	0.2	0.27	0.36	0.42	0.54	0.64	1	0.84	0.85	1.74	1.31	0.93	1.08	1.45	1.94	1.79	2.25	5.28
Simulated SEL mean	−0.06	−0.08	−0.1	−0.15	−0.16	−0.24	−0.29	−0.44	−0.5	−0.7	−0.76	−0.99	−1.31	−1.31	−1.4	−1.5	−1.7	−1.54	−1.23	0.47

The effects of duty-cycling were evaluated using the measured continuous datasets (Figure 5-12) and the simulated 1-minute SELs generated from Gamma-distributed data in the same manner as the real data sets. The resulting distribution of errors versus autocorrelation coefficient is shown in Table 5-5.

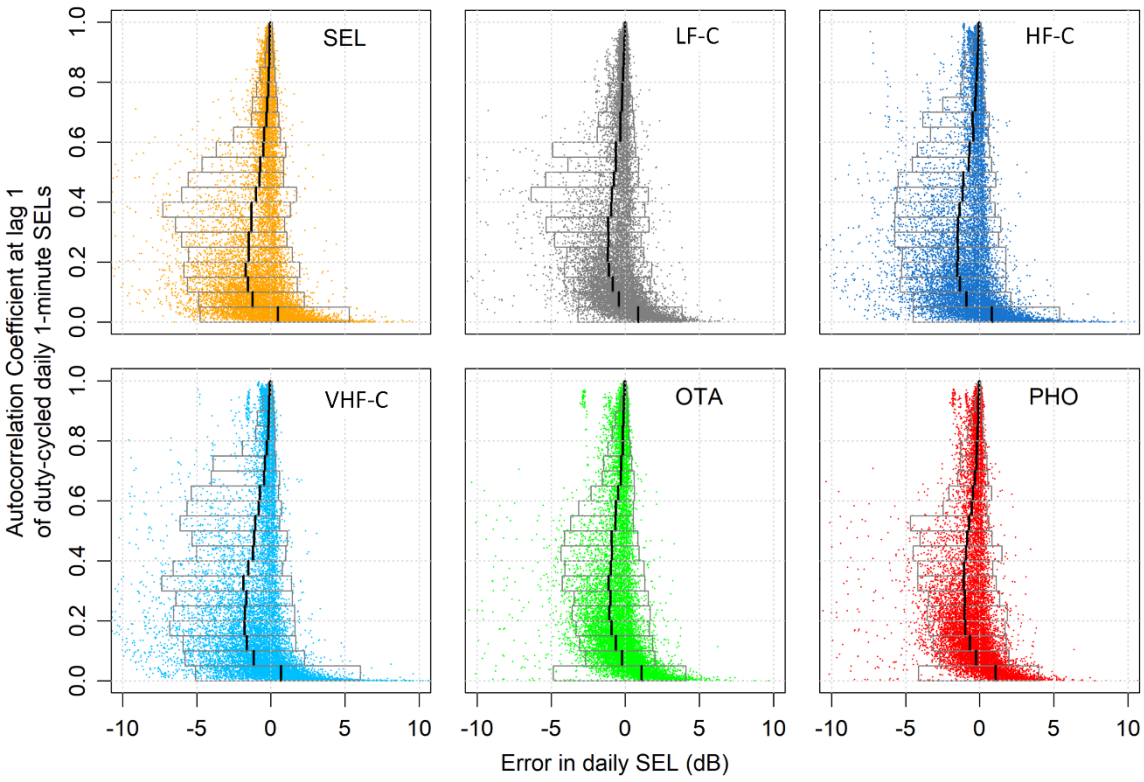

Figure 5-12. Distribution of errors in daily SEL versus the daily autocorrelation coefficient calculated with data from the Chukchi 2015 (C), Vancouver-Fraser Port Authority (F), Block Island (H & I), and Baffin Bay (J). The boxes drawn over the data show the 95% positive and negative confidence intervals for each 5% change in correlation coefficient. The black bars are the expected bias in the estimates. The abbreviations for the weighting functions are The auditory frequency weighting functions shown are: SEL – 10+ Hz (10 Hz and above); LF-C – low-frequency cetacean; HF-C – high-frequency cetaceans; VHF-C – very high-frequency cetaceans; PHO – Phocid seals; and OTA – otariid seals.

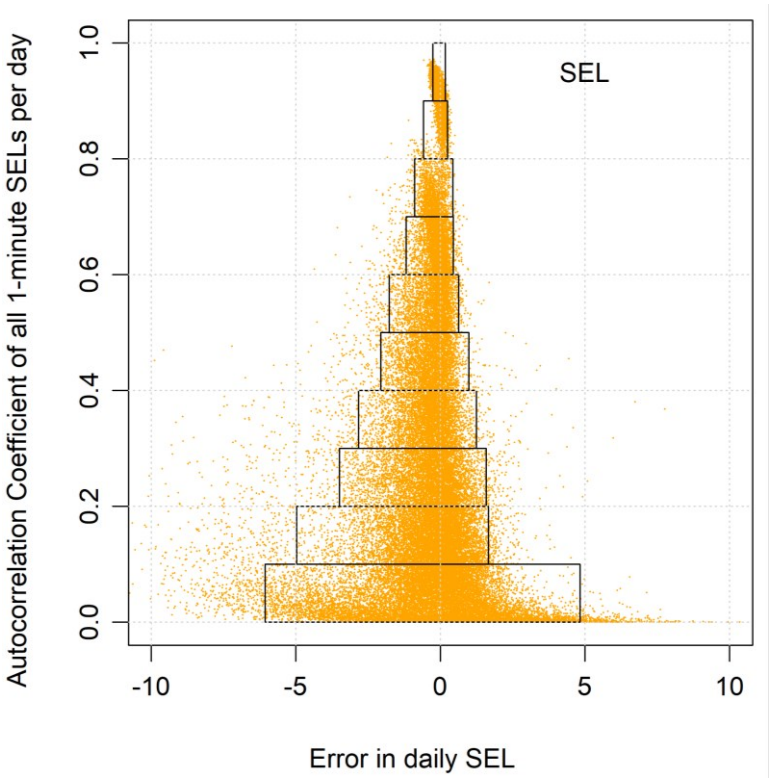

Figure 5-13. Distribution of errors in daily SELs versus the daily autocorrelation coefficient calculated from the seven Gamma-distributed random data sets described in Table 5-3

CHAPTER 6 USING KURTOSIS AND EFFECTIVE QUIET TO CLASSIFY HUMAN SOUNDS AS IMPULSIVE OR NON-IMPULSIVE

This chapter contains a draft manuscript that was submitted to the Journal of the Acoustical Society of America in March 2019. The data in this chapter is drawn from a wide range of projects that I've been involved with at JASCO, with numerous staff who have assisted with the original data collection and analysis. All data analysis in this Chapter was performed with MATLAB software by Bruce Martin as well figures generated in '***R***'.

The co-author, Klaus Lucke, assisted with reviews of the material on hearing and the effects of sound on marine life. He also contributed the data from (Lucke et al. 2009) that was re-analyzed to determine the auditory frequency weighted sound exposure levels.

This material was presented and discussed extensively at the Effects of Noise on Aquatic Life conference in Den Haag, 7-12 July 2019. During those discussions it became clear that there was not sufficient biological data to recommend thresholds for kurtosis to distinguish sounds as impulsive or non-impulsive in the marine environment and much more research is required. Thus, Section 6.4.C and Table 6-7 in particular will not be part of the published versions of this work.

Title: *Using Kurtosis and Effective Quiet to Classify Human Sounds as Impulsive or Non-impulsive.*

S. Bruce Martin*[6], Klaus Lucke[2]

[1]Dalhousie University, Department of Oceanography, 1355 Oxford Street, PO Box 15000, Halifax, Nova Scotia, Canada B3H 4R2

Email: sbmartin@dal.ca

[2]JASCO Applied Sciences, Australia, 1/14 Hook Street, Capalaba, Queensland 4157, Australia

Running Title: Classifying the Impulsiveness of Underwater Sounds.

Date Submitted: ~15 March 2019

* Also at JASCO Applied Sciences Canada, Suite 202, 32 Troop Avenue, Dartmouth NS, B3B 1Z1.

ABSTRACT

Regulations designed to mitigate the effects of man-made sounds on marine life set thresholds on the maximum daily sound exposure levels. Lower thresholds are proscribed for impulsive sounds compared to non-impulsive sounds, but no quantitative metric for identifying impulsive sounds are provided in the regulations. Four metrics of impulsiveness are considered: skewness, kurtosis, the crest factor and the difference between the impulse- and slow- time-weighted sound pressure levels. Biologically relevant values for the metrics were computed by first applying an auditory frequency weighting filter. Applying these metrics to statistical noise distributions and real-world ocean sounds shows that kurtosis is the most effective metric for identifying impulses. Only sounds above the sound pressure level threshold called effective quiet are considered loud enough to accumulate over time and cause hearing injury. A functional definition for effective quiet is proposed: the level for temporary threshold shift from non-impulsive noise, less 50 dB. Using kurtosis and effective quiet, new classifications of human sources as impulsive or non-impulsive are proposed that depend on functional hearing groups. Under the proposed changes vibratory pile driving and echosounders are impulsive sources. Naval sonar and vessels may be impulsive or non-impulsive depending on the functional hearing group.

AIP Codes: 43.30.Nb

Keywords: Kurtosis; Marine Soundscape; Anthropogenic Noise; Effective Quiet, marine echo sounder

6.1. INTRODUCTION

It has been known for centuries that humans suffer noise induced hearing loss when exposed to loud sound (Akay 1978). The hearing loss may be a temporary threshold shift (TTS) in hearing sensitivity or a permanent threshold shift (PTS). Eldred et al. (1955) proposed the equal energy hypothesis (EEH) which states that equivalent hearing injury will occur for loud sources over a short duration as for lower level sources over a long duration if the sound exposure levels are the same; i.e. noise induced hearing loss depends on intensity and duration. The intensity of sound perceived by a listener depends on their hearing capabilities. Weighting functions are used to emphasize frequencies where the listener's hearing sensitivity to noise is high and de-emphasize frequencies where sensitivity is low. For the marine mammal species functional hearing groups have been defined based on similarities in their hearing capabilities and sound production. Cetaceans are divided into low- (LF), high- (HF) and very high- (VHF) frequency cetaceans (Southall et al. 2019b).

The EEH is the foundation of regulations to protect human hearing (NIOSH 1998) and is an integral part of regulations to limit the impact of human activities on marine mammals (Southall et al. 2007, NMFS 2018, Southall et al. 2019b). Since Eldred et al. (1955) numerous measurements have shown that mammals, including marine mammals, are affected differently by non-impulsive and impulsive sources of sound and therefore the equal energy hypothesis by itself does not adequately predict the effects of sound on hearing (Ward 1962, Finneran 2015b, Kastelein et al. 2015). The temporal pattern of the arrival of impulsive sounds, as well as their frequency content, duration and amplitude affect the onset and magnitude of temporary threshold shifts (Buck et al. 1984, Danielson

et al. 1991b, Finneran et al. 2002, Kastelein et al. 2014a). For non-impulsive sounds, exposure to longer durations of lower sound pressure levels can result in larger TTS effects than exposure to the same SEL from shorter but higher amplitude sounds (Mooney et al. 2009, Kastelein et al. 2012a). Regulations designed to mitigate the effects of sound on marine mammals have distilled the complexity of temporal and amplitude effects into separate equal energy threshold levels for non-impulsive and impulsive sounds, where the impulsive TTS thresholds are 8-13 dB below the non-impulsive thresholds (Southall et al. 2019b). Initial guidelines for other marine taxa are discussed in Popper et al. (2014b).

Qualitatively, impulses are characterized as being broadband, short (< 1 second), having high peak pressures and short rise times (NIOSH 1998, NMFS 2018). While quantitative definitions for the difference between impulsive and non-impulsive sounds are missing from the regulations, several impulsive metrics have been suggested for aerial and underwater sounds. Southall et al. (2007) proposed that regulations should use the definition of Harris (1998) that an impulse is present if there is more than a 3 dB difference between the impulse time weighted SPL and the slow-time weighted SPL (referred to here as the Harris impulse factor). Pekkarinen and Starck (1983) proposed that an A-weighted crest factor greater than 15 dB was a predictor of impulse hazards for human workers. Other statistical measures that could be considered are skewness and kurtosis. Kurtosis was proposed by Erdreich (1986) as an indicator of impulsiveness for assessing effects of noise on factory workers. Kurtosis has also been used to in studies of the effects of noise on terrestrial mammals (Hamernik et al. 2003, Qiu et al. 2013a) and as a characteristic to describe seismic impulses during an exposure study of harbor

porpoise (Kastelein et al. 2017). Hamernik, Qiu and collaborators have shown that PTS increases with kurtosis for the same SEL up to a kurtosis of 40 (Qiu et al. 2013b).

Due to effects like refraction, absorption and scattering, long-range underwater propagation attenuates high frequencies more than low frequencies. Multi-path reflections influence the temporal pattern of a sound by adding extra arrivals at longer ranges (Martin et al. 2017). It has been proposed that because these effects change the structure of an impulse over distance, at some range from the source the sound is no longer impulsive and ought to be considered non-impulsive. Since non-impulsive and impulsive sounds have different thresholds within the regulations to protect hearing of marine mammals, it is important to have an objective metric that measures the impulsiveness of sounds. There are no agreed metrics for quantitative delineation of impulses from non-impulsive sound, so sounds are currently grouped by source. Impact pile driving and seismic airgun surveys are considered impulsive sources, while vessels and vibratory pile driving are considered non-impulsive sources. Sonar pulses, both high frequency pulses from multibeam sonars and echosounders as well as lower frequency pulses from naval sonar, are grouped by the American regulator (NMFS 2018) with the non-impulsive sources due to their narrowband nature, but are considered impulsive by the European Union Task Group on Noise (Van der Graaf et al. 2012).

There is minimum level of sound required to start accumulating energy for estimating hearing injury since mammals do not suffer threshold shift in normal acoustic environments even when integrating over very long periods. This safe level is known as ‘effective quiet’ (Ward et al. 1976b) and it is poorly understood or quantified for any species, including humans. Below the level of effective quiet the impulsive or non-

impulsive nature of a sound is irrelevant for assessing auditory impairment, although it may be a consideration for studies of disturbance or masking of biologically important sounds. It is desirable to develop a 'general rule' for assessing effective quiet since simple measures that are straight-forward to use in practice improves compliance with regulatory policy. The proposed limit for effective quiet is an auditory frequency weighted one-minute SEL 32 dB below the Southall et al. (2019b) daily TTS threshold for non-impulsive sources ($10 \cdot \log_{10}$(1440 minutes / day) = 31.6 dB). The one-minute auditory frequency weighted SPL is 18 dB below the one-minute SEL (since $10 \cdot \log_{10}$(60 seconds / minute) = 17.7 dB). Thus the proposed level for effective quiet is equivalently a sound pressure level 50 dB below the auditory frequency-weighted Southall et al. (2019b) daily TTS threshold for non-impulsive sources. The proposed one-minute auditory frequency weighted SEL effective quiet thresholds are 147, 146, and 121 dB re 1 $\mu Pa^2 \cdot s$ for low-, high-, and very high- frequency cetaceans, respectively. The equivalent one-minute auditory frequency weighted SPL effective quiet thresholds are of 129, 128, and 103 dB re 1 μPa^2, s for low-, high-, and very high frequency cetaceans, respectively.

The proposed limits for effective quiet may be compared to the limited experimental results available to assess their validity. Mooney et al. (2009) found that effective quiet for bottlenose dolphins exposed to octave band noise centered at 5.6 kHz was 150-160 dB re 1 μPa^2. Using the level of 150 dB re 1 μPa^2, the high-frequency cetacean auditory frequency weighted SPL for the sound used is approximately 145 dB re 1 μPa^2, 17 dB above the proposed threshold. Similarly the sounds used in Kastelein et al. (2012b) that did not cause significant TTS in harbor porpoise had an auditory frequency weighted SPL of 108 dB re 1 μPa^2, which is 5 dB above the proposed limit. The lowest sound exposure

level at 16 kHz that caused TTS in harbour porpoise after one hour was 159 dB re 1 $\mu Pa^2 \cdot s$, which is equivalent to a one minute very-high frequency weighted SEL of 138 dB re 1 $\mu Pa^2 \cdot s$ (Kastelein et al (2019) in Press). Observations of sound levels that did not cause TTS in odontocetes from impulsive sounds are at least 15 dB above the proposed limits (Finneran et al. 2000, Lucke et al. 2009, Kastelein et al. 2017). There is evidence that long exposures (multiple hours) to low intensity sound leads to higher hearing impairment than an equivalent SEL from a higher sound level for shorter durations (e.g. Kastelein et al. 2012b). The proposed thresholds for effective quiet may need to be carefully considered if there is realistic expectation that an animal will be exposed to sounds above the threshold for many consecutive hours.

The question addressed here is: between the level of effective quiet and loud sounds that are expected to cause auditory impairment, which human sounds in the ocean are impulsive and which non-impulsive? There is also a related question: what metric and threshold should be used to identify the presence of impulses? The results are expected to inform the development of regulatory thresholds for marine mammals by providing the auditory frequency weighted sound exposure levels and impulsive metrics for real-world recordings of human marine activities as well as the sounds employed in benchmark studies of the effects of sound on marine mammals.

6.2. METHODS

6.2.1. Simulations of Random Data and Sound Exposure Data Sets

To demonstrate the range of values generated by different impulsive metrics, the metrics were applied to Gaussian random data as well as two Gamma and two Rayleigh

random noise distributions. The Gamma and Rayleigh distribution parameters were chosen to provide one case with and one case without high amplitude tails.

Numerous studies of TTS on marine mammals have been conducted in controlled settings (Finneran 2015c). These studies informed the development of the auditory frequency weighting functions and TTS thresholds in Finneran (2016) and (Southall et al. 2019b). To complement the real-world data, the impulsive metrics are computed for simulations of the fatiguing signals from Finneran *et al* (simulating explosives, 2000, using intermittent tones, 2010), Popov *et al* (using band-limited noise, 2013), and Kastelein *et al* (using band-limited noise in 2012b, and 2014b, and with simulated 6.5 kHz sonar sweeps, 2015). General descriptions of these sounds are included in the results tables (Table 6-5). All simulations were performed at a sample rate of 512000 Hz. Signals that were not band-limited noise were added to 100 dB re 1 μPa^2 Gaussian noise as the ambient background. Transient signals were tapered with a 5% Tukey window to remove start-up effects.

6.2.2. Real-World Data Sets

Six short-term data sets containing high amplitude human generated sounds were analyzed to provide an indication of their kurtosis and auditory frequency weighted sound exposure levels. Five long-term data sets were analyzed to provide results that one would expect from typical passive acoustic monitoring projects. All recordings were performed using an autonomous multi-channel acoustic recorder (AMAR, JASCO Applied Sciences). The selected data sets have no substantial contributions from flow induced noise or other acoustic artefacts.

The short-term data includes examples of a seismic survey, vibratory and impact pile driving, oil and gas drilling, vessel passages and naval sonar (Figure 6-1). An additional data set from recorded in 2000 m water depth in the Gully Marine Protected Area (MPA) was analyzed as a reference data set as it contains no detectable human sound sources or biologic calls. Vibratory pile driving data (data set A) were collected 10 m from the insertion of a 3 m diameter pile in the Hudson River using a Super Kong 600 vibratory hammer. The seismic survey data (data set B) were collected in Baffin Bay, West of Greenland (for more information see Frouin-Mouy et al. 2017, Martin et al. 2017). In the data considered here, a 3480 in^3 airgun array was towed from 36 km south of the recorder (starting at 03:00, 4 Sept 2012) to 2 km north in water 600 m deep. Note the presence of a 12 kHz multibeam sonar on the seismic vessel that is present throughout the 5 minutes of data shown. Several naval sonars (data set C) with centre frequencies from 1200 Hz to 5500 Hz were recorded by chance with a recorder in 1600 m deep water during the 'ObSERVE' baseline monitoring program off Ireland (Kowarski et al. 2018, or www.dccae.gov.ie/ObSERVE). Recordings at a distance of 1900 m from the Block Island Wind Farm (data set D) provide an example of the SEL and kurtosis from impact pile driving (for more on this data set see Martin et al in press). An example of fisheries echosounder sounds (data set E) are provided from the passage a 58 m fishing vessel by the Georgia Strait Observatory (https://bit.ly/2RNSnQ0). Finally, the sounds from shallow-water oil and gas drilling program (data set F) in the Chukchi Sea are an example of sound from dynamic positioning operations, in this case from a semi-submersible drillship. Table 6-1 contains further information on each data set.

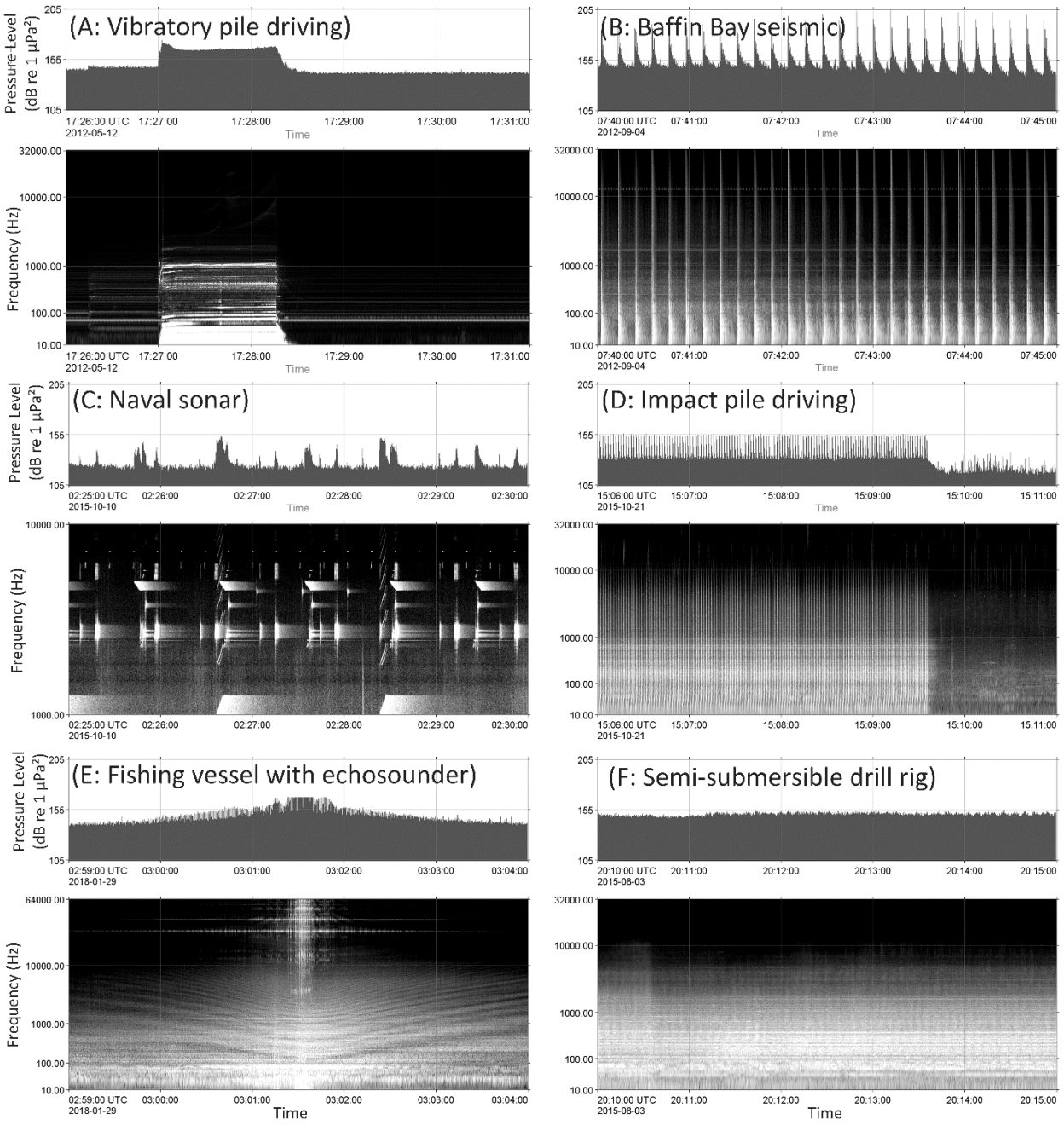

Figure 6-1. Snapshots of the data analyzed; recorded sound types are: (A) Vibratory pile driving, (B) Seismic airgun survey, (C) Naval sonar, (D) impact pile driving, (E) Vessel passage, (F) Dynamic positioning of a vessel. All snapshots show 5 minutes of data. For each example the top panel is the peak sound pressure level and the bottom panel is the spectrogram (FFT parameters: 0.2 seconds of data, 0.1 second overlap, 2 Hz resolution (0.3 seconds zero padding), Hann window; spectrograms are normalized to optimize the visual representation of the data). The vertical axes in the spectrograms are log-frequency. Dataset (C) is restricted to 1000 – 10000 Hz to better visualize the sonar pulses.

Table 6-1. Short-term acoustic recordings used in this study.

Location ID	Location name	Data represented	Latitude (degrees North)	Longitude (degrees East)	Recorder depth (m)	Sample rate
A	Hudson River	Vibratory Pile Driving	43.04	73.53	7	64 kHz
B	Baffin Bay	Seismic Survey	74.16	61.98	603	64 kHz
C	GMIT Observe Mooring 1	Naval Sonar Exercise	55.63	-9.73	1620	32 kHz[1]
D	Block Island Wind Farm	Impact pile driving at 1900 m	41.06	-71.45	42	64 kHz
E	Vancouver-Fraser Port Authority	Heavy Port Traffic and fisheries echosounder	49.05	-123.3	170	128 kHz
F	Chukchi Sea, 2015	Semi-submersible drill rig	71.19	-163.5	51	64 kHz

[1]The ObSERVE data are the only recording sampled at less than 64 kHz, which is the minimum sample rate recommended for measuring the high- and very high-frequency weighted SEL from human sources (Martin et al., in Press). Since the sonar's energy does not exceed 10 kHz, the 32 kHz sample rate is acceptable for this source.

The five long-term data sets were each 6-10 weeks long, sampled at 250 or 375 kHz on a duty cycle between 1 minute out of 15 to 1 minute out of 30. The first data set was collected in 120 m of water at the head of Lilly Canyon at the eastern edge of the Grand Banks. This location was at least 70 km from seismic surveys throughout the selected recording. The second data set was collected in water 870 m deep on the Blake Escarpment as part of the Atlantic Deep-water Eco-system Observatory Network project (www.adeon.unh.edu). The third data set was collected in water 1280 m deep in the Orphan Basin off Newfoundland, Canada, and included sound from seismic surveys that passed within several kilometers of the recorder. The fourth data were collected in water 2300 m deep off Nova Scotia, Canada. The selected data period included five days with Naval sonar exercises in the area. The final data were from the same Vancouver-Fraser Port Authority observatory as short-term data set E which were included to assess the

sound exposure level and kurtosis from a variety of vessels. All of the long-term data are presented as a single group; a total of 26,864 minutes of data were analyzed.

6.2.3. Metrics Computed

This analysis used the sound exposure level and four possible measures of impulsiveness: skewness, kurtosis, crest factor and the Harris impulse factor metrics which are defined below. The impulsive metrics were computed on the data's time series. Biologically relevant values of these metrics were obtained by using filtered time-series where the filters were FIR implementations of the auditory frequency weighting functions defined in Southall et al. (2019b). The metrics were also computed on a broadband time series that was FIR filtered to remove energy below 10 Hz. The filters were designed in MATLAB using the following code:

```
NfilterPoints = samplingFrequency;
freqs = linspace(0, samplingFrequency/2, 1000);
response = zeros(size(freqs));
for p = 1:length(response)
    response(p) = getWeighting(auditoryFilterName, freqs(p));
end
response = sqrt(response);  % because filtering is done on voltage data not power
freqs = freqs / (samplingFrequency/2);
d = fdesign.arbmag('N,F,A',NfilterPoints,freqs,response);
Hd = design(d,'freqsamp');
```

where *getWeighting* is a user provided function that generates the amplitude response of the auditory frequency weighting function. Tougaard and Beedholm (2019) provide examples and software for computing the weighting functions. The responses for the 10 Hz and above filter were [0, .01, .8, 1, 1, 1] at frequencies of [0, 7, 10, 14, 100, 0.5*fs] Hz. The filters were applied to the time series in MATLAB using the command:

```
filtered = fftfilt(Hd.numerator, rawTimeSeries).
```

Man-made sound sources are most likely to exceed the auditory frequency weighted SEL thresholds for the low- and very high-frequency cetaceans functional hearing groups rather than those for mid-frequency cetaceans (see Martin et al 2019 in Press). Therefore, the sound exposure levels and kurtosis for these groups are discussed in more detail in this analysis. The high-frequency cetacean hearing group is also discussed because of the extensive hearing threshold experiments that have been conducted with this group. Pinnipeds and sirenians are not discussed, however, the results are expected to be applicable to these groups as well. Similarly, all other marine taxa are not discussed since we do not have auditory frequency weighting functions or TTS thresholds for any other group. The methods and results obtained are expected to be directly applicable once the required functions and thresholds are determined.

Impulsive metrics were computed using a 1-minute time window which is a standard soundscape analysis duration (Ainslie et al. 2018) and has the advantage of providing metric values without concern for whether data are impulsive as it integrates over multiple transients (e.g. Figure 6-1). It also meets the criterion from Hamernik et al. (2003) that kurtosis be computed on at least a 30-second window.

Sound exposure level is defined as 10 dB times the logarithm (base 10) of the sound exposure, which is the integral of the squared sound pressure (*p(t)*) over some period of time, *T*, normalized by a reference squared pressure p_o^2 and reference time T_o (Equation 6-1, see also ISO (2017b))

$$L_{E,T} = 10\log_{10}\left(\frac{1}{T_o p_o^2}\int_0^T p^2(t)\,dt\right) \text{ dB re 1 } \mu\text{Pa}^2\cdot\text{s} \qquad (6\text{-}1)$$

Where T_o is normally 1 second and p_o is 1 µPa, so that the unit of $L_{E,T}$ are dB re 1 µPa²·s. For this analysis the auditory frequency weighted SEL were computed from the filtered time series.

Skewness is a measure of the asymmetry in the probability distribution of a real-value variable about its mean. It is above zero when a signal has high amplitude outliers, and it is below zero when there are many low amplitude outliers. Skewness, γ, is the third moment of the time series normalized by the variance to the 3/2 (Equation 6-2).

$$\gamma = \frac{1}{t_2 - t_1}\sum_{t_1}^{t_2}[p(t) - \bar{p}]^3 \Big/ \left(\frac{1}{t_2 - t_1}\sum_{t_1}^{t_2}[p(t) - \bar{p}]^2\right)^{3/2} \tag{6-2}$$

Kurtosis is another measure of the asymmetry of a probability distribution of a real-valued variable. Kurtosis, β, is the fourth moment of the time series divided by the square of the second moment (Equation 6-3).

$$\beta = \frac{\mu_4}{\mu_2^2};\ \mu_2 = \frac{1}{t_2 - t_1}\sum_{t_1}^{t_2}[p(t) - \bar{p}]^2\ ;\ \mu_4 = \frac{1}{t_2 - t_1}\sum_{t_1}^{t_2}[p(t) - \bar{p}]^4 \tag{6-3}$$

Unlike skewness kurtosis is an unsigned property which results in a different representation of the time and amplitude distribution of impulses in a time series than skewness. The kurtosis of Gaussian distributed random data is 3 while time series with strong sinusoidal signals have a kurtosis in the range of 0-3 and time series with transients have kurtosis above 3.

The crest factor is the peak sound pressure level minus the root mean square sound pressure level over some duration, here it is computed for each minute of data. An auditory frequency weighted crest factor greater than 15 was proposed by Pekkarinen and Starck (1983) as an indicator of impulsive sounds being present.

The Harris (1998) impulse factor is the maximum value for each minute of the impulse time-weighted sound pressure level minus the slow time-weighted sound pressure level. The time-weighted SPL are related to the sound level meter time-response settings (ANSI S1.4-1983 R2006). See Tougaard and Beedholm (2019) for examples of how to compute the time weighted SPLs. Southall et al. (2007), based on Harris (1998), recommended a 3 dB threshold for the impulse factor as an interim threshold for distinguishing impulses and non-impulsive sounds.

6.3. RESULTS

6.3.1. Synthetic Data

The random distributed noise data were expected to have low impulsive metric values indicative of non-impulsive sound sources. All five of the random noise distributions evaluated have similar skewness, kurtosis, crest factors and Harris impulse factors (Table 6-2). Applying the low-frequency auditory frequency weighting made minor differences to the metric results for the randomly distributed data because more than one-half of the 256 kHz bandwidth of the synthetic signals were filtered out. The Harris impulse factor was below the proposed threshold of 3 for all distributions and auditory frequency weighting functions. The weighted crest factor threshold of 15 proposed by Pekkarinen and Starck (1983) is the crest factor for a Gaussian distribution, and thus probably too low to use as an indicator of impulsive noise. The skewness was very close to zero for all distributions. The Gamma distributed random data with shape parameter 1 and scale 2 had the most samples with high amplitudes and had the highest kurtosis. However, a kurtosis of 4 is not sufficiently above the Gaussian distribution

value of metric 3 to indicate the strong presence of impulses. Thus, all four of the metrics indicate random distributed data is non-impulsive, as expected.

Table 6-2. 1-minute impulse metrics for random distributed data with typical noise amplitude distributions weighted by the low (LF) and very high (VHF) frequency cetacean Southall et al. (2019b) auditory frequency weighting functions. The metric values that are proposed as indicators of impulsiveness are shown in brackets.

Distribution	Parameters	Skewness			Kurtosis (40)			Crest factor (15)			Harris (1998) impulse factor (3)		
		Un-weighted	LF weighted	VHF weighted	Un-weighted	LF weighted	VHF weighted	Un-weighted	LF weighted	VHF weighted	Un-weighted	LF weighted	VHF weighted
Gaussian	Mean 0 Var 1	0	0	0	3	3	2.7	15	15	15	1.0	2.4	1.3
Gamma	Shape 1 Scale 2	0	0	0	4	3.2	4	19.2	15.7	20	1.3	2.5	1.5
Gamma	Shape 6 Scale 1	0	0	0	2.6	2.9	2.6	13.6	14	13.3	0.84	2.5	1.4
Rayleigh	B 2	0	0	0	2.7	2.9	2.7	13.8	14	13.8	0.9	2.3	1.2
Rayleigh	B 10	0	0	0	2.7	2.9	2.7	14	14	13.5	0.9	2.2	1.2

6.3.2. Real-world Data

The short-term real-world data's impulsive metrics covered a wide range of values and deviated substantially from the random data's values (Table 6-2, Table 6-3). Unlike the randomly distributed data, applying the Southall et al. (2019b) auditory frequency weighting functions changed the impulsive metric values for the real-world data. The kurtosis, crest factor and Harris impulse factor all increased for the very high-frequency weighted time series while the skewness decreased (Table 6-3). The Harris impulse factor is restricted to a maximum value of 23, which is related to the ratio of the areas under the impulsive and slow time-weighting functions. Similarly, the crest factor is constrained to

be between ~15 (the value for Gaussian random data), and an absolute maximum value equal to the broadband dynamic range of the analog-to-digital data collection system, which is between 90 and 110 dB for most acoustic recorders. Thus, crest factor and the Harris impulse factor have constrained response amplitudes that depend primarily on the signal amplitude. The results show that kurtosis, crest factor and Harris impulse factor are well correlated and respond similarly to changes in the data, while the skewness was less correlated with the other metrics (Figure 6-2). Therefore, the skewness was not considered further in this analysis. Of the three metrics whose values represent impulsiveness in the data, the kurtosis was selected for further consideration since its value depends on factors including signal rise time and pulse rate. This result is supported by the use of kurtosis for studying impulses with humans as well as terrestrial mammals (Hamernik et al. 2010, Qiu et al. 2013a).

Table 6-3. The range (minimum to maximum) of the 1-minute impulse metrics for the short-term real-world data sets weighted by the low (LF) and auditory frequency weighting functions. The number of minutes in the data sets is shown in brackets in the second column. The metric values that are proposed as indicators of impulsiveness are shown in brackets in the first row. Un-weighted data are 10 Hz and above high-pass filtered.

Data set ID	Data type (and duration of data analysed)	Skewness			Kurtosis (40)			Crest factor (15)			Harris (1998) impulse factor (3)		
		Un-weighted	LF weighted	VHF weighted	Un-weighted	LF weighted	VHF weighted	Un-weighted	LF weighted	VHF weighted	Un-weighted	LF weighted	VHF weighted
	Gully MPA Ambient noise (30 min)	-0.02 — 0.02	-0.07 — 0.01	-0.03 — -0.02	3.0— 3.7	3.0— 5.4	2.97 — 2.98	14.4 — 17.5	13.5 — 22.4	14.2 — 17.1	7.5— 13.7	3.3— 16.7	1.2— 1.4
A	Vibratory Pile Driving (90 min)	-0.22- 1.18	-1.68- 3.07	-4.72- 5.93	1.3- 407	2.2- 807	4.8- 5174	6.3- 33.2	12.8- 37.7	18.6- 47.4	4.2- 20.5	4.6- 22.0	4.9- 22.9
B	Seismic Survey (300 min)	- 13.7 — 10.1	-4.5— 4.1	-3.5 —6.5	8.7— 1362	3.4— 1620	3.2— 7819	18.9 — 39.2	16.3 — 41.8	17.3 — 47.7	14.3- 23.0	10.2 —23	5.2— 22.9
C	Naval Sonar (6 min)	-0.01 — 0.02	-0.01 — 0.02	- 0.15 — -0.01	20.6 — 38.2	21.2 — 48.0	29.7 — 53.1	24.7 — 38.2	27.8 — 37.7	25.8 — 27.7	15.8 — 19.1	17.0 — 22.0	17.3 — 18.1
D	Impact Pile Driving (50 min)	- 0.85 — 0.47	- 0.31 — 0.39	- 0.37 — 0.23	62.0 — 96.9	19.4 — 37.0	3.3— 134	24.4 — 34.2	3.3— 62	25.6 — 42.2	18.2 — 19.2	15.2 — 17.4	9.0— 20.9
E	Vessels and echosounder (60 min)	- 0.07 — 0.21	- 0.07 — 0.21	-1.0— 0.12	3.0— 17.4	3.0— 17.4	4.2— 358	13.9 — 28.3	13.9 — 28.3	25.9 — 37.8	5.0— 15.9	5.0— 15.9	8.1— 20.6
F	Dynamic Positioning (30 min)	0.00 — 0.04	0.00 — 0.04	- 0.01 — 0.01	2.9— 3.3	2.9— 3.4	3.1— 21.2	13.0 — 16.7	13.0 — 16.7	16.2 — 38.3	6.6— 8.4	6.1— 8.4	2.9— 14.5

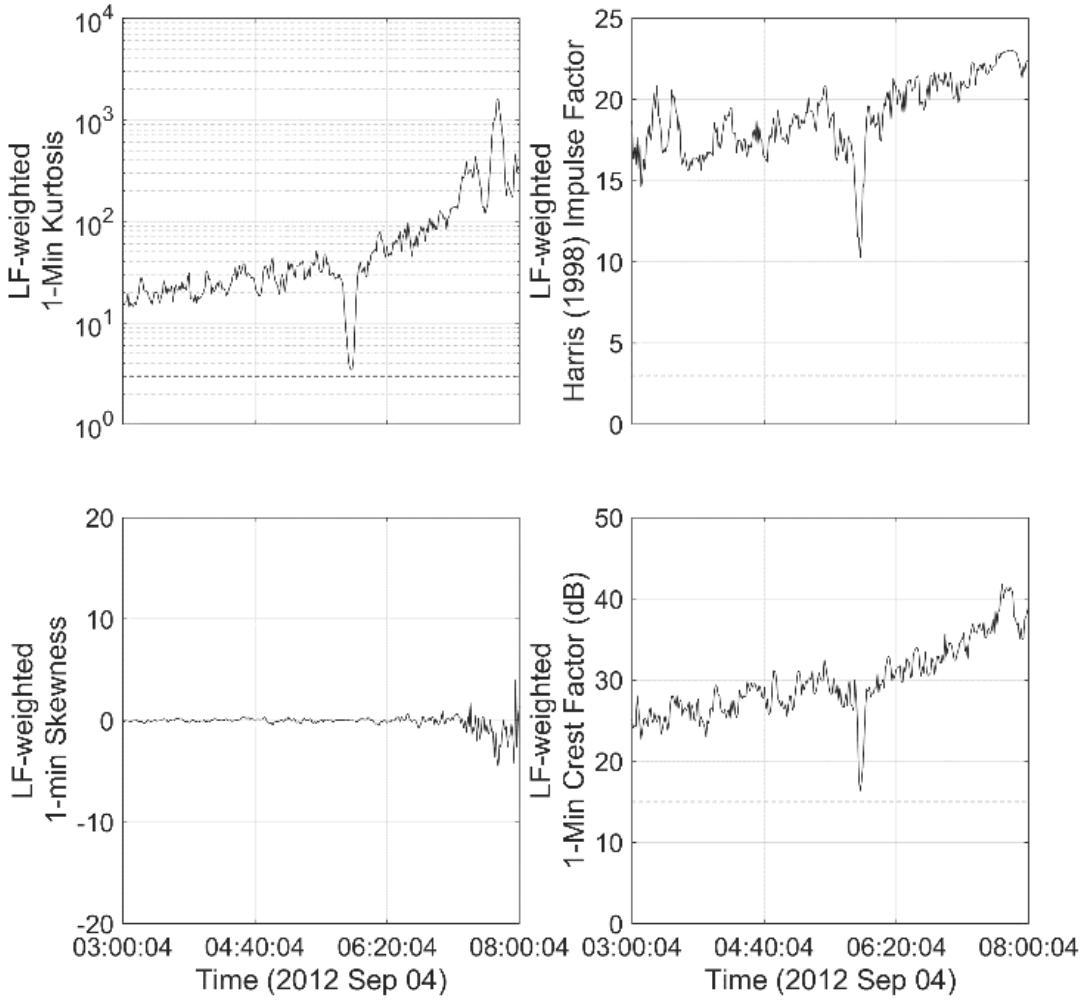

Figure 6-2. Low-frequency auditory frequency weighted 1-minute impulse metrics for the Baffin Bay seismic data (data set B). The decrease in kurtosis, crest factor and Harris impulse factor at ~06:00 is associated with another vessel passing directly over the recorder. This vessel's sound levels exceeded the seismic sound levels for a short period and made the low-frequency cetacean auditory frequency weighted metrics more non-impulsive-like.

Figure 6-3 shows the per-minute low- and very high-frequency cetacean auditory frequency weighted kurtosis and SEL for the short-term real-world data. The ambient noise data from the Gully Marine Protected Area with no sources present were processed as a baseline and had un-weighted as well as the low- and very high-frequency cetacean weighted kurtosis stay near 3, an indication that as expected, open ocean sound behaves

like random distributed noise when no detectable sources are present. The dynamic positioning noise data (F) also had a kurtosis of 3 for the 30 minutes shown (and generally throughout the full two months of data recorded). The seismic data (B) has a kurtosis that generally increased with SEL. The very high-frequency weighted kurtosis was 3 when the pulses did not contribute to the per-minute SEL. The low-frequency weighted kurtosis was in the range of 20-30 when the seismic source was 36 km from the recorder when the weighted per-minute SEL was ~140 dB re 1 $\mu Pa^2 \cdot s$. Just before 06:00 another vessel without a seismic array passed over the recorder. The energy from this vessel was higher than that from the seismic survey and the low-frequency weighted kurtosis dropped to nearly 3, but the very high-frequency weighted SEL rose quickly to almost 400. The very high-frequency weighted kurtosis from the vessel was caused by close-range cavitation noise as well as thumps and squeals from the ship's operation.

The kurtosis from impact pile driving was near or above the threshold of 40 at both 1900 m (data set D) as well as at 9100 m (not shown) during impact pile driving and dropped to lower values when pile driving ended. The very high-frequency weighted SEL and kurtosis both increased throughout the pile driving due to greater high frequency energy in the emitted sound as the pile penetration increased (Martin 2019, in press). The vibratory pile driving itself had a low kurtosis for all weighting functions, however, the complete soundscape from tugs, barges, cranes and compressors had a wide variety of kurtosis values, that were higher for the very high-frequency auditory frequency weighted kurtosis. The combination of different sources around vibratory pile driving appears to makes the total operation impulsive.

The kurtosis associated with the naval sonar (data set C) was ~40 for the low, high- and very high-frequency weighted time series. The kurtosis associated with the overpass of a fishing vessel with echo-sounders on (data set E) was near the non-impulsive noise indication value of 3 for the low-frequency weighted time series except at the closest point of approach (CPA). In contrast the very high-frequency weighted kurtosis at this location (Straits of Georgia) were elevated throughout the 60 minutes and reached almost 400 during the CPA period. The *per-minute* very high-frequency weighted SEL during the overpass exceeded 156.7 dB re 1 $\mu Pa^2 \cdot s$ – which is above the 24-hour Southall et al. (2019b) threshold of 155 dB re 1 $\mu Pa^2 \cdot s$ for permanent threshold shift from impulses for very high frequency cetaceans – even though the data was clipped and did not record the full amplitude of the fisheries echosounder.

.

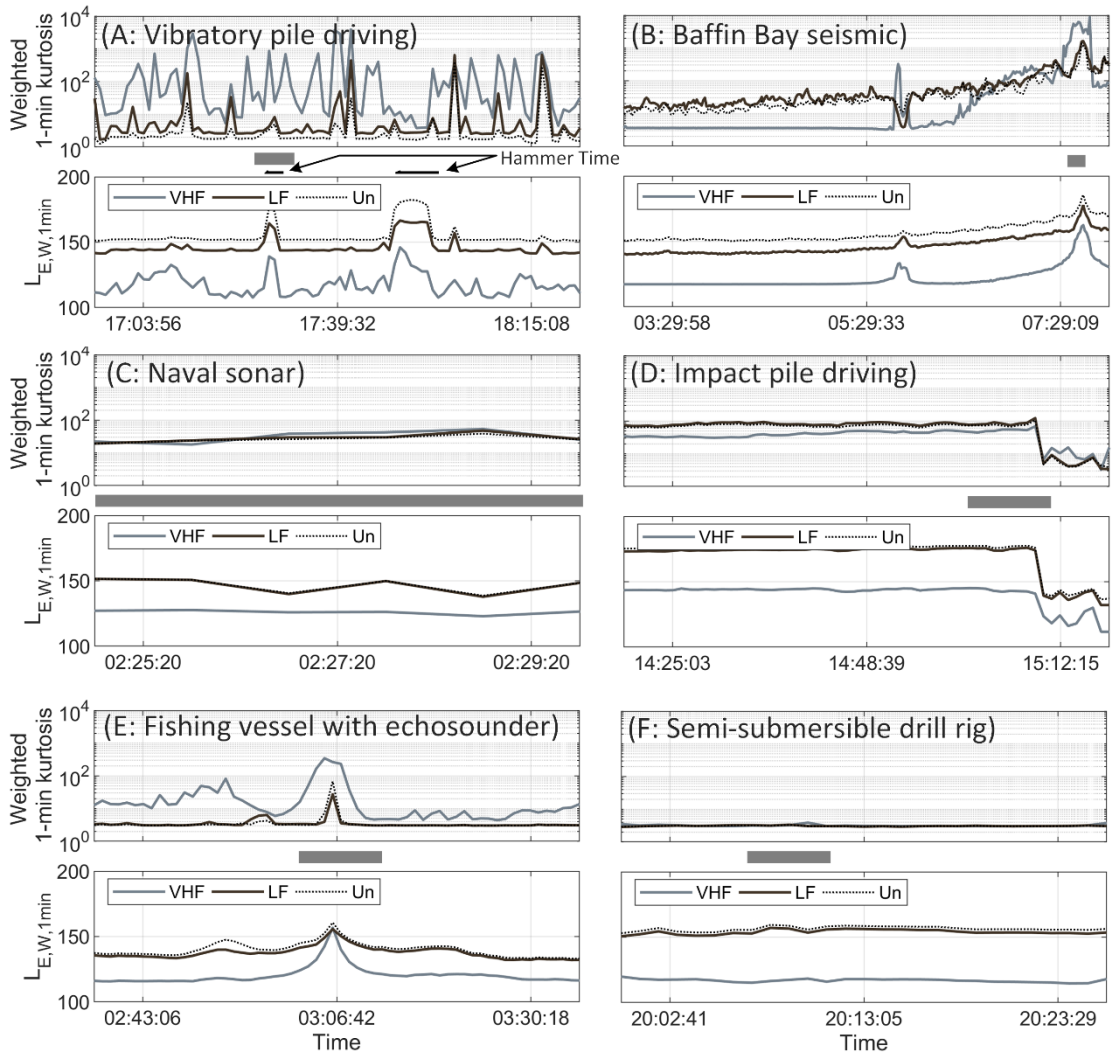

Figure 6-3. One-minute Southall et al. (2019b) auditory frequency weighted kurtosis (top panel) and SEL (bottom panel) for the six real-world data sets (Figure 6-1). Weighting function applied: Un – unweighted data (10 Hz and above), LF – low-frequency cetaceans, VHF – very high-frequency cetaceans. The gray boxes between the panels show the time windows displayed in Figure 6-1. The very high-frequency auditory frequency weighted per-minute SEL was self-noise limited at ~117 dB re 1 µPa²·s for the seismic data (B).

The long-term data had a total of 26,864 minutes of data analyzed. Of those, 88, 3, and 445 minutes exceeded the low-, high- and very high-frequency auditory frequency weighted sound exposure levels for effective quiet, respectively (Figure 6-4, Table 6-4). For each of the minutes above one of the auditory frequency weighted SEL effective

quiet thresholds, the data were manually reviewed to determine the sound source. Rain occasionally exceeded the very high-frequency cetacean auditory frequency weighted threshold at Lilly Canyon, Blake Escarpment and in the Port of Vancouver. The rain data always had a kurtosis near 3 (Figure 6-4). Seismic survey sounds that exceeded the low-frequency cetacean effective quiet threshold always had a kurtosis above 30 and above 20,000 for high-frequency cetaceans. When high-frequency cetacean auditory frequency weighted, the SEL and kurtosis of seismic pulses were similar to the levels when very high-frequency weighted, however, the difference in effective quiet thresholds resulted in none of them having high enough per-minute SEL to be considered for integration into the daily SEL

Sound from vessels exceeded the low-frequency cetacean effective quiet threshold 38 times, but only twice did had a kurtosis above 40; the median kurtosis was 3.6. When very high-frequency weighted, 209 minutes exceeded the effective quiet threshold and 97 of those minutes had a kurtosis higher than 40. Echosounders exceeded the very high-frequency effective quiet threshold on numerous dates at Lilly Canyon, with kurtosis value in the range of 20 – 3600. At the Port of Vancouver echosounders had kurtosis values between 3.1 – 2963 when low frequency-cetacean weighted and 28 – 143,700 when very high frequency-cetacean weighted. Naval sonars exceeded the effective quiet thresholds at Blake Escarpment and off Nova Scotia. Naval sonar was the only source that exceeded the high-frequency weighted effective quiet threshold. The sonar data generally had kurtosis between 30 and 60 for all auditory frequency weightings; two events had higher kurtosis. The most commonly detected sound source with SEL above the very high-frequency auditory frequency weighted effective quiet threshold were

marine mammal clicks and whistles. Minutes with whistles had a lower kurtosis than the data with clicks only.

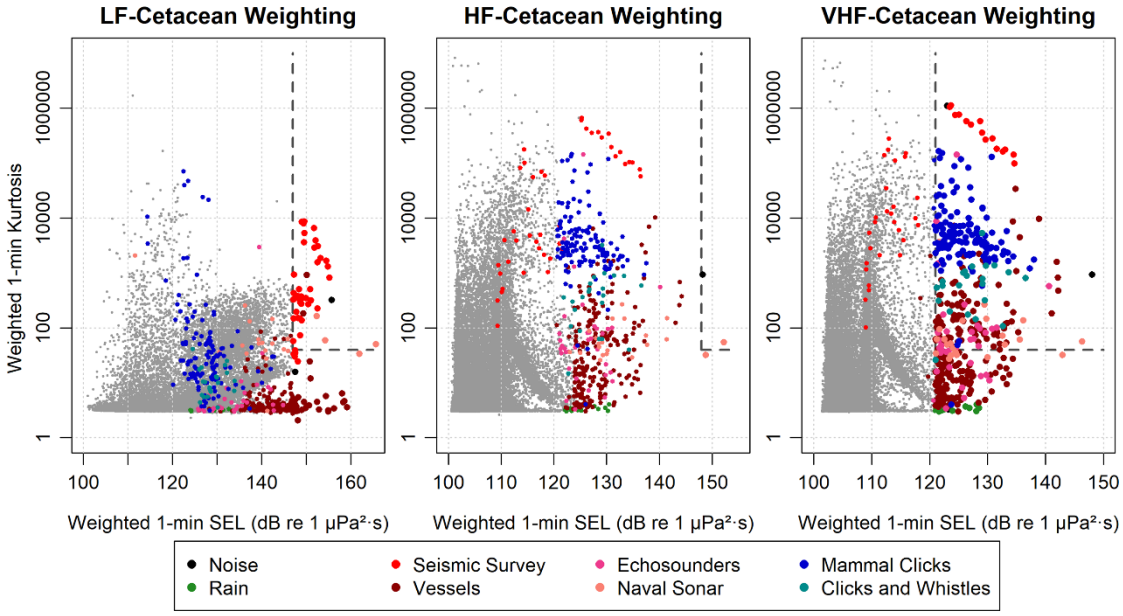

Figure 6-4. Scatter-plots of the low-, mid- and high-frequency cetacean auditory frequency weighted 1-minute sound exposure levels and kurtosis for the long-term passive acoustic monitoring data. The point color indicates the sound source identified by manual analysis for any minute that exceeded the effective quiet threshold for at least one of the three (LF-, HF-,VHF-) auditory frequency weighting functions (Southall et al. 2019b). The dashed lines mark the auditory frequency weighted limits of effective quiet (vertical) and kurtosis of 40 (horizontal). Any data points above and right of the lines are impulsive and loud enough to accumulate to cause TTS. There are three noise events included that were random high amplitude impulses.

Table 6-4. Effective Quiet auditory frequency weighted SEL threshold exceedance counts and auditory frequency weighted kurtosis greater than 40 counts for the long-term data. The right- hand columns identify the sources of the SEL exceedances and exceedances of both thresholds. A total of 26,864 minutes of data were analyzed.

Southall et al. (2019b). Cetacean Auditory Frequency Weighting Group	Number of minutes that exceed SEL threshold	Number of minutes that exceed kurtosis threshold of 40	Number of minutes that exceed both thresholds	Number of minutes that exceed SEL threshold / both thresholds						
				Rain	Seismic Surveys	Vessels	Echosounders	Naval Sonar	Mammal Clicks	Clicks and Whistles
Low	88	2759	44	0/0	43/38	38/2	0/0	4/3	0/0	0/0
High	3	5967	2	0/0	0/0	0/0	0/0	2/1	0/0	0/0
Very High	445	6583	298	13/0	15/15	209/ 97	34/22	22/15	126/ 125	22/21

6.3.3. Controlled Sound Exposure Data

Table 6-5 contains the kurtosis values for low-, high- and very high-frequency cetacean auditory frequency weightings of the controlled sound exposure data. The band-limited Gaussian noise data of Popov et al. (2013) and Kastelein et al. (2012b) had a kurtosis of 3 indicative of randomly distributed noise for all marine mammal auditory frequency weightings. The constant frequency data emulating the signals employed by Finneran et al. (2010) and Kastelein et al. (2014b) as well as the frequency-modulated sweeps used by (Kastelein et al. 2015) reduced the kurtosis to levels below the randomly distributed value of ~3 for all weightings when the signal was present for the entire minute, but caused the kurtosis to increase if the sound was intermittent during the minute. The change in kurtosis showed a frequency-weighting dependence – i.e. 6-7 kHz frequency modulated sweeps investigated by Kastelein et al. (2015) had a higher kurtosis when very high-frequency weighted than low-frequency weighted. Truly impulsive sounds, such as simulated explosive sounds (Finneran et al. 2000) generated extremely

high kurtosis values that increased by factors of 3-4 for the high- and very high-frequency weightings compared to the low-frequency weighting.

The kurtosis of different linearly swept frequency modulated sonar pulse trains similar to those in Kastelein et al. (2015) depended on the pulse duration and pulses per minute (Table 6-6). Kurtosis was higher when the impulses were shorter and spaced farther apart in time. The unweighted (10 Hz and above) kurtosis does not depend on the bandwidth of the sweep.

Table 6-5. Impulse metrics of fatiguing sounds from controlled threshold shift experiments weighted by the low (LF), high (HF) and very high (VHF) frequency cetacean Southall et al. (2019b) auditory frequency weighting functions. The test subjects exposed were TT: bottlenose dolphins (*Tursiops truncatus*); DL: Beluga Whales *(Delphinapterus leucas*); PP: Harbor Porpoise (*Phocoena phocoena*). Un-weighted data are 10 Hz and above high-pass filtered.

Study	Subject species	Fatiguing Sound	Measurement Condition	One-minute weighted kurtosis			
				Un- weighted	LF weighted	HF weighted	VHF weighted
Popov et al. (2013)	DL	Half-octave noise at 11.2, 22.5, 45 and 90 kHz at 165 dB re 1 µPa² for 1, 3, 10 or 30 minutes.	11.2 kHz	3	3	3	3
			22.5 kHz	3	3	3	3
			45 kHz	3	3	3	3
			90 kHz	3	3	3	3
Kastelein et al. (2012b)	PP	Octave band noise centered at 4 kHz at 124, 136 or 148 dB re 1 µPa² for 7.5, 15, 30, 60, 120 or 240 minutes		3	3	3	3
Kastelein et al. (2014b)	PP	6.5 kHz CW tone at 118, 124, 130, 136, 142, 148 or 154 dB re 1 µPa² for 60 minutes.		1.5	1.5	1.5	1.5

Study	Subject species	Fatiguing Sound	Measurement Condition	One-minute weighted kurtosis			
				Un- weighted	LF weighted	HF weighted	VHF weighted
Finneran et al. (2000)	TT & DL	Signal resembling explosions with sharp compression to rarefaction transition; maximum SEL 179 dB re 1 μPa²·s and peak-to-peak SPL of 221 dB re 1 μPa² (estimated mid-frequency weighted SEL of 172 dB re 1 $\mu Pa^2 \cdot s$)	500 kg HBX-1 at 1.7 km	423k	306k	900k	1.2 M
Finneran et al. (2010)	TT	3 kHz tones at 192 dB re 1 μPa², 16-s long or 64-s long.	16 s	7.6	7.6	7.6	8.8
			64 s	1.5	1.5	1.5	1.5
(Kastelein et al. 2015)	PP	1 second long 6-7 kHz FM upsweeps at 166 dB re 1 μPa² at either at duty cycle (DC) of 1 sweep every 10 seconds or non-impulsive repetition.	10% DC	15.4	15.4	15.9	16.3
			100% DC	1.5	1.5	1.6	1.6

Table 6-6. Comparison of the 1-minute kurtosis for different combinations of frequency modulated sweeps similar to those employed in Kastelein et al. (2015). The centre frequency for all sweeps was 6500 Hz. The values shown are not frequency weighted.

Bandwidth (Hz)	Pulses Per Minute	Pulse Duration (s)	Kurtosis
500	10	1	9.3
1000	10	1	9.3
1000	6	1	15.4
1000	5	1	18.5
1000	1	1	90
10000	1	1	90
100	1	1	90
100	1	.005	17982
100	15	.005	1200
100	60	.005	300
100	300	.005	60
2000	1	.1	900

Bandwidth (Hz)	Pulses Per Minute	Pulse Duration (s)	Kurtosis
10000	1	.002	4440
1000	60	0.5	3

6.4. DISCUSSION

Kurtosis is the most sensitive metric considered for measuring the impulsiveness of ocean sounds. It is recommended that the kurtosis be computed on the auditory frequency weighted time series since it is expected that the weighted kurtosis more accurately represents the sound perceived by each mammal group. Kurtosis of ocean ambient noise is near the random distribution value of 3 for the 10 Hz and above time series and each of the marine mammal auditory frequency weighted time series. This suggests that the large range of kurtosis values measured in the real-world human generated sounds represent a change to the soundscape from what is natural. The SEL increases as the range to human sources decreases which increases the probability of auditory impairment; similarly, the kurtosis increases as the range decreases. The kurtosis was also elevated at low SEL when sound levels are not expected to result in auditory impairment, such as during periods when the per-minute very high-frequency weighted SEL is below 120 dB re 1 $\mu Pa^2 \cdot s$ in the Port of Vancouver (E).

This section discusses kurtosis in the context of its predictive power for auditory impairment and presents new classifications for man-made marine sounds that depends on the functional hearing group but not on range. Sonar is discussed in detail..

A. KURTOSIS AS A PREDICTOR OF AUDITORY IMPAIRMENT IN MARINE MAMMALS

The relationship between kurtosis, SEL and hearing impairment has been the subject of extensive experiments by Hamernik, Qiu and their colleagues using chinchillas as an animal model for human hearing. They have demonstrated that: 1) PTS increased with kurtosis, up to about a kurtosis of 40; above this threshold increasing kurtosis did not increase auditory effect, but increasing the energy did, i.e. EEH applies normally again above a kurtosis of 40; 2) the value of kurtosis for the time series used in their experiments reaches a relatively stable value for exposure durations greater than 30 seconds; 3) the extent of auditory effects is related to the bandwidth of the transients that make the sound non-Gaussian, with wider bandwidths resulting in stronger effects; 4) kurtosis is a good predictor for auditory effects whether the source of non-Gaussian variability are impulses or not; 5) the EEH does not apply when there are different kurtosis values in exposures with equal energy, but it broadly does apply for exposures with constant kurtosis; and 6) the frequency-weighted kurtosis is a good predictor for hearing loss from signals with narrower bandwidths (Hamernik et al. 2003, Qiu et al. 2006, Hamernik et al. 2007, Hamernik et al. 2010, Qiu et al. 2013a).

Differences in how marine mammals protect themselves from loud sounds compared to terrestrial mammals could affect the kurtosis threshold associated with auditory impairment and injury. Terrestrial mammals protect their hearing from loud sound exposures through the acoustic reflex that tightens the middle ear ossicles in most species groups (Hung and Dallos 1972) and neural attenuation in bats (Suga and Shimozawa 1974). Similar to the bats, some odontocete species have been shown to have

a sophisticated automatic gain control that uses neural attenuation to rapidly change their hearing sensitivity so that they can detect their echolocation echoes in the presence of their outgoing pulses as well as clicks and echoes from other members of their group (Nachtigall and Supin 2008). They are able to learn to attenuate their hearing at a precise time if a warning sound is received up to 30 seconds prior to a loud sound (Nachtigall et al. 2018). For all mammals if there is no warning of loud sounds the inner ear receives the full energy of impulsive sounds which leads to increased damage compared to non-impulsive sounds at the same energy (Akay 1978, Finneran 2015b).

For terrestrial mammals impulses at a rate of ~1 per second are particularly damaging since the acoustic reflex generally relaxes after 1 second, and all impulses arriving at the inner ear have maximum effect (Ward 1962, Buck et al. 1984, Danielson et al. 1991a). Producing sounds once-per-second does not yield the maximum kurtosis (Table 6-6), which indicates that the temporal pattern of sound and its effects on hearing are not fully predicted by kurtosis for terrestrial mammals. The once-per-second sensitivity most likely does not apply to odontocetes that can predict loud sounds and attenuate their neural response. Hearing mechanisms of toothed whales (odontocetes) and pinnipeds are partially understood, but there is no direct data on hearing of baleen whales (mysticetes). Thus, it is unknown if once-per-second sensitivity is applicable to mysticetes or any of the other marine mammal taxa. If the once-per-second sensitivity does apply to marine life, we should to be particularly careful of the possible effects of impact pile driving (e.g. data set D) and echosounders (data set E) on marine life as these sources have repetition rates of approximately once per second.

Despite the potential limitations of applying the terrestrial results to marine taxa, the effectiveness of kurtosis as a predictor for hearing impairment in terrestrial mammals indicates that the kurtosis of underwater sounds should be considered for future investigations of the effects of noise on marine life. To be conservative it is reasonable to assume that loud human-generated sounds are more likely to have effects on marine life resembling those caused by impulsive signals as the kurtosis rises and that sounds will have fully impulsive effects when the weighted kurtosis reaches 40. Studies of the dependence of auditory effects on kurtosis in marine life is needed to refine this threshold.

B. Combining Kurtosis and Effective Quiet to Determine when Sounds are Impulsive

The sounds generated by each of the anthropogenic sources in the short-term data sets had per-minute weighted SEL above the proposed limits for effective quiet (Figure 6-3). For those minutes that exceed the one-minute effective quiet SEL limits it is relevant to determine the nature of the sounds – impulsive or non-impulsive? For both the low and very high frequency cetaceans, the auditory frequency weighted one-minute kurtosis of the seismic survey (data set B) was approximately 100 when the per-minute weighted SEL exceeded the proposed thresholds for effective quiet. The low- and very high-frequency per-minute SEL exceeded the threshold at ranges of 12.7 and 7.2 km from the vessel, respectively. The kurtosis and SEL continued to rise as the vessel approached the recording location. The naval sonar (data set C) had auditory frequency weighted kurtosis between 20 and 40 for both auditory frequency weightings, and at the recording location had auditory frequency weighted SEL just above the effective quiet threshold. At

1900 m from the impact pile driving (data set D) the low-frequency weighted kurtosis was near 100, while the very high-frequency weighted kurtosis increased from 20 to 50. The auditory frequency weighted SEL of the vessel with fisheries echosounders (data set E) exceeded the very high-frequency cetacean effective quiet threshold for six minutes on either side of the closest point of approach (CPA), which equated to 1.7 km. The auditory frequency weighted kurtosis was ~10 when the SEL exceeded effective quiet and exceeded 40 for three minutes on either side of CPA (~800 m) at which time the SEL was above 126 dB re 1 $\mu Pa^2 \cdot s$. The sounds 1 km from the dynamically positioned semi-submersible drill rig (data set F) were below effective quiet for very high-frequency cetaceans and above threshold for the low-frequency cetaceans. The auditory-frequency weighted kurtosis was ~3 for both groups.

A total of 481 minutes of the 26,864 analyzed in the long-term data exceeded at least one of the auditory frequency weighted thresholds for effective quiet (Table 6-4). Approximately 1/3 (153/445) of the very high-frequency cetacean exceedances of the effective quiet threshold were caused by sperm whale clicks or dolphin clicks and whistles (Table 6-4). None of these events caused exceedances for the high-frequency cetaceans that generated the clicks and whistles, mostly due to the 25-dB difference in effective quiet thresholds between the HF- and VHF-cetaceans. The high-frequency cetacean weighted kurtosis were similar to those for very high-frequency cetaceans. Since the animals are generating the signals that cause the kurtosis, these results suggest that the high- and very high-frequency cetaceans live in an acoustic environment where high kurtosis is normal. However, effective quiet exceedances only occurred for very high-frequency cetaceans (porpoise). It would be useful to test the hearing thresholds for any

of the dolphin species (*Cephalorhynchus spp.* and *Lagenorhynchus spp.*) that are part of the very high-cetacean group to see if their sensitivity is similar to those measured in porpoises or dolphins.

Human sound sources accounted for 312 of the SEL exceedances of effective quiet, of which 179 also exceeded the kurtosis threshold of 40. In the short-term data, impact pile-driving and seismic airgun survey sound had high kurtosis values for low- and very high-frequency cetacean auditory frequency weightings. Vessel sound had a kurtosis below the threshold of 40 when low-frequency cetacean auditory frequency weighted, but above 40 when very high-frequency weighted. In the long-term data, vessel sound exceeded the kurtosis threshold of 40 in two of the 38 occurrences of the sound exceeding the effective quiet threshold. However, when very high-frequency cetacean weighted, vessels exceeded both thresholds 97 times in 209 occurrences. This result is interesting for two reasons. First, it shows that vessel sound 'matters' to very high-frequency cetaceans more often than for low-frequency cetaceans. Second, it shows how kurtosis generally increases when low frequencies are removed from the time series. The vessel sounds that generated the high SEL and kurtosis when very high-frequency cetacean

auditory frequency weighted was a mix of cavitation sounds, mechanical knocking, and rubbing or rasping sounds (e.g. Figure 6-5).

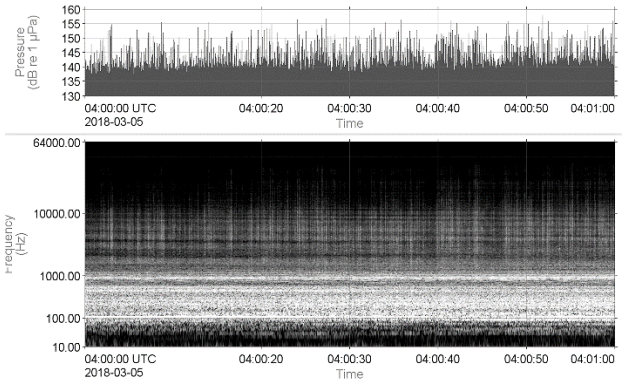

Figure 6-5. Example of a 1-minute recording of vessel sound recorded at the Port of Vancouver that had low-frequency auditory frequency weighted kurtosis of 5.6, and very high-frequency weighted kurtosis of 122.

Naval sonar as well as navigational and fisheries echosounders were considered in this analysis. The NMFS (2018) regulations identify sonars as non-impulsive sound sources which is not supported by the kurtosis metric for the sonars analyzed here. The short-term real-world naval sonar data had a kurtosis between 20 and 40 for both the low and very high frequency weighted time series which suggest impulsive properties. The short-term data has sounds from four different sonars operating together, which likely decreases the kurtosis due to the additional impulses per minute (Table 6-6). The naval sonar events detected in the long-term data had weighted kurtosis between 30-60 with a few events having higher kurtosis values. As an example of lower kurtosis for a single sonar, the single sonar intermittent sonar pulses simulated in Kastelein et al. (2015) that had a one-minute kurtosis of 15 (Table 6-5). Echosounders generated high kurtosis in the short-term data (data set E) but a range of kurtosis in the long-term data. Echosounders are characterized by short pulse lengths which yields a high kurtosis compared to the

longer pulse lengths of naval sonars (Figure 6-3, Table 6-6). However, these sonars have a higher pulse rate than naval sonars, which reduces the kurtosis (Table 6-6). At longer ranges propagation effects increase the received duration of the echosounder pulses which further decreases the kurtosis.

The relevance of the kurtosis for all sonars, and the marine environment in general, requires careful consideration and dedicated experiments. Sonars have a very stable pulse rate, which potentially allows odontocetes, including the more sensitive high-frequency cetaceans like porpoise, to predict the pulse arrival and adapt their hearing sensitivity (Nachtigall et al. 2018). The long-term real-world data showed that the high- and very high-frequency cetaceans live in an acoustic environment where high levels of kurtosis are normal. An experiment to assess TTS onset for echosounders and multibeam sonars in odontocetes, especially porpoise, is strongly recommended. Experiments similar to those of Hamernik, Qiu and collegues (2003, 2007, 2010, 2013a) that test the degree of TTS in marine mammals for sounds with different kurtosis at the same SEL, as well as the same kurtosis at different SEL, should be conducted. Broadening the experiments to include a wider range of marine taxa and careful consideration of how the hearing mechanisms of low-frequency cetaceans are affected by sonar is also recommended.

C. Recommended Classification of Source Type by Animal Group

The results of this study indicate that sounds can not be identified as impulsive or non-impulsive solely based on their characteristics at the source for two reasons. First, the biologically relevant kurtosis value changes with auditory frequency weighting. Second, odontocetes live in a high kurtosis soundscape, and some (if not all) species may have the

ability to reduce their hearing sensitivity when impulses arrive repeatedly at regular intervals; if this proves to be the case it would suggest that these species likely are affected differently by repetitive impulsive sounds than other marine taxa. It is proposed that sounds should be classified as impulsive or non-impulsive based on the source type as well as functional hearing group (Table 6-7). For the purposes of Table 6-7, all other marine taxa which tend to only be able to hear sounds below 1 kHz are assigned the same source classifications as low-frequency cetaceans which are the only mammal group that hears in this frequency range. While not all vessels have high levels of kurtosis when the low frequencies are filtered out, approximately half do, and therefore the vessels are proposed to be impulsive for odontocetes and pinnipeds. Naval sonar has low kurtosis values compared to odontocete clicks, pile driving and seismic. Therefore, it is proposed that naval sonar be classified as non-impulsive for the high- and very high-frequency cetaceans, but impulsive for the other marine taxa. Note that many fish, turtle and invertebrates likely can't hear the high frequencies of naval sonar and echosounders. Due to the random and impulsive nature of the operations around vibratory pile driving, it is recommended that vibratory pile driving be considered impulsive (see Figure 6-3(A) and Martin et al. (2012a)).

Table 6-7. Recommended assignment of human sounds sources as impulsive (I) or non-impulsive (NI) for different groups of marine life. Sonars are likely inaudible (IA) to most species besides marine mammals.

	Low-frequency Cetacean	Mid-frequency Cetaceans	High-Frequency Cetaceans	Otariid and Phocid Seals	All other marine taxa
Vessels	NI	I	I	I	NI
Dynamic Positioned Vessels	NI	NI	NI	NI	NI
Vibratory Pile Driving	I	I	I	I	I
Impact Pile Driving	I	I	I	I	I
Naval Sonar	I	NI	NI	I	I, IA
Echosounders and multi-beam sonar	I	I	I	I	I, IA
Seismic Airguns	I	I	I	I	I

There will inevitably be situations where it is unclear whether a sound source ought to considered impulsive or non-impulsive. The following procedure is proposed to resolve these situations:

1. Compute auditory frequency weighted time series using the filter method (see Section 6-2.C).
2. Compute the auditory frequency weighted per-minute sound exposure level and kurtosis.
3. Compute the daily SEL for the per-minute SEL greater than the threshold for effective quiet, defined as 32 dB below the Southall et al. (2019b) TTS threshold

for non-impulsive sound (or a one-minute SPL 50 dB below the Southall et al. (2019b) TTS threshold, see Section 6.1). Determine the SEL for the minutes with a kurtosis greater than 40 and less than 40 separately, nominally the impulsive and non-impulsive SELs. If the impulsive SEL is within 6 dB of the total, compare the SEL to the Southall et al. (2019b) thresholds for impulsive sound, otherwise compare to the thresholds for non-impulsive sound to assess the possibility of the sound exceeding the regulatory thresholds. Use the appropriate thresholds and weighting functions to assess the effects on other marine taxa.

The threshold of 6 dB was chosen to be conservative since the threshold for kurtosis is high at 40 rather than a more conservative level at which impulsive effects are likely beginning to appear. Further, this threshold respects the results that show impulsive sounds have greater effects on hearing when they occur in a background of high non-impulsive sound levels (Hamernik et al. 1974).

6.5. ACKNOWLEDGEMENTS

The authors thank the following organizations for including their data sets in this analysis:

- TTS data were collected as part of the research project MINOS+ funded by the German Federal Ministry for the Environment, Nature Conservation and Nuclear Safety, Grant No. Fkz 0329946B; data were used with permission of Prof. Ursula Siebert, Institute for Terrestrial and Aquatic Wildlife Research (ITAW), Germany.
- Shell Global Solutions for the Baffin Bay and Chukchi Sea 2015 data;

- Deepwater Wind / Block Island Wind Farm for the Block Island data;
- The Irish Department of Communications, Climate Action and Environment for the short-term naval sonar data collected by the ObSERVE Project.
- The Department of Fisheries and Oceans Canada, Oceans and Coastal Management Division, Maritimes Region for the Gully MPA was provided by
- The Environmental Studies Research Fund, which provided support for JASCO Applied Sciences to collect the deep-water data off Nova Scotia and the Department of Fisheries and Oceans Canada, North-west Atlantic Fisheries Centre to collect the Lilly Canyon data.

Thanks to all the JASCO Applied Sciences teams and vessel crews who participated in the data collection programs whose data was used in this manuscript. Thanks to Andrew Martin for assisting with the manual analysis of the long-term data.

CHAPTER 7 CONCLUSIONS AND RECOMMENDATIONS

7.1. SUMMARY

The research in this thesis provides new information on marine soundscapes and the characteristics of human source sources. Data from 14 different recording programs were analyzed. The data are notable for three aspects: the range of soundscapes considered, the durations of each data set, and the high sample rates: almost all of the data were collected at 64 kHz or higher which provides data on sound sources up to 30 kHz, much higher than many previous projects. The tools developed and described in this thesis are intended to be accessible to students, researchers and regulators and thus expand our knowledge of marine soundscape and the possible effects of human sound sources on marine life.

The key contribution of this thesis is the recommendation to use one-minute analysis windows for characterizing soundscapes and the injurious effects of human sounds on marine life. The combination of one-minute sound exposure level and kurtosis represents the amplitude and impulsiveness of a soundscape and can identify those soundscapes affected by human sound sources. Using one-minute windows, without detectors, is a simple and robust means of measuring the sound levels from human sources such as seismic, vessels and pile-driving which can then be regressed against range to predict hearing injury isopleth radii.

This thesis proposes a marine mammal threshold for effective quiet that is based on the auditory frequency weighted one-minute sound exposure level. By analyzing the change in kurtosis with SEL, it is demonstrated that sounds retain their impulsive

character when the SEL is above the threshold for effective quiet and therefore the transition of sounds from impulsive to non-impulsive as they propagate is inconsequential for purposes of assessing hearing injury.

With respect to specific human sound sources in the marine soundscape, this research has shown:

1. For seismic airgun survey sound:
    a. The one-minute SPL was increased by ~28 dB throughout the survey program for a 3-D survey where the average minimum daily range to the vessels was 42 km.
    b. Even though the sound energy is concentrated below 100 Hz, there is substantial sound at higher frequencies. Seismic sound elevated the 1-minute SEL by 20 dB in the 16 kHz octave band at a range of 6 km from the array.
    c. In the waters of Baffin Bay that are 600-800 m deep, multi-path arrivals are distinct impulses out to ranges of at least 40 km. This environment is similar to the Outer Continental Shelf of the United States that is currently open for bids to conduct seismic surveys.
2. For impact pile driving sound:
    a. The radiated sound levels depend on the strike energy and pile penetration depth into the sediment. Both of these are frequency dependent effects, especially the pile penetration. Current pile source models do not appear to

adequately consider these effects, nor do they function at high enough frequencies to predict the effects on pinnipeds and odontocetes, the two groups of marine mammals that inhabit coastal waters where pile driving for wind turbine installations occurs.

b. Inclined, or raked, piles are a directional sound source, with more sound propagating when the pile is inclined away from the receiver. The combination of inclination, strike energy, and pile penetration effects can lead to the biological effects isopleths varying by an order of magnitude between the start of piling and the completion, when considering the highest sound direction compared to the quietest.

c. The damped cylindrical spreading model for pile sound propagation proposed by Lippert et al. (2018) was supported by the data from Block Island Wind Farm, as was the linear relationship between SEL and peak SPL of Lippert et al. (2015).

d. The random effects coefficients of a linear mixed model contained information about the acoustic propagation environment, including identifying days with similar sound speed profiles and differences in the average attenuations of different, but closely spaced, radials.

3. Echosounders: fisheries and navigational echosounders were observed by chance in two of the data sets. In both cases the source changed the soundscape and generated sound levels high enough to cause permanent threshold shifts in very

high frequency cetaceans. Use of these sources, and presumably multibeam sonars, should be carefully considered before being employed in marine mammal habitats.

4. Vessels: Vessel data had higher levels of kurtosis, an indicator of impulsiveness, than expected. Future marine noise regulations should carefully consider the nature of most vessel signatures to determine vessels are better categorized as non-impulsive or impulsive. Dynamic positioning vessel noise did not contain impulses.

7.2. Data Collection and Analysis Recommendations

To collect data for soundscape characterization I recommend the following minimum configuration:

- Record for a minimum of 1 minute at a time. Longer recordings are desirable for many applications, especially detecting marine life that vocalizes infrequently.
- Record with a duty cycle of at least 1 minute out of every 30 minutes. Higher duty cycles are recommended whenever possible, especially in soundscapes that change rapidly. Continuous recording is recommended for measuring sound exposure levels and peak sound pressure levels for regulatory compliance, or for projects that must characterize human sound sources.
- Sampling rates should be 64 kHz or higher to adequately describe most human sound sources. This sample rate is also the minimum to measure the sound

exposure level of human sources when applying the high- and very high-frequency cetacean auditory frequency weighting functions.

- When designing a measurement program, it is important to understand the physical and acoustic propagation environments. If possible, model the acoustic propagation and chose a measurement location and depth that optimizes the probability of detecting the sounds of interest. All else being equal, place your recorder and hydrophone at the seabed – this location generally minimizes flow-induced noise and simplifies the mooring design.

The results of this thesis have shown that substantial information about a soundscape can be obtained using 1-minute analysis windows and two metrics – kurtosis and sound exposure. The recommended steps are:

1. Compute the 10 Hz and above time series and the auditory frequency weighted times series of interest using the filter method (see Section 2.3.5).
2. Compute the auditory frequency weighted per-minute sound exposure and kurtosis. The impulsive or non-impulsive nature of sounds is only relevant when the per-minute SEL exceeds the proposed threshold for effective quiet. The distribution of daily or monthly per-minute kurtosis values provides information on the short-term impulsiveness of the soundscape. A per-minute kurtosis threshold that indicates when impulsive effects on marine life begin to occur needs to be researched.
3. Compute the per-day and per-month auto-correlation of the 1-minute sound exposures:

a. The daily autocorrelation should be used to determine the uncertainty in the daily SEL.

b. The monthly autocorrelation correlation at 3-hour lag provides information on the general nature of the soundscape. If the unweighted daily SEL is below 160 dB re 1 $\mu Pa^2 \cdot s$, the 10 Hz and above SEL is within 3 dB of the low-frequency cetacean auditory frequency weighted SEL and the monthly autocorrelation coefficient is above 0.6 at three hours lag, the soundscape likely does not have a substantial anthropogenic contribution.

4. Compute the total daily weighted sound exposure levels. A plot of the marine mammal auditory frequency weighted daily SEL over a deployment provides an excellent high-level overview of the soundscape and how it is separated in broad frequency bands. The difference between the 10 Hz and above SEL and the low-frequency cetacean weighted SEL indicates how much sound energy is below 100 Hz. The difference between the pinniped, low frequency cetacean and very high-frequency cetacean weighted SEL indicates when the primary sound sources are below 4 kHz and above 10 kHz. A temporal pattern in daily SEL indicates cadences linked to anthropogenic, solar or lunar cycles.

7.3. Limitations and Future Research

This research focused on hearing injury to marine mammals from impulsive human sound sources because peer-reviewed regulations on maximum sound exposures exist. It was possible to develop the regulations because odontocete and pinniped marine mammals are amenable to training and testing in captivity, and thus measurements of

their hearing thresholds, critical bands, critical ratios and onset of temporary threshold shifts have been made and extrapolated to the species that were not measured. Few similar results are available for the bulk of marine taxa, all of which have different hearing systems than marine mammals, and few of which we are able to train and test with behavioural methods. Most marine life appears to respond to the motion caused by sound waves rather than the pressure. Measuring motion challenges our existing tools that use pressure as the primary quantity, which we then analyze in the frequency domain. Motion combines time and frequency in ways that are complex to understand.

To better understand the effects of human sound we need tools to record and quantify sound in ways that are relevant to all marine life. This includes masking and behavioural reactions that are likely more pervasive effects than hearing injury and their long-term consequences are poorly understood. Moving forward requires collaboration of experts in biology, physiology, physics, sensor systems, and signal processing. Biologists and physiologists will need to determine how fish and invertebrates sense sound, including thresholds and frequency ranges. Physicists and sensor systems experts will develop the sensors to measure sound in ways that mimic animal hearing. The data from these sensors will be analyzed with relevant metrics that are related to thresholds of response by marine life – as determined by the biologists and physiologists.

In the near-term, the work in this thesis should be extended to provide an accepted suite of metrics that characterize sounds in ways relevant to effects of sound on marine life. This thesis and the literature have established that in many applications SEL is the preferred metric for sound energy. This thesis proposes kurtosis as the preferred metric

for impulsiveness. For both of these metrics, this thesis has proposed using frequency-weighted metrics for studying the effects on marine mammals. The appropriateness of the weightings, and relevant weightings for all other marine life, remain to be determined. Other metrics are needed to express: 1) the periodicity of sounds, which is related to the ability of an animal to predict the arrival of a loud sound and self-mitigate; 2) the displacement caused by a sound, which is likely related to swimbladder injuries in fish; and 3) measures of acceleration and / or rise-time of sounds that are related to both injury and the startle reflex in all taxa.

REFERENCES

[FHWG] Fisheries Hydroacoustic Working Group. 2008. *Agreement in Principle for Interim Criteria for Injury to Fish from Pile Driving Activities*. June 12, 2008 edition. http://www.dot.ca.gov/hq/env/bio/files/fhwgcriteria_agree.pdf.

[IMO] International Maritime Organisation. 2014. *Noise from commercial shipping and its adverse impacts on marine life, MEPC 66/17*. http://ocr.org/ocr/pdfs/policy/2014_Shipping_Noise_Guidelines_IMO.pdf.

[ISO] International Organization for Standardization. 2017a. *ISO 18405.2:2017. Underwater acoustics—Terminology*. Geneva. https://www.iso.org/obp/ui/#iso:std:iso:18405:ed-1:v1:en.

[ISO] International Organization for Standardization. 2017b. *ISO/DIS 18405.2:2017. Underwater acoustics—Terminology*. Geneva. https://www.iso.org/standard/62406.html.

[NIOSH] National Institute for Occupational Safety and Health. 1998. *Criteria for a recommended standard: Occupational noise exposure*. Document Number 98-126. U.S. Department of Health and Human Services, NIOSH, Cincinnati, Ohio. 122 p.

[NMFS] National Marine Fisheries Service. 2016. *Technical Guidance for Assessing the Effects of Anthropogenic Sound on Marine Mammal Hearing: Underwater Acoustic Thresholds for Onset of Permanent and Temporary Threshold Shifts*. U.S. Department of Commerce, NOAA. NOAA Technical Memorandum NMFS-OPR-55. 178 p. http://www.nmfs.noaa.gov/pr/acoustics/Acoustic%20Guidance%20Files/opr-55_acoustic_guidance_tech_memo.pdf.

[NMFS] National Marine Fisheries Service (U.S.). 2018. *2018 Revision to: Technical Guidance for Assessing the Effects of Anthropogenic Sound on Marine Mammal Hearing (Version 2.0): Underwater Thresholds for Onset of Permanent and Temporary Threshold Shifts*. U.S. Department of Commerce, NOAA. NOAA Technical Memorandum NMFS-OPR-59. 167 p. https://www.fisheries.noaa.gov/webdam/download/75962998.

[NMFS] National Marine Fisheries Service (US) and [NOAA] National Oceanic and Atmospheric Administration. 1995. Small takes of marine mammals incidental to specified activities; offshore seismic activities in southern California: Notice of issuance of an incidental harassment authorization. *Federal Register* 60(200): 53753-53760.

[NOAA] National Oceanic and Atmospheric Administration. 2001. *Joint Interim Report: Bahamas Marine Mammals Stranding Event of 15-16 March 2000*, 59 pp. U.S. Department of Commerce, National Marine Fisheries Service (US), US Navy. www.nmfs.noaa.gov/pr/pdfs/health/stranding_bahamas2000.pdf.

[NOAA] National Oceanic and Atmospheric Administration. 2012. *Guidance document: Data collection methods to characterize impact and vibratory pile driving source levels relevant to marine mammals*. U.S. Department of Commerce, National Marine Fisheries Service, 7 pp. Memorandum from NMFS Northwest Region and Northwest Fisheries Science Center.

[NOAA] National Oceanic and Atmospheric Administration. 2013. *Draft guidance for assessing the effects of anthropogenic sound on marine mammals: Acoustic threshold levels for onset of permanent and temporary threshold shifts*, December 2013, 76 pp. Silver Spring,

Maryland: NMFS Office of Protected Resources. http://www.nmfs.noaa.gov/pr/acoustics/draft_acoustic_guidance_2013.pdf.

[NOAA] National Oceanic and Atmospheric Administration. 2015. *Draft guidance for assessing the effects of anthropogenic sound on marine mammal hearing: Underwater acoustic threshold levels for onset of permanent and temporary threshold shifts*, July 2015, 180 pp. Silver Spring, Maryland: NMFS Office of Protected Resources. http://www.nmfs.noaa.gov/pr/acoustics/draft%20acoustic%20guidance%20July%202015.pdf.

[NOAA] National Oceanic and Atmospheric Administration. 2016. *Underwater Noise and Marine Life* (webpage). http://cetsound.noaa.gov/index. (Accessed 5 April 2016).

[NOAA] National Oceanic and Atmospheric Administration and U.S. Department of Commerce. 2016. *Draft Guidance for Assessing The Effects of Anthropogenic Sound on Marine Mammal Hearing*. 24 p. http://www.nmfs.noaa.gov/pr/acoustics/draft_guidance_march_2016_.pdf.

[NOAA] National Oceanic and Atmospheric Administration (U.S.). 1998. Incidental taking of marine mammals; Acoustic harassment. *Federal Register* 63(143): 40103.

[NRC] National Research Council. 2003. *Ocean Noise and Marine Mammals*. National Research Council (U.S.), Ocean Studies Board, Committee on Potential Impacts of Ambient Noise in the Ocean on Marine Mammals. The National Academies Press, Washington, DC. http://www.nap.edu/openbook.php?record_id=10564.

[NRC] National Research Council. 2005. *Marine Mammal Populations and Ocean Noise: Determining when Ocean Noise Causes Biologically Significant Effects*. National Academy Press, Washington, DC.

[UN] United Nations. 2017. *IMO (International Maritime Organization) Profile: Overview* (webpage). Copyright UN-Business Action Hub and United Nations. https://business.un.org/en/entities/13. (Accessed 31 Mar 2017).

Ahroon, W.A., R.P. Hamernik, and R.I. Davis. 1993. Complex noise exposures: an energy analysis. *Journal of the Acoustical Society of America* 93(2): 997-1006. http://link.aip.org/link/?JAS/93/997/1.

Ainslie, M.A. and J.G. McColm. 1998. A simplified formula for viscous and chemical absorption in sea water. *Journal of the Acoustical Society of America* 103(3): 1671-1672.

Ainslie, M.A., P.H. Dahl, C.A. De Jong, and R.M. Laws. 2014a. *Practical Spreading Laws: the Snakes and Ladders of Shallow Water Acoustics*. *UA2014 - 2nd International Conference and Exhibition on Underwater Acoustics*, Island of Rhodes, Greece, pp. 879-886.

Ainslie, M.A., P.H. Dahl, C.A.F. de Jong, and R.M. Laws. 2014b. *Practical Spreading Laws: The Snakes and Ladders of Shallow Water Acoustics*. *UA2014 - 2nd International Conference and Exhibition on Underwater Acoustics*, 22-27 Jun 2014, Island of Rhodes, Greece, pp. 879-886.

Ainslie, M.A., J.L. Miksis-Olds, S.B. Martin, K. Heaney, C.A.F. de Jong, A.M. von Benda-Beckmann, and A.P. Lyons. 2018. *ADEON Underwater Soundscape and Modeling Metadata Standard*. Version 1.0. Technical report by JASCO Applied Sciences for ADEON Prime Contract No. M16PC00003.

Akay, A. 1978. A review of impact noise. *Journal of the Acoustical Society of America* 64(4): 977-987. https://doi.org/10.1121/1.2773928.

André, M., K. Kaifu, M. Solé, M. van der Schaar, T. Akamatsu, A. Balastegui, A.M. Sánchez, and J.V. Castell. 2016. Contribution to the understanding of particle motion perception in marine invertebrates. (Chapter 6) *In* Popper, A. and A. Hawkins (eds.). *The Effects of Noise on Aquatic Life II*. Springer. pp. 47-55.

Andrew, R.K., B.M. Howe, and J.A. Mercer. 2011. Long-time trends in ship traffic noise for four sites off the North American West Coast. *Journal of the Acoustical Society of America* 129(2): 642-651. http://www.ore.hawaii.edu/OE/Prof.Howe_PDF/Andrew_et_al_2011_Long_term_trends_JAS000642.pdf.

ANSI S1.4-1983. R2006. *American National Standard Specification for Sound Level Meters*. American National Standards Institute, New York.

ANSI S1.1-1994. R2004. *American National Standard Acoustical Terminology*. American National Standards Institute, New York.

Au, W.W., R.A. Kastelein, T. Rippe, and N.M. Schooneman. 1999. Transmission beam pattern and echolocation signals of a harbor porpoise (*Phocoena phocoena*). *Journal of the Acoustical Society of America* 106(6): 3699-3705.

Au, W.W.L., R.W. Floyd, R.H. Penner, and A.E. Murchison. 1974. Measurement of echolocation signals of the Atlantic bottlenose dolphin, *Tursiops truncatus* Montagu, in open waters. *Journal of the Acoustical Society of America* 56(4): 1280-1290.

Au, W.W.L. and M.C. Hastings. 2008. *Principles of Marine Bioacoustics*. Springer. 510 p. http://link.springer.com/book/10.1007%2F978-0-387-78365-9.

Bailey, H., B. Senior, D. Simmons, J. Rusin, G. Picken, and P. Thompson, M. 2010. Assessing underwater noise levels during pile-driving at an offshore windfarm and its potential effects on marine mammals. *Marine Pollution Bulletin* 60(6): 888-897. http://doi.org/10.1016/j.marpolbul.2010.01.003.

Betke, K. 2008. *Measurement of Wind Turbine Construction Noise at Horns Rev II*. Report Number 1256-08-a-KB. Report from ITAP–Institut für technische und angewandte Physik GmbH, Oldenburg, Germany, for BioConsultSH, Husun, Germany. 30 p.

Blackwell, S.B., J.W. Lawson, and M.T. Williams. 2004. Tolerance by ringed seals (*Phoca hispida*) to impact pipe-driving and construction sounds at an oil production island. *Journal of the Acoustical Society of America* 115(5): 2346-2357. http://scitation.aip.org/content/asa/journal/jasa/115/5/10.1121/1.1701899.

Blackwell, S.B., C.S. Nations, T.L. McDonald, A.M. Thode, D. Mathias, K.H. Kim, C.R. Greene, Jr., and A.M. Macrander. 2015. Effects of airgun sounds on bowhead whale calling rates: evidence for two behavioral thresholds. *PLoS ONE* 10(6): e0125720. http://journals.plos.org/plosone/article?id=10.1371/journal.pone.0125720.

Blix, A.S., L. Walløe, and E.B. Messelt. 2013. On how whales avoid decompression sickness and why they sometimes strand. 216(18): 3385-3387. http://jeb.biologists.org/content/jexbio/216/18/3385.full.pdf.

Bohnenstiehl, D.R., C.M. Scheip, H. Matsumoto, and R.P. Dziak. 2012. Acoustics variability of air gun signals recorded at intermediate ranges within the Lau Basin. *Geochemistry, Geophysics, Geosystems* 13(11).

Brandt, M.J., A. Diederichs, K. Betke, and G. Nehls. 2011. Responses of harbour porpoises to pile driving at the Horns Rev II offshore wind farm in the Danish North Sea. *Marine Ecology Progress Series* 421: 205-216.

Brandt, M.J., A.-C. Dragon, A. Diederichs, A. Schubert, V. Kosarev, G. Nehls, V. Wahl, A. Michalik, A. Braasch, et al. 2016. *Effects of offshore pile driving on harbour porpoise abundance in the German Bight. Assessment of Noise Effects. Final Report*. Created by BioConsult SH GmbH & Co KG, IBL Umweltplanung GmbH, Institut für Angewandte Ökosystemforschung GmbH for Offshore Forum Windenergie. http://bioconsult-sh.de/site/assets/files/1573/1573.pdf.

Branstetter, B.K., K. Bakhtiari, A. Black, J.S. Trickey, J.J. Finneran, and H. Aihara. 2016. Energetic and informational masking of complex sounds by a bottlenose dolphin (*Tursiops truncatus*). *Journal of the Acoustical Society of America* 140(3): 1904-1917. https://doi.org/10.1121/1.4962530.

Breitzke, M. and T. Bohlen. 2010. Modelling sound propagation in the Southern Ocean to estimate the acoustic impact of seismic research surveys on marine mammals. *Geophysical Journal International* 181(2): 818-846.

Buck, K., A. Dancer, and R. Franke. 1984. Effect of the temporal pattern of a given noise dose on TTS in guinea pigs. 76(4): 1090-1097. https://asa.scitation.org/doi/abs/10.1121/1.391401.

Caldwell, J. and W. Dragoset. 2000. A brief overview of seismic air-gun arrays. *The Leading Edge* 19(8): 898-902.

Carroll, A.G., R. Przeslawski, A. Duncan, M. Gunning, and B. Bruce. 2017. A critical review of the potential impacts of marine seismic surveys on fish & invertebrates. *Marine Pollution Bulletin* 114: 9-24. http://www.sciencedirect.com/science/article/pii/S0025326X16309584.

Casper, B.M., M.E. Smith, M.B. Halvorsen, H. Sun, T.J. Carlson, and A.N. Popper. 2013. Effects of exposure to pile driving sounds on fish inner ear tissues. *Comparative Biochemistry and Physiology Part A: Molecular & Integrative Physiology* 166(2): 352-360. http://www.sciencedirect.com/science/article/pii/S109564331300189X.

Casper, B.M., M.B. Halvorsen, T.J. Carlson, and A.N. Popper. 2017a. Onset of barotrauma injuries related to number of pile driving strike exposures in hybrid striped bass. *The Journal of the Acoustical Society of America* 141(6): 4380-4387. https://asa.scitation.org/doi/abs/10.1121/1.4984976.

Casper, B.M., M.B. Halvorsen, T.J. Carlson, and A.N. Popper. 2017b. Onset of barotrauma injuries related to number of pile driving strike exposures in hybrid striped bass. *Journal of the Acoustical Society of America* 141(6): 4380-4387. https://doi.org/10.1121/1.4984976.

Cato, D.H. 2008. Ocean ambient noise: Its measurement and its significance to marine animals. *Proceedings of the Institute of Acoustics* 30(5): 1-9.

Chapman, R.N. and A. Price. 2011. Low frequency deep ocean ambient noise trend in the Northeast Pacific Ocean. *Journal of the Acoustical Society of America* 129(5): EL161-EL165. http://dx.doi.org/doi/10.1121/1.3567084.

Charifi, M., M. Sow, P. Ciret, S. Benomar, and J.-C. Massabuau. 2017. The sense of hearing in the Pacific oyster, *Magallana gigas*. *PLOS ONE* 12(10): e0185353. https://doi.org/10.1371/journal.pone.0185353.

Cholewiak, D., A.I. DeAngelis, D.L. Palka, P.J. Corkeron, and S.M. Van Parijs. 2017. Beaked whales demonstrate a marked acoustic response to the use of shipboard echosounders. *Royal Society Open Science* 4(12). http://rsos.royalsocietypublishing.org/content/royopensci/4/12/170940.full.pdf.

Clark, C.W., W.T. Ellison, B.L. Southall, L. Hatch, S.M. Van Parijs, A. Frankel, and D. Ponirakis. 2009. Acoustic masking in marine ecosystems: Intuitions, analysis, and implication. *Marine Ecology Progress Series* 395: 201-222. http://www.int-res.com/abstracts/meps/v395/p201-222/

Collins, M.D. 1993. A split-step Padé solution for the parabolic equation method. *Journal of the Acoustical Society of America* 93(4): 1736-1742.

Costa, D.P., L. Schwarz, P. Robinson, R.S. Schick, P.A. Morris, R. Condit, D.E. Crocker, and A.M. Kilpatrick. 2016. A Bioenergetics Approach to Understanding the Population Consequences of Disturbance: Elephant Seals as a Model System. (Chapter 19) *In* Popper, A.N. and A.D. Hawkins (eds.). *The Effects of Noise on Aquatic Life II*. Volume 875. NY, USA. pp. 161-169. https://doi.org/10.1007/978-1-4939-2981-8_19.

Cox, T.M., T. Ragen, A. Read, E. Vos, R. Baird, K. Balcomb, J. Barlow, J. Caldwell, T. Cranford, et al. 2006. Understanding the impacts of anthropogenic sound on beaked whales. *Journal of Cetacean Research and Management* 7(3): 177-187. http://www.researchgate.net/publication/224554761_Understanding_the_impacts_of_anthropogenic_sound_on_beaked_whales/file/60b7d51e46006d38ae.pdf.

D'Amico, A., R. Gisiner, D. Ketten, J. Hammock, C. Johnson, P. Tyack, and J. Mead. 2009. Beaked whale strandings and naval exercises. *Aquatic Mammals* 35(4): 452-472.

Dahl, P.H. 2015. The Underwater Sound Field from Impact Pile Driving and Its Potential Effects on Marine Life. *Acoustics Today* 11(2): 7.

Dähne, M., A. Gilles, K. Lucke, V. Peschko, S. Adler, K. Krügel, J. Sundermeyer, and U. Siebert. 2013. Effects of pile-driving on harbour porpoises (*Phocoena phocoena*) at the first offshore wind farm in Germany. *Environmental Research Letters* 8(2): 025002.

Dalen, J., E. Dragsund, and A. Næss. 2007. *Effects of seismic surveys on fish, fish catches and sea mammals*. Document Number Report no. 2007-0512. Report by DNV Energy for the Cooperation group - Fishery Industry and Petroleum Industry, Høvik, Norway. 27 p.

Danielson, R., D. Henderson, M.A. Gratton, L. Bianchi, and R. Salvi. 1991a. The importance of ‘‘temporal pattern’’ in traumatic impulse noise exposures. *Journal of the Acoustical Society of America* 90(1): 209-218. https://doi.org/10.1121/1.402361.

Danielson, R., D. Henderson, M.A. Gratton, L. Bianchi, and R. Salvi. 1991b. The importance of ‘‘temporal pattern’’ in traumatic impulse noise exposures. 90(1): 209-218. https://asa.scitation.org/doi/abs/10.1121/1.402361.

Day, R., D., R.D. McCauley, Q.P. Fitzgibbon, K. Hartmann, J.M. Semmens, and Institute for Marine and Antarctic Studies. 2016. *Assessing the Impact of Marine Seismic Surveys on Southeast Australian Scallop and Lobster Fisheries. FRDC Project No 2012/008*. Impacts of Marine Seismic Surveys on Scallop and Lobster Fisheries. Fisheries Ressearch & Development Corporation, University of Tasmania, Hobart. 159 p.

Deruiter, S.L., B.L. Southall, J. Calambokidis, W.M. Zimmer, D. Sadykova, E.A. Falcone, A.S. Friedlaender, J.E. Joseph, D. Moretti, et al. 2013. First direct measurements of behavioural responses by Cuvier's beaked whales to mid-frequency active sonar. *Biology Letters* 9(4): 1-5.

Di Iorio, L., C. Gervaise, V. Jaud, A.A. Robson, and L. Chauvaud. 2012. Hydrophone detects cracking sounds: Non-intrusive monitoring of bivalve movement. *Journal of Experimental Marine Biology and Ecology* 432-433: 9-16. https://doi.org/10.1016/j.jembe.2012.07.010.

Dombroski, J.R.G., S.E. Parks, K.R. Groch, P.A.C. Flores, and R.S. Sousa-Lima. 2016. Vocalizations produced by southern right whale (*Eubalaena australis*) mother-calf pairs in a calving ground off Brazil. *Journal of the Acoustical Society of America* 140(3): 1850-1857. https://doi.org/10.1121/1.4962231.

Dooling, R.J., M.R. Leek, and A.N. Popper. 2015. Effects of noise on fishes: What we can learn from humans and birds. *Integrative Zoology* 10: 29-37.

Doughty, C.E., J. Roman, S. Faurby, A. Wolf, A. Haque, E.S. Bakker, Y. Malhi, J.B. Dunning, and J.-C. Svenning. 2016. Global nutrient transport in a world of giants. *Proceedings of the National Academy of Sciences* 113(4): 868-873. https://doi.org/10.1073/pnas.1502549112.

Dragoset, W.H. 1990. Air-gun array specs: A tutorial. *The Leading Edge* 9(1): 24-32.

Edmonds, N.J., C.J. Firmin, D. Goldsmith, R.C. Faulkner, and D.T. Wood. 2016. A review of crustacean sensitivity to high amplitude underwater noise: Data needs for effective risk assessment in relation to UK commercial species. *Marine Pollution Bulletin* 108(1–2): 5-11. http://www.sciencedirect.com/science/article/pii/S0025326X16302892.

Eldred, K.M., W. Gannon, and H.E. Von Gierke. 1955. *Criteria for short time exposure of personnel to high intensity jet aircraft noise*. Report Number WADC TN 55-355. U.S. Air Force, Aero Space Medical Lab, Wright Patterson Air Force Base, OH, USA.

Eldredge, D.H. and W.P. Covell. 1958. A laboratory method for the study of acoustic trauma. *Laryngoscope* 68(3): 465-477. https://doi.org/10.1002/lary.5540680328.

Ellison, W.T. and A.S. Frankel. 2012. A common sense approach to source metrics. *In* Popper, A.N. and A. Hawkins (eds.). *The Effects of Noise on Aquatic Life*. Springer. pp. 433-438.

Ellison, W.T., B.L. Southall, C.W. Clark, and A.S. Frankel. 2012. A new context-based approach to assess marine mammal behavioral responses to anthropogenic sounds. *Conservation Biology* 26(1): 21-28.

Ellison, W.T., R. Racca, C.W. Clark, B. Streever, A.S. Frankel, E. Fleishman, R. Angliss, J. Berger, D. Ketten, et al. 2016. Modeling the aggregated exposure and responses of bowhead whales *Balaena mysticetus* to multiple sources of anthropogenic underwater sound. *Endangered Species Research*. http://www.int-res.com/articles/esr2016/30/n030p095.pdf.

Erbe, C. 2008. Critical ratios of beluga whales (*Delphinapterus leucas*) and masked signal duration. *Journal of the Acoustical Society of America* 124(4): 2216-2223. http://asadl.org/jasa/resource/1/jasman/v124/i4/p2216_s1?isAuthorized=no.

Erbe, C. 2013. International regulation of underwater noise. *Acoustics Australia* 41(1): 12-19.

Erbe, C., C. Reichmuth, K. Cunningham, K. Lucke, and R. Dooling. 2016. Communication masking in marine mammals: A review and research strategy. *Marine Pollution Bulletin* 103(1): 15-38. https://doi.org/10.1016/j.marpolbul.2015.12.007.

Erdreich, J. 1986. A distribution based definition of impulse noise. *Journal of the Acoustical Society of America* 79(4): 990-998. http://link.aip.org/link/?JAS/79/990/1.

Etter, P.C. 1996. *Underwater Acoustic Modeling - Principles, Techniques, and Applications*. Second edition. E & FN Spon, London, UK. 344 p.

Fewtrell, J.L. and R.D. McCauley. 2012. Impact of air gun noise on the behaviour of marine fish and squid. *Marine Pollution Bulletin* 64(5): 984-993. http://www.sciencedirect.com/science/article/pii/S0025326X12000872.

Finneran, J.J., C.E. Schlundt, D.A. Carder, J.A. Clark, J.A. Young, J.B. Gaspin, and S.H. Ridgway. 2000. Auditory and behavioral responses of bottlenose dolphins (*Tursiops truncatus*) and a beluga whale (*Delphinapterus leucas*) to impulsive sounds resembling distant signatures of underwater explosions. *Journal of the Acoustical Society of America* 108(1): 417-431. http://link.aip.org/link/?JAS/108/417/1.

Finneran, J.J., C.E. Schlundt, R. Dear, D.A. Carder, and S.H. Ridgway. 2002. Temporary shift in masked hearing thresholds in odontocetes after exposure to single underwater impulses from a seismic watergun. *Journal of the Acoustical Society of America* 111(6): 2929-2940.

Finneran, J.J., D.A. Carder, C.E. Schlundt, and R.L. Dear. 2010. Growth and recovery of temporary threshold shift at 3 kHz in bottlenose dolphins: Experimental data and mathematical modelsa. *Journal of the Acoustical Society of America* 127(5): 3256-3266.

Finneran, J.J., J.S. Trickey, B.K. Branstetter, C.E. Schlundt, and K. Jenkins. 2011. *Auditory effects of multiple underwater impulses on bottlenose dolphins (Tursiops truncatus)*. *Journal of the Acoustical Society of America*. pp. 2561-2561.

Finneran, J.J. and A.K. Jenkins. 2012. *Criteria and thresholds for U.S. Navy acoustic and explosive effects analysis*. SPAWAR Systems Center Pacific, San Diego, California.

Finneran, J.J. 2015a. Noise-induced hearing loss in marine mammals: A review of temporary threshold shift studies from 1996 to 2015. *The Journal of the Acoustical Society of America* 138(3): 1702-1726. https://asa.scitation.org/doi/abs/10.1121/1.4927418.

Finneran, J.J. 2015b. *Auditory weighting functions and TTS/PTS exposure functions for cetaceans and marine carnivores*. San Diego: SSC Pacific.

Finneran, J.J. 2015c. Noise-induced hearing loss in marine mammals: A review of temporary threshold shift studies from 1996 to 2015. *Journal of the Acoustical Society of America* 138(3): 1702-1726. https://doi.org/10.1121/1.4927418.

Finneran, J.J. 2016. *Auditory weighting functions and TTS/PTS exposure functions for marine mammals exposed to underwater noise*. Technical Report. 49 p.

François, R.E. and G.R. Garrison. 1982a. Sound absorption based on ocean measurements: Part I: Pure water and magnesium sulfate contributions. *Journal of the Acoustical Society of America* 72(3): 896-907.

François, R.E. and G.R. Garrison. 1982b. Sound absorption based on ocean measurements: Part II: Boric acid contribution and equation for total absorption. *Journal of the Acoustical Society of America* 72(6): 1879-1890.

Frouin-Mouy, H., K. Kowarski, B. Martin, and K. Bröker. 2017. Seasonal trends in acoustic detection of marine mammals in Baffin Bay and Melville Bay, Northwest Greenland. *Arctic* 70(1): 59-76. http://arctic.journalhosting.ucalgary.ca/arctic/index.php/arctic/article/view/4632.

Gaspard, J.C., G.B. Bauer, R.L. Reep, K. Dziuk, A. Cardwell, L. Read, and D.A. Mann. 2012. Audiogram and auditory critical ratios of two Florida manatees (*Trichechus manatus latirostris*). *Journal of Experimental Biology* 215(9): 1442-1447. https://jeb.biologists.org/content/216/14/2769.

Gedamke, J., N. Gales, and S. Frydman. 2011. Assessing risk of baleen whale hearing loss from seismic surveys: The effect of uncertainty and individual variation. *Journal of the Acoustical Society of America* 129(1): 496-506. http://www.ncbi.nlm.nih.gov/pubmed/21303030.

Gisiner, R.C. 2016. Sound and Marine Seismic Surveys. *Acoustics Today* 12(4): 10-18. http://acousticstoday.org/wp-content/uploads/2016/12/Seismic-Surveys.pdf.

Goldbogen, J.A., B.L. Southall, S.L. Deruiter, J. Calambokidis, A.S. Friedlaender, E.L. Hazen, E.A. Falcone, G.S. Schorr, A. Douglas, et al. 2013. Blue whales respond to simulated mid-frequency military sonar. *Proceedings of the Royal Society B* 280(1765): 1-8.

Goold, J.C. and P.J. Fish. 1998. Broadband spectra of seismic survey air-gun emissions, with reference to dolphin auditory thresholds. *Journal of the Acoustical Society of America* 103(4): 2177-2184.

Gordon, J., D. Gillespie, J. Potter, A. Frantzis, M.P. Simmonds, R. Swift, and D. Thompson. 2003. A review of the effects of seismic surveys on marine mammals. *Marine Technology Society Journal* 37(4): 16-34. http://www.ingentaconnect.com/content/mts/mtsj/2003/00000037/00000004/art00003.

Guan, S., J. Vignola, J. Judge, and D. Turo. 2015. Airgun inter-pulse noise field during a seismic survey in an Arctic ultra shallow marine environment. *Journal of the Acoustical Society of America* 138(6): 3447-3457.

Guerra, M., A.M. Thode, S.B. Blackwell, and A. Michael Macrander. 2011. Quantifying seismic survey reverberation off the Alaskan North Slope. *Journal of the Acoustical Society of America* 130(5): 3046–3058. http://dx.doi.org/10.1121/1.3628326.

Hall, D.A., A. Irwin, M. Edmondson-Jones, S. Phillips, and J.E.W. Poxon. 2013. An exploratory evaluation of perceptual, psychoacoustic and acoustical properties of urban soundscapes. *Applied Acoustics* 74(2): 248-254. https://doi.org/10.1016/j.apacoust.2011.03.006.

Halvorsen, M.B., B.M. Casper, C.M. Woodley, T.J. Carlson, and A.N. Popper. 2011. *Hydroacoustic impacts on fish from pile installation*. NCHRP Research Results Digest Report Number 363, Project 25-28. National Cooperative Highway Research Program, Transportation Research Board, National Academy of Sciences, Washington DC, USA. http://www.trb.org/Publications/Blurbs/166159.aspx.

Halvorsen, M.B., B.M. Casper, F. Matthews, T.J. Carlson, and A.N. Popper. 2012a. Effects of exposure to pile-driving sounds on the lake sturgeon, Nile tilapia and hogchoker. *Proceedings of the Royal Society B: Biological Sciences* 279(1748): 4705-4714. http://www.ncbi.nlm.nih.gov/pubmed/23055066.

Halvorsen, M.B., B.M. Casper, C.M. Woodley, T.J. Carlson, and A.N. Popper. 2012b. Threshold for onset of injury in Chinook salmon from exposure to impulsive pile driving sounds. *PLoS ONE* 7(6): e38968.

Hamernik, R., W. Qiu, and R. Davis. 2010. The use of the kurtosis metric in the evaluation of industrial noise exposures. 128(4): 2456-2456. https://asa.scitation.org/doi/abs/10.1121/1.3508793.

Hamernik, R.P., D. Henderson, J.J. Crossley, and R.J. Salvi. 1974. Interaction of continuous and impulse noise: Audiometric and histological effects. *Journal of the Acoustical Society of America* 55(1): 117-121. https://doi.org/10.1121/1.1928141.

Hamernik, R.P., W. Qiu, and B. Davis. 2003. The effects of the amplitude distribution of equal energy exposures on noise-induced hearing loss: The kurtosis metric. 114(1): 386-395. https://asa.scitation.org/doi/abs/10.1121/1.1582446.

Hamernik, R.P., W. Qiu, and B. Davis. 2007. Hearing loss from interrupted, intermittent, and time varying non-Gaussian noise exposure: The applicability of the equal energy hypothesis. 122(4): 2245-2254. https://asa.scitation.org/doi/abs/10.1121/1.2775160.

Harris, C.M. 1998. *Handbook of acoustical measurements and noise control*. 3rd edition. Acoustical Society of America, Huntington, NY.

Harwood, J., S. King, R. Schick, C. Donovan, and C. Booth. 2014. *Protocol for Implementing the Interim Population Consequences of Disturbance (PCoD) Approach: Quantifying and Assessing the Effects of UK Offshore Renewable Energy Developments on Marine Mammal Populations*. Scottish Marine and Freshwater Science. Volume 5, No. 2 Report Number SMRUL-TCE-2013-014. 97 p. http://www.scotland.gov.uk/Resource/0044/00443360.pdf.

Hatch, L.T., C.W. Clark, S.M. Van Parijs, A.S. Frankel, and D.W. Ponirakis. 2012. Quantifying loss of acoustic communication space for right whales in and around a U.S. National Marine Sanctuary. *Conservation Biology* 26(5): 983-994.

Hawkins, A.D. and A.N. Popper. 2017. A sound approach to assessing the impact of underwater noise on marine fishes and invertebrates. *ICES Journal of Marine Science* 74(3): 635-651. https://doi.org/10.1093/icesjms/fsw205.

Hawkins, R.S., J.L. Miksis-Olds, and C.M. Smith. 2014. Variation in low-frequency estimates of sound levels based on different units of analysis. *Journal of the Acoustical Society of America* 135(2): 705-711. https://doi.org/10.1121/1.4861252.

Heinzel, G., A. Rüdiger, and R. Schilling. 2002. Spectrum and spectral density estimation by the Discrete Fourier transform (DFT), including a comprehensive list of window functions and some new at-top windows.

Henderson, D. and R.P. Hamernik. 1986. Impulse noise: Critical review. *Journal of the Acoustical Society of America* 80(2): 569-584. http://link.aip.org/link/?JAS/80/569/1.

Hermannsen, L., J. Tougaard, K. Beedholm, J. Nabe-Nielsen, and P.T. Madsen. 2015. Characteristics and propagation of airgun pulses in shallow water with implications for effects on small marine mammals. *PLoS ONE* 10(7): e0133436. http://journals.plos.org/plosone/article?id=10.1371/journal.pone.0133436.

Hildebrand, J.A. 2009. Anthropogenic and natural sources of ambient noise in the ocean. *Marine Ecology Progress Series* 395: 5-20.

Hirsh, I.J. and W.D. Ward. 1952. Recovery of the Auditory Threshold after Strong Acoustic Stimulation. 24(2): 131-141. https://asa.scitation.org/doi/abs/10.1121/1.1906867.

Holles, S., S.D. Simpson, A.N. Radford, L. Berten, and D. Lecchini. 2013. Boat noise disrupts orientation behaviour in a coral reef fish. *Marine Ecology Progress Series* 485: 295-300.

Houser, D.S., W. Yost, R. Burkard, J.J. Finneran, C. Reichmuth, and J. Mulsow. 2017. A review of the history, development and application of auditory weighting functions in humans and marine mammals. *Journal of the Acoustical Society of America* 141(3): 1371-1413. https://doi.org/10.1121/1.4976086.

Hughes, A.R., D.A. Mann, and D.L. Kimbro. 2014. Predatory fish sounds can alter crab foraging behaviour and influence bivalve abundance. *Proceedings of the Royal Society B: Biological Sciences* 281(1788): 20140715. https://royalsocietypublishing.org/doi/abs/10.1098/rspb.2014.0715 %X The risk of predation can have large effects on ecological communities via changes in prey behaviour, morphology and reproduction. Although prey can use a variety of sensory signals to detect predation risk, relatively little is known regarding the effects of predator acoustic cues on prey foraging behaviour. Here we show that an ecologically important marine crab species can detect sound across a range of frequencies, probably in response to particle acceleration. Further, crabs suppress their resource consumption in the presence of experimental acoustic stimuli from multiple predatory fish species, and the sign and strength of this response is similar to that elicited by water-borne chemical cues. When acoustic and chemical cues were combined, consumption differed from expectations based on independent cue effects, suggesting redundancies among cue types. These results highlight that predator acoustic cues may influence prey behaviour across a range of vertebrate and invertebrate taxa, with the potential for cascading effects on resource abundance.

Hung, I.J. and P. Dallos. 1972. Study of the Acoustic Reflex in Human Beings. I. Dynamic Characteristics. 52(4B): 1168-1180. https://asa.scitation.org/doi/abs/10.1121/1.1913229.

International Electrotechnical Commission. 2004. *Electroacoustics–Sound level meters (IEC 61672:2003-2004)*. Geneva.

Jennings, P. and R. Cain. 2013. A framework for improving urban soundscapes. *Applied Acoustics* 74(2): 293-299.

Jensen, F.B., W.A. Kuperman, M.B. Porter, and H. Schmidt. 2011. *Computational Ocean Acoustics*. 2nd edition. AIP Series in Modern Acourics and Signal Processing. AIP Press - Springer, New York. 794 p.

Jepson, P.D., M. Arbelo, R. Deaville, I.A.P. Patterson, P. Castro, J.R. Baker, E. Degollada, H.M. Ross, P. Herraez, et al. 2003. Gas-bubble lesions in stranded cetaceans. *Nature* 425(6958): 575-576.

Johnson, C.S. 1968. Relation between absolute threshold and duration-of-time pulses in the bottlenosed porpoise. *Journal of the Acoustical Society of America* 43: 757-763.

Kaiser, J.F. 1990. *On a simple algorithm to calculate the 'energy' of a signal*. *International Conference on Acoustics, Speech, and Signal Processing*, 3-6 Apr 1990. IEEE, pp. 381-384.

Kandia, V. and Y. Stylianou. 2006. Detection of sperm whale clicks based on the Teager-Kaiser energy operator. *Applied Acoustics* 67: 1144-1163.

Kastelein, R.A., L. Hoek, P.J. Wensveen, J.M. Terhune, and C.A.F. de Jong. 2010. The effect of signal duration on the underwater hearing thresholds of two harbor seals (*Phoca vitulina*) for single tonal signals between 0.2 and 40 kHz. *Journal of the Acoustical Society of America* 127(2): 1135-1145. https://doi.org/10.1121/1.3283019.

Kastelein, R.A., R. Gransier, L. Hoek, A. Macleod, and J.M. Terhune. 2012a. Hearing threshold shifts and recovery in harbor seals (Phoca vitulina) after octave-band noise exposure at 4 kHz. 132(4): 2745-2761. https://asa.scitation.org/doi/abs/10.1121/1.4747013.

Kastelein, R.A., R. Gransier, L. Hoek, and J. Olthuis. 2012b. Temporary threshold shifts and recovery in a harbor porpoise (Phocoena phocoena) after octave-band noise at 4 kHz. 132(5): 3525-3537. https://asa.scitation.org/doi/abs/10.1121/1.4757641.

Kastelein, R.A., R. Gransier, L. Hoek, and J. Olthuis. 2012c. Temporary threshold shifts and recovery in a harbor porpoise (*Phocoena phocoena*) after octave-band noise at 4 kHz. *Journal of the Acoustical Society of America* 132(5): 3525-3537. https://doi.org/10.1121/1.4757641.

Kastelein, R.A., L. Hoek, and R. Gransier. 2013a. Hearing thresholds of two harbor seals (*Phoca vitulina*) for playbacks of multiple pile driving strike sounds. *Journal of the Acoustical Society of America* 134(3): 2307-2312. https://doi.org/10.1121/1.4817889.

Kastelein, R.A., D. van Heerden, R. Gransier, and L. Hoek. 2013b. Behavioral responses of a harbor porpoise (*Phocoena phocoena*) to playbacks of broadband pile driving sounds. *Marine Environmental Research* 92: 206-214. http://doi.org/10.1016/j.marenvres.2013.09.020.

Kastelein, R.A., L. Hoek, R. Gransier, M. Rambags, and N. Claeys. 2014a. Effect of level, duration, and inter-pulse interval of 1–2 kHz sonar signal exposures on harbor porpoise hearing. 136(1): 412-422. https://asa.scitation.org/doi/abs/10.1121/1.4883596.

Kastelein, R.A., J. Schop, R. Gransier, and L. Hoek. 2014b. Frequency of greatest temporary hearing threshold shift in harbor porpoises (Phocoena phocoena) depends on the noise level. 136(3): 1410-1418. https://asa.scitation.org/doi/abs/10.1121/1.4892794.

Kastelein, R.A., R. Gransier, J. Schop, and L. Hoek. 2015. Effects of exposure to intermittent and continuous 6–7 kHz sonar sweeps on harbor porpoise (*Phocoena phocoena*) hearing. *Journal of the Acoustical Society of America* 137(4): 1623-1633. http://scitation.aip.org/content/asa/journal/jasa/137/4/10.1121/1.4916590.

Kastelein, R.A., L. Helder-Hoek, S. Van de Voorde, A.M. von Benda-Beckmann, F.-P.A. Lam, E. Jansen, C.A.F. de Jong, and M.A. Ainslie. 2017. Temporary hearing threshold shift in a harbor porpoise (*Phocoena phocoena*) after exposure to multiple airgun sounds. *Journal of the Acoustical Society of America* 142(4): 2430-2442. https://doi.org/10.1121/1.5007720.

King, S., R.S. Schick, C. Donovan, C.G. Booth, M. Burgman, L. Thomas, and J. Harwood. 2015. An Interim Framework for Assessing the Population Consequences of Disturbance. *Methods in Ecology and Evolution* 6(10): 1150–1158

Kinsler, L.E., A.R. Frey, A.B. Coppens, and J.V. Sanders. 2000. *Fundamentals of acoustics*. 4th edition. John Wiley & Sons Inc., New York.

Koller, M. 2016. robustlmm: An R Package for Robust Estimation of Linear Mixed-Effects Models. *Journal of Statistical Software* 75(6): 1-24. https://www.jstatsoft.org/v075/i06.

Kowarski, K.A., J. Delarue, B. Martin, J. O'Brien, R. Meade, O. Ó Cadhla, and S.D. Berrow. 2018. Signals from the deep: Spatial and temporal acoustic occurrence of beaked whales off western Ireland. *PLOS ONE* 13(6). https://doi.org/10.1371/journal.pone.0199431.

Kyhn, L.A., D. Boertmann, J. Tougaard, K. Johansen, and A. Mosbech. 2011. *Guidelines to environmental impact assessment of seismic activities in Greenland waters*. 3rd revised edition, Dec 2011, Danish Center for Environment and Energy. 61 p.

Ladich, F. and R.R. Fay. 2013. Auditory evoked potential audiometry in fish. *Reviews in Fish Biology and Fisheries* 23(3): 317-364. http://link.springer.com/article/10.1007/s11160-012-9297-z/fulltext.html.

Lammers, M.O., S. Stieb, W.W.L. Au, T.A. Mooney, R.E. Brainard, and K. Wong. 2006. Temporal, geographic, and density variations in the acoustic activity of snapping shrimp. *Journal of the Acoustical Society of America* 120(5): 3013-3013.

Le, T.N., L.V. Straatman, J. Lea, and B. Westerberg. 2017. Current insights in noise-induced hearing loss: a literature review of the underlying mechanism, pathophysiology, asymmetry, and management options. *Journal of otolaryngology - head & neck surgery = Le Journal d'oto-rhino-laryngologie et de chirurgie cervico-faciale* 46(1): 41-41. https://www.ncbi.nlm.nih.gov/pubmed/28535812
https://www.ncbi.nlm.nih.gov/pmc/PMC5442866/.

Leggat, L.J., H.M. Merklinger, and J.L. Kennedy. 1981. *LNG Carrier Underwater Noise Study for Baffin Bay*. Defence Research Establishment Atlantic, Dartmouth, Nova Scotia. 32 p.

Lippert, S., M. Nijhof, T. Lippert, D. Wilkes, A. Gavrilov, K. Heitmann, M. Ruhnau, O. von Estorff, A. Schäfke, et al. 2016. COMPILE—A Generic Benchmark Case for Predictions of Marine Pile-Driving Noise. *IEEE Journal of Oceanic Engineering* 41(4): 1061-1071. https://doi.org/10.1109/JOE.2016.2524738.

Lippert, T. and O.v. Estorff. 2014. The significance of parameter uncertainties for the prediction of offshore pile driving noise. 136(5): 2463-2471. https://asa.scitation.org/doi/abs/10.1121/1.4896458.

Lippert, T., M. Galindo-Romero, A.N. Gavrilov, and O. von Estorff. 2015. Empirical estimation of peak pressure level from sound exposure level. Part II: Offshore impact pile driving noise. *Journal of the Acoustical Society of America* 138(3): EL287-EL292. http://dx.doi.org/10.1121/1.4929742.

Lippert, T., M.A. Ainslie, and O. von Estorff. 2018. Pile driving acoustics made simple: Damped cylindrical spreading model. *Journal of the Acoustical Society of America* 143(1): 310-317. https://doi.org/10.1121/1.5011158.

Lucke, K., U. Siebert, P. Lepper, A., and M.-A. Blanchet. 2009. Temporary shift in masked hearing thresholds in a harbor porpoise (*Phocoena phocoena*) after exposure to seismic airgun stimuli. *Journal of the Acoustical Society of America* 125(6): 4060-4070.

Lucke, K., E. Winter, F.-P. Lam, G. Scowcroft, A. Hawkins, and A.N. Popper. 2014. International harmonization of approaches to define underwater noise exposure criteria. *Journal of the Acoustical Society of America* 135(4): 2404-2404.

MacGillivray, A. 2014. A model for underwater sound levels generated by marine impact pile driving. *Proceedings of Meetings on Acoustics* 20(1): 045008. http://scitation.aip.org/content/asa/journal/poma/20/1/10.1121/2.0000030.

MacGillivray, A. 2018a. Underwater noise from pile driving of conductor casing at a deep-water oil platform. *The Journal of the Acoustical Society of America* 143(1): 450-459. https://doi.org/10.1121/1.5021554.

MacGillivray, A.O. 2006. *Acoustic Modelling Study of Seismic Airgun Noise in Queen Charlotte Basin*. MSc Thesis. University of Victoria, Victoria, BC. 98 p.

MacGillivray, A.O. and N.R. Chapman. 2012. Modeling underwater sound propagation from an airgun array using the parabolic equation method. *Canadian Acoustics* 40(1): 19-25. http://jcaa.caa-aca.ca/index.php/jcaa/article/view/2502.

MacGillivray, A.O., R. Racca, and Z. Li. 2014. Marine mammal audibility of selected shallow-water survey sources. *Journal of the Acoustical Society of America* 135(1): EL35-EL40. http://scitation.aip.org/content/asa/journal/jasa/135/1/10.1121/1.4838296.

MacGillivray, A.O. 2018b. Underwater noise from pile driving of conductor casing at a deep-water oil platform. *Journal of the Acoustical Society of America* 143(1): 450-459. https://doi.org/10.1121/1.5021554.

Madsen, P.T., I. Kerr, and R. Payne. 2004. Echolocation clicks of two free-ranging, oceanic delphinids with different food preferences: False killer whales *Pseudorca crassidens* and Risso's dolphins *Grampus griseus*. *Journal of Experimental Biology* 207(11): 1811-1823.

Madsen, P.T. 2005. Marine mammals and noise: Problems with root mean square sound pressure levels for transients. *Journal of the Acoustical Society of America* 117(6): 3952-3957. http://link.aip.org/link/?JAS/117/3952/1.

Madsen, P.T., M. Johnson, P.J.O. Miller, N. Aguilar Soto, J. Lynch, and P. Tyack. 2006a. Quantitative measures of air-gun pulses recorded on sperm whales (*Physeter*

macrocephalus) using acoustic tags during controlled exposure experiments. *Journal of the Acoustical Society of America* 120(4): 2366-2379. http://scitation.aip.org/content/asa/journal/jasa/120/4/10.1121/1.2229287.

Madsen, P.T., M. Wahlberg, J. Tougaard, K. Lucke, and P.L. Tyack. 2006b. Wind turbine underwater noise and marine mammals: Implications of current knowledge and data needs. *Marine Ecology Progress Series* 309: 279-295. http://darchive.mbl.edu/bitstream/handle/1912/4503/m309p279.pdf?sequence=1&isAllowed=y.

Martin, B., A. MacGillivray, J. MacDonnell, J. Vallarta, T. Deveau, G. Warner, D. Zeddies, X. Mouy, and J. Krebs. 2012a. *Underwater Acoustic Monitoring of the Tappan Zee Bridge Pile Installation Demonstration Project: Comprehensive Report*. Document Number 00355, Version 1.3. Technical report for AECOM by JASCO Applied Sciences. 139 p. http://www.newnybridge.com/documents/feis/vol2/f-5a-pidp-final-report-2012-07-07.pdf

Martin, B., J. MacDonnell, A.O. MacGillivray, and D. Hannay. 2016. Comparing methods for estimating the injury and behavioral disturbance radii from sound source characterization measurements. *Journal of the Acoustical Society of America* 139(4): 2147-2148. http://dx.doi.org/10.1121/1.4950345.

Martin, K.J., S.C. Alessi, J.C. Gaspard, A.D. Tucker, G.B. Bauer, and D.A. Mann. 2012b. Underwater hearing in the loggerhead turtle (*Caretta caretta*): A comparison of behavioral and auditory evoked potential audiograms. *Journal of Experimental Biology* 215(17): 3001-3009. http://jeb.biologists.org/content/jexbio/215/17/3001.full.pdf.

Martin, S.B., M.-N.R. Matthews, J.T. MacDonnell, and K. Bröker. 2017. Characteristics of seismic survey pulses and the ambient soundscape in Baffin Bay and Melville Bay, West Greenland. *Journal of the Acoustical Society of America* 142(6): 3331-3346. https://doi.org/10.1121/1.5014049.

Martin, S.B., K.A. Kowarski, E.E. Maxner, and C.C. Wilson. 2019. *Acoustic Monitoring During Scotian Basin Exploration Project: Summer 2018*. Document Number 01687, Version 2.0. Technical report by JASCO Applied Sciences for BP Canada Energy Group ULC. https://www.bp.com/content/dam/bp-country/en_ca/canada/documents/NS_Drilling_Pgm/Acoustic-Monitoring-During-Scotian-Basin-Exploration-Project-Summer-2018.pdf.

Matthews, M.-N.R. 2012a. *Underwater Sound Modelling of Shell's 2013 Shelburne Basin 3 D Seismic Survey*. Document Number 00421, Version 5.0. Technical report for LGL Limited (St. John's, NL) by JASCO Applied Sciences. 45 p.

Matthews, M.-N.R. 2012b. *Underwater Sound Propagation from an Airgun Array in Baffin Bay: Shell 2012 Seismic Surveys in Baffin Bay Blocks 5 & 8*. Document Number 00307, Version 5.0. Technical report for LGL Ltd., Environmental Research Associates by JASCO Applied Sciences.

Matthews, M.-N.R. 2013. *Underwater Sound Propagation from an Airgun Array in Baffin Bay: Shell 2013 Seismic Surveys in Baffin Bay, Blocks 5 & 8*. Document Number 00617. Version 2.0. Technical report by JASCO Applied Sciences Ltd. for Shell Global Solutions International B. V.

Matthews, M.-N.R. and A.O. MacGillivray. 2013. Comparing modeled and measured sound levels from a seismic survey in the Canadian Beaufort Sea. *Proceedings of Meetings on*

Acoustics 19(1): 1-8. http://scitation.aip.org/content/asa/journal/poma/19/1/10.1121/1.4800553.

Matuschek, R. and K. Betke. 2009. Measurment of construction noise during pile driving of offshore research platforms and wind farms. *Proceedings of NAG-DAGA 2009 International Conference on Acoustics*. Rotterdam, Netherlands. pp. 262-265.

McCauley, R.D., R.D. Day, K.M. Swadling, Q.P. Fitzgibbon, R.A. Watson, and J.M. Semmens. 2017. Widely used marine seismic survey air gun operations negatively impact zooplankton. *Nature Ecology & Evolution* 1(7): 1-8. https://doi.org/10.1038/s41559-017-0195.

McDonald, M.A., J.A. Hildebrand, and S.M. Wiggins. 2006. Increases in deep ocean ambient noise in the Northeast Pacific west of San Nicolas Island, California. *Journal of the Acoustical Society of America* 120(2): 711-718.

Melcon, M.L., A.J. Cummins, S.M. Kerosky, L.K. Roche, S.M. Wiggins, and J.A. Hildebrand. 2012. Blue whales respond to anthropogenic noise. *PLoS ONE* 7(2): 1-6. http://www.plosone.org/article/info%3Adoi%2F10.1371%2Fjournal.pone.0032681.

Miksis, J.L., S.B. Martin, and P.L. Tyack. 2018. Exploring the Ocean Through Soundscapes. *Acoustics Today* 14(1): 26-34. https://acousticstoday.org/wp-content/uploads/2018/03/Exploring-the-Ocean-Through-Soundscapes.pdf.

Miller, P., P. Kvadsheim, F. Lam, P.L. Tyack, C. Curé, S.L. DeRuiter, L. Kleivane, L. Sivle, S. van IJsselmuide, et al. 2015. First indications that northern bottlenose whales are sensitive to behavioural disturbance from anthropogenic noise. *Royal Society Open Science* 2(6): 140484.

Mooney, T.A., P.E. Nachtigall, M. Breese, S. Vlachos, and W.W.L. Au. 2009. Predicting temporary threshold shifts in a bottlenose dolphin (*Tursiops truncatus*): The effects of noise level and duration. *Journal of the Acoustical Society of America* 125(3): 1816-1826. https://darchive.mblwhoilibrary.org/bitstream/handle/1912/2741/JASA_Mooney-etal.pdf?sequence=1&origin=publication_detail.

Mooney, T.A., R.T. Hanlon, J. Christensen-Dalsgaard, P.T. Madsen, D.R. Ketten, and P.E. Nachtigall. 2010. Sound detection by the longfin squid (Loligo pealeii) studied with auditory evoked potentials: sensitivity to low-frequency particle motion and not pressure. *Journal of Experimental Biology* 213(21): 3748-3759. http://jeb.biologists.org/content/213/21/3748.abstract.

Nachtigall, P.E. and A.Y. Supin. 2008. A false killer whale adjusts its hearing when it echolocates. *Journal of Experimental Biology* 211(11): 1714-1718. https://jeb.biologists.org/content/211/11/1714.

Nachtigall, P.E., A. Supin, A.F. Pacini, and R.A. Kastelein. 2018. Four odontocete species change hearing levels when warned of impending loud sound. *Integrative Zoology* 13(2): 160-165. https://doi.org/10.1111/1749-4877.12286.

Nieukirk, S.L., D.K. Mellinger, S.E. Moore, K. Klinck, R.P. Dziak, and J. Goslin. 2012. Sounds from airguns and fin whales recorded in the mid-Atlantic Ocean, 1999–2009. *Journal of the Acoustical Society of America* 131(2): 1102-1112.

Nordeide, J.T. and E. Kjellsby. 1999. Sound from spawning cod at their spawning grounds. *ICES Journal of Marine Science* 56(3): 326-332. http://icesjms.oxfordjournals.org/content/56/3/326.abstract.

Nowacek, D.P., L.H. Thorne, D.W. Johnston, and P.L. Tyack. 2007. Responses of cetaceans to anthropogenic noise. *Mammal Review* 37(2): 81-115.

Nowacek, D.P., K. Bröker, G. Donovan, G. Gailey, R. Racca, R.R. Reeves, A.I. Vedenev, D.W. Weller, and B.L. Southall. 2013. Responsible practices for minimizing and monitoring environmental impacts of marine seismic surveys with an emphasis on marine mammals. *Aquatic Mammals* 39(4): 356-377.

Nowacek, D.P., C.W. Clark, D. Mann, P.J. Miller, H.C. Rosenbaum, J.S. Golden, M. Jasny, J. Kraska, and B.L. Southall. 2015. Marine seismic surveys and ocean noise: time for coordinated and prudent planning. *Frontiers in Ecology and the Environment* 13(7): 378-386. http://www.esajournals.org/doi/abs/10.1890/130286?journalCode=fron&.

Parmentier, E., L. Berten, P. Rigo, F. Aubrun, S.L. Nedelec, S.D. Simpson, and D. Lecchini. 2015. The influence of various reef sounds on coral-fish larvae behaviour. *Journal of Fish Biology* 86(5): 1507-1518. https://doi.org/10.1111/jfb.12651.

Parmentier, E., R. Diogo, and M.L. Fine. 2017. Multiple exaptations leading to fish sound production. *Fish and Fisheries* 18(5): 958-966. https://doi.org/10.1111/faf.12217.

Payne, R. and D. Webb. 1971. Orientation by means of long range acoustic signaling in baleen whales. *Annals of the New York Academy of Sciences* 188: 110-142.

Payne, R.S. and S. McVay. 1971. Songs of humpback whales. *Science* 173(3997): 585-597.

Pekkarinen, J. and J. Starck. 1983. Impulse Noise in a Shipyard. *11th International Congress on Acoustics*. Paris, France. pp. 195-198.

Pettit, E.C., K.M. Lee, J.P. Brann, J.A. Nystuen, P.S. Wilson, and S. O'Neel. 2015. Unusually loud ambient noise in tidewater glacier fjords: A signal of ice melt. *Geophysical Research Letters* 42(7): 2309-2316.

Piercy, J.J., D.J. Smith, E.A. Codling, A.J. Hill, and S.D. Simpson. 2016. The good, the bad, and the distant: Soundscape cues for larval fish. *Advances in Experimental Medicine and Biology* 875: 829-837.

Pijanowski, B.C., A. Farina, S.H. Gage, S.L. Dumyahn, and B.L. Krause. 2011. What is soundscape ecology? An introduction and overview of an emerging new science. *Landscape Ecology* 26(9): 1213-1232. https://doi.org/10.1007/s10980-011-9600-8.

Pine, M., D.E. Hannay, S.J. Insely, W.D. Halliday, and F. Juanes. 2018. Assessing vessel slowdown as an option for reducing acoustic masking for Arctic cod in the western Canadian Arctic. *Journal of the Acoustical Society of America* 144(3). https://doi.org/10.1121/1.5067412.

Pinheiro, J., D. Bates, S. DebRoy, D. Sarkar, and R Core Team. 2017. *nlme: Linear and Nonlinear Mixed Effects Models*. R package version 3.1-131. https://CRAN.R-project.org/package=nlme.

Pirotta, E., R. Milor, N. Quick, D. Moretti, N. Di Marzio, P. Tyack, I. Boyd, and G. Hastie. 2012. Vessel noise affects beaked whale behavior: Results of a dedicated acoustic response study. *PLoS ONE* 7(8): e42535.

Plomp, R. and M. Bouman. 1959. Relation between hearing threshold and duration for tone pulses. *Journal of the Acoustical Society of America* 31(6): 749-758.

Popov, V.V., A.Y. Supin, V.V. Rozhnov, D.I. Nechaev, E.V. Sysuyeva, V.O. Klishin, M.G. Pletenko, and M.B. Tarakanov. 2013. Hearing threshold shifts and recovery after noise exposure in beluga whales, Delphinapterus leucas. *Journal of Experimental Biology* 216(Pt 9): 1587-96. NLM.

Popper, A.N., M. Salmon, and K.W. Horch. 2001. Acoustic detection and communication by decapod crustaceans. *Journal of Comparative Physiology A: Neuroethology, Sensory, Neural, and Behavioral Physiology* 187(2): 83-89. http://dx.doi.org/10.1007/s003590100184.

Popper, A.N., A.D. Hawkins, R.R. Fay, D.A. Mann, S. Bartol, T.J. Carlson, S. Coombs, W.T. Ellison, R.L. Gentry, et al. 2014a. Sound exposure guidelines. *In ASA S3/SC1. 4 TR-2014 Sound Exposure Guidelines for Fishes and Sea Turtles: A Technical Report prepared by ANSI-Accredited Standards Committee S3/SC1 and registered with ANSI*. Springer. pp. 33-51.

Popper, A.N., A.D. Hawkins, R.R. Fay, D.A. Mann, S. Bartol, T.J. Carlson, S. Coombs, W.T. Ellison, R.L. Gentry, et al. 2014b. *Sound Exposure Guidelines for Fishes and Sea Turtles: A Technical Report prepared by ANSI-Accredited Standards Committee S3/SC1 and registered with ANSI*. SpringerBriefs in Oceanography, Volume ASA S3/SC1.4 TR-2014. ASA Press.

Popper, A.N. and A.D. Hawkins. 2018. The importance of particle motion to fishes and invertebrates Physical aspects of swimbladder function. *Journal of the Acoustical Society of America* 143(1): 470-488. https://doi.org/10.1121/1.5021594.

Popper, A.N., A.D. Hawkins, and A. R. 2018. The importance of particle motion to fishes and invertebrates
Physical aspects of swimbladder function. *The Journal of the Acoustical Society of America* 143(1): 470-488. https://asa.scitation.org/doi/abs/10.1121/1.5021594.

Pye, H.J. and W.H. Watson, III. 2004. Sound detection and production in the American lobster, *Homarus americanus*: Sensitivity range and behavioral implications. *Journal of the Acoustical Society of America* 115(5): 2486-2486.

Qiu, W., R.P. Hamernik, and B. Davis. 2006. The kurtosis metric as an adjunct to energy in the prediction of trauma from continuous, nonGaussian noise exposures. 120(6): 3901-3906. https://asa.scitation.org/doi/abs/10.1121/1.2372455.

Qiu, W., R.P. Hamernik, and R.I. Davis. 2013a. The value of a kurtosis metric in estimating the hazard to hearing of complex industrial noise exposures. 133(5): 2856-2866. https://asa.scitation.org/doi/abs/10.1121/1.4799813.

Qiu, W., R.P. Hamernik, and R.I. Davis. 2013b. The value of a kurtosis metric in estimating the hazard to hearing of complex industrial noise exposures. *Journal of the Acoustical Society of America* 133(5): 2856-2866. https://doi.org/10.1121/1.4799813.

Reinhall, P.G. and P.H. Dahl. 2011. *An Investigation of Underwater Sound Propagation from Pile Driving*. Document Number WA-RD 781.1. Prepared for the State of Washington Department of Transportation. 39 p. http://www.wsdot.wa.gov/research/reports/fullreports/781.1.pdf.

Richardson, W.J., B. Würsig, and C.R. Greene, Jr. 1986. Reactions of bowhead whales, *Balaena mysticetus*, to seismic exploration in the Canadian Beaufort Sea. *Journal of the Acoustical Society of America* 79(4): 1117-1128.

Richardson, W.J., G.W. Miller, and C.R. Greene, Jr. 1999. Displacement of migrating bowhead whales by sounds from seismic surveys in shallow waters of the Beaufort Sea. *Journal of the Acoustical Society of America* 106(4): 2281-2281. http://link.aip.org/link/?JAS/106/2281/3.

Risch, D., P.J. Corkeron, W.T. Ellison, and S.M. Van Parijs. 2012. Changes in humpback whale song occurrence in response to an acoustic source 200 km away. *PLoS ONE* 7(1): e29741. http://www.plosone.org/article/info%3Adoi%2F10.1371%2Fjournal.pone.0029741#pone-0029741-g003.

Roberts, L. and M. Elliott. 2017. Good or bad vibrations? Impacts of anthropogenic vibration on the marine epibenthos. *Science of The Total Environment* 595: 255-268. https://doi.org/10.1016/j.scitotenv.2017.03.117.

Robertson, F.C., W.R. Koski, T.A. Thomas, W.J. Richardson, B. Würsig, and A.W. Trites. 2013. Seismic operations have variable effects on dive-cycle behavior of bowhead whales in the Beaufort Sea. *Endangered Species Research* 21(2): 143-160. http://www.int-res.com/abstracts/esr/v21/n2/p143-160/.

Robinson, S.P., P.A. Lepper, and J. Ablitt. 2007. The measurement of the underwater radiated noise from marine piling including characterisation of a" soft start" period. *Oceans 2007-Europe*. 18-21 Jun 2007. IEEE, Aberdeen, UK. pp. 732-737. https://doi.org/10.1109/OCEANSE.2007.4302326.

Rodríguez, E., C.S. Morris, Y.J.E. Belz, E.C. Chapin, J.M. Martin, W. Daffer, and S. Hensley. 2005. *An Assessment of the SRTM Topographic Products*. Document Number JPL D-31639. Jet Propulsion Laboratory, Pasadena, CA.

Rolland, R.M., S.E. Parks, K.E. Hunt, M. Castellote, P.J. Corkeron, D.P. Nowacek, S.K. Wasser, and S.D. Kraus. 2012. Evidence that ship noise increases stress in right whales. *Proceedings of the Royal Society B: Biological Sciences*. http://rspb.royalsocietypublishing.org/content/royprsb/early/2012/02/01/rspb.2011.2429.full.pdf.

Roman, J., J.A. Estes, L. Morissette, C. Smith, D. Costa, J. McCarthy, J.B. Nation, S. Nicol, A. Pershing, et al. 2014. Whales as marine ecosystem engineers. *Frontiers in Ecology and the Environment* 12(7): 377-385.

Roth, E.H., J.A. Hildebrand, and S.M. Wiggins. 2012. Underwater ambient noise on the Chukchi Sea continental slope from 2006-2009. *Journal of the Acoustical Society of America* 131(1): 104-110.

Samson, J.E., T.A. Mooney, S.W. Gussekloo, and R.T. Hanlon. 2016. A brief review of cephalopod behavioral responses to sound. *Advances in Experimental Medicine and Biology* 875: 969-975.

Sand, O. and A.D. Hawkins. 1973. Acoustic properties of the cod swim bladder. *Journal of Experimental Biology* 58: 797-820. http://jeb.biologists.org/content/58/3/797.

Saunders, J.C., W.F. Rintelmann, and G.R. Bock. 1979. Frequency selectivity in bird and man: A comparison among critical ratios, critical bands and psychophysical tuning curves. *Hearing Research* 1(4): 303-323. https://doi.org/10.1016/0378-5955(79)90003-0.

Scharf, B. 1970. Critical bands. *In* Tobias, J.V. (ed.). *Foundations of Modern Auditory Theory*. Volume 1. Academic Press, New York. pp. 157–202.

Shannon, G., M.F. McKenna, L.M. Angeloni, K.R. Crooks, K.M. Fristrup, E. Brown, K.A. Warner, M.D. Nelson, C. White, et al. 2016. A synthesis of two decades of research documenting the effects of noise on wildlife. *Biological Reviews* 91(4): 982-1005. http://dx.doi.org/10.1111/brv.12207.

Sills, J.M., B.L. Southall, and C. Reichmuth. 2014. Amphibious hearing in spotted seals (*Phoca largha*): Underwater audiograms, aerial audiograms and critical ratio measurements. *Journal of Experimental Biology* 217: 726-734.

Sills, J.M., B.L. Southall, and C. Reichmuth. 2015. Amphibious hearing in ringed seals (*Pusa hispida*): Underwater audiograms, aerial audiograms and critical ratio measurements. *Journal of Experimental Biology* 218(14): 2250-2259. http://jeb.biologists.org/content/jexbio/218/14/2250.full.pdf.

Simard, Y., N. Roy, C. Gervaise, and S. Giard. 2016. Analysis and modeling of 255 source levels of merchant ships from an acoustic observatory along St. Lawrence Seaway. *Journal of the Acoustical Society of America* 140(3): 2002-2018.

Simpson, S.D., A.N. Radford, S. Holles, M.C. Ferarri, D.P. Chivers, M.I. McCormick, and M.G. Meekan. 2016. Small-Boat Noise Impacts Natural Settlement Behavior of Coral Reef Fish Larvae. *In* Popper, A. and A. Hawkins (eds.). *The Effects of Noise on Aquatic Life II*. Springer, New York. pp. 1041-1048.

Smith, M. and R. R. Gilley. 2008. *Testing the equal energy hypothesis in noise-exposed fishes*, Volume 17. 343-345 p.

Snyder, M.A. 2007. *Long-term ambient noise statistics in the Gulf of Mexico*. Doctor of Philosophy Thesis, Doctoral. University of New Orleans, New Orleans. 162 p.

Southall, B.L., A.E. Bowles, W.T. Ellison, J.J. Finneran, R.L. Gentry, C.R. Greene, Jr., D. Kastak, D.R. Ketten, J.H. Miller, et al. 2007. Marine mammal noise exposure criteria: Initial scientific recommendations. *Aquatic Mammals* 33(4): 411-521.

Southall, B.L., S.L. DeRuiter, A. Friedlaender, A.K. Stimpert, J.A. Goldbogen, E. Hazen, C. Casey, S. Fregosi, D.E. Cade, et al. 2019a. Behavioral responses of individual blue whales (*Balaenoptera musculus*) to mid-frequency military sonar. *Journal of Experimental Biology* 222(5). http://jeb.biologists.org/content/jexbio/222/5/jeb190637.full.pdf.

Southall, B.L., J.J. Finneran, C. Reichmuth, P.E. Nachtigall, D.R. Ketten, A.E. Bowles, W.T. Ellison, D.P. Nowacek, and P.L. Tyack. 2019b. Marine Mammal Noise Exposure Criteria:

Updated Scientific Recommendations for Residual Hearing Effects. *Aquatic Mammals* 45(2): 125-232. https://doi.org/10.1578/AM.45.2.2019.125.

Spiga, I., J. Fox, and R. Benson. 2012. Effects of Short-and Long-Term Exposure to Boat Noise on Cortisol Levels in Juvenile Fish. (Chapter 55) *In* Popper, A.N. and A. Hawkins (eds.). *The Effects of Noise on Aquatic Life*. Volume 730. Springer New York. pp. 251-253 Translated from English.

Spiga, I., G.S. Caldwell, and R. Bruintjes. 2016. Influence of Pile Driving on the Clearance Rate of the Blue Mussel, *Mytilus edulis* (L.). *Proceedings of Meetings on Acoustics: Fourth International Conference on the Effects of Noise on Aquatic Life*. Volume 27(1), 10–16 July 2016, Dublin, Ireland. http://dx.doi.org/10.1121/2.0000277.

Stadler, J.H. and D.P. Woodbury. 2009. *Assessing the effects to fishes from pile driving: Application of new hydroacoustic criteria*. *Inter-Noise 2009: Innovations in Practical Noise Control*, 2009 August 23-26, Ottawa, Canada.

Suga, N. and T. Shimozawa. 1974. Site of Neural Attenuation of Responses to Self-Vocalized Sounds in Echolocating Bats. 183(4130): 1211-1213. http://science.sciencemag.org/content/sci/183/4130/1211.full.pdf.

Tashmukhambetov, A.M., G.E. Ioup, J.W. Ioup, N.A. Sidorovskaia, and J.J. Newcomb. 2008. Three-dimensional seismic array characterization study: Experiment and modeling. *Journal of the Acoustical Society of America* 123(6): 4094-4108.

Teague, W.J., M.J. Carron, and P.J. Hogan. 1990. A comparison between the Generalized Digital Environmental Model and Levitus climatologies. *Journal of Geophysical Research* 95(C5): 7167-7183.

Thode, A., K.H. Kim, C.R. Greene, Jr., and E. Roth. 2010. Long range transmission loss of broadband seismic pulses in the Arctic under ice-free conditions. *Journal of the Acoustical Society of America* 128(4): EL181-EL187. http://scitation.aip.org/content/asa/journal/jasa/128/4/10.1121/1.3479686.

Thomisch, K., O. Boebel, D.P. Zitterbart, F. Samaran, S. Van Parijs, and I. Van Opzeeland. 2015. Effects of subsampling of passive acoustic recordings on acoustic metrics. *Journal of the Acoustical Society of America* 138(1): 267-278.

Tougaard, J., J. Carstensen, J. Teilmann, H. Skov, and P. Rasmussen. 2009. Pile driving zone of responsiveness extends beyond 20 km for harbor porpoises (*Phocoena phocoena* (L.)). *Journal of the Acoustical Society of America* 126(1): 11-14.

Tougaard, J., A.J. Wright, and P.T. Madsen. 2014. Cetacean noise criteria revisited in the light of proposed exposure limits for harbour porpoises. *Marine pollution bulletin*: 1-13.

Tougaard, J., A.J. Wright, and P.T. Madsen. 2015. Cetacean noise criteria revisited in the light of proposed exposure limits for harbour porpoises. *Marine Pollution Bulletin* 90(1): 196-208.

Tougaard, J. and K. Beedholm. 2019. Practical implementation of auditory time and frequency weighting in marine bioacoustics. *Applied Acoustics* 145: 137-143. https://doi.org/10.1016/j.apacoust.2018.09.022.

Tyack, P.L., W.M. Zimmer, D. Moretti, B.L. Southall, D.E. Claridge, J.W. Durban, C.W. Clark, A. D'Amico, N. DiMarzio, et al. 2011. Beaked whales respond to simulated and actual navy sonar. *PLoS ONE* 6(3): e17009.

Urick, R.J. 1983. *Principles of Underwater Sound*. 3rd edition. McGraw-Hill, New York, London. 423 p.

Van der Graaf, A., M. Ainslie, M. André, K. Brensing, J. Dalen, R. Dekeling, S. Robinson, M. Tasker, F. Thomsen, et al. 2012. *European Marine Strategy Framework Directive - Good Environmental Status (MSFD GES): Report of the Technical Subgroup on Underwater Noise and Other Forms of Energy*. Brussels.

Venables, W.N. and B.D. Ripley. 2002. *Modern Applied Statistics with S*. Fourth edition. Springer. http://www.stats.ox.ac.uk/pub/MASS4.

Vermeij, M.J.A., K.L. Marhaver, C.M. Huijbers, I. Nagelkerken, and S.D. Simpson. 2010. Coral larvae move toward reef sounds. *PLoS ONE* 5(5): e10660. http://dx.doi.org/10.1371%2Fjournal.pone.0010660.

Ward, W.D. 1962. Effect of Temporal Spacing on Temporary Threshold Shift from Impulses. *Journal of the Acoustical Society of America* 34(9A): 1230-1232. https://doi.org/10.1121/1.1918309.

Ward, W.D., E.M. Cushing, and E.M. Burns. 1976a. Effective quiet and moderate TTS: Implications for noise exposure standards. *Journal of the Acoustical Society of America* 59(1): 160-165. https://doi.org/10.1121/1.380835.

Ward, W.D., E.M. Cushing, and E.M. Burns. 1976b. Effective quiet and moderate TTS: Implications for noise exposure standards. *The Journal of the Acoustical Society of America* 59(1): 160-165. https://asa.scitation.org/doi/abs/10.1121/1.380835.

Ward, W.D. 1997. Effects of high-intensity sound. *In* Crocker, M.J. (ed.). *Encyclopedia of acoustics*. Volume III. John Wiley and Sons, New York. pp. 1497-1507.

Wartzok, D., A.N. Popper, J. Gordon, and J. Merrill. 2003. Factors affecting the responses of marine mammals to acoustic disturbance. *Marine Technology Society Journal* 37(4): 6-15. http://www.ingentaconnect.com/content/mts/mtsj/2003/00000037/00000004/art00002 http://dx.doi.org/10.4031/002533203787537041.

Welch, P. 1967. The use of fast Fourier transform for the estimation of power spectra: A method based on time averaging over short, modified periodograms. *IEEE Transactions on Audio and Electroacoustics* 15(2): 70-73.

Wenz, G.M. 1962. Acoustic ambient noise in the ocean: Spectra and sources. *Journal of the Acoustical Society of America* 34(12): 1936-1956.

Whitehead, H. and L. Rendell. 2014. *The Cultural Lives of Whales and Dolphins*. University of Chicago Press. 408 p.

Wilkes, D.R. and A.N. Gavrilov. 2017. Sound radiation from impact-driven raked piles. *The Journal of the Acoustical Society of America* 142(1): 1-11. https://asa.scitation.org/doi/abs/10.1121/1.4990021.

Wisniewska, D.M., L.A. Kyhn, J. Tougaard, M. Simon, Y.-T. Lin, A. Newhall, K. Beedholm, J. Lynch, and P.T. Madsen. 2014. *Propagation of airgun pulses in Baffin Bay 2012*. Scientific Report from DCE – Danish Centre for Environment and Energy. Document Number 109. http://dce2.au.dk/pub/SR109.pdf.

Wood, J., B.L. Southall, and D.J. Tollit. 2012. *PG&E offshore 3 D Seismic Survey Project EIR-Marine Mammal Technical Draft Report*. SMRU Ltd.

Zampolli, M., M.J.J. Nijhof, C.A.F. de Jong, M.A. Ainslie, E.H.W. Jansen, and B.A.J. Quesson. 2013. Validation of finite element computations for the quantitative prediction of underwater noise from impact pile driving. *Journal of the Acoustical Society of America* 133(1): 72-81.

APPENDIX A. COPYRIGHT PERMISSIONS

26 Aug 2019
Journal of the Acoustical Society of America
1305 Walt Whitman Road
Meliville, NY 11747, acousticalsociety.org

I am preparing my PhD thesis for submission to the Faculty of Graduate Studies at Dalhousie University, Halifax, Nova Scotia, Canada. I am seeking your permission to include manuscript versions of the following papers as a chapter in the thesis:

Martin, S.B., C. Morris, K. Bröker, and C. O'Neill. 2019. Sound exposure level as a metric for analyzing and managing underwater soundscapes. *Journal of the Acoustical Society of America* 146(1): 135-149. https://doi.org/10.1121/1.5113578.

Martin, S.B. and D.R. Barclay. 2019. Determining the dependence of marine pile driving sound levels on strike energy, pile penetration, and propagation effects using a linear mixed model based on damped cylindrical spreading. *Journal of the Acoustical Society of America* 146(1): 109-121. https://doi.org/10.1121/1.5114797.

Martin, S.B., M.-N.R. Matthews, J.T. MacDonnell, and K. Bröker. 2017. Characteristics of seismic survey pulses and the ambient soundscape in Baffin Bay and Melville Bay, West Greenland. *Journal of the Acoustical Society of America* 142(6): 3331-3346. https://doi.org/10.1121/1.5014049.

The versions I propose to include in the thesis have been edited to reflect the comments received from my Thesis Review Committee and to improve the flow of the thesis, where relevant.

Canadian graduate theses are reproduced by the Library and Archives of Canada (formerly National Library of Canada) through a non-exclusive, world-wide license to reproduce, loan, distribute, or sell theses. I am also seeking your permission for the material described above to be reproduced and distributed by the LAC(NLC). Further details about the LAC(NLC) thesis program are available on the LAC(NLC) website (www.nlc-bnc.ca).

Full publication details and a copy of this permission letter will be included in the thesis.

Yours sincerely,

Steven Bruce Martin, PhD
Dalhousie University Department of Oceanography

Permission is granted for:

a) the inclusion of the material described above in your thesis.

b) for the material described above to be included in the copy of your thesis that is sent to the Library and Archives of Canada (formerly National Library of Canada) for reproduction and distribution.

Name: Susann Brailey

Title: Manager, Rights Permission, AIP

Signature: _____

Date: 26 / 08 / 2019